GNGTS 2024

SEISMICITY, VOLCANOES, DATA AND MODELS

Session 1.1

Recent advances in the study of earthquakes, faults and seismogenic processes in natural and experimental faults

Convenors of the session:
Paolo Galli (DPC) – paolo.galli@protezionecivile.it
Massimo Cocco (INGV) – massimo.cocco@ingv.it
Luisa Valoroso (INGV) – luisa.valoroso@ingv.it

The goal of this session is to present and discuss recent advances in earthquake and fault mechanics through observations, multidisciplinary data, and modeling of natural and experimental faults.
We encourage the submission of contributions on the following topics:

- **Investigations of the Quaternary and structural background of active faults**
- **Paleoseismology and archaeoseismology**
- **Insights of the 2023 Kahramanmaraş (Turkey) and High Atlas Mts. (Morocco) earthquakes**
- **Characterization of capable faults for seismic microzonation studies, in tectonic and volcanic settings**
- **Revisions of historical and instrumental earthquakes and catalogues**
- **Case histories of instrumental and historical seismic sequences**
- **Advanced earthquake location methods, both for research and monitoring purposes**
- **GPS and InSAR data for the evaluation of inter-, post- and co-seismic deformation**
- **Source modelling through the inversion of seismic, geodetic and/or other multidisciplinary datasets**
- **Multidisciplinary, multiscale geophysical imaging for seismotectonic studies**
- **3D modelling for seismotectonics**
- **Insights into the mechanics of earthquake and faulting form from numerical modeling and laboratory experiments**
- **Rocks rheology and role of fluids in the seismogenesis: from laboratory experiments to the Earth crust**

Estimate of seismic fracture surface energy from pseudotachylyte-bearing faults

S. Aldrighetti[1], G. Di Toro[1,2], G. Pennacchioni[1]

[1] *Dipartimento di Geoscienze, Università degli Studi di Padova, Padua, Italy*
[2] *Sezione di Roma 1, Istituto Nazionale di Geofisica e Vulcanologia, Rome, Italy*

Earthquakes are the result of propagation (at km s^{-1}) of a rupture and associated slip (at m s^{-1}) along a fault (Scholz, 2019). The total energy involved in a seismic event is unknown, but qualitatively most of the energy is dissipated by rock fracturing and frictional heat. Seismic fracture energy G (J m^{-2}) is the energy dissipated in the rupture propagation and can be estimated by the inversion of seismic waves (Abercrombie and Rice, 2005; Tinti et al., 2005; Cocco et al., 2023). However, the physical significance of G remains elusive. G may include the contributions of both rock fracturing (energy to form new rock surfaces U_S, J m^{-2}) and fault frictional heating (Q, J m^{-2}). Here we determine both U_S and Q in natural and experimental pseudotachylyte-bearing faults following the approach used by Pittarello et al. (2008). Pseudotachylytes are solidified frictional melts produced during seismic slip. In these rocks: (i) U_S is proportional to the surface of the new fragments produced in both the slip zone and in the wall rocks; and (ii) Q is proportional to the volume of frictional melt.

The selected natural pseudotachylytes are from the East-West-striking, dextral, strike-slip Gole Larghe Fault Zone (Adamello, Italy; Di Toro and Pennacchioni, 2004). To estimate U_S we used Electron Back-Scatter Electrons (EBSD), High Resolution Mid Angle Back-Scattered Electrons (HRMABSD) and Cathodoluminescence-Field Emission-Scanning Electron Microscopy (CL-FESEM). In particular, CL-FESEM imaging reveals a microfracture network in the wall rocks that cannot be detected with other techniques used (Fig. 1).

In the pseudotachylyte-bearing fault, the microstructural analysis reveals (i) a high degree of fragmentation of the wall rock adjacent to the pseudotachylyte fault vein (formed along the slip surface), with clast size down to < 90 nm in diameter, and (ii) a systematic difference in fracture density and orientation of the microfractures on the two opposite wall rock sides of the fault (Fig. 1). In fact, in the northern wall rock the fracture density is low and the microfractures are oriented preferentially East-West, while in the southern wall rock the fracture density is high and oriented preferentially North-South (Fig. 1). This asymmetric distribution of microfracture damage is consistent with the stress perturbation at the crack tip associated with the propagation of the seismic rupture (Di Toro et al., 2005). This suggests that the microfractures developed during coseismic slip and, therefore, can be used to estimate U_S.

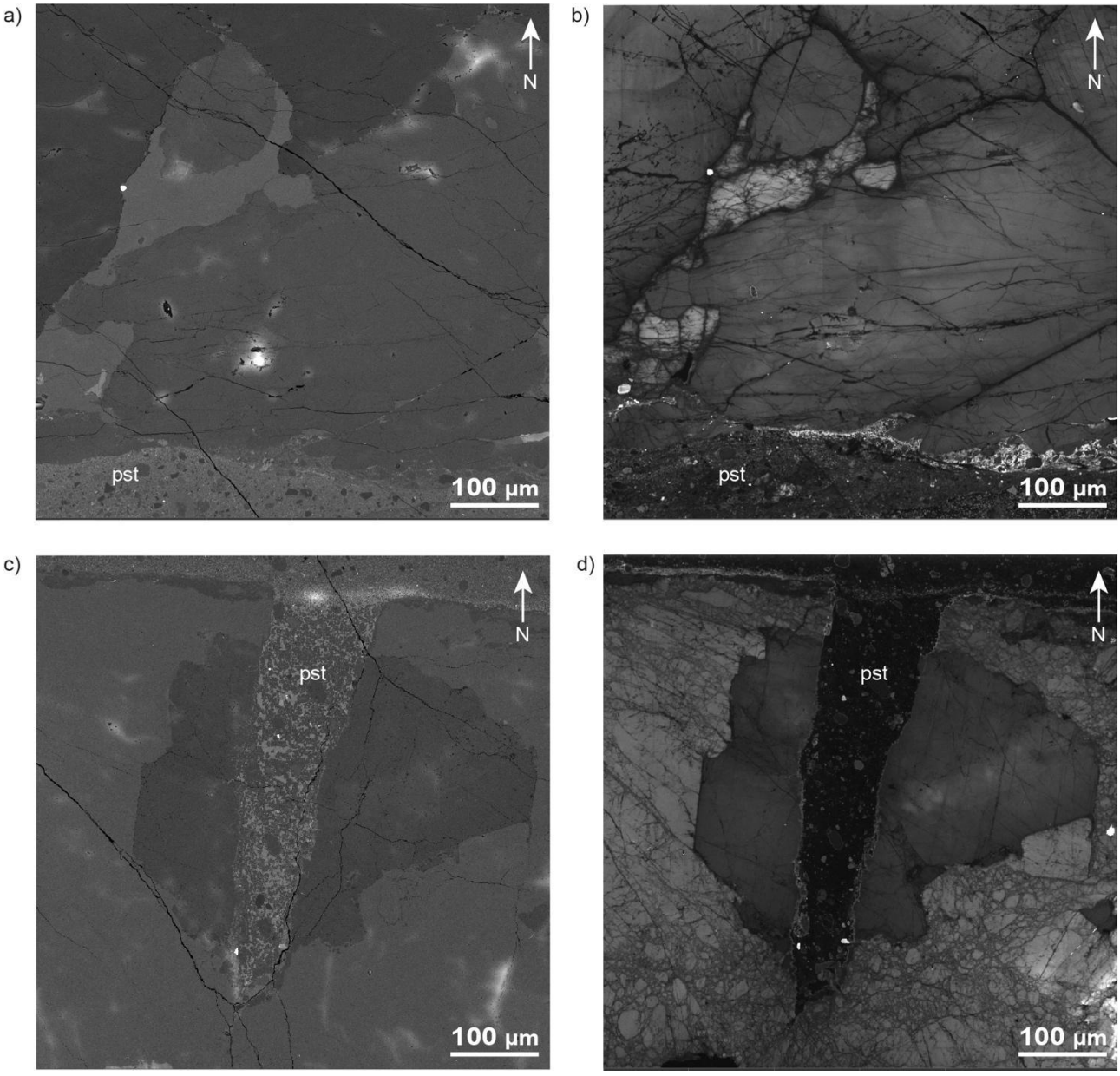

Fig. 1: Microfracture pattern in the two wall rocks of the selected pseudotachylyte-bearing fault. a) BSE-FESEM and b) CL-FESEM microimages of the northern wall rock, displaying low damage and preferential subhorizontal orientation of the microfractures. c) BSE-FESEM and d) CL-FESEM microimages of the southern wall rock, showing instead extreme damage surrounding a pseudotachylyte injection vein, and a preferential subvertical strike of the microfractures. All microimages are taken at the boundary pseudotachylyte-wall rock. Note how in BSE-FESEM microimages the microfracture pattern is extremely underestimated. pst=pseudotachylyte.

Fracture density decreases exponentially from the pseudotachylyte-wall rock contact towards the wall rock. The rock volumes with highest coseismic damage at the contact with the pseudotachylytes are assumed to be representative of the host-rock damage preceding frictional melting along the slip zone (Pittarello et al., 2008). Based on this assumption, U_S is estimated in the range from 0.008 to 1.35 MJ m^{-2}. Q was estimated from the thickness of the pseudotachylyte vein (Pittarello et al., 2008) to be ~32 MJ m^{-2}. In the case of the Gole Larghe Fault, numerical

modelling yield fracture energies G in the range 8-67 MJ m^{-2} (Di Toro et al., 2005) suggesting that U_S is subordinate component of G and that most of the seismological fracture energy is heat.

References

Abercrombie, R. E., and Rice, J. R.; 2005: *Can observations of earthquake scaling constrain slip weakening?* Geophys. J. Int., 162(2), 406–424. https://doi.org/10.1111/j.1365-246X.2005.02579.x.

Cocco, M., Aretusini, S., Cornelio, C., Nielsen, S. B., Spagnuolo, E., Tinti, E., and Di Toro, G.; 2023: *Fracture Energy and Breakdown Work During Earthquakes.* Ann. Rev. Earth Planet. Sci., 51(1), null. https://doi.org/10.1146/annurev-earth-071822-100304.

Di Toro, G., Nielsen, S., and Pennacchioni, G.; 2005: *Earthquake rupture dynamics frozen in exhumed ancient faults.* Nature, 436(7053), Article 7053. https://doi.org/10.1038/nature03910.

Di Toro, G., and Pennacchioni, G.; 2004: *Superheated friction-induced melts in zoned pseudotachylytes within the Adamello tonalites (Italian Southern Alps).* J. Struct. Geol., 26(10), 1783–1801. https://doi.org/10.1016/j.jsg.2004.03.001.

Pittarello, L., Di Toro, G., Bizzarri, A., Pennacchioni, G., Hadizadeh, J., and Cocco, M.; 2008: *Energy partitioning during seismic slip in pseudotachylyte-bearing faults (Gole Larghe Fault, Adamello, Italy).* Earth Planet. Sci. Lett., 269(1), 131–139. https://doi.org/10.1016/j.epsl.2008.01.052.

Scholz, C. H.; 2019: *The Mechanics of Earthquakes and Faulting.* Cambridge University Press.

Tinti, E., Spudich, P., and Cocco, M.; 2005: *Earthquake fracture energy inferred from kinematic rupture models on extended faults.* J. Geophys. Res: Solid Earth, 110(B12). https://doi.org/10.1029/2005JB003644.

Corresponding author: silvia.aldrighetti.1@phd.unipd.it

Offshore fault geometry revealed from earthquake locations using new state-of-art techniques: the case of the 2022 Adriatic Sea earthquake sequence

Like An*[1], Francesco Grigoli[2], Bogdan Enescu[1,3], Mauro Buttinelli[4], Mario Anselmi[4], Irene Molinari[4], and Yoshihiro Ito[5]

[1]Department of Geophysics, Graduate School of Science, Kyoto University, Kyoto, Japan
[2]Department of Earth Sciences, University of Pisa, Pisa, Italy
[3]National Institute for Earth Physics, Magurele, Bucharest, Romania
[4]National Institute of Geophysics and Volcanology, Italy
[5]Disaster Prevention Research Institute, Kyoto University, Uji, Kyoto, Japan

On November 9, 2022, 6:07 AM (UTC), a sequence of two M>5 earthquakes (mainshock of Mw 5.5) occurred 30 km NE off the coast of Fano, Italy. Since locating offshore earthquakes is challenging, we have applied a combined approach to constrain the geometry and depth of the sequence events better. Six M3+ events were first relocated using a travel time stacking method. Next, using the six M3+ earthquakes as reference events, we applied a differential travel-time method to reconstruct the earthquake cluster geometry and locate the remaining events, including the mainshock. The results reveal a 25-35 degree SW dipping cluster. The depth of the mainshock hypocenter obtained using this procedure agrees well with that determined by depth phases. This study's relatively sharp earthquake cluster geometry is consistent with the thrust faults revealed by a local seismic reflection survey and focal mechanism solutions. These approaches are particularly useful for offshore monitoring of industrial operations (e.g., Carbon Dioxide and Methane storage).

Corresponding author:
Like An (like.an.65h@st.kyoto-u.ac.jp),
Mauro Buttinelli (mauro.buttinelli@ingv.it)

Focus on the seismic behavior of the Morrone Fault: the Majella-Morrone experiment

M. Anselmi[1], S. Bagh[1], C. Chiarabba[1], P. De Gori[1], R. Fonzetti[3], A. Govoni[1], I. Menichelli [1,3], G. Pezzo[1], G. Saccorotti[1], F. Silverii[1]

[1] Istituto Nazionale di Geofisica e Vulcanologia, Roma, Italy
[2] Istituto Nazionale di Geofisica e Vulcanologia, Pisa, Italy
[3] Università degli Studi di Roma Tre, Roma, Italy

In the framework of the PON-GRINT project, a working group of INGV researchers, along with some Ph.D. students, carried out a passive seismic experiment, still ongoing. The field activities began in May 2022 in the Abruzzi region (Central Italy). Between May and October 2022, twenty-three (23) temporary seismic stations were deployed in a ~ 250 km^2 area extending from the Sulmona-Pratola Peligna plain to the eastern flank of Monte Morrone.

The location of the study area is in the Central Apennines, southeast of the area struck by the 2009 L'Aquila seismic sequence. The whole Apennine chain consists of thrust and fold systems, the space-time E and NE migration of which are related to the westward subduction of the Adriatic lithosphere and its progressive eastward flexural retreat (Patacca et al. 2008 and references therein). Since the Pliocene, and during the entire Quaternary, the chain was affected by extensional tectonics, contemporaneous to its significant uplift (Galadini et al. 2003a and references therein). The extensional faults have resulted in the formation of several intermontane basins (e.g. the Fucino, Sulmona, L'Aquila) that are filled by continental deposits of Plio-Quaternary age (Bosi et al. 2003; Galadini and Messina 2004).

In particular, the Apennine sector focused in this study, located in the southern-eastern Abruzzi region, has been struck by some large magnitude earthquakes , i.e. the seismic events of 1706 (Maw = 6.6) and 1933 (Maw = 5.7), as well as by the shocks of the 1349 and 1456 seismic sequences (Maw = 6.6 and 7.0, Romano et al. 2013 and references therein). The literature available indicates also the 1456, 1706 and 1933 earthquakes originated in this area (Galadini and Galli 2007; Fracassi and Valensise 2007). Many studies have been carried out to define the seismotectonic characteristics of this Apennine sector. Some probably active faults have been detected along the south-western slopes of Mt. Morrone (Bosi 1975), and in the area located between Mt. Morrone, the Maiella Massif and the Cinque Miglia plain.

Although the last 20 years have been characterised by low-magnitude seismicity, the presence of the Morrone Fault (whose instrumental seismic activity is still debated) motivates the carrying out of the experiment to record the microseismicity occurred in the whole area and also the eventual seismic activity released by the Morrone Fault structure.

The field activity results in building a temporary network, integrated with regional and national seismic networks, with an average station inter-distance of about 7-8 Km. In addition, along with the seismic network, we deployed a subset of seismic stations to make an almost straight transect across the Monte-Morrone, with the goal of defining the fault structure profile by using seismic noise recordings. After almost 12 months of recordings the straight transect was shifted, following the strike of the focused fault, to the north-west, still across the Monte Morrone (Fig.1).

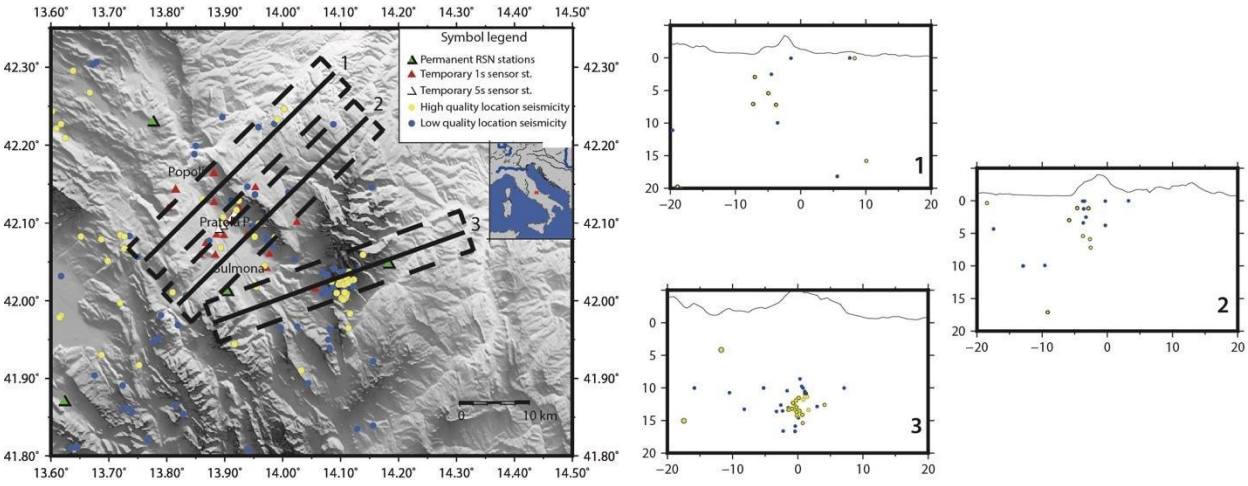

Fig.1 . Map with a temporary network of the experiment: 19 short period + 4 extended period sensors. The seismicity was recorded between November 2022 and January 2023.

The preliminary analysis of the recorded data seems to show a scarce seismicity within the temporary network, mainly clustered in two different areas: one at the north-western side of Monte Morrone and the other between the southeastern part of Monte Morrone and Maiella, probably related to the Caramanico fault that boards the western flank of the Maiella anticline (Fig. 1).

References

Bosi C (1975) Osservazioni preliminare su faglie probabilmente attive nell'Appennino Centrale. Bol Soc Geol Ital 94:827–859

Bosi C, Galadini F, Giaccio B, Messina P, Sposato A (2003). Plio-Quaternary continental deposits in the Latium-Abruzzi Apennines: the correlation of geological events across different intermontane basins. Il Quat (Ital J Quat Sci) 16:55–76

Fracassi U, Valensise G (2007). Unveiling the sources of the catastrophic 1456 multiple earthquake: hints to an unexplored tectonic mechanism in southern Italy. Bull Seism Soc Am 97:725–748

Galadini F, Galli P, Moro M (2003a). Paleoseismology of silent faults in the central Apennines (Italy): the Campo Imperatore fault (Gran Sasso range fault system). Ann Geophys 46:793–813

Galadini F, Messina P (2004). Early-Middle Pleistocene eastward migration of the Abruzzi Apennine (central Italy) extensional domain. J Geodyn 37:57–81

Galadini F, Galli P (2007). Inquadramento sismotettonico della regione interessata dai terremoti del 1703 e 1706. Bullettino della Deputazione di Storia Patria degli Abruzzi. Settecento abruzzese: eventi sismici, mutamenti economico-sociali e ricerca storiografica. In: a cura di Raffaele Colapietra, Giacinto Marinangeli, Colacchi (ed) Atti del convegno L'Aquila 29-30-31 ottobre 2004, Paolo Muzi. L'Aquila 2007, pp 1158

Patacca E, Scandone P, Di Luzio E, Cavinato GP, Parotto M (2008) Structural architecture of the central Apennines: interpretation of the CROP 11 seismic profile from the Adriatic coast to the orographic divide. Tectonics 27:TC3006, 36 pp

Romano, M. A., De Nardis, R., Lavecchia, G., Garbin, M., Peruzza, L., Priolo, E., ... & Ferrarini, F. (2013). Preliminary analysis of the microearthquakes-faults association in the Sulmona basin (central Apennines, Italy). Rendiconti Online della Società Geologica Italiana, 29, 150-153

Corresponding author: mario.anselmi@ingv.it

One Earthquake, Two Scenarios: The Baffling Case of the 1467 Siena Earthquake.

A. Arrighetti[1], B. Gelli[2], V. Castelli[3]

[1] École normale supérieure - Université PSL (AOROC UMR 8546), Paris, France;
[2] Università degli Studi di Siena, Italia; [3] INGV, Bologna/Ancona, Italia

Historical seismology is a work in progress: the overall picture of a given historical earthquake, no matter how long taken for granted, can sometimes change, either thanks to the discovery of "new" (i.e. previously unknown or unheeded) historical sources, or by considering the research output of other disciplines.

Historical seismologists tend to give precedence in their studies to written evidence, derived (when a choice is possible) from the sources 1) most likely to provide information useful to fulfill their main objectives (i.e. assessing macroseismic data points, reconstructing macroseismic fields and damage scenarios), and 2) not requiring long-drawn out, possibly unsuccessful searches that would hardly fit with their generally tight deadlines. Unavoidably, this approach mean to discard interesting but elusive evidence, whose records are buried too deep to make a search cost-effective, or were never written down at all but survive as the marks which past earthquakes left on buildings. It is up to the scholar to find ways and means to interpret these unwritten records, even if the readings taken are not always conclusive.

The archaeoseismological study of historic towns and buildings allows to gain in-depth knowledge of how a given earthquake interacted with architectures and building components and in some cases, it can also provide evidence of the social, economic, or even political consequences of some earthquakes. The project *PROTECT – Knowledge for PReventiON - Technique s for repairing seismic damage from the medieval period to the modern era* (financed by the European Union's Horizon 2020 research and innovation program together with a Marie Skłodowska-Curie Individual Fellowship) applies, on an entirely experimental basis, the methods of archaeoseismological analysis to the historic centre of Siena (Tuscany), to improve the knowledge of its context for purposes of seismic risk reduction. By weaving together the information gathered by different humanistic and scientific disciplines, the PROTECT project aims to define an operational protocol for the archaeoseismological reading of the historic centre of Siena (or part of it). This protocol could be exported to other Italian/European towns, with a view to improve our understanding of their historic heritage and the best ways to protect it from seismic risk.

The PROTECT project started in December 2021 with a first step aimed at a general analysis of the historic city centre with reference to a specific earthquake. After an initial look at the seismic history of Siena, the choice fell on the August-September 1467 seismic sequence (Fig. 1).

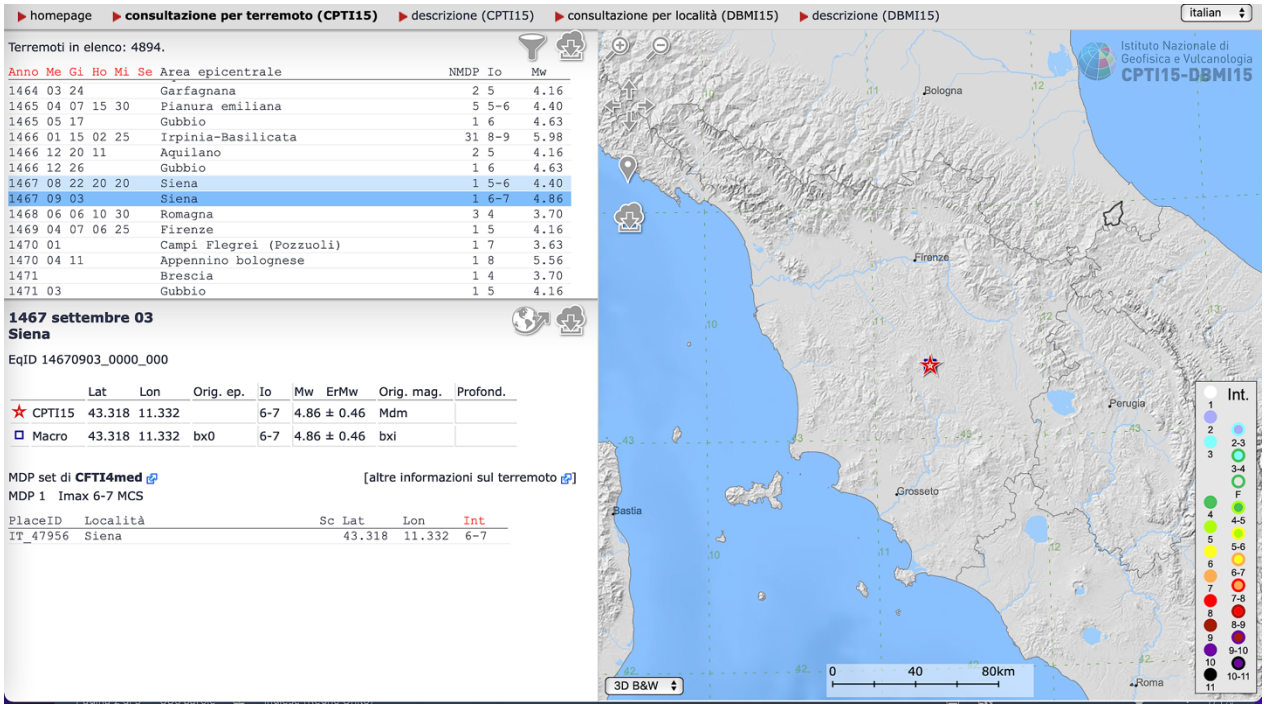

Fig. 1 – The 1467 Siena seismic sequence according to CPTI15 v. 4.0 (Rovida et al., 2022).

What led to the choice of this comparatively “minor” earthquake (Mw 4.8 according to Rovida et al., 2022) was dictated by the awareness that the Archivio di Stato of Siena preserved a a so far unexploited source of exceptional documentary value, the “Lira” of the year 1468. This is a huge collection of tax statements compiled less than a year after the earthquake, by all Sienese citizens and including details on the state of repair of their property. A careful sifting of this “Lira” allows to extract a “snapshot” of the state of conservation of Sienese buildings in 1468. The thematic cartography derived from the collected data was transferred into a GIS environment and the data obtained from this analysis have been used as the basis for undertaking some specific archaeological expeditious analyses of architectural complexes in the historic centre of Siena in order to verify whether the historical source data were legible in the stratigraphy of the buildings.

This paper presents the preliminary results of the analysis carried out within the PROTECT project on the 1467 Siena earthquake. The picture of the seismic sequence – as handed down by the Italian “seismological tradition” and reconstructed by two separate teams of historical seismologists (Castelli et al., 1996; Guidoboni et al., 2007) on the basis of a set of mainly narrative, contemporary or nearly contemporary sources - is challenged by the output of the consultation of the “Lira” of 1468. Was the 1467 earthquake a stronger and more damaging event than contemporary witnesses made it out to have been? Or, perhaps, did its moderate shaking interact with buildings whose vulnerability was already enhanced by some other factor? As it often happens in historical investigation, looking at a “well-known” situation from an unusual point of view makes way for new interpretative perspectives.

Acknowledgments

The project *PROTECT - Knowledge for PReventiOn. Technique for reparing seismic damage from medieval period To modern era* is being funded within the EU program “Horizon 2020 research and innovation” dell’Unione Europea by a Marie Skłodowska-Curie Individual Fellowship (grant agreement No. 101018762) at the Ecole Normale Superiéure of Paris, under the scientific responsibility of Andrea Arrighetti.

References

Castelli V., Monachesi G., Moroni A., Stucchi M. (1996). Revisione dei principali terremoti d'interesse per il territorio toscano, vol. 1: Dall’anno 1000 al 1731, GNDT/CNR, Rapporto interno, Macerata-Milano, https://emidius.mi.ingv.it/ASMI/study/CASAL996

Guidoboni E., Ferrari G., Mariotti D., Comastri A., Tarabusi G., Valensise G. (2007) CFTI4Med, Catalogue of Strong Earthquakes in Italy (461 B.C.-1997) and Mediterranean Area (760 B.C.-1500), INGV-SGA, http://storing.ingv.it/cfti4med/

Rovida A., Locati M., Camassi R., Lolli B., Gasperini P., Antonucci A. (2022). Catalogo Parametrico dei Terremoti Italiani (CPTI15), versione 4.0, Istituto Nazionale di Geofisica e Vulcanologia (INGV), https://doi.org/10.13127/CPTI/CPTI15.4.

Corresponding author: viviana.castelli@ingv.it

A reappraisal of the March 1952 Linera seismic sequence: the case study of the S. Tecla fault (Mt. Etna)

R. Azzaro[1], M.S. Barbano[1,2,3], D. Musumeci[4], G. Orefice[2]

[1] *Istituto Nazionale di Geofisica e Vulcanologia, Osservatorio Etneo, Catania, Italy*
[2] *Dipartimento di Scienze Biologiche, Geologiche e Ambientali, Università di Catania, Italy*
[3] *CRUST - Interuniversity Center for 3D Seismotectonics with Territorial Applications, Chieti, Italy*
[4] *Dipartimento di Scienze Umanistiche, Università di Catania, Italy*

Introduction

The Mt. Etna region is characterised by a very frequent seismic activity, in several cases even destructive, occurring often in form of seismic sequences during both eruptive periods and volcanic quiescence too (Bevilacqua et al., 2022). This volcano-tectonic seismicity has a significant impact particularly in the eastern flank of the volcano where earthquakes, typically featuring very shallow focal depths (h < 3 km) and magnitude rarely exceeding M_L 5, are related to the intense tectonic activity of the Timpe fault system (Azzaro et al., 2017). The short recurrence times for damaging earthquakes, capable of producing macroseismic effects up to degree IX in the European macroseismic scale (hereinafter EMS, see Grünthal, 1998), gives rise to a very high level of seismic hazard in these densely urbanised area of the volcano (Azzaro et al., 2016).

Long-term seismicity at Etna is very well known by the local macroseismic catalogue (hereinafter CMTE, see Azzaro and D'Amico, 2014) which parametrises, starting from a general revision of the historical sources documenting past earthquakes (Azzaro et al., 2000), also fore- and after-shocks and provides indication on the causative faults. This makes it possible to reconstruct the seismic history of each seismogenic structure (Azzaro et al, 2013). In this framework, the S. Tecla fault shows a high seismic potential (Fig. 1a), with a number of strong and minor events rupturing different segments of the structure (Azzaro et al, 2017). The strongest known earthquake is the 1914 event, which entirely ruptured along strike destroying the locality of Linera and surroundings; the maximum intensity was assessed to reach degree IX-X EMS and the equivalent magnitude estimated as M_L 5.2.

An event with similar features is the 19 March 1952 earthquake (Fig. 1b), that almost destroyed again Linera along the central sector of the S. Tecla fault and was preceded by a seismic sequence affecting the northern segment of the fault, south to the town of Zafferana Etnea. The mainshock is reported in the CMTE catalogue according to the intensity dataset by Patanè and Imposa (1995), the only one available, and was not revised in the phase of the catalogue compilation since this study was recent. The maximum intensity was assessed as VII-VIII EMS, corresponding to an equivalent magnitude of M_L 4.0.

In recent years we acquired some sparse information suggesting that this event may be underestimated in the study by Patanè and Imposa (1995). These authors reconstructed the macroseismic field relying on oral testimonies collected more than 30 years after the event, and by very few other sources (two editions of the local newspaper *La Sicilia* of 3 and 20 March 1952, and a technical report). For this reason, we decided to revise it starting from zero with a new historical investigation.

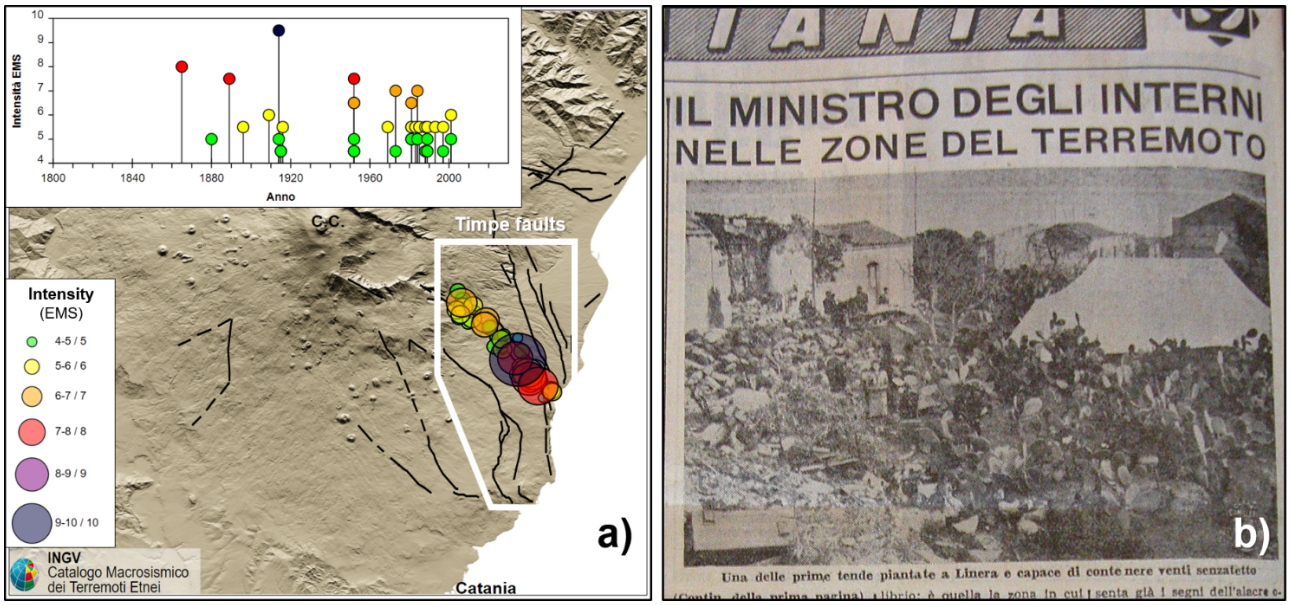

Fig. 1 – a) Main historical earthquakes associated with the S. Tecla fault and related seismic history (from https://doi.org/10.13127/cmte); b) front page of the local newspaper *Corriere di Sicilia* (24-3-1952), reporting the first tent camp set in Linera and the visit of the Minister of the Interior.

The historical sources

In order to revise the 1952 seismic sequence, we followed a strategy tested during the revision of other historical events, particularly the complex sequence of 1968 in western Sicily (see methodological approach in Azzaro et al., 2020). In brief, we performed a search of the contemporaneous sources and classified information as we were simulating, *a-posteriori*, a macroseismic survey carried out day-by-day. In this way we were able to follow in detail the evolution of the sequence and the progression of damage effects on the territory. To this end, we searched the potential sources in different repositories such as local or government archives, municipal libraries, ecclesial archives etc.

As a result, we collected a wide spectrum of sources (Fig. 2): coeval scientific papers, macroseismic questionnaires (seismic postcards or *Cartoline macrosismiche*), archive documents, local diaries and newspapers. As regards the latter, local press is a valuable source of information since news on earthquakes' effects and rescue operations are published daily. In addition, as for other earthquakes of "modern epoch", photographs and two *Istituto Luce* videos were also retrieved.

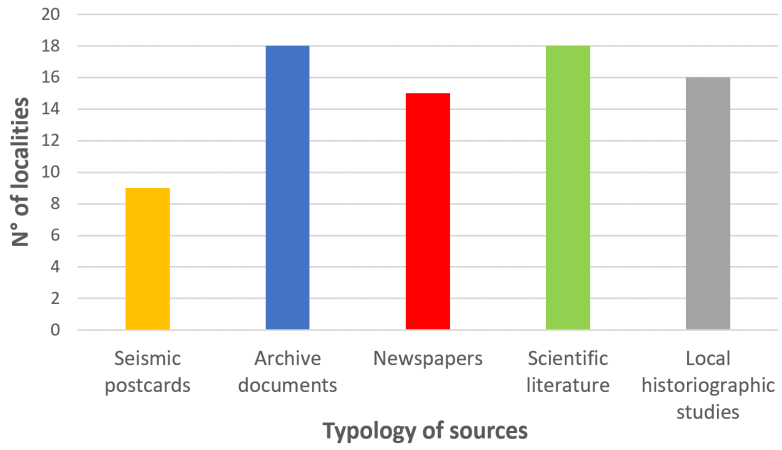

Fig. 2 – Coeval sources reporting information and data on the 1952 seismic sequence along the S. Tecla fault. The number of localities cited in the documents is also indicated.

Analysis and preliminary results

Among the retrieved documents, we found of great interest some tables saved in the State Archive of Catania, compiled by the technicians of the Civil Engineers following the mainshock of 19 March. These tables provide the precise situation of the cumulative damage produced by the seismic sequence in the affected municipalities (Acireale, S. Venerina and Zafferana), classified by ISTAT census sections; the associated number of buildings per sections is also indicated. In particular, the percentages of damaged edifices are divided into three categories: totally unusable, partially unusable, usable even if damaged. This “operative” level of damage was then associated with the grades of damage (D) expected in the EMS, as follows: totally unusable D4-5, partially unusable D3, usable D1-2.

In order to define the vulnerability classes of buildings prevailing in the damage area, we used photos and videos collected in the historical investigation, together with the descriptions on the state of buildings provided in some technical reports. Since we worked at the scale of census sections, the percentage of the different typologies of buildings in the 1950 was estimated according to Pessina et al. (2021) (Tab. 1). In this way, from the analysis of quantity and grade of damage for the different building vulnerability classes in each locality, it has been possible to assess the EMS intensity.

Tab. 1 – Statistical distribution of the EMS vulnerability classes vs buildings’ age (from Pessina et al., 2021).

Age	Vulnerability class [%]		
	A	*B*	*C1*
<1919	74	23	3
’19–‘45	52	40	8
’46–‘60	25	47	28
’61–‘71	4	31	65
’72–‘91	2	19	79

The study allowed to reconstruct in detail the March 1952 seismic sequence and to obtain the intensity data points (IDPs) for the mainshock as well as for two strong foreshocks. The first event occurred on 1 March (12.35 GTM) and had epicenter near Zafferana, where produced diffuse but minor damage (I_0 = VI-VII EMS); it was followed the day after (14.14 GTM) by a stronger shock increasing damage in the same area (I_0 = VII EMS). In the following days there were several other minor shocks of low intensity, locally felt by people; the seismic sequence culminates with the mainshock on 19 March (08.13 GMT, I_0 = VIII-IX EMS), which produced very heavy damage in Linera and other localities nearby, causing two victims and around sixty injured. Aftershocks (not damaging) followed for some days.

Fig. 3 shows the IDPs determined for the mainshock of 19 March: Linera suffered the partial destruction (I = VIII-IX EMS) whereas Bongiardo and Rocca d'Api (I = VIII) had a number of partial/ total collapses especially for the most vulnerable buildings. As usual for the shallow volcano-tectonic earthquakes at Etna (Azzaro et al., 2006), the intensity attenuation is very strong so damage effects disappear quickly at a few kilometers of distance from the causative fault (in Catania the event was only felt). Impressive coseismic faulting phenomena accompanied this earthquake as well as the two strong foreshocks of 1 and 2 March.

This macroseismic field is basically different compared to the one by Patanè and Imposa (1995), both in terms of maximum intensity – I_{max} = VIII-IX vs VII-VIII EMS, respectively – and for the number of IDPs.

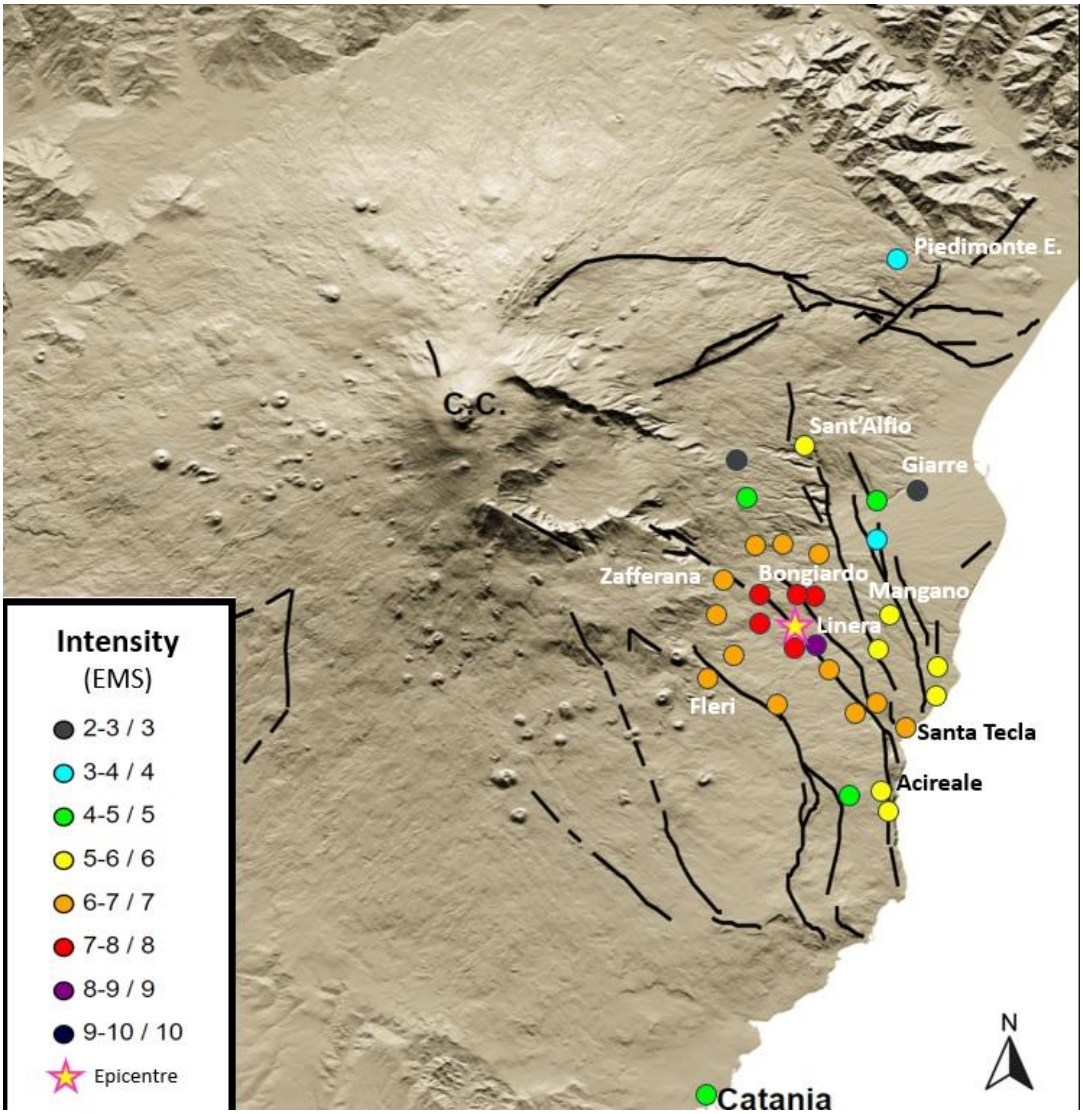

Fig. 3 – Intensity map of the 19 March 1952 earthquake (08.13 GMT) obtained by this study.

In conclusion, the March 1952 seismic sequence ruptured the entire S. Tecla fault, first the northern segment with the foreshocks' activity and then the central-southern part with the mainshock. This determined, from a macroseismic point of view, a cumulative picture of damage not solvable by the analysis of the historical sources. However, the revision produced in this study confirmed that the mainshock was previously underestimated as for the maximum intensity, this determining changes on the earthquake parameters to be reported in the CMTE catalogue: now the epicentral intensity I_0 increases up to VIII-IX EMS, and the corresponding equivalent magnitude up to M_L 4.6. Results also have implications in terms of local hazard assessment, allow a more precise reconstruction of the seismic history of this fault and therefore a more reliable evaluation of its seismic potential.

References

Azzaro R., M.S. Barbano, B. Antichi and R. Rigano; 2000: *Catalogo Macrosismico dei Terremoti Etnei dal 1832 al 1998*. Acta Vulcanologica, 12 (1-2), 3-36 (with CD-ROM).

Azzaro R., Barbano M.S., D'Amico S. and Tuvè T.; 2006: *The attenuation of seismic intensity in the Etna region and comparison with other Italian volcanic districts*. Annals of Geophysics, 49 (4/5), 1003-1020.

Azzaro R., D'Amico S., Peruzza L. and Tuvè, T.; 2013: *Probabilistic seismic hazard at Mt. Etna (Italy): the contribution of local fault activity in mid-term assessment*. Journal of Volcanology and Geothermal Research, 251, 158-169.

Azzaro R. and D'Amico S.; 2014: *Catalogo Macrosismico dei Terremoti Etnei (CMTE), 1633-2023*. Istituto Nazionale di Geofisica e Vulcanologia (INGV), https://doi.org/10.13127/cmte

Azzaro R., D'Amico S. and Tuvè T.; 2016: *Seismic hazard assessment in the volcanic region of Mt. Etna (Italy): a probabilistic approach based on macroseismic data applied to volcano-tectonic seismicity*. Bulletin of Earthquake Engineering, 17 (7), 1813-1825.

Azzaro R., Barberi G., D'Amico S., Pace B., Peruzza L. and Tuvè T.; 2017: *When probabilistic seismic hazard climbs volcanoes: the Mt Etna case, Italy. Part I: model components for sources parametrization*. Natural Hazards Earth System Science, 17, 1981-2017.

Azzaro R., Barbano M.S., Tertulliani A. and Pirrotta C.; 2020: *A reappraisal of the 1968 Valle del Belìce seismic sequence (Western Sicily): a case study of intensity assessment with cumulated damage effects*. Annals of Geophysics, 63 (1), SE105, 1 Appendix, Doi: https://doi.org/10.4401/ag-8308.

Bevilacqua A., Azzaro R., Branca S., D'Amico S., Flandoli F. and Neri A.; 2022: *Quantifying the statistical relationships between flank eruptions and major earthquakes at Mt. Etna volcano (Italy)*. Journal Geophysical Research: Solid Earth, 127, e2022JB024145, https://doi.org/10.1029/2022JB024145.

Grünthal G.; 1998: *European Macroseismic Scale 1998 (EMS-98)*. In: Cahiers du Centre Européen de Géodynamique et de Séismologie. European Seismological Commission, Subcommission on Engineering Seismology, Working Group Macroseismic Scale, 15 (Luxembourg, Conseil de l'Europe).

Patanè G. and Imposa S.; 1995: *Atlante delle isosiste dei terremoti etnei dal 1971 al 1991*. Pubbl. GNGTS-Ist. Geologia e Geofisica Università di Catania, 81 pp.

Pessina V., Meroni F., Azzaro R. and D'Amico S.; 2021: *Applying simulated seismic damage scenarios in the volcanic region of Mount Etna (Sicily): a case-study from the M_W 4.9, 2018 Earthquake*. Front. Earth Sci., Sec. Solid Earth Geophysics 9, https://doi.org/10.3389/feart.2021.629184

Corresponding author: raffaele.azzaro@ingv.it

Three-dimensional magnetotelluric inversion applied in a sector of the Irpinia Fault System (Southern Apennine)

M. Balasco[1], M. De Girolamo[2], D. Di Gennaro[3], G. Romano[3], A. Siniscalchi[3]

[1] Istituto di Metodologie per l'Analisi Ambientale, CNR – Tito Scalo, PZ
[2] Istituto di Geofisica e Vulcanologia INGV, Roma
[3] Università degli Studi di Bari

The magnetotelluric (MT) method is a powerful tool to investigate seismotectonic regions thanks to its capability to image volumetric electrical conductivity variations related to presence of interconnected fluids and partial melt (Bedrosian et al. 2014), especially if correlated with other geophysical observations (Balasco et al. 2022).

In this presentation we show a preliminary 3-D electrical resistivity model obtained sector of the Irpinia Fault System (80x60km) acquiring n. 30 broad band magnetotelluric (MT) soundings at approximately intervals of 5 km, using the inversion code ModEM3DMT (Kelbert et al. 2014).

The study area includes epicentral zones of the two greatest seismic events occurred in the last 100 years in the Southern Italy, 1930 and 1980 earthquakes. Mefite d'Ansanto, the largest source of natural CO2 gas emission measured on the Earth in a non-volcanic environment, also falls in the investigated area (Chiodini et al. 2010).

Many testing were performed building different starting models varying the dimension of horizontal and vertical grid cells, model covariance, and initial damping factors to get the best resultant model for our data. The sea-effect was also taken into account because the coastline is very near to the investigated area.

3-D inversion approach has become fundamental for MT data interpretation with respect to the 2-D inversion that frequently cannot explain important features from geologically complex regions.

Unfortunately, the routine of 3-D codes require high-end workstation or parallel machines, and long computational time. Even if our preliminary MT model of the Irpinia sector is still coarse, the results are promising also take into account a good agreement with other geophysical observations. In particular, the geostructural interpretation of the 3D MT model will also benefit from the seismic data of the ISNET, INGV network and DETECT experiment (DEnse mulTi-paramEtriC observations and 4D high resoluTion imaging, Picozzi et al. 2022).

References

Balasco, M., Cavalcante, F., Romano, G., Serlenga, V., Siniscalchi, A., Stabile, T. A., Lapenna, V. (2021). New insights into the High Agri Valley deep structure revealed by magnetotelluric imaging and seismic tomography (Southern Apennine, Italy), Tectonophysics, 808, Art. n. 228817. doi: 10.1016/j.tecto.2021.228817.

Bedrosian P.A., Feucht D.W. (2014) Structure and tectonics of the northwestern United States from Earthscope USArray magnetotelluric data. Earth Planet Sci Lett 402:275–289.

Chiodini G, Granieri D, Avino R, Caliro S, Costa A, Minopoli C, Vilardo G (2010) Nonvolcanic CO2 Earth degassing: case of Mefite d'Ansanto (southern Apennines), Italy. Geophys Res Lett 37:L11303.

Kelbert A, Meqbel N, Egbert G, Tandon K (2014) ModEM: a modular system for inversion of electromagnetic geophysical data. Computat Geosci 66:40–53.

Picozzi, M., Iaccarino, A. G., Bindi, D., Cotton, F., Festa, G., Strollo, A., Zollo, A., Stabile, T. A., Adinolfi, G. M., Martino, C., Amoroso, O., De Matteis, R., Convertito, V., Spallarossa, D., DESERT, T. (2022): The DEnse mulTi-paramEtriC observations and 4D high resoluTion imaging (DETECT) experiment, a new paradigm for near-fault observations - Abstracts, EGU General Assembly 2022 (Vienna, Austria, Online 2022).

Corresponding author: marianna.balasco@cnr.it

The harsh life of an earthquake in the region that doesn't exist

S. Baranello[1,2], R. Camassi[1], V. Castelli[1]

1 Istituto Nazionale di Geofisica e Vulcanologia, Bologna, Italy
2 Università degli studi di Bologna – Dipartimento di Fisica e Astronomia

The historical research on earthquakes often clashes with harsh reality: if the earthquake is not destructive, if it occurs during a particularly complex historical period, dominated by wars, epidemics, and other misfortunes, there is the possibility of its memory being lost. Sometimes, in addition to the scant production of testimonies about the earthquake and its impact, possible problems arise in the preservation of such testimonies. And finally, the obstacle course of the historical seismologist can find many doors closed today. Literally.
And this happens especially in the region that doesn't exist...
When any of these circumstances (or all of them) occur, research must necessarily pursue not only written testimonies but also simple clues, indirect evidence of the earthquake's occurrence, such as local traditions, the presence of a local earthquake-related cult, etc.
Baratta (1901) devotes only a few very generic lines to the Molise earthquake of May 1712. First of all, he says that an earthquake was felt in early May in Naples, and that it caused panic among the Neapolitans. To this news, Baratta adds that an earthquake was also felt in Campobasso where "some houses and churches were ruined." Finally, he mentions several shocks that were felt in Benevento between May and June 15.
Baratta's sources are respectively a summary of the *Bologna* Gazette published by De Rossi (1889) and a brief mention of Campobasso by Sarnelli (1716).
In the Postpischl (1985) catalogue, these pieces of information are summarized into an event dated generically to May 1712, located in Bojano, with an epicentral intensity of VIII MCS (Tab. 1).

	Year	Mo	Da	Ho	Mi	Lat	Lon	Int	Ref	Epic. Zone
POS85	1712	5		-	-	41 30	14 30	VIII	75	BOIANO
CPTI15	1712	05	08	-	-	41.561	14.660	6-7	AMGNDT995	Campobasso

Tab. 1 – The earthquake of May 1712 in the catalogues by Postpischl (1985) and Rovida et al. (2022)

In the early 1990s, in the frame of the “Hazard Project” - that led to the compilation of various versions of the parametric catalogue, along with the in-depth study of many hundreds of medium-high-energy earthquakes - approximately 250 earthquakes were swiftly reviewed through a simple

verification of seismological compilations. These revisions were then synthesized a few years ago in the data sheets called AMGNDT995 [Macroseismic Archive GNDT, 1995].
The AMGNDT995 data sheet dedicated to the 1712 earthquake considers various information not clearly attributable to a single event and downgrades the earthquake, dated May 8th, locating it in Campobasso with an epicentral intensity uncertain between VI and VII MCS. The study suggests that the assertion that houses and churches were 'ruined' refers to a level of moderate, non-structural damage. This interpretation has been incorporated into the CPTI catalogue in its various versions.
Recently, in the frame of a research project aimed at improving the preliminary AMGNDT995 studies, the case of the 1712 earthquake has been reopened, following the report of the presence of the cult of San Michele in Ripalimosani, connected to the averted danger during an earthquake dated May 1712 [Mascia, 2000].
Along with this reference, attributed to an oral tradition, similar references have been identified respectively in Lucito and Monteodorisio. To verify this information and deepen the research, two avenues were pursued: the first, at the local level, aimed at verifying local historiography and archival evidence. Unfortunately, the research on this front has not progressed as it was hoped. The consultation of materials stored at the State Archive of Campobasso was unsuccessful. It was impossible to examine the documents preserved at the Provincial Library "P. Albino", that has been closed to the public for several years due to technical and structural problems (it is still unclear if and when it will be reopened). The Diocesan Historical Library "V. Fusco" was also consulted, with negative results. Luckily enough, however, additional journalistic sources ([Gazzetta di] Bologna, 1712.05.24; 1712.06.14; [Avvisi di] Napoli, 1712.05.14; 1712.05.17; Il Corriere Ordinario, 1712.06.08) were found, which significantly enriched the information framework (Tab. 2).
Overall, this is certainly a very interesting and complex situation regarding a certainly important earthquake that affected a very large area of central Italy (Fig. 1).

Year	Mo	Da	Ho	Mi	Localities	Lat	Lon	Is
1712	05	08	04	30	Campobasso	41.561	14.660	7
1712	05	08	04	30	Avellino	40.914	14.793	6
1712	05	08	04	30	Benevento	41.131	14.778	6
1712	05	08	04	30	Piedimonte Matese	41.354	14.371	6
1712	05	08	04	30	Alife	41.328	14.331	6
1712	05	08	04	30	Napoli	40.849	14.25	4-5
1712	05	08	04	30	Piedimonte San Germano	41.496	13.749	3
1712	05	08	04	30	Chieti	42.352	14.168	HF
1712	05	08	04	30	Lucito	41.731	14.688	HF?
1712	05	08	04	30	Monteodorisio	42.086	14.652	HF?
1712	05	08	04	30	Ripalimosani	41.613	14.666	HF?

Tab. 2 – Intensity observed for the earthquake of 8 May 1712

This case, certainly not unique, is exemplary of a very broad research space that would require a long-term work plan today. The current Italian parametric catalogue, despite being among the most advanced in the world, contains many hundreds of earthquakes with extremely poor basic data, which should be completely reassessed. At the same time, data losses, informational gaps, and misunderstandings are always possible and would deserve work from a long-term perspective, a condition that today appears entirely illusory.

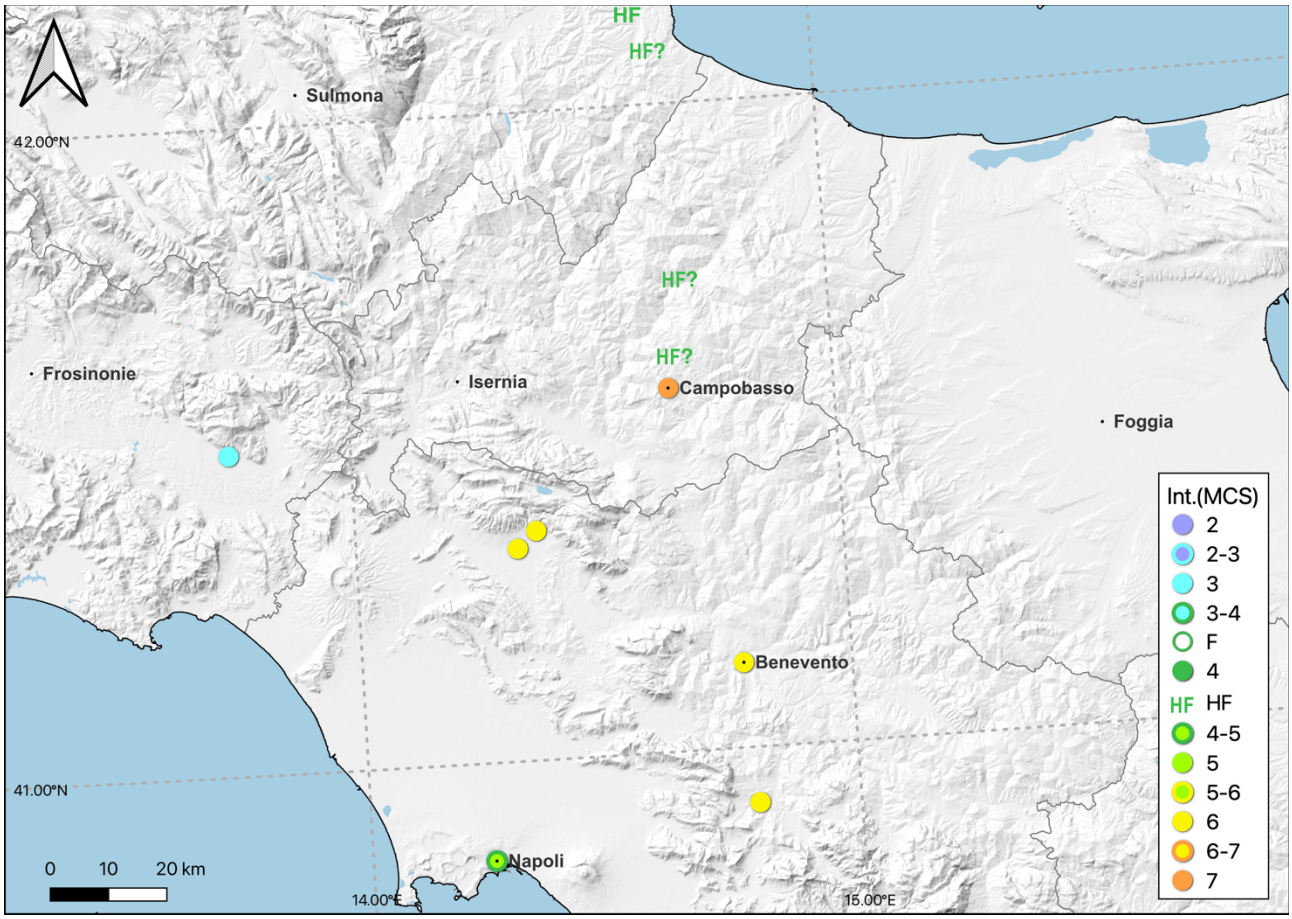

Fig. 1 – Distribution map of the distribution of the effects of the earthquake of 8 May 1712

References

[Gazzetta di] Bologna, 1712.05.24; 1712.06.14.

[Avvisi di] Napoli, 1712.05.14; 1712.05.17.

Il Corriere Ordinario, 1712.06.08.

De Rossi, M.S.; (Ed.) (1889): Documenti raccolti dal defunto conte Antonio Malvasia per la storia dei terremoti ed eruzioni vulcaniche massime d'Italia. Memorie della Pontificia Accademia dei Nuovi Lincei, 5, 169-289.

Mascia G.; (2000): Aspetti del culto popolare di San Michele Arcangelo nel Molise. In: Gioielli M., Madonne, Santi e Pastori. Culti e feste lungo i tratturi del Molise, Palladino Editore, Campobasso,

Postpischl D.; (1985): Catalogo dei terremoti italiani dall'anno 1000 al 1980. Progetto Finalizzato Geodinamica. Quaderni de La Ricerca Scientifica, n. 114, vol.2B

Rovida A., Locati M., Camassi R., Lolli B., Gasperini P., Antonucci A.; (2022): Catalogo Parametrico dei Terremoti Italiani (CPTI15), versione 4.0. Istituto Nazionale di Geofisica e Vulcanologia (INGV). https://doi.org/10.13127/CPTI/CPTI15.4

Sarnelli P.; (1716): Lettere Ecclesiastiche, VII, Appresso Antonio Bortoli, Venezia.

Corresponding author: sofia.baranello@ingv.it

New insights into the seismogenic potential of a low-strain rate region: active faulting in the Siena basin (Cava Capanni quarry, Tuscany)

Andrea Brogi[1,2], Paola Vannoli[3], Martina Zucchi[1], Pierfrancesco Burrato[3], Umberto Fracassi[3], Gianluca Valensise[3], Hsun-Ming Hu[4,5], Chuan-Chou Shen[4,5]

[1] Department of Earth and Geoenvironmental Sciences (University of Bari, Italy)
[2] CNR-IGG, Institute for Geosciences and Georesources (C.N.R., Italy)
[3] Istituto Nazionale di Geofisica e Vulcanologia (Italy)
[4] High-Precision Mass Spectrometry and Environment Change Laboratory (HISPEC), Department of Geosciences, (National Taiwan University, Taiwan, ROC)
[5] Research Center for Future Earth (National Taiwan University, Taiwan, ROC)

We investigate the active tectonics and earthquake potential of a system of active faults located along the eastern Siena Basin, a slowly deforming portion of southern Tuscany falling within the inner Northern Apennines. This region, although classified as a low hazard area (Stucchi et al., 2011; Meletti et al., 2021), has been frequently hit by low magnitude seismic sequences occurring in the uppermost 10 km of the crust, and often concentrated in clusters that appear unrelated to major known seismogenic zones, but also, by rare damaging earthquakes in the Mw range 5.0-6.0. The historical earthquake record includes events such as the 7 August 1414, Mw 5.7, Colline Metallifere; the 13 April 1558, Mw 6.0, Valdarno superiore and the 25 August 1909, Mw 5.3, Crete Senesi, earthquakes (Rovida et al., 2022). As of today, very little is known concerning the geometry of their causative faults, the maximum earthquake potential of such faults and their kinematic characteristics.

The Siena Basin is a Neogene structural depression that developed during the extensional evolution of the inner Northern Apennines along NNW- to NW-striking Plio-Quaternary normal faults, and is filled by an up to 600 m thick sequence of marine terrigenous and continental deposits (e.g. Martini et al., 2021).

Different N-, NE- and WNW-striking fault systems active in Zanclean-latest Quaternary times were described in the eastern Siena Basin (Brogi, 2004; Bambini et al., 2010; Ghinassi et al., 2021). The N-striking faults are Pliocene in age and are associated with the latest evolution of the Siena Basin (Brogi, 2011), whereas the youngest, WNW- and NE-striking faults are Neogene-latest Quaternary in age and appear to control the location of thermal springs and the resulting pattern of travertine deposition. The WNW-striking faults are the youngest structures and still control the ascent of thermal water, gas emissions, and travertine deposition in some areas (e.g., Minissale et al., 2002; Minissale, 2004; Brogi and Capezzuoli, 2009; Bambini et al., 2010). These deposits are especially

useful in active tectonics studies due to (a) the close genetic relationships between active faulting and travertine deposition, (b) the optimal recording and preservation of any brittle deformation events, (c) the quick and permanent sealing of such episodes due to the circulation of pressurized fluids (e.g., Hancock et al., 1999).

We describe in detail and for the first time an active, capable and seismogenic fault system that we identified in the saw-cut walls of Cava Capanni, an active travertine quarry near Serre di Rapolano, few km south-east of the city of Siena. As a matter of fact, the Late Pleistocene-Holocene travertine deposits of the eastern Siena Basin preserved the record of several past earthquakes, in the form of earthquake-induced soft-sediment deformation structures and co-seismic injection of overpressured hydrothermal fluids, in different quarries and archeological sites (e.g. the Campo Muri site near the Serre di Rapolano fissure ridge; Brogi et al., 2017).

To document the geometrical and kinematic characteristics of the active faults, we conducted a detailed geological and structural field survey of the quarry outcrop, collected samples for U-Th dating, and made a virtual outcrop model (VOM) of Cava Capanni using a set of photos taken using an airborne drone.

The active fault system we mapped consists of at least three main WNW-ESE-striking fault segments, rupturing up to the ground surface a sequence of travertine younger than 45 ka. The system has a total vertical displacement of 111 cm, and can be followed in the quarry over a distance of 200+ m. However, its total mapped length is ~700 m, as it continues eastwards for at least 500 m, cutting the Jurassic Tuscan succession and the overlying Zanclean deposits, before disappearing due to the heavy vegetation cover. To the west of the quarry, the fault zone disappears below the Holocene colluvial deposits of the Siena Basin. In addition to the main splays, the fault system exhibits many fractures, collectively defining a several tens of meters-wide damage zone. The fractures are near-parallel to parallel to the main fault segments and locally exhibit anastomosed traces associated with linkage zones (releasing step-overs) and relay ramps, testifying for the transtensive kinematics of the system.

The walls of the faults are covered by cm-thick, well-cemented carbonate siltstone, which often also fills the fractures of the damage zone. Such material derives from sediment liquefaction at the base of the travertine succession, as suggested by the occurrence of fossil remains, forming three generations of clastic dykes that were presumably injected in the fault zone during earthquake-induced shaking. Following this observation, we suggest that the measured displacement is the result of at least three earthquakes.

The Cava Capanni fault system is evidence of a poorly understood but regionally-extensive and potentially seismogenic tectonic mechanism. Based on total displacement and using standard empirical relationships, we estimate that it may generate earthquakes in the Mw range 6.0-6.3 recurring every ~10^4 years. Its orientation and kinematics are compatible with the activity of faults orthogonal to the main chain axis (“anti-Apennines striking”), in contrast with the current tectonic regime of the axial and outer zone of the Northern Apennines, where extension and compression are accommodated by Apennines-parallel faults.

References

Slejko D., Caporali A., Stirling M. and Barba S.; 2010: Occurrence probability of moderate to large earthquakes in Italy based on new geophysical methods. J. Seismol., 14, 27-51, DOI 10.1007/s10950-009-9175-x.

Bambini A.M., Brogi A., Cornamusini G., Costantini A., Foresi L.M. and Lazzarotto A.; 2010: Geologia dell'area di Rapolano Terme in Provincia di Siena (Appennino Settentrionale). Italian Journal of Geosciences 129, 457–95.

Brogi A.; 2004: Miocene low-angle detachments and upper crust megaboudinage in the Mt. Amiata geothermal area (Northern Apennines, Italy). Geodin. Acta 17, 375–387.

Brogi A.; 2011: Bowl-shaped basin related to low-angle detachment during continental extension: the case of the controversial Neogene Siena Basin (central Italy, Northern Apennines). Tectonophysics, 499, 54–76.

Brogi A. and Capezzuoli E.; 2009: Travertine deposition and faulting: The fault-related travertine fissure-ridge at Terme S. Giovanni, Rapolano Terme (Italy). International Journal of Earth Sciences 98 (4), 931–947, DOI 10.1007/s00531-007-0290-z.

Brogi A., Capezzuoli E., Kele S., Baykara M.O. and Shen C-C.; 2017: Key travertine tectofacies for neotectonics and palaeoseismicity reconstruction: Effects of hydrothermal overpressured fluid injection. Journal of the Geological Society 174 (4), 679–699, DOI 10.1144/jgs2016-124.

Ghinassi M., Aldinucci M., Bianchi V., Brogi A., Capezzuoli E., Yu T.-L. and Shen C.-C.; 2021: Lifecycle of an Intermontane Plio-Pleistocene Fluvial Valley of the Northern Apennines: From Marine-Driven Incision to Tectonic Segmentation and Infill. Geosciences, 11, 141, DOI 10.3390/geosciences11030141.

Hancock P. L., Chalmers R.M.L., Altunel E. and Çakir Z.; 1999: Travitonics: using travertines in active fault studies. J. Structural Geology, 21, 903-916.

Martini I., Ambrosetti E., Brogi A., Aldinuicci M., Zwaan F. and Sandrelli F.; 2021: Polyphase extensional basins: interplay between tectonics and sedimentation in the Neogene Siena-Radicofani Basin (Northern Apennines, Italy). International Journal of Earth Sciences, 110, 1,729–1,751, DOI 10.1007/s00531-021-02038-4.

Meletti C., Marzocchi W., D'Amico V., Lanzano G., Luzi L., Martinelli F., Pace B., Rovida A., Taroni M., Visini F. and the MPS19 Working Group; 2021: The new Italian Seismic Hazard Model (MPS19). Annals of Geophysics 64, 1, DOI 10.4401/ag-8579.

Minissale A.; 2004: Origin, transport, and discharge of CO2 in central Italy. Earth-Science Rev., 66, 89-141, DOI 10.1016/j.earscirev.2003.09.001.

Minissale A., Vaselli O., Tassi F., Magro G. and Grechi G.P.; 2002: Fluid mixing in carbonate aquifers near Rapolano (central Italy): chemical and isotopic constraints. Appl. Geochem., 17, 1,329–1,342. DOI 10.4401/ag-3188.

Rovida A., Locati M., Camassi R., Lolli B., Gasperini P. and Antonucci A.; 2022: Catalogo Parametrico dei Terremoti Italiani (CPTI15), versione 4.0. Istituto Nazionale di Geofisica e Vulcanologia (INGV), DOI 10.13127/CPTI/CPTI15.4.

Stucchi M., Meletti C., Montaldo V., Crowley H., Calvi G.M. and Boschi E.; 2011: Seismic hazard assessment (2003-2009) for the Italian building code. Bull. Seism. Soc. Am. 101, 1,885-1,911.

Corresponding author: andrea.brogi@uniba.it

Fluid-rock interaction in eclogite-facies meta-peridotites (Erro-Tobbio Unit, Ligurian Alps)

S. Cacciari[1], G. Pennacchioni[1], M. Scambelluri[2], E. Cannaò[3], G. Toffol[1]

[1] *Università degli Studi di Padova, Italy*
[2] *Università degli Studi di Genova, Italy*
[3] *Università degli Studi di Milano - La Statale, Italy*

The investigation of exhumed blueschist/eclogite-facies ophiolitic serpentinites can provide information on dehydration reactions, fluid activity and, possibly, seismicity occurring at subduction zones intermediate depths. Fluids are progressively released during subduction by breakdown reactions occurring within serpentinites and meta-sediments, leading to periodic fluid pressure build up that may eventually result in brittle failure (dehydration embrittlement mechanism). This mechanism is likely responsible for triggering deep Episodic Tremor and Slow Slip events (deep ETS), composed of correlated tectonic tremor (low-frequency seismic swarms) and aseismic slow-slip events (SSEs). These events are observed along the subduction interface at depth ranges of 25-60 km (*Behr and Bürgmann, 2021*), a rheologically heterogeneous domain characterized by high Vp/Vs ratio, indicating the presence of pressurized fluids. Rheological heterogeneities (i.e. mantle peridotites affected by different degrees of serpentinization) allow for strain partitioning into low-strain domains, developing crack-seal veining and radiating tremor, and high-strain domains accommodating SSEs. These events are geophysically well constrained, however, only a few exhumed geological assemblages have been interpreted as geological records for deep ETS so far.

The Erro-Tobbio meta-peridotite (Voltri Massif, Western Alps) records fluid-rock interactions and associated deformation occurred mostly within the “deep ETS” depth range (Fig.1). The uneven serpentinization experienced by the lherzolite protoliths at the ocean floor and at the forearc region, led to partitioning of the eclogite-facies deformation into high-strain domains of serpentinite mylonites (interpreted as horizons of SSEs), hosting overprinting brittle and ductile structures and low strain domains of undeformed meta-peridotites (interpreted as the asperities reaching failure and triggering tremor), mainly affected by brittle deformation. These rocks, therefore, display association of tens-of-cm-thick mylonitic horizons with a pervasive network of metamorphic olivine (Ol_2) and Ti-clinohumite (*Ti-chu*) veins and reaction bands related to breakdown of brucite (*Brc*) and antigorite (*Atg*) to *Ol* at 350-500 °C (*Hermann et al., 2000*).

At the mesoscale, the *Ol, Ti-chu* reaction bands can be grouped into two main sets: (i) Ol-fabric-1 (OlF1), steeply-dipping around 320°, oriented at high angle (~ 60°) to the mylonites, (ii) Ol-fabric-2 (OlF2) which trends parallel to the mylonitic domains and progressively increases in spatial density towards the mylonites. Locally, the structural arrangement is more complex and includes multiple sets of olivine veins.

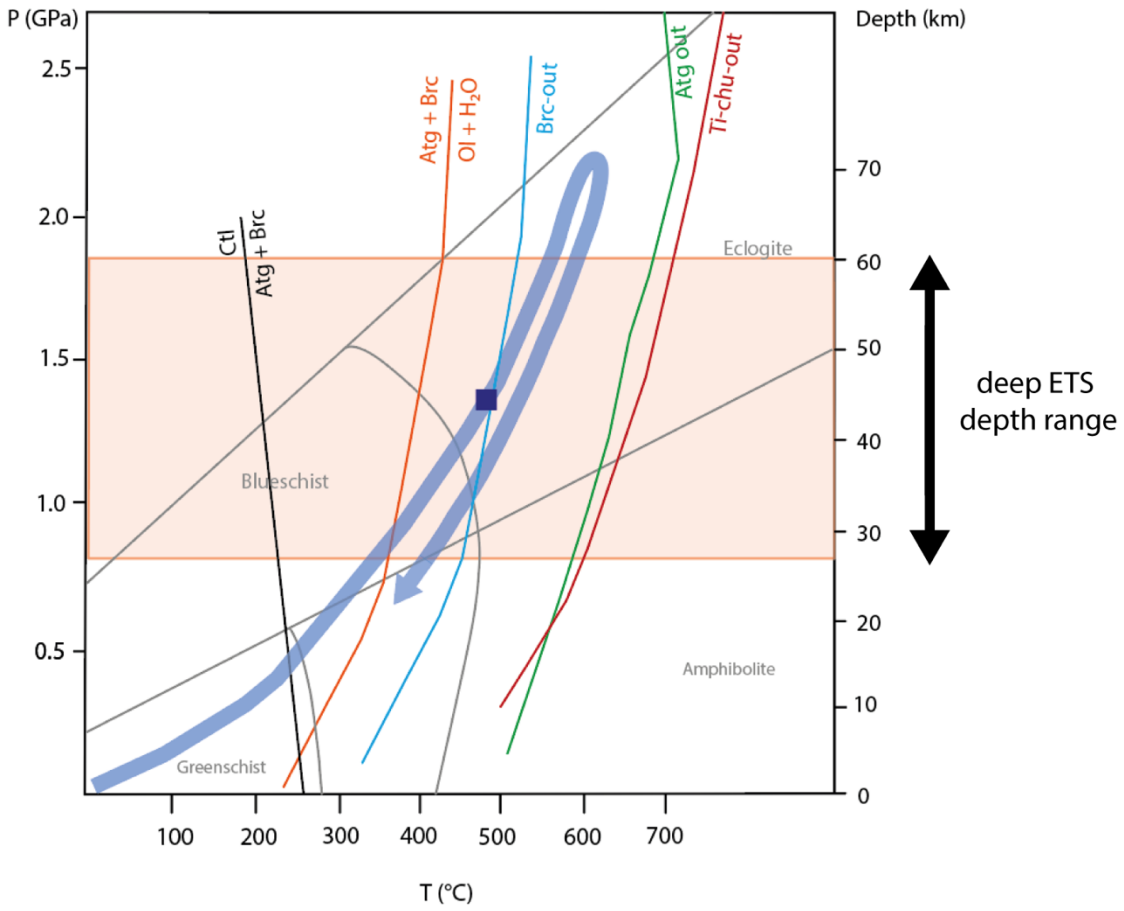

Figure 1. Erro-Tobbio Unit P-T path. The blue rectangle marks the possible conditions of formation of the metamorphic olivine veins and reaction bands

The N-S trending mylonitic horizons include: (i) type 1 mylonites, composed of a planar foliation marked by olivine reaction bands (OlF2), and (ii) type 2 mylonites, displaying a chaotic structure. The southern part of the outcrop contains, in addition, sub-horizontal, cm-thick veins of *Ol + Ti-chu + Chl*, and conjugated right stepping en-echelon arrays of *Ol + Ti-chu* veins.

At the microscale, the meta-peridotite matrix within the undeformed domains consists of coarse *Al-rich Atg* statically replacing mantle olivine (Ol_1) and clinopyroxene (*Cpx*). In these domains, OlF1 is arranged into conjugate *Ol*, *Ti-chu* reaction bands, and radial aggregates, in which *Al-free Atg* replaces Ol_2 along a network of microcracks. These reaction bands include relics of coarse *Al-rich Atg* and *Brc*, suggesting that the formation of Ol_2 localized along *Brc*-rich zones. Coronitic granoblastic olivine grows at the contact between *Brc* and *Atg*, reflecting the dehydration reaction $Atg + Br \rightarrow Ol + H_2O$; a similar mineral phase (Ol_3) was observed within previous Ol_2 sites within the reaction bands. This phase is characterized by a Mg/Si ratio typical of olivine, still, TEM analysis will be performed to unambiguously identify this phase. Ol_1 relics appear structurally linked to the fine-grained Ol_2 that constitutes the reaction-bands. EBSD maps acquired on a reaction band, reveal epitaxial growth of Ol_2 over Atg_1 and Ol_1. Ol_2 grains are iso-oriented with Atg_1 and Ol_1 in areas close to the Ol_1 relics, and the misorientation of the Ol_2 grains increases with the distance from the Ol_1 relics.

Along the mylonitic horizons, the *Al-rich Atg* forming the matrix is affected by ductile deformation, and OlF2 reaction bands mark a foliation parallel to that of *Atg*. Ol_1 relics are also involved in the deformation. Considering Ol_2, EBSD maps revealed the absence of a relationship between the metamorphic olivine (Ol_2), the surrounding *Al-rich Atg* and the Ol_1 relics.

Ol + Ti-chu + Mt + Clinochlore (C-Chl) + Di assemblage was observed within the thicker veins of the southern part of the outcrop and *Ol + Ti-chu* assemblage within the en-echelon veins. The contact between these two sets is sealed by *Mt* and fine-grained *Ol* arranged to form an oblique fabric. From the hand-specimen and the thin sections the following sequence of events was determined: (i) development of horizontal *Atg* veins, hosting µm-sized *Ol* and *Ti-chu* grains, (ii) formation of the *Ol + Ti-chu + Atg + C-chl + Di* vein subparallel to the *Atg* vein, decorated by locally sheared, orthogonal *Atg* lamellae, and of the en-echelon veins (iii) reactivation of the veins through the formation of Atg-bearing microcracks (iv) late veins of calcite and chrysotile crosscutting the previous structures.

In-situ determination of trace elements through LA-ICP-MS allowed the determination of the sources of fluids released during the subduction process and involved in the deformation. The geochemical analyses focused on the distribution of fluid-mobile elements (FMEs: *As, Sb, Ba, W, Li, B*) within the different minerals, as tracers of fluid-rock interactions occurring during dehydration reactions in subducted serpentinites. Enrichment in FMEs detected within the metamorphic olivine and in the Al-free antigorite provide evidence of infiltration of external, sedimentary-derived fluids, indicating an opening of the system during deformation at eclogite-facies conditions, consistently with the results reported by *Scambelluri et al. (2012)* and *Clarke et al. (2020).*

These observations suggest the possible occurrence of two stages of *Atg* dehydration, and an intermediate stage of hydration, occurring within the stability field of *Atg, Brc* and *Ol*. The first extensive dehydration following oceanic serpentinization led to the formation of the metamorphic olivine (Ol_2) arranged along the reaction bands and the veins. The new stage of hydration was localized along *Atg*-bearing microcracks formed especially within the reaction bands, which were, in turn, likely affected by dehydration, leading to growth of granoblastic olivine (Ol_3).

References

Behr W. M., Bürgmann R.; 2021: *What's down there? The structures, materials and environment of deep-seated slow slip and tremor.* Phil. Trans. R. Soc. A 379: 20200218. doi: 10.1098/rsta.2020.0218

Clarke E., De Hoog J. C. M., Kirstein L. A., Harvey J., Debret B.; 2020: *Metamorphic olivine record external fluid infiltration during serpentinite dehydration.* Geochem. Persp. Let. 16, 25–29. doi: 10.7185/geochemlet.2039 25

Hermann J., Müntener O., Scambelluri M.; 2000: *The importance of serpentinite mylonites for subduction and exhumation of oceanic crust.* Tectonophysics 327, 225±238. doi: 10.1016/ S0040-1951(00)00171-2

Scambelluri M., Tonarini S.; 2012: *Boron isotope evidence for shallow fluid transfer across subduction zones by serpentinized mantle.* Geology 40, 10, 907–910. doi: 10.1130/G33233.1

Corresponding author: serena.cacciari@phd.unipd.it

Stress drop scaling is still a very controversial topic: is it real or apparent?

G. Calderoni[1]

[1] *Istituto Nazionale di Geofisica e Vulcanologia (INGV, Italy)*

The stress drop scaling is still an unresolved issue and continues to be controversial in the scientific community. However, knowledge of seismic source scaling parameters plays a fundamental role in assessing the seismic forecasting in a given area and in improving ground motion predictions for seismic hazard mitigation. For this reason, this study compares the Brune stress drop of the earthquake sequence that struck the 2010-2014 Pollino area in the southern Apennines with those estimated for other earthquakes that occurred in different areas of the Apennines during the following seismic sequences: 2009 L'Aquila (Calderoni et al., 2013), 2016-2017 Amatrice (Calderoni & Abercrombie 2023), 2013-2014 Sannio-Matese (Calderoni et al., 2023) and 2019 Northern Edge of the Calabrian Arc Subduction Zone (Calderoni et al., 2020). Three different methods are used, and the results are compared with previous studies.In the first procedure (Calderoni et al. 2019) a two-step approach is used to model the attenuation and then estimate the source parameters from individual earthquake spectra. In the second procedure, an EGF approach is applied. In the third procedure, a modified EGF approach is applied using a scaling law derived by Calderoni et al., (2013) for the L'Aquila 2009 seismic sequence. To gain deeper insights into the interpretation of the result, the structural complexities and tectonic barriers that control seismic activity in the Pollino area are considered (Cirillo et al., 2022).

References

Calderoni, G., & Abercrombie, R. E. (2023). Investigating spectral estimates of stress drop for small to moderate earthquakes with heterogeneous slip distribution: Examples from the 2016– 2017 Amatrice earthquake sequence. Journal of Geophysical Research: Solid Earth, 128, e2022JB025022. https://doi.org/10.1029/2022JB025022

Calderoni, G., L. Improta, and R. Di Giovambattista (2023). Investigating the Role of Fluids in the Source Parameters of the 2013–2014 Mw 5 Matese Seismic Sequence, Southern Italy, Seismol. Res. Lett. XX, 1–21, doi: 10.1785/0220230046.

Calderoni, G., A. Gervasi, M. La Rocca, and G. Ventura (2020). Strike-Slip Earthquakes at the Northern Edge of the Calabrian Arc Subduction Zone, Seismol. Res. Lett. XX, 1–13, doi: 10.1785/0220200251.

Calderoni, G., Rovelli, A., & Singh, S. K. (2013). Stress drop and source scaling of the 2009 April L'Aquila earthquakes. Geophysical Journal International, 192(1), 260–264. https://doi.org/10.1093/gji/ggs011.

Rovelli, A., & Calderoni, G. (2014). Stress drops of the 1997–1998 Colfiorito, central Italy earthquakes: Hints for a common behaviour of normal-faults in the Apennines. Pure and Applied Geophysics, 171(10), 2731–2746. https://doi.org/10.1007/s00024-014-0856-1

Corresponding author: giovanna.calderoni@ingv.it

A “new” Aeolian event in the 20th century: the 19th June 1916 earthquake in Filicudi Island.

C.H. Caracciolo

Istituto Nazionale di Geofisica e Vulcanologia, Sezione di Bologna, Italy

This "work in progress" paper is part of the revision of 20th-century Aeolian seismicity, contributing to the update of the Historical Seismological Database.

In 1916, the second year of the war in Europe and the first in Italy, public opinion was centred on battles, military movements, and news from various fronts, including the sea and the sky. The cost of civil navigation became perilous due to bombardments from ships and attacks with torpedoes from submarines. Against this historical backdrop, Italy experienced intense geological activity, notably the Romagna seismic sequence. Additionally, the Aeolian Islands, particularly Stromboli, witnessed significant lava flows and eruptions, reaching a peak in early July. Two months later, on September 3rd, a moderate earthquake shook Salina island, causing minimal damage to only a few houses, as reported by Molin et al. (2008).

An additional event, absent from recent catalogues (CPTI15, CFTI5med), took place in the archipelago on June 19th. It was likely overshadowed by the news about the war and the eruptions of Stromboli.

However, the PFG catalogue (Postpischl, 1985) records six earthquakes felt in the archipelago between June 12th and 20th, 1916, based on information from De Fiore (1917), Martinelli (1916) and Carrozzo et al. (1975).

Record	Data	Hour	Intensity	Reference	Epicentral Area
25557	1916 06 12	21:00	V - VI	De Fiore (1917)	Basso Tirreno
25558	1916 06 12	21:15	III	Martinelli (1916); Carrozzo et al. (1975)	Basso Tirreno
25560	1916 06 14	21:15	III	De Fiore (1917)	Basso Tirreno
25568	1916 06 17	09:00	V	Carrozzo et. al. (1975)	Basso Tirreno
25575	1916 06 19	21:00	V	Martinelli (1916)	Salina
25578	1916 06 20	02:00	III	Martinelli (1916)	Salina

Tab. 1. Earthquakes in the Aeolian Archipelago during June 1916 according to the catalogue PFG (Postpischl, 1985).

Likely, De Fiore served as the primary source for the other authors, despite the apparent (and likely incorrect) year of the Martinelli publication. Nonetheless, it remains unclear from where Martinelli sourced the data.

In his brief narrative, De Fiore recounts a journey to the Aeolian Islands, just a few months after the events, with the purpose of reporting to the government about the contemporary Stromboli eruption. During this visit, he learned about the earthquakes in Filicudi and decided to investigate further.

Then he visited the island and met local inhabitants, particularly two municipal officials, who shared information about several earthquakes that took place since June. The strongest was said to have occurred on the evening of June 12th. According to De Fiore, there were other two notable earthquakes on July 17th and September 22nd.

While he expressed uncertainty about the precise intensity ("Mercalli V-VI?"), his description suggests a higher degree:

> “It was very strong (V-VI on the Mercalli scale) and caused damage, in some cases significant, to the roofs of houses (constructed, according to local customs, with layers of a kind of beaten concrete forming slightly arched vaults) that appeared in various directions; detachments in the walls, where they formed angles or joined; fractures in the keystones of arches and lintels of doors and windows. There were also rockslides, which I witnessed.” (De Fiore, 1917).

Although De Fiore didn't specify the number of houses damaged, the text implicitly indicates two degrees of damage: "in some cases significant" and less important in others. Therefore, damaged houses were not "exceptions" in the macroseismic scenario, and the uncertainty can be proposed between 6 and 7 degrees on the MCS scale.

De Fiore added that the effects of the earthquake were stronger in the town of Pecorini and that it was also strongly felt in two other islands, Alicudi and Salina, without reporting any damage.

De Fiore's report would be sufficient to update a 20th-century Aeolian earthquake catalogue. However, De Fiore and Martinelli do not align on the sequence of events. Above all, archival documents cast doubt on De Fiore's information regarding the data of the strongest event. According to administrative documentation (Interior Ministry) and seismological records (macroseismic postcards), the earthquake occurred on June 19th, exactly one week after the date indicated by De Fiore. Specifically, on June 20th, Angelo Buganza, the Prefect of Messina province, sent a telegram to the Ministry of the Interior reporting that the previous evening, at 22:00 hours,

a strong earthquake was felt in Filicudi with some damage. He added that a member of the civil engineers would be sent to verify the damage (ACS TUC).

Almost four months later, on October 9th, the Prefect sent a report to Rome with the results of two trips conducted by members of the Civil Engineers Department. According to that document, on Filicudi Island, more than 80% of the buildings were somehow damaged: 60% of the total had light damage, while 17% were heavily damaged, and 4% should be demolished (ACS. MInt.).

This scenario is sufficient for estimating an intensity level of 7 MCS, encompassing the entire island. However, considering Pecorini as the most impacted place (according to De Fiore), allows for the application of the general effects to this locality. On the contrary, for the European Macroseismic Scale (EMS98), the percentage of houses affected and the degree of damage in an urban entity is crucial for estimating the macroseismic intensity. In this case probably the most damaged houses could be situated in Pecorini and the intensity could reach 8 EMS98. Yet, it is only a hypothesis.

In the broader macroseismic scenario, it is noteworthy that the nearby islands of Alicudi and Salina felt the earthquake strongly, though it did not cause any damage. According to the macroseismic postcards (UCMG), in Salina, people fled from their houses, while in Stromboli, individuals felt the earthquake both inside and outside their homes, without experiencing fear. Additionally, the Palermitan newspaper *L'Ora* reported that all residents in Lipari felt a strong earthquake.

The following Table shows the estimated intensities (MCS) for the Aeolian archipelago considering the localities indicated by the sources (Pecorini a Mare, Lipari) or the more important of each island (Santa Marina Salina, San Vincenzo, Alicudi Porto).

Località	**Lat.**	**Lon.**	**Int. MCS**
Pecorini a Mare	38.563	14.567	7
Alicudi Porto	38.535	14.361	5
Santa Marina Salina	38.562	14.873	5
Lipari	38.467	14.955	4-5
Stromboli (San Vincenzo)	38.806	15.235	4

Table 2. Macroseismic Intensities for the Aeolian Earthquake on June 19th, 1916.

Conclusions

This "work in progress" has unveiled a new Aeolian earthquake, pinpointed on June 19th, at 21:00 GMT approximately, in the Filicudi island. At this juncture, it is possible to estimate an Imax of 7 MCS in the town of Pecorini and gauge the perception in the other islands of the Archipelago. However, further research is necessary to establish the entire sequence, considering that various sources indicate additional earthquakes produced further damage, while national and regional authorities were deliberating on how and when to provide financial assistance to the island's residents.

References

Carrozzo, M.T., Cosentino, M., Ferlito, A., Giorgetti, F., Patanè, G., Riuscetti, M.; 1975: Earthquakes Catalogue of Calabria and Sicily (1783-1973).

CFTI5med; 2018: Guidoboni E., Ferrari G., Mariotti D., Comastri A., Tarabusi G., Sgattoni G., Valensise G. - CFTI5Med, Catalogo dei Forti Terremoti in Italia (461 a.C.-1997) e nell'area Mediterranea (760 a.C.-1500). Istituto Nazionale di Geofisica e Vulcanologia (INGV).

CPTI15; 2022: Rovida A., Locati M., Camassi R., Lolli B., Gasperini P., Antonucci A. Catalogo Parametrico dei Terremoti Italiani (CPTI15), versione 4.0. Istituto Nazionale di Geofisica e Vulcanologia (INGV). https://doi.org/10.13127/CPTI/CPTI15.4

De Fiore O.; 1917: I terremoti di Filicudi (isole Eolie) nel 1916. Bollettino della Società Geografica Italiana, v. IV-V. f.2.

Martinelli G.; 1916(!): Macrosismi avvertiti in Italia durante il 1916. Bollettino della Società Sismologica Italiana, v. 20, pp.228-245.

Molin D., Bernardini F., Camassi R., Caracciolo C.H., Castelli V., Ercolani E., Postpischl L.; 2008: *Materiali per un catalogo dei terremoti italiani: revisione della sismicità minore del territorio nazionale*. Quaderni di Geofisica, 57, Istituto Nazionale di Geofisica e Vulcanologia (INGV), Roma, 75 pp.

L'Ora [Palermo], "Terremoto a Lipari", 22-23.06.1916.

Postpischl D.; 1985: (PFG) Catalogo dei terremoti italiani dall'anno 1000 al 1980. Progetto Finalizzato Geodinamica. Quaderni de «La Ricerca Scientifica», n.114, v.2B.

Archival Documents

ACS: MInt. Archivio Centrale dello Stato. Ministero degli Interni. Divisione Servizi Speciali. Servizi in dipendenza dei terremoti. Affari Generali. b. 4 - Filicudi.

ACS: TUC. Archivio Centrale dello Stato. Ministero degli Interni. Telegrammi dell'Ufficio Cifra, "Arrivi", 16.06.1916 - 28.06.1916.

UCGM: Macroseismic Postcards of the *Ufficio Centrale di Meteorologia e Geodinamica*, Macroseismic Archive, Istituto Nazionale di Geofisica e Vulcanologia, Rome, June 1916.

Corresponding author: carlos.caracciolo@ingv.it

A new 3D seismotectonic model of the Pedeapenninic Front between Parma and Bologna (Italy): new perspectives on Seismic Hazard Assessment

G. Carloni[1*] , G. Vignaroli[1], T. Gusmeo[1], L. Martelli[2], G. Viola[1]

[1] Università di Bologna-Dipartimento di Scienze Biologiche, Geologiche e Ambientali
[2] Regione Emilia-Romagna – Area geologia, suoli e sismica
** now at: Provincia di Ferrara – Settore Pianificazione Territoriale e Urbanistica*

Introduction

Understanding how surface brittle deformation patterns of seismic areas relate to their seismogenic source(s) is crucial for seismic hazard assessment protocols and should significantly rely on deterministic geological inputs. Aiming at a better picture of the subsurface along the Pedeapenninic Front of the Northern Apennines (Italy), we built a new 3D seismotectonic model (Fig. 1) of the area between Parma and Bologna incorporating new geological surface constraints with a wealth of subsurface geological and geophysical data, in order to locate, characterise and parametrize the active and seismogenic faults that define the seismotectonic framework of the region. The investigated area extends from the mountainous internal sector of the Northern Apennines, to the south, to the flat Po Plain in the north. Adria-related Tuscan Units crop out in the axial sector and are overthrust by the allochthonous Ligurian and Epiligurian Units. Pliocene and younger units crop out along the Pedeapenninic Front (Boccaletti et al., 1985; DeCelles and Giles, 1996; Boccaletti et al., 2011). Compressive tectonics is currently on-going in the external part of the chain, with the Pedeapenninic Front and the Po Plain blind thrusts striking NW-SE (Jolivet and Faccenna, 2000; Bennet et al., 2012). This thrust system is dissected by transverse normal and transpressive/transtensive faults.

This work provides the scientific community with a 3D seismotectonic model to be used for practical purposes, such as the assessment of seismic hazard in specific areas of interest as well as scientific and educational purposes. The methodological approach used to generate this 3D model, and its associated database, also serves as an inspiring workflow for characterising active and seismogenic faults in other geological settings elsewhere, where seismogenic faults are buried and not directly accessible for field studies.

3D model architecture

The database of the seismotectonic model (Fig. 1) is organized in three levels:

i) The first level consists of folders and subfolders containing 2D input data imported into the software Leapfrog Works, version 2023.2. The georeferenced data are: eight new geological cross-sections deriving from detailed fieldwork carried out along the Pedeapenninic margin; six different cross sections from the two seismotectonic maps of the Emilia-Romagna region (Boccaletti et al., 2004; Martelli et al., 2016); twenty-three geological cross sections from the CARG project (Martelli et al., 2009; Gasperi et al., 2005; Panini et al., 2002; Bettelli et al., 2002; Pizziolo et al., 2002; Cerrina Feroni et al., 2002; Plesi et al., 2002); 113 boreholes and eighteen deep seismic lines from the ViDePi project (https://www.videpi.com/videpi/videpi.asp); hypocenters from > 8000 seismic events extracted from the national catalogs (ISIDe Working Group, 2007; Rovida et al., 2020, 2022) and seventy-nine focal mechanisms from Martelli et al. (2016);

ii) The second level stores 3D geometries created directly within the model from the above input data, such as polylines and meshes;

iii) The third level contains the seismotectonic model with eight reconstructed chronostratigraphic units and fifty-seven mapped active faults.

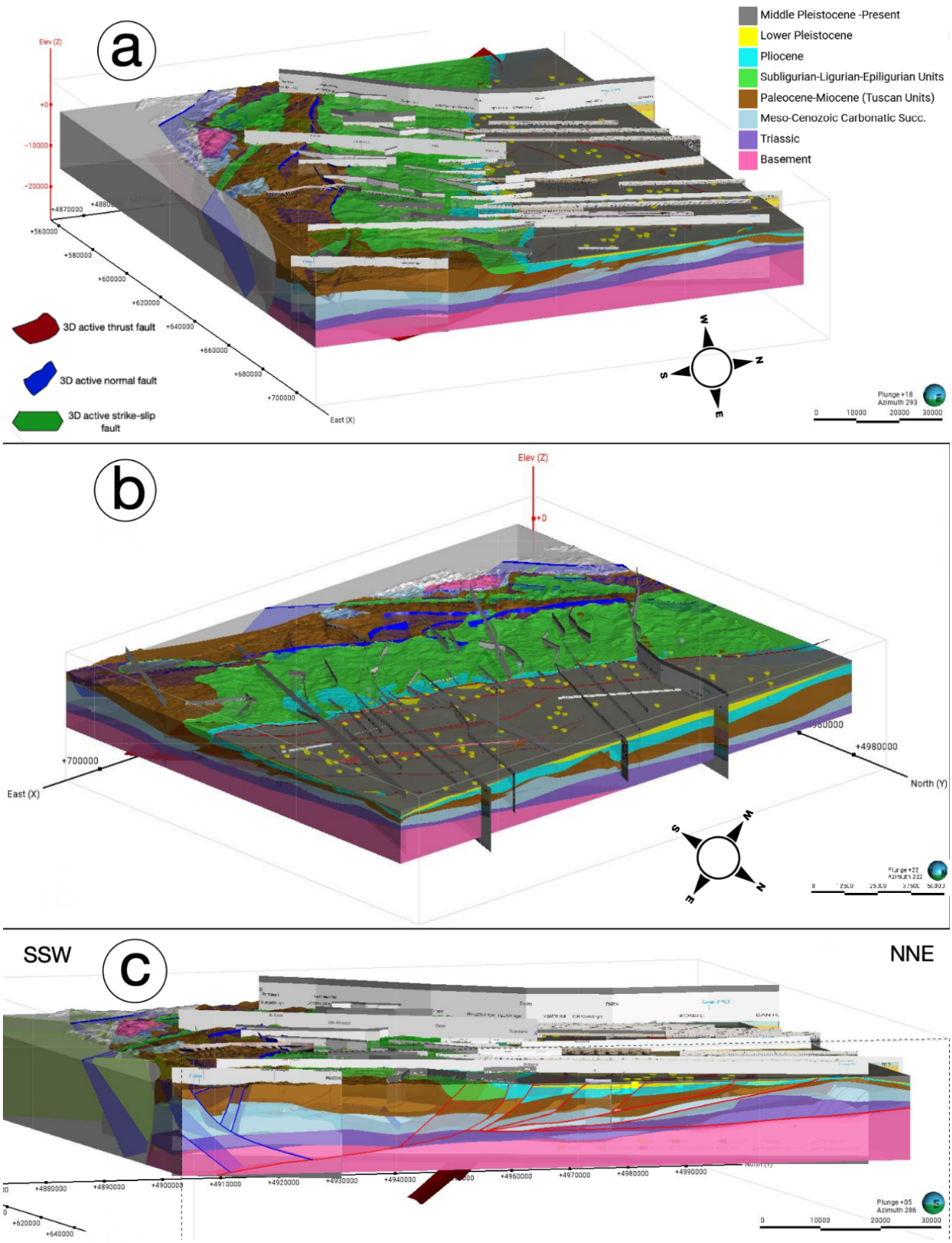

Figure 1: Views from the ESE (a) and the NE (b) of the 3D seismotectonic model, and a NNE-SSW cross-section (c).

Parametrisation of active and seismogenic faults

For each active and/or seismogenic fault populating the 3D database, an attribute table (Fig. 2b) was populated listing their main characteristics, such as:

- geometric parameters directly measured in the model (fault trace length, depth, dip direction, dip angle in Fig. 2a).

- kinematic parameters (Fig. 2a), such as kinematics (estimated based on geological considerations and existing literature), displacement along the fault strike, and slip rate. The displacement was calculated in the 3D model by creating a series of evenly spaced (every 2 km) cross-sections, with the spacing distance chosen based on the size of the analysed structures and the desired level of detail and continuity. On these sections we mapped the position of the intersection points of each chronostratigraphic boundary displaced above and below the fault. The 3D coordinates of these points in the hanging wall and footwall were then extracted and used to seamlessly calculate the three components of displacement and their resultant along the fault strike. To calculate the average slip rate, the previously calculated displacements were sorted according to the age of deposition of the displaced chronostratigraphic limits.

- historical and instrumental seismicity data and available focal mechanisms to obtain the seismological parameters of the studied faults (Fig. 2a). Specific seismic clusters that could be clearly assigned to specific seismogenic faults were analysed to extract the maximum recorded magnitude for a specific fault and to identify the time periods during which the major seismic sequences occurred. For the remaining parameters (slip per event, return period, maximum possible magnitude), we employed well known seismological formulas (e.g., Kanamori & Anderson, 1975; Leonard, 2010).

Active and Seismogenic faults' attribute table ⓐ

Geometric parameters	Applied technique
Fault trace Length (km)	Measured from the 3D model
Depth min. (km)	Measured from the 3D model
Depth max. (km)	Measured from the 3D model
Dip min. (°)	Measured from the 3D model
Dip max. (°)	Measured from the 3D model
Average dip (°)	Measured from the 3D model
Dip Direction (°)	Measured from the 3D model
Kinematic parameters	
Kinematics	From geological constraints and literature data
Average Diplacement calculated for each chronostratigraphic limit	Calculated from serial cross-sections in the 3D model
Average Slip_rate calculated for each chronostratigraphic limit	Average Displacement/age of deposition of the displaced level
Seismological parameters	
Average Slip per Event (Mw>4.5) (yr)	D=M0/μS (Kanamori & Anderson, 1975)
Average Return Period (yr)	Slip per event/ Average Slip Rate
Return Period (Mw>4.5) max.	Slip per event/Slip Rate max.
Return Period (Mw>4.5) min.	Slip per event/Slip Rate min.
Max. registered Mw	Historical/Instrumental seismicity
Max. possible Mw	M_{max}=4.24+1.67 x log(Fault trace length) (Leonard, 2010)
Significant seismic events	Historical/Instrumental seismicity
Quality code of the reconstructed 3D geometry	
References	

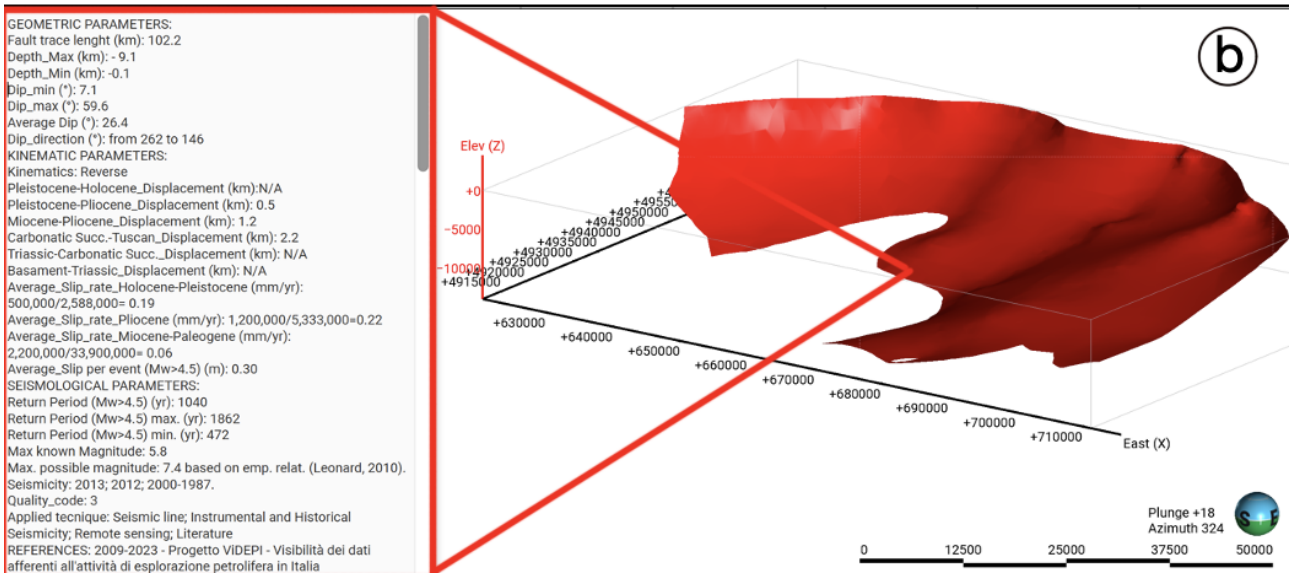

Figure 2: a) List of the main geometric, kinematic, and seismological parameters that have been included in the attribute table of each active and/or seismogenic fault, to the left, and the methodologies by which they have been calculated, to the right. b) An example of what an attribute table looks like when querying a fault within the 3D model.

Model validation

First of all, we validated the assessment procedure of the model through the visual juxtaposition of chronostratigraphic units and faults, as delineated by the input information, against their corresponding 3D modelled geometries. We compared the plan view of the 3D seismotectonic model with the original 2D seismotectonic map of the Emilia-Romagna Region (Martelli et al., 2016; Fig. 3a). Then, we generated six sections from the 3D model using the dedicated *slicer* tool in Leapfrog Work, and we compared them with the real cross-sections used as input (Fig. 3b). This comparison clearly demonstrates the high quality of the model and the correct reproduction of the main mapped geometries. The observed differences are due to the simplification of the geological system and are intentionally overlooked to highlight only the geology of interest. The main horizons and faults that could be easily correlated between different domains were interpolated and created. Therefore, all the lower hierarchical structures are missing in the model sections (to the left in Fig. 3b), because it is impossible to correlate them laterally with the data available in the literature. Another important point to consider when comparing the obtained results with the input data is that, in some model-generated sections, the attitude of the deeper stratigraphic units was inferred beyond the extent of the 2D input sections when the available data allowed for it This type of validation is therefore feasible in areas where 2D input data exist, while the remaining areas of the model are the result of our interpretation.

We further refined the validation of the 3D model by employing data from the existing literature and basic geological knowledge to verify the accuracy of the reconstructed geometries. This evaluation step aimed to determine if the modelled geometries can be considered meaningful and compared with the real geological structures. For the mapped faults, for example, we verified whether their reconstruction is geometrically and kinematically compatible with the thrust-type structures and extensional faults (Anderson, 1951; Fossen, 2016) located in the frontal and in the internal sectors, respectively, of the Northern Apennines fold-and-thrust belt. The geometric, kinematic, and seismological parameters in the attribute table of each fault were compared with the available literature data (ITHACA Working Group, 2019; Basili et al., 2008), thus confirming that the parameters calculated by this model are indeed comparable with those reported in the literature.

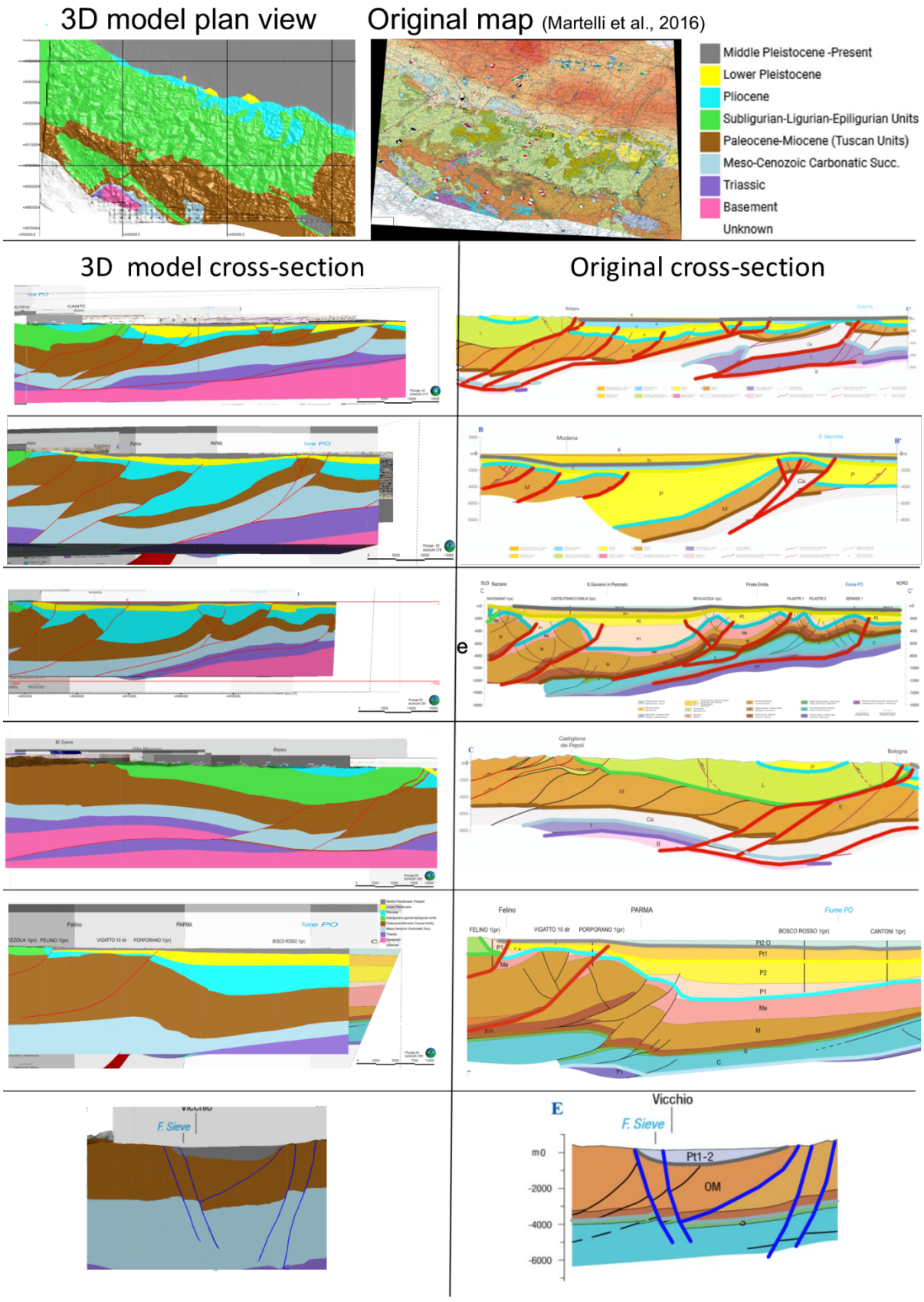

Figure 3: a) Visual comparison between the map view of the 3D seismotectonic model and the real 2D map from Martelli et al., 2016. b) Visual comparison between six slices from the 3D model (to the left) taken in correspondence of the 2D seismotectonic cross-sections (to the right) given as 2D inputs (Boccaletti et al., 2004; Martelli et al., 2016).

References

Anderson E.M., 1951. *The Dynamics of Faulting.* Transactions of the Edinburgh Geological Society, 8, 387-402.

Basili, R., Valensise, G., Vannoli, P., Burrato, P., 2008. T*he Database of Individual Seismogenic Sources (DISS), version 3: Summarizing 20 years of research on Italy's earthquake geology.* Tectonophysics, 453, 20–43.

Bennett, R.A., Serpelloni, E., Hreinsdóttir, S., Brandon, M.T., Buble, G., Basic, T., Casale, G., Cavaliere, A., Anzidei, M., Marjonovic, M., Minelli, G., Molli, G., Montanari, A., 2012. *Syn-convergent extension observed using the RETREAT GPS network, northern Apennines, Italy.* Journal of Geophysical Research: Solid Earth 117. https://doi.org/10.1029/2011JB008744

Bettelli, G., Boccaletti, M., Cibin, U., Panini, F., Poccianti, C., Rosselli, S., Sani, F., 2002. *Note illustrative della Carta Geologica d'Italia alla scala 1:50.000, Foglio 217, Neviano degli Arduini.* Servizio Geologico d'Italia-Regione Emilia-Romagna, p. 112.

Bettelli, G., Panini, F., Cibin, Pizziolo, M., 2002. *Note illustrative della Carta Geologica d'Italia alla scala 1:50.000, Foglio 236, Pavullo nel Frignano.* Servizio Geologico d'Italia-Regione Emilia-Romagna, p. 112.

Boccaletti, M., Coli, M., Eva, C., Ferrari, G., Giglia, G., Lazzarotto, A., Merlanti, F., Nicolich, R., Papani, G., Postpischl, D., 1985. *Considerations on the seismotectonics of the Northern Apennines.* Tectonophyiscs 117, 7–38.

Boccaletti M., Bonini, M., Corti, G., Gasperini, P., Martelli, L., Piccardi L., Tanini, G., Vannucci, G., 2004. *Seismotectonic map of the Emilia-Romagna Region.*

Boccaletti, M., Corti, G., Martelli, L., 2011. *Recent and active tectonics of the external zone of the Northern Apennines (Italy)*. International Journal of Earth Sciences 100, 1331–1348. https://doi.org/10.1007/s00531-010-0545-y

Cerrita Feroni, A., Ottria, G., Vescovi, P., 2002. *Note illustrative della Carta Geologica d'Italia alla scala 1:50.000, Foglio 252, Barberino di Mugello.* Servizio Geologico d'Italia-Regione Emilia-Romagna, p. 130.

DeCelles, P.G., Giles, K.A., 1996. *Foreland basin system*. Basin Research 8, 105–124.

Fossen, H. 2016. *Structural Geology* (Cambridge university press, 2016).

Gasperi, G., Bettelli, G., Panini, F., Pizziolo, M., 2005. *Note illustrative della Carta Geologica d'Italia alla scala 1:50.000, Foglio 219, Sassuolo.* Servizio Geologico d'Italia-Regione Emilia-Romagna, p. 197.

ISIDe Working Group, 2007, *Italian Seismological Instrumental and Parametric Database (ISIDe).* Istituto Nazionale di Geofisica e Vulcanologia (INGV). https://doi.org/10.13127/ISIDe .

ISPRA- Istituto Superiore per la Protezione e la Ricerca Ambientale. *Progetto CARG-Carta Geologica d'Italia alla scala 1:50.000, Regione Emilia-Romagna.* https://www.isprambiente.gov.it/Media/carg/emilia.html

ITHACA Working Group, 2019. *ITHACA (ITaly HAzard from CApable faulting), A database of active capable faults of the Italian territory. Version December 2019*. ISPRA Geological Survey of Italy. Web Portal: http://sgi.isprambiente.it/ithaca/viewer/index.html

Jolivet, L., Faccenna, C., 2000. *Mediterranean extension and the Africa-Eurasia collision*. Tectonics 19, 1095–1106. https://doi.org/10.1029/2000TC900018

Kanamori, H., Anderson, D.L., 1975. *Theoretical basis of some empirical relations in seismology*. Bulletin of the Seismological Society of America; 65 (5), 1073–1095.

Leonard, M., 2010. *Earthquake fault scaling: Self-consistent relating of rupture length, width, average displacement, and moment release*. Bull. Seismol. Soc. Am. 100 (5A), 1971–1988. https://doi.org/10.1785/0120090189

Martelli, L. et al. 2016, *Carta Sismotettonica della Regione Emilia- Romagna e aree limitrofe. Scala 1:250.000* https://ambiente.regione.emilia-romagna.it/it/geologia/pubblicazioni/cartografia-geo-tematica/carta-sismotettonica-della-regione-emilia-romagna-e-aree-limitrofe-edizione-2016

Martelli L., Benini, A., De Nardo, M.T., Severi, P., 2009. *Note illustrative della Carta Geologica d'Italia alla scala 1:50.000, Foglio 220, Casalecchio di Reno*. Servizio Geologico d'Italia-Regione Emilia-Romagna, p.124.

Panini, F., Bettelli, G., Pizziolo, M., 2002. *Note illustrative della Carta Geologica d'Italia alla scala 1:50.000, Foglio 237, Sasso Marconi*. Servizio Geologico d'Italia-Regione Emilia-Romagna, p.176.

Pizziolo, M., Segadelli, S., Vaiani, S.C., 2002. *Note illustrative della Carta Geologica d'Italia alla scala 1:50.000, Foglio 200, Reggio nell'Emilia*. Servizio Geologico d'Italia-Regione Emilia-Romagna, p.110.

Plesi, G., et al., 2002. *Note illustrative della Carta Geologica d'Italia alla scala 1:50.000, Foglio 235, Pievepelago*. Servizio Geologico d'Italia-Regione Emilia-Romagna, p.138.

Progetto ViDEPI. *Visibilità dei dati afferenti all'attività di esplorazione petrolifera in Italia. Ministero dello sviluppo economico DGRME-Società Geologica Italiana-Assomineraria* (cc) BY-Contenuti distribuiti con Licenza Creative Commons Attribuzione 3.0 Italia. https://www.videpi.com/videpi/videpi.asp

Rovida, A., Locati, M., Camassi, R., Lolli, B., Gasperini, P., 2020. *The Italian earthquake catalogue CPTI15.* Bulletin of Earthquake Engineering, 18(7), 2953-2984.

Rovida, A., Locati, M., Camassi, R., Lolli, B., Gasperini, P., Antonucci, A., 2022. Catalogo Parametrico dei Terremoti Italiani (CPTI15), versione 4.0. Istituto Nazionale di Geofisica e Vulcanologia (INGV). https://doi.org/10.13127/CPTI/CPTI15.4

Acknowledgements

We thank Dr. Alberto Martini of the Emilia-Romagna geological survey (RER-SGSS) for providing the high-resolution geological cross-sections and maps of the CARG and seismotectonic sheets. We would also like to express our special thanks to the entire Deformation, Fluids, and Tectonics (DFT) group of the Department of Biological, Geological, and Environmental Sciences in Bologna for their comments and constructive discussions during the development of this project.

Corresponding author: giacomo.carloni@provincia.fe.it

What about the predecessors of the February 2023 earthquakes in Eastern Anatolia?

V. Castelli[1], K. Sesetyan[1,2], A.A. Gomez Capera[3], C. Meletti[4], M. Stucchi[1]

[1]Istituto Nazionale di Geofisica e Vulcanologia - Sezione di Bologna, Bologna/Ancona, Italy;
[2]Bogazici University, Kandilli Observatory and Earthquake Research Institute, Dept. of Earthquake Engineering, Istanbul, Turkey;
[3]Istituto Nazionale di Geofisica e Vulcanologia - Sezione di Milano, Milano, Italy;
[4]Istituto Nazionale di Geofisica e Vulcanologia - Sezione di Pisa, Pisa, Italy.

When large earthquakes occur, it is natural enough to wonder about their likely predecessors (if any). This is why, after the earthquakes of February 2023, we began a review of the historical seismic record of Eastern Anatolia (Fig. 1).

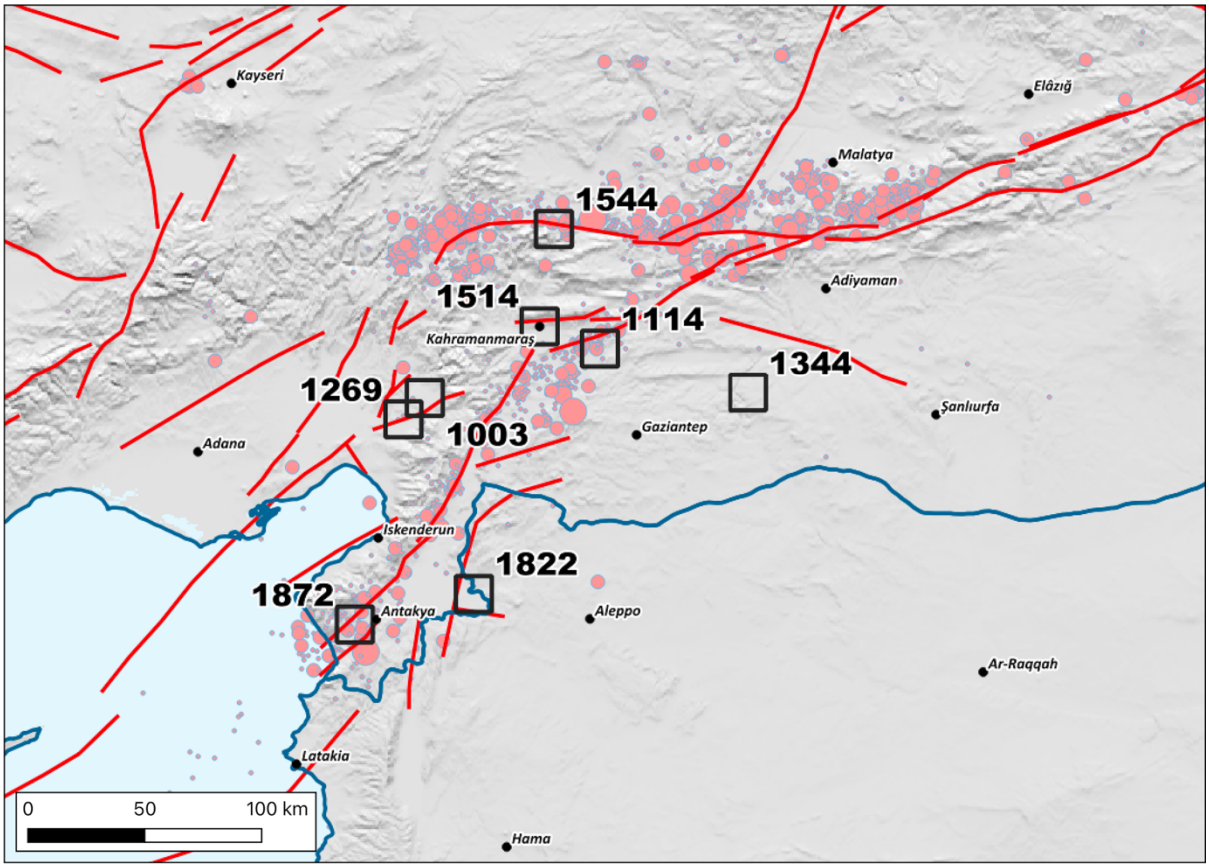

Figure 1. The 2023 seismic sequence superimposed on the major historical earthquakes of the area. Faults traces (in red) from www.seismofaults.eu/. Digital Elevation Model from www.hawaii.edu/its/webservice/

Our investigation concentrated on six major earthquakes/sequences occurred after 1000 AD (1003, 1114/1115, 1269, 1344, 1513/1514 and 1544). The earthquakes of 1822, 1872 and 1893 are better known and do not require priority investigation.

The geopolitical history of this region is very complex, with many changes of rulers along the centuries, but its long-term seismic history is rather well known. Many earthquakes are on record both before and since the date - some 2100 years ago - when the region became a Roman province. Many of its main towns (Aleppo and Antakya for instance) have a long-term history that includes eyewitness observations of many strong earthquakes.

Historical earthquake records for this area were collected and studied several times. The latest studies are Soysal et al. (1981), Ambraseys and Finkel (1995), Guidoboni & Comastri (2005), Sbeinati et al. (2005), Tan et al. (2008). N.N. Ambraseys wrote many papers on this subject and compendiated his work in Ambraseys (2009). However, time, epicentral location and size of many earthquakes are debatable and earthquake catalogues propose contrasting values for the same events.

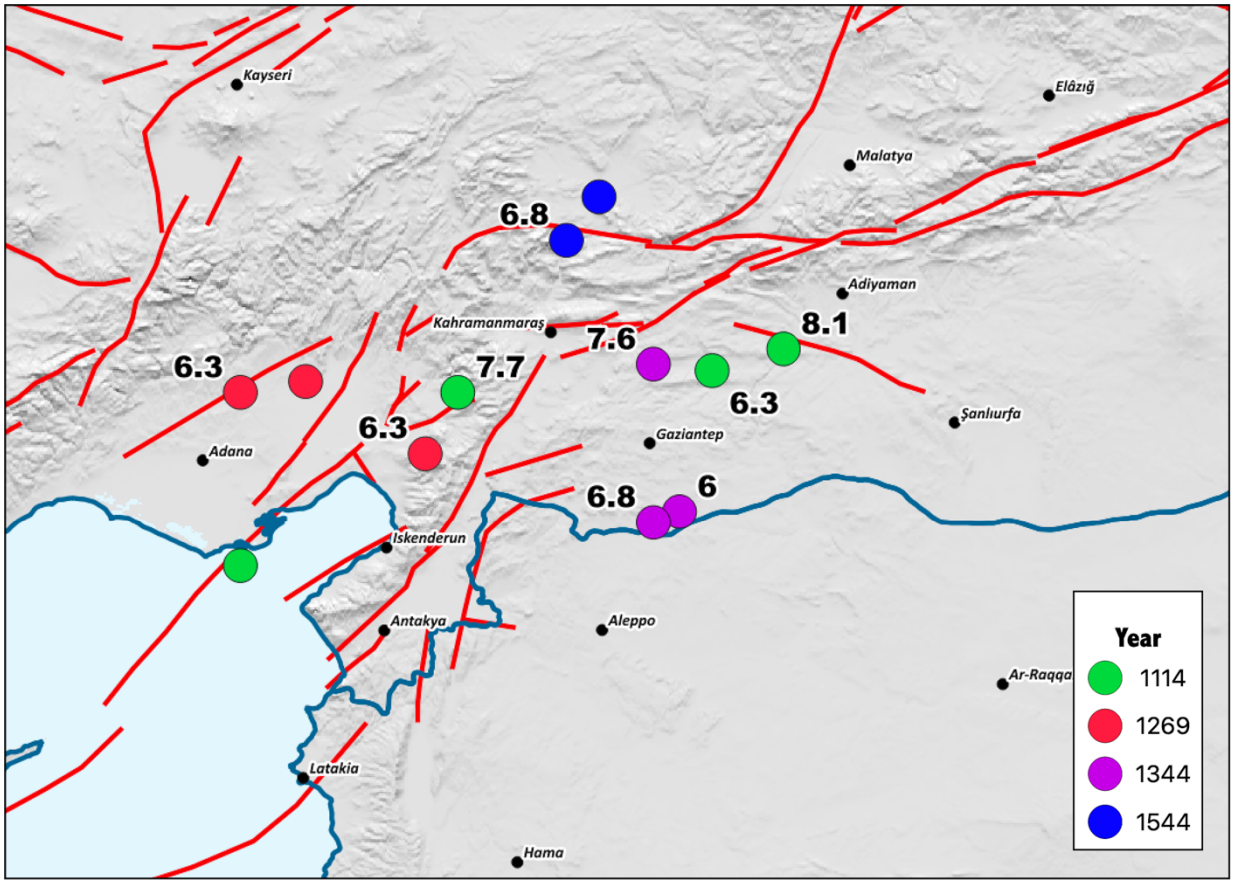

Figure 2. Epicentres and M from Sbeinati et al. (2005), CFTI5Med (2019), Tan et al. (2008). Io from Soysal et al. (1981).

Our work consisted of: a) retrieving and analyzing the main historical sources for each earthquake; b) identifying the localities mentioned in the sources and assessing macroseismic intensities from the original information; c) determining earthquake parameters (Io, Mw and - whenever possible - source azimuth) with the “Boxer” method (Gasperini et al., 1999), after properly calibrating the relevant coefficient by using recent earthquakes of the Anatolian region.

Fig. 3 presents the seismological results of this work: Mw (with uncertainty equal to 0.3) and the "boxes" obtained with the Gasperini et al. (1999) procedure and representing the surface projection of the possible earthquake sources: the epicentre is in the middle of the "box".

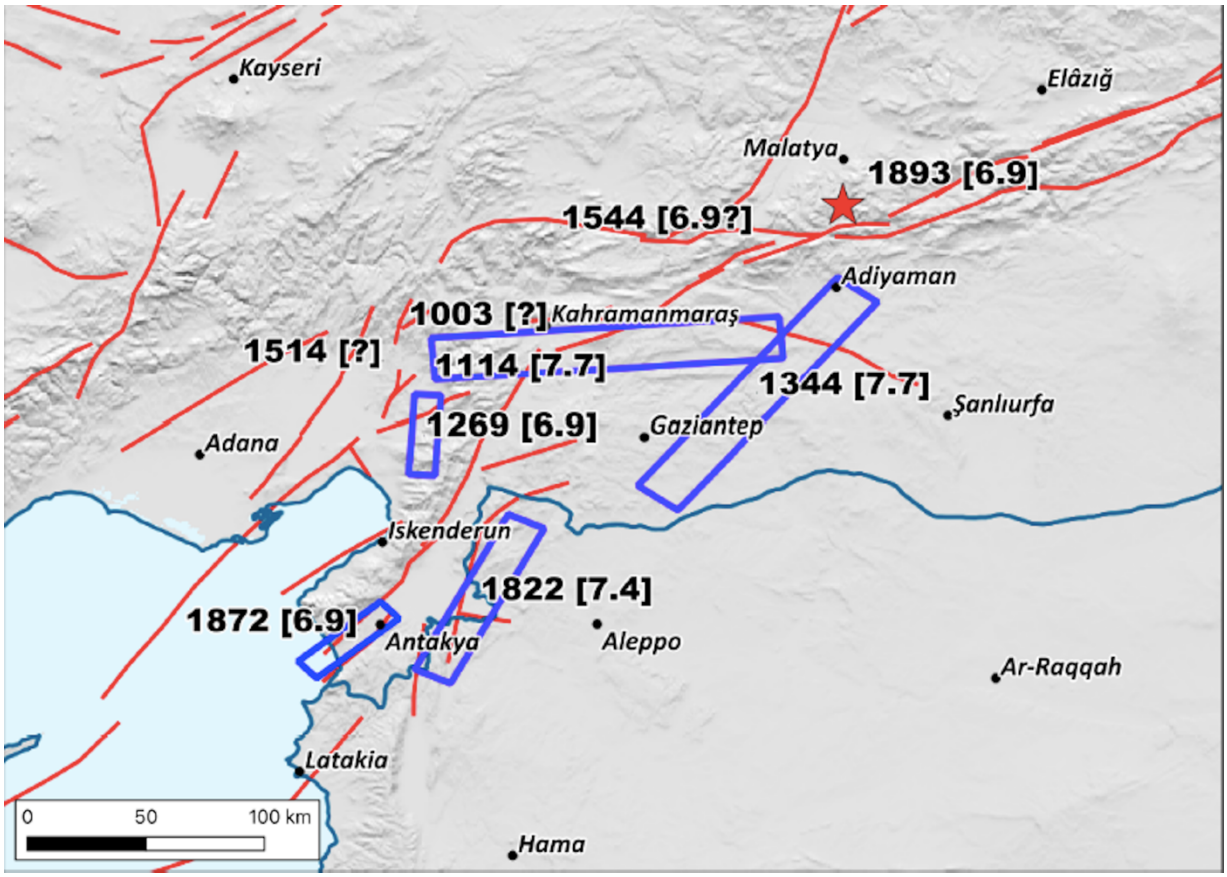

Figure 3. Seismogenic boxes or epicentral areas determined in our study.

The epicentral location and Mw calculated for the main earthquake of 1114 are close to those of the first event of 6 February, 2023. The "box" seems to match the Pazarcik segment of the EAFZ (we refer hereafter to the fault definitions used by Duman and Emre, 2013 and by Duman et al., 2018). The 1269 earthquake was less energetic than the 1114 one, and its parameters are less well constrained. Its "box" suggests the Amanos segment as the likeliest source, with the Toprakkale segment as an alternative candidate. The **1344** earthquake is rather well known and was indeed a very large one. On account of its location it was not considered in the debate on the 2023 earthquake source. However, the identification of its source would be helpful for the understanding of seismicity in this region. As for the **1513/1514** earthquake, the first interpretation by Ambraseys (1988) was -and still is – considered as the absolute truth by literature, leading to a strong connection with the Pazarcık segment. Unfortunately, this interpretation is founded on poor information, as later stated by Ambraseys (2009) and confirmed by us. Though we cannot provide reliable epicentral location and magnitude estimates, we believe that the Toprakkale or Karataş segments could represent a more appropriate option for the source. Similar considerations can be proposed for the **1544** earthquake, whose informative background is

also very weak. It could be located in the area where the recent M7.6 took place (Çardak fault), with Mw around 6.9.

References

Ambraseys N.N.; 1989: Temporary seismic quiescence: SE Turkey. Geophys. J. Int. 96, 311–331.

Ambraseys N.N.; 2009: Earthquakes in the Eastern Mediterranean and the Middle East: a multidisciplinary study of 2000 years of seismicity. Cambridge University Press, 947 p.

Ambraseys N.N., Finkel C.; 1995: The seismicity of Turkey and adjacent areas, a historical review, 1500-1800. Eren, 240 p.

Duman T.Y., Emre Ö.; 2013: The East Anatolian fault: geometry, segmentation and jog characteristics.Geol. Soc. Lond. Spec. Publ. 372, 495–529.

Duman T.Y., Çan T., Emre Ö., Kadirioğlu F.T., Başarır Baştürk N., Kılıç T., Arslan S., Özalp S., Kartal R.F., Kalafat D., Karakaya F.; 2018: Seismotectonic database of Turkey. Bulletin of Earthquake Engineering, 16, 3277-3316.

Gasperini P., Bernardini F., Valensise G., Boschi E.; 1999: Defining seismogenic sources from historical felt reports. Bull. Seismol. Soc. Am. 89, 94–110.

Gasperini P., Vannucci G., Tripone D., Boschi E.; 2010: The location and sizing of historical earthquakes using attenuation of macroseismic intensity with distance. Bull. Seismol. Soc. Am. 100, 2035–2066.

Guidoboni E., Comastri A.; 2005: Catalogue of Earthquakes and Tsunamis in the Mediterranean from the 11th to the 15th Century, Istituto Nazionale di Geofisica e Vulcanologia, 1037 p.

Guidoboni E., Ferrari G., Tarabusi G., Sgattoni G., Comastri A., Mariotti D., Ciuccarelli C., Bianchi M.G., Valensise G.; 2019: CFTI5Med, the new release of the catalogue of strong earthquakes in Italy and in the Mediterranean area, Scientific Data 6, Article number: 80 (2019). doi: https://doi.org/10.1038/s41597-019-0091-9

Sbeinati M.R., Darawcheh R., Mouty M.; 2005: The historical earthquakes of Syria: an analysis of large and moderate earthquakes from 1365 BC to 1900 AD. Ann. Geoph. 48(3), 347–435.

Soysal H., Sipahioğlu S., Kolçak D., Altınok Y.; 1981: Türkiye ve çevresinin tarihsel deprem kataloğu MÖ 2100 – MS 1900, TUBITAK Project, no. TBAG.341, Istanbul.

Tan O., Tapırdamaz M.C., Yörük A.; 2008: The Earthquake Catalogues for Turkey. Turkish J. Earth Sci.17, 405–418.

Corresponding author: viviana.castelli@ingv.it

«Se dice *etiam* per teremoti esser sommerso et ruinato tre terre» (How a large historical earthquake was born).

V. Castelli [1]

[1] *Istituto Nazionale di Geofisica e Vulcanologia-Sezione di Bologna, Bologna/Ancona, Italy*

There was once a physician (called Andrea Alpago or Maestro Andrea da Belluno, from his NE Italy hometown) who went to work for the Venetian consulate in Damascus around 1487, stayed there up to 1517, learned Arabic and was the first European ever to translate Avicenna's works from the original (Levi della Vida, 1960). Thanks to his linguistic skills Maestro Andrea became an expert advisor on the political and commercial situation of the entire East (from Egypt and Turkey to Arabia and India) and in particular on the "Signor Sophi" or "Suffi", i.e. the Shah of Persia Ismāʿīl, founder of the Safawid dynasty (1502-1524), whose alliance Venice was then seeking to obtain against the Turks. Between 1504 and 1514, Maestro Andrea sent to the Venetian government many confidential reports, that were copied by Marino Sanudo in his *Diarii* (De Bertoldi, 1888). In a report dated on 10 March 1514, Mastro Andrea, describes at length the doings of the new Turkish sovereign, Selim I "the Grim", in Anatolia (he was liquidating all his internal enemies – namely his stepbrothers and nephews - before starting a war against Egypt and Persia). The report ends, as an afterthought, with this piece of information: "Se dice *etiam* per teremoti esser sommerso e ruinato tre terre del Soltan a li confini del Turcho, videlicet Malathia et Terso et Adena".

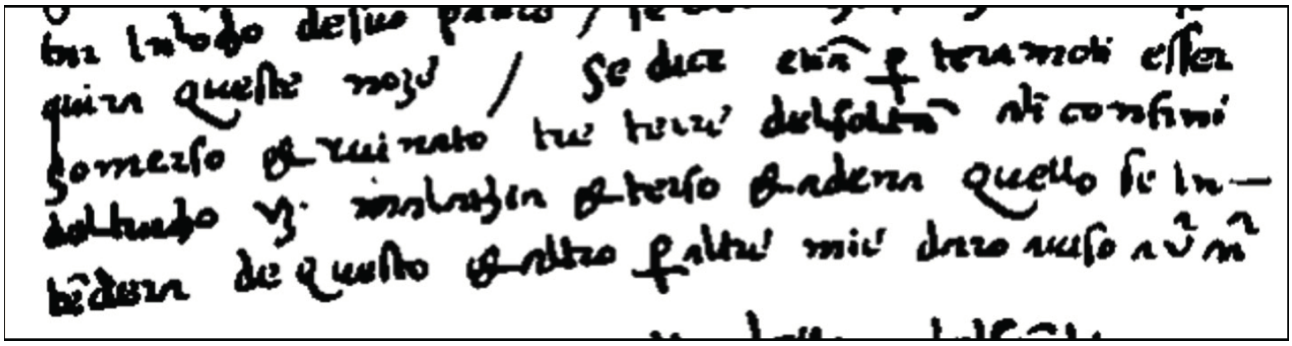

Fig. 1 – Excerpt of the report written Maestro Andrea on 10 March 1514, as transcribed in Venice by Marin Sanudo sometime in the second half of 1514 (Biblioteca Nazionale Marciana, Venice).

This is the earliest, and only contemporary testimony of an earthquake about which very little is known. It must have happened before the letter was written, but was it in late 1513 or early 1514? It heavily damaged (as shown by the verbs "submerged" and "ruined") at least three towns of SE Anatolia, but it seems curious that two of them - Tarsus and Adana - are close to each other, while

the third – Malatya – is more than 300 km away (Fig. 2). What happened in between? Could someone - either Maestro Andrea who wrote by hearsay ("se dice") or Sanudo who copied him - have made a mistake in trascribing one of these names? Could some other place-name have been wrongly transcribed as "Malatya"?

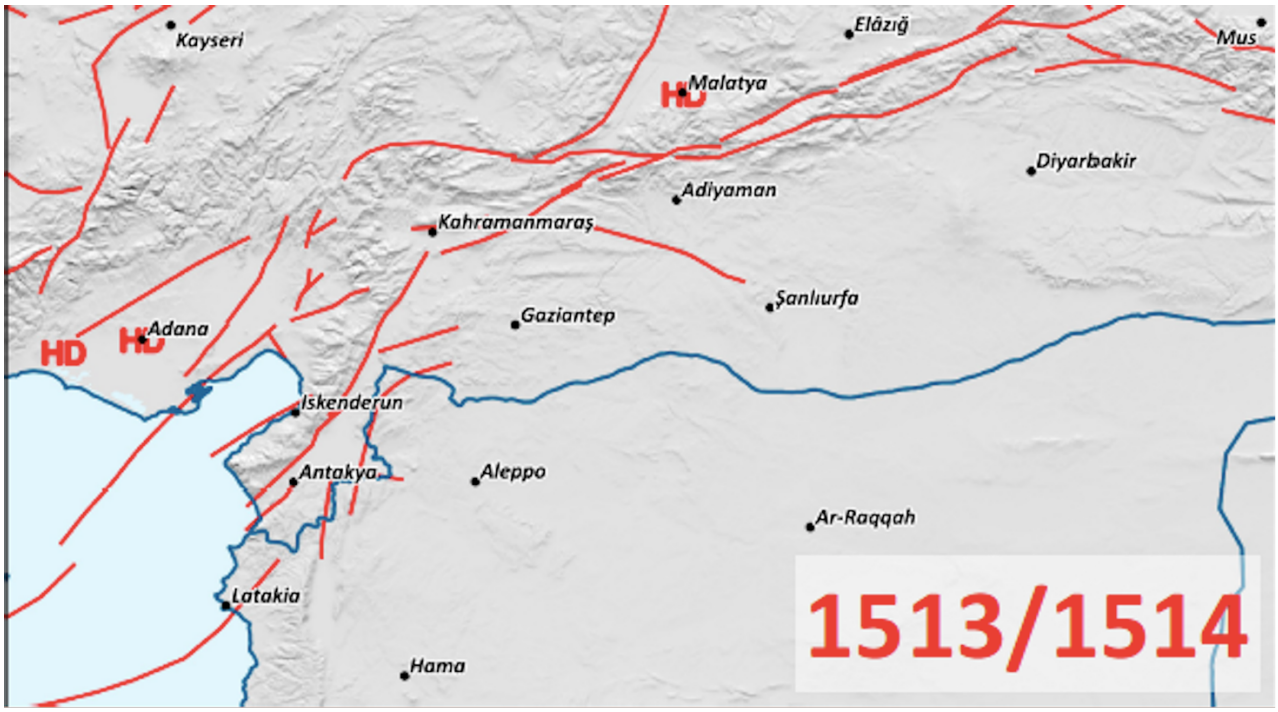

Fig. 2 – Macroseismic data points assessed for the earthquake of the year 1513/1514.

Sanudo copied the information on the earthquake, saving it for future use. It surfaced, with literary flourishes, in a Venetian chronicle of the years 1512-1514 (Barbaro, 16th c.), and after this chronicle was published (1842) in a 19th century geological treatise (Abich, 1882) that in its turn was one of the sources for Calvi (1941). Seismological studies and catalogues then followed in Calvi's wake, locating the earthquake either generically in "Cilicia" (the region to which Tarsus and Adana belong), or in Malatya, with Io 6 (Ergunay et al., 1967) or 7 (Soysal et al., 1981). Them came Ambraseys (1989), that went back to the somewhat romanced narration provided by Barbaro (16th c.), calculating Mw 7.4 and locating the epicentre not far from Maras, on the Pazarcik segment of the Eastern Anatolian Fault with I=IX (maximum intensity observed… but where?).

Subsequent seismological literature on the Eastern Anatolian Fault, both before and since the 2023 earthquake took and still takes the interpretation of the 1513 or 1514 earthquake provided by Ambraseys (1989) as absolute truth: the 1514 earthquake must have been located near Maras, with a M 7 at least and be a most likely predecessor of the February 2023 earthquake. Yet Ambraseys had changed his mind on this account, concluding that "without further details this information is insufficient to indicate the precise date and area over which this earthquake was felt" (Ambraseys, 2009). And, looking back to the original source of information on it, one must surely agree with him.

And how many such “large” earthquakes, based on information as poor as this, could be still taken for granted by overconfident geologists and seismologists, only because they happen to fit with some cherished theory?

References

Abich H.; 1882: Geologie des Armenisches Hochlandes, Wien.

Ambraseys N.N.; 1989: Temporary seismic quiescence. Geophysical Journal, 96, 311-331.

Ambraseys N.N.; 2009: Earthquakes in the Eastern Mediterranean and the Middle East: a multidisciplinary study of 2000 years of seismicity, Cambridge UK..

Barbaro D.; (16th c.): Storia Veneziana di D.B. dall’anno 1512 al 1515, Archivio Storico Italiano, vol. 77, 1842.

Calvi W.; 1941: Erdbebenkatalog der Turkei und Einiger Benaehbarter Gebiete, Yayinlanmamis, Rep. No 276, MTA Enstitüsu; Ankara.

De Bertoldi G.; 1888: Notizie e lettere di Andrea Alpago Medico in Damasco tratte dai Diarii di Marino Sanuto (Nozze Alpago-Novello-Valduga), Belluno.

Levi della Vida G.; 1960: «ALPAGO Andrea». Dizionario Biografico degli Italiani, vol. 2 (online).

Sanudo M.; 16th c.: I Diarii di M.S.(MCCCCXCVI-MDXXXIII) dall' autografo Marciano ital. cl. VII codd. CDXIX-CDLXXVII, vol. XVIII, Venezia, 1877.

Soysal H., Sipahioglu S., Kolcak D., Altinok Y.; 1981: Turkiye ve cevresinin tarihsel deprem katalogu MO” 2100 – MS 1900, TUBITAK Project, no. TBAG.341, Istanbul.

Corresponding author: viviana.castelli@ingv.it

Active Transpressive Faulting Along the High Atlas Mountains: the 8 September 2023, M_W 6.8, Morocco Earthquake

D. Cheloni[1], N. A. Famiglietti[2], R. Caputo[3], C. Tolomei[1], A. Vicari[2]

[1] Istituto Nazionale di Geofisica e Vulcanologia, Rome, Italy
[2] Istituto Nazionale di Geofisica e Vulcanologia, Sezione Irpina, Italy
[3] Department of Physics & Earth Sciences, Ferrara University, Italy

The 2023 Morocco earthquake sequence started on September 8th 2023 with a MW 6.8 event in the western sector of the High Atlas Mountains (Fig. 1), triggering significant aftershocks (including a M4.9 event). The earthquake caused extensive damage, claiming at least 2900 lives and affecting around 320,000 people. The seismicity in Morocco is attributed to the convergent motion between the African and Eurasian plates, with the Atlas region experiencing moderate seismic activity. Morocco's seismic history includes notable events like the 1994, 2014 and 2016 earthquakes in the Rif and Alboran Sea and the 1960 Agadir earthquake. The 2023 event, the strongest recorded in modern times, occurred in the High Atlas region. The seismic regime is characterized by a present-day compressional regime with active deformation along the High Atlas, accommodating about 1.7 mm/yr of WNW-ESE shortening (Serpelloni et al. 2007).

We employed Interferometric Synthetic Aperture Radar (InSAR) data from Sentinel-1 and ALOS-2 satellites to study ground displacement associated with the mainshock of the 2023 seismic sequence. The coseismic deformation field displayed a WSW-ENE elongated ellipse, suggesting a blind rupture. Two fault scenarios were investigated using geodetic modelling: an NNW-dipping fault in agreement with the focal mechanism and an SSW-dipping fault consistent with seismic data. We performed the geodetic modelling using the formulation of Okada (1985), following a standard two-steps procedure (e.g. Atzori et al., 2009; Cheloni et al., 2020). Both models effectively explained the observed data, indicating ambiguity in fault identification. Coulomb stress analysis implicated stress redistribution in aftershock occurrence.

Uncertainties in fault dip direction persisted, with seismic databases showing discrepancies in aftershock distribution. On the other hand, gravity and heat-flow data (Teixell et al., 2005), coupled with geodynamic considerations, favoured the SSW-dipping fault model. The analysis suggests that the high-angle fault model is unrealistic based on rheological arguments and regional geodynamic constraints. Integrating interferometric analyses with geological, tectonic, and seismological data could be crucial for resolving ambiguities in satellite-based models. The study therefore

underscores the complexity of fault identification and the need for a multidisciplinary approach in understanding seismic events.

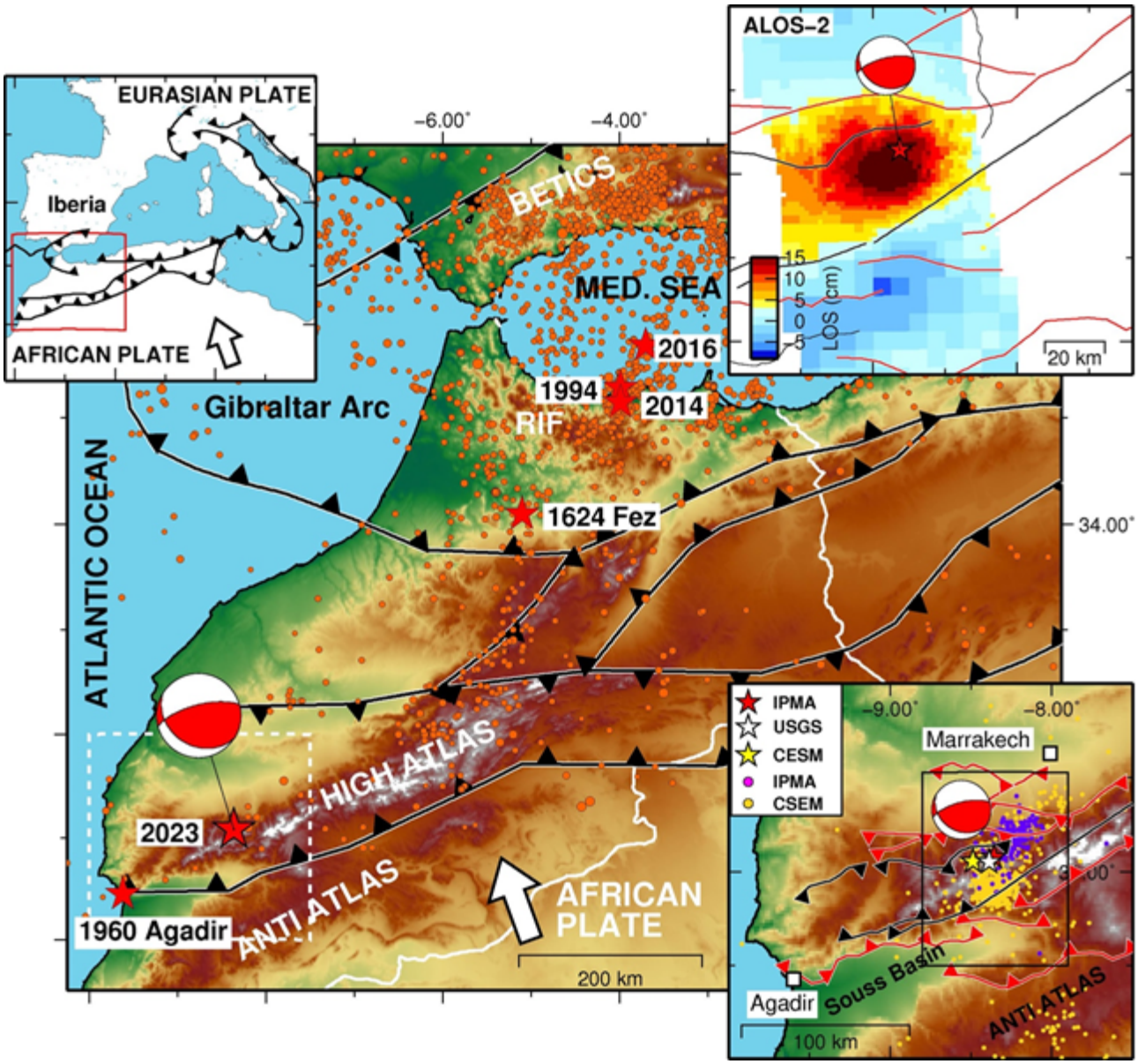

Fig. 1 – Seismotectonic settings of the study area. Solid barbed lines represent the major tectonic lineaments of the area. Orange circles are instrumental seismicity from the ESHM20 catalog (Grunthal and Whalstrom, 2012; Rovida and Antonucci, 2021); red stars are the greatest seismic events (M>6). The bottom inset is a sketch map of the active faults (Sebrier et al., 2016) and of the 2023 seismic sequence in Morocco; the box is the area of the right upper inset showing the ALOS-2 displacement map. The left upper inset is a tectonic sketch of the western Mediterranean region.

References

Atzori S., Hunstad I., Chini M., Salvi S., Tolomei C., Bignami C., Stramondo S., Trasatti E., Antonioli A., Boschi E.; 2009: Finite fault inversion of DInSAR coseismic displacement of the 2009 L'Aquila earthquake (Central Italy). Geophys. Res. Lett., 36(15), doi:10.1029/2009GL039293.

Cheloni D., Akinci A.; 2020: Source modelling and strong ground motion simulations for the 24 January 2020 M_W 6.8 Elazig earthquake, Turkey. Geophys. J. Int., 223, doi:10.1093/gji/ggaa350.

Grunthal G., Whalstrom R.; 2012: The European-Mediterranean Catalogue (EMEC) for the last millennium. Journal of Seismology, 16(3), doi:10.1007/s10950-012-9302-y.

Okada Y.; 1985: Surface deformation due to shear and tensile faults in a half-space. Bull. Seism. Soc. Am., 75(4), doi:10.1785/BSSA0750041135.

Rovida A., Antonucci A.; (2021): EPICA – European PreInstrumental Earthquake CAtalogue, version 1.1 [Data set]. Istituto Nazionale di Geofiscia e Vulcanologia (INGV), doi:10.13127/epica.1.1.

Sebrier M., Siame L., Zouine El M., Winter T., Missenard Y., Laturmy P.; 2006: Active tectonics in the Moroccan high Atlas. Geosciences, 338, doi:10.1016/j.crte.2005.12.001.

Serpelloni E., Vannucci G., Pondrelli S., Argnani A., Casula G., Anzidei M., Baldi P., Gasperini P.; 2007: Kinematics of the Western Africa-Eurasia plate boundary from focal mechanisms and GPS data. Geophys. J. Int., 169(3), doi:10.1111/j.1365-246X.2007.03367.x.

Teixell A., Avarza P., Zeyen H., Fernandez M., Arboleya M.-L.; 2005: Effects of mantle upwelling in a compressional setting: the Atlas Mountains of Morocco. Terra Nova, 17, doi:10.1111/j.1365-3121-2005.00633.x.

Corresponding author: daniele.cheloni@ingv.it

Geodetic Modelling of the 2023 M_W 7.8 and 7.6 Türkiye Earthquake Sequence

D. Cheloni[1], N. A. Famiglietti[2], A. Akinci[1], R. Caputo[3], A. Vicari[2]

[1] Istituto Nazionale di Geofisica e Vulcanologia, Rome, Italy

[2] Istituto Nazionale di Geofisica e Vulcanologia, Sezione Irpina, Italy

[3] Department of Physics & Earth Sciences, Ferrara University, Italy

On 6 February 2023 a M_W 7.8 earthquake occurred at 01:17 UTC in south-eastern Türkiye, near the Pazarcık district in Kahramanmaraş province close to the northern border of Syria (Fig. 1). It was followed 9 hours later by a M_W 7.6 earthquake approximately 90 km to the north, resulting in widespread destruction of buildings and significant loss of life. The largest aftershocks occurred on 6 February and 20 February, and their magnitudes have been assessed as M_W 6.7 and 6.4, respectively. According to the information provided by the Earthquake Department of the Disaster and Emergency Presidency (AFAD) there were over 50,000 reported fatalities and over 100,000 injuries from the devastating seismic sequence. The earthquakes were reported to be on different segments of the well-known left-lateral continental strike-slip East Anatolian Fault Zone (EAFZ), which is one of the two major active strike-slip fault systems in Türkiye, other being the right-lateral North Anatolian Fault Zone (NAFZ). In this study, we analyse the main features of the rupture process during the Kahramanmaras seismic sequence. In this respect, we use Interferometric Synthetic Aperture Radar (InSAR) and Global Navigation Satellite System (GNSS) data to investigate the ground displacement field (inset Fig. 1) and to infer, by using elastic dislocation modelling, the fault geometry and slip distribution of the causative fault segments.

We performed fault slip modelling using rectangular dislocations embedded in an elastic, homogeneous and isotropic half-space (Okada, 1985). We constrain the trace of the rupture surface of the earthquake doublet by examination of the displacements in the near-field InSAR data, extending the fault planes to a depth of 20 km running through the relocated seismicity (Lomax, 2023). The geodetic data is thus inverted for slip magnitude on each fault patch, inferring the optimal geometry iterating over dips and rake angles of the fault planes (Cheloni et al., 2019). In our inversion scheme, we consider 3 main fault segments with variable orientation for the M_W 7.8 main shock (Amanos, Pazarcık and Erkenek segments) and 2 main fault segments for the M_W 7.6 event (the Çardak-Savrun fault and an eastward segment located along the Nurhak complexity). In addition, we also include a segment located in the Narlı Fault Zone, a small splay

fault between the Pazarcık and Erkenek segments, and the Pütürge segment located between the previous 2020 Elaziğ seismic sequence and the north-eastern termination of the 2023 earthquake sequence.

The coseismic slip model on the preferred fault network geometry shows the activation of different fault segments during the 2023 Kahramanmaraş seismic sequence. In particular, the M_W 7.8 earthquake ruptured the Amanos segment to the south and the Pazarcık and Erkenek segment to the north (for a total length of about 300 km), in agreement with previous studies (e.g. Barbot et al., 2023), with little slip resolved along the Narlı segment where the mainshock nucleated (Melgar et al., 2023). The maximum slip is observed along the Pazarcık segment (peak slip of about 10 m). In contrast, the geodetic modelling of the M_W 7.6 earthquake, nucleated in the middle of the E-W trending Çardak-Savrun fault and propagated westward to the Savrun fault and eastward along the Nurhak complexity, indicated a more localized rupture primarily within the Çardak-Savrun segment (for a total length of about 150 km), with up to 15 m of slip. Finally, at the southern termination of the mainshock rupture, our modelling revealed that the 20 February M_W 6.4 aftershock activated the Antakya fault. Including the 2020 Elaziğ and 1971 Bingöl sequences, most of the EAFZ has been recently reactivated; similarly considering the well-known XX century earthquakes succession that reactivated the NAFZ (Stein et al., 1997), within the broader regional scale fault system associated to the lithospheric Arabia indenter, the N-S Dead Sea Trasform fault system could possibly be the focus of future ruptures.

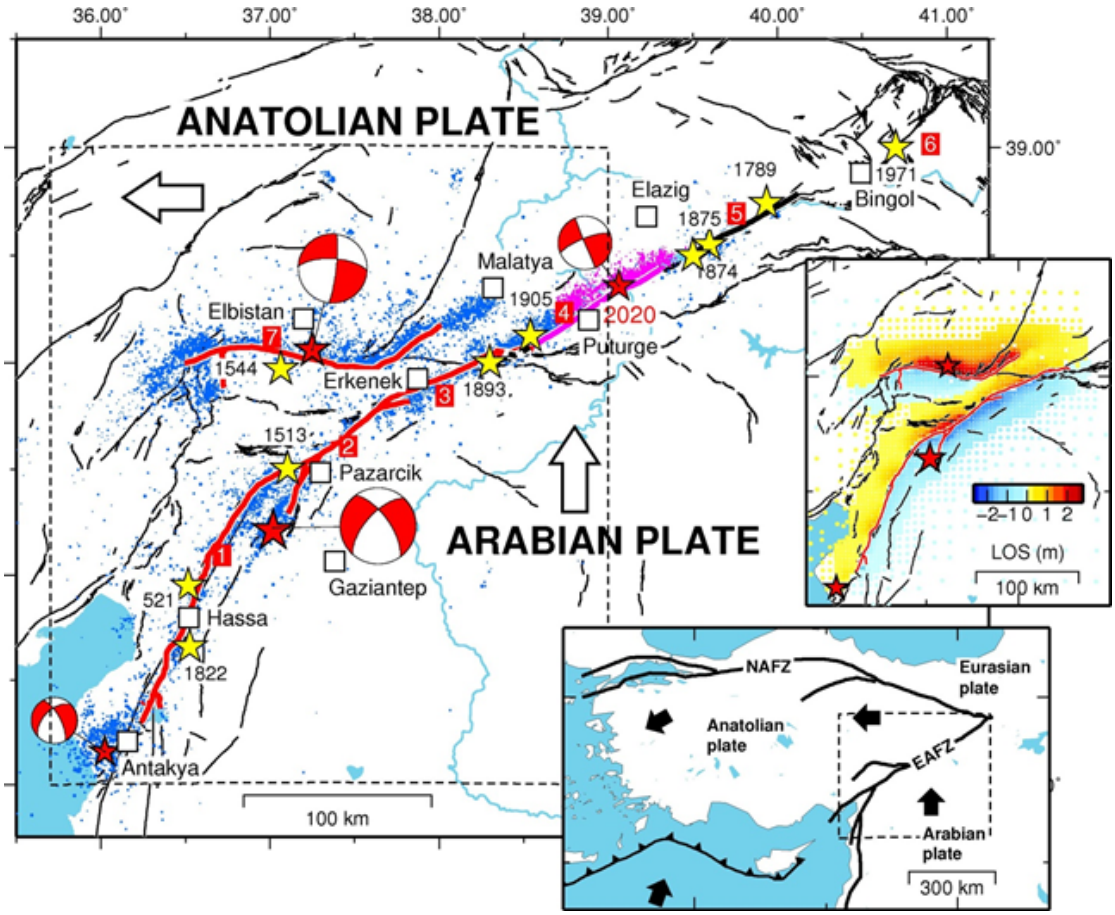

Fig. 1 – Seismotectonic settings of the study area. The solid lines are the main fault segments of the EAFZ (after Duman and Emre, 2013): (1) Amanos, (2) Pazarcık, (3) Erkenek, (4) Pütürge, (5) Palu, (6) Bingöl and (7) Sürgü-Çardak -Savrun segments, respectively. Seismicity: the blue dots are relocated aftershocks of the 2023 sequence (Lomax, 2023); red stars are the location of the main events and their moment tensor solution (KOERI); yellow stars represent the major historical events (Ambraseys 1989). The bottom inset shows a sketch of the main fault systems in and around Turkey, and the dashed box is the area of the main figure. The upper inset shows an example of InSAR data: the unwrapped interferogram showing the cumulative coseismic displacement field from the ALOS-2 ascending track.

References

Ambraseys N.N.; 1989: Temporary seismic quiescence: SE Turkey. Geophys. J. Int., 96(2), doi:10.1111/j.1365-246X.1989.tb04453.x.

Barbot S., Luo H., Want T., Hamiel Y., Piatibratova O., Javed M.T., Braitenberg C., Gurbuz G.; 2023: Slip distribution of the February 6, 2023 Mw 7.8 and Mw 7.6, Kahramanmaras Turkey earthquake sequence in the East Anatolian Fault Zone. Seismica, 2(3), doi:10.26443/seismica.v.2i3.502.

Cheloni D., Falcucci E., Gori S.; 2019: Half-Graben Rupture Geometry of the 30 October 2016 Mw 6.6 Mt. Vettore-Mt. Bove Earthquake. J. Geophys. Res., 124, doi:10.1029/2018JB015851.

Duman T.Y., Emre O.; 2013: The East Anatolian Fault: geometry, segmentation and jog characteristics. Geol. Soc. Lond. Spec. Publ., 372, doi:10.1144/SP372.14.

Okada Y.; 1985: Surface deformation due to shear and tensile faults in a half-space. Bull. Seism. Soc. Am., 75(4), doi:10.1785/BSSA0750041135.

Lomax A.; 2023: Precise, NLL.SSST-coherence hypocenter catalog for the 2023 Mw 7.8 and Mw 7.6 Turkey earthquake sequence, March 2023. https://zenodo.org/record/7699882#.ZAjBfuzMI-Q, doi:10.5281/zenodo.7699882.

Melgar, D., Taymaz T., Ganas A., Crowell B., Ocalan T., Kahraman M., Tsitorni V., Yolsal-Cevikbil S., Valkaniotis S., Irmark T.S., Eken T., Erman C., Ozkan B., Dogan A.H., Altuntas C.; 2023: Sub- and super-shear ruptures during the 2023 Mw 7.8 and Mw 7.6 earthquake doublet in SE Turkiye. Seismica 2(3), doi:10.26443/seismica.v.2i3.387.

Stein, R.S., Barka A.A., Dieterich J.H.; 1997: Progressive failure on the North Anatolian fault since 1939 by earthquake stress triggering. Geophys. J. Int., 128, doi:10.1111/j.1365-246X.1997.tb05321.x.

Corresponding author: daniele.cheloni@ingv.it

Seismic cycle in bituminous dolostones (Central Apennines, Italy)

M. Chinello[1], E. Bersan, M. Fondriest[1], T. Tesei[1], G. Di Toro[1,2]

[1]Dipartimento di Geoscienze, Università degli studi di Padova, Padua, Italy

[2]Istituto Nazionale di Geofisica e Vulcanologia (INGV), Rome, Italy

Central Apennines in Italy is one of the most seismically active areas in the Mediterranean (e.g., L'Aquila 2009, Mw 6.3 earthquake), with mainshocks and aftershocks propagating along extensional faults cutting km-thick sequences of carbonates. As a consequence, fault rock assemblages may record the seismic cycle under a wide range of loading conditions, temperatures, and fluid-rock interactions that activates several mechanical and chemical processes (i.e., fracturing, crystal-plastic deformation, dissolution and precipitation).

We document the interplay between these deformation mechanisms in normal faults cutting through bituminous dolostones in the Central Apennines. We sampled faults with increasing displacement (from 1-2 mm to a few meters) and with ultra-polished slip surfaces ("mirror-like surface").

Microstructural analysis of the slip zones show evidence of cataclasis, pressure solution and smearing of bitumen. Furthermore, the fault surfaces with higher displacement also record multiple slip events with ingression of carbonate-rich fluids and fragments of older slip zones sealed by calcite precipitation. Sometimes, these fragments derive from bitumen-rich slip zones with evidence of viscous flow. We propose that these microstructures preserve the evidence of multiple cycles of: high strain rate coseismic embrittlement (i.e., fragments of previous slip zones associated to fluid ingression), long-term aseismic or post-seismic creep (i.e., bitumen viscous flow and pressure solution) and fault locking/sealing (i.e., calcite precipitation). Since mirror-like surfaces can form both during seismic slip (Fondriest et al., 2013; Siman-Tov et al., 2015; Ohl et al., 2020; Pozzi et al., 2018) and aseismic creep (Tesei et al., 2017; Verbene et al., 2013), this study presents a natural case of different processes acting in the same slip zones throughout the seismic cycle.

References

Fondriest, M. et al.; 2013: Mirror-like faults and power dissipation during earthquakes. Geology 41, 1175–1178.

Ohl, M. et al.; 2020: Mechanisms of fault mirror formation and fault healing in carbonate rocks. Earth Planet. Sci. Lett. 530, 115886.

Pozzi, G., et al; 2018: A new interpretation for the nature and significance of mirror-like surfaces in experimental carbonate-hosted seismic faults. Geology 46, 583–586.

Siman-Tov, S., et al.; 2015: Fault mirrors along carbonate faults: Formation and destruction during shear experiments. Earth Planet. Sci. Lett. 430, 367–376.

Tesei, T. et al.; 2017: Friction and scale-dependent deformation processes of large experimental carbonate faults. J. Struct. Geol. 100, 12–23.

Verberne, B. A. et al.; 2013: Nanocrystalline slip zones in calcite fault gouge show intense crystallographic preferred orientation: Crystal plasticity at subseismic slip rates at 18-150 °C. Geology 41, 863–866.

Corresponding author: miriana.chinello@phd.unipd.it

Diffusivity analysis of clustered seismicity in Central-Southern Apennines

G.M. Cipressi[1], A. Vuan[4,5], M.A. Romano[4], G. Lavecchia[2,3], R. de Nardis[2,3]

[1]Department of Engineering and Geology, University "G. d' Annunzio" of Chieti-Pescara, Italy
[2]DiSPuTer - University of Chieti-Pescara 'G. d'Annunzio', Italy
[3]CRUST- Interuniversity Center for 3D Seismotectonics with Territorial Applications, Italy
[4]National Institute of Oceanography and Applied Geophysics (OGS), Italy
[5] National Institute of Geophysics and Volcanology (INGV), Italy

Seismic swarms are defined as a set of clustered earthquakes with high spatio-temporal variability and with the absence of a main shock. They can originate in different tectonic contexts related to the migration of deep fluids that can alter the stress field (Roland et al., 2009). In particular, the diffusivity parameter, defined by Shapiro et al. (1997) and linked to the migration of the hypocenters over time, allows us to associate the swarms' temporal duration with the rocks' permeability characteristics. Swarms characterized by long durations (years) and low diffusivity values (10^{-3}-10^{-2} m^2/sec) are associated with low permeability fault systems. On the contrary, shorter durations (days) and high diffusivity values (0.5-1 m^2/sec or greater) indicate the presence of highly permeable systems in which seismicity is induced by the rise of fluids at high pressures (Amezawa et al., 2021). We focus on the clustered seismicity in the central-southern Apennines, which extends from the south of L'Aquila to Benevento, to analyze the spatio-temporal characteristics of the swarms and the relationship between their temporal duration and diffusivity.

Compared to the rest of the chain, this sector is characterized by (1) low seismicity rates, which do not allow us to follow the evolution of seismicity and the mechanisms underlying it, and (2) a high seismic risk, as demonstrated by the strongest and most destructive sequences recorded within the historical catalogs which magnitude M ~ 7.

We analyzed the seismicity reported in the catalog of absolute locations CLASS (Latorre et al., 2022), which describes Italian seismic activity over the past 37 years (1981-2018). Additionally, we augmented the catalog within a 7-year time window (2012-2018) using a template matching technique (Vuan et al., 2018). This choice was made based on the optimal distribution and operation of the seismic network. The initial catalog is improved, lowering the completeness magnitude by more than one degree (+ 20,000 events with -1.5<M<5.0). This approach allowed the analysis and comparison of clustered seismicity in two catalogs with different time extensions and resolutions.

Clustered seismicity is defined relative to the background using a nearest-neighbour technique (Zaliapin & Ben-Zion, 2020). Due to the great spatio-temporal variability of the seismic phenomenon, no univocal methods in the literature can establish the spatial dimension and duration of the single cluster. The low seismicity rates of this area require a very detailed analysis

on a small space-time scale and different methodological approaches. For the spatial definition, we used the Kernel Density calculation to determine an event's density probability in each radius. The time duration is defined using the approach described by Roland et al. 2009 based on the evaluation of the percentage of seismicity rate.

We identified 53 polyphasic seismic clusters in the complete catalog (37-year time window), and 30 in the improved catalog (7-year time window). The clusters were subsequently divided into swarms and sequences. The diffusivity was calculated for each cluster using the Shapiro et al. (1997) relationship.

Most of the seismicity is expressed as swarm-type and characterized by high diffusivity values (≥ 1m^2/sec) with short temporal durations (days-months). This result confirms that the clustered seismicity is linked to highly permeable fault zones and the natural injection of fluids under pressure. The swarms present in this sector of the Apennine chain can, therefore, be linked to the deep migration of CO_2-rich fluids (Chiodini et al., 2004), which exploit pre-existing fault zones as a preferential path.

References

Amezawa Y., Taeta T., Kosuga M. (2021) Migration diffusivity as a controlling factor in the duration of earthquake swarms; https://doi.org/10.1186/s40623-021-01480-7

Chiodini, G., C. Cardellini, A. Amato, E. Boschi, S. Caliro, F. Frondini, and G. Ventura (2004). Carbon dioxide Earth degassing and seismogenesis in central and southern Italy, Geophys. Res. Lett., 31, L07615. doi: 10.1029/2004GL019480

Latorre D., Di Stefano R., Castello B., Michele M., Chiaraluce L. (2022) Catalogo delle Localizzazioni ASSolute (CLASS): locations (Version 1). Istituto Nazionale di Geofisica e Vulcanologia (INGV). https://doi.org/10.13127/class.1.0

Roland E., McGuire J.J. (2009) Earthquake swarms on transform faults https://doi.org/10.1111/j.1365-246X.2009.04214.x

Shapiro A.S., Huenges E., Borm G. (1997) Estimating the crust permeability from fluid-injection-induced seismic emission at the KTB site https://doi.org/10.1111/j.1365-246X.1997.tb01215.x

Vuan A., Sugan M., Amati G., Kato A. (2018). Improving the Detection of Low-Magnitude Seismicity Preceding the Mw 6.3 L'Aquila Earthquake: Development of a Scalable Code Based on the Cross Correlation of Template Earthquakes.doi:10.1785/0120170106

Zaliapin, I., & Ben-Zion, Y. (2020). Earthquake declustering using the nearest-neighbor approach in space- time-magnitude domain. Journal of Geophysical Research: Solid Earth, 125, e2018JB017120. https://doi.org/ 10.1029/2018JB017120

Corresponding author: gemmacipressi@gmail.com

Estimating the source parameters of a moderate earthquake using the second seismic moments

A.Cuius[1,2], A. Saraò[3], H. Meng[4], G. Costa[1]

[1] *Department of Mathematics and Geosciences, University of Trieste, Trieste, Italy*
[2] *National Institute of Geophysics and Volcanology, INGV, Roma, Italy*
[3] *National Institute of Geophysics and Applied Geophysics, OGS, Trieste, Italy*
[4] *Department of Earth and Space Sciences, Southern University of Science and Technology, Shenzhen, Guangdong, China*

Introduction

The study of earthquake generation and associated seismic parameters such as seismic moment, rupture size, rupture velocity and direction, and stress drop is crucial for understanding earthquake dynamics and the underlying physics of the seismic process. This information plays an important role in the estimation of ground shaking near the earthquake source and in the assessment of seismic hazard, even for low to moderate magnitude earthquakes.

The kinematic properties of small earthquakes are often difficult to determine, and simple models are often used to represent these events, although improved records show that source complexity is common even for small earthquake ruptures (e.g. Calderoni and Abercrombie, 2023 and reference therein).

A critical task in determining finite source attributes for moderate and low magnitude earthquakes requires good removal of path and site effects. To address this problem, several methods based on empirical Green's function (EGF) deconvolution have been developed in recent decades. Although the EGF offers several advantages, its application is associated with some difficulties, as there are often no focal mechanisms for small earthquakes and source effects have been observed even for low energy events (Calderoni et al. 2023).

The simplest general representation of an earthquake that contains information about the rupture extent and directivity is the point-source representation plus the variances or second-degree moments of the moment-release distribution. The hypocenter and the origin time of the earthquake correspond to the spatial and temporal average (first degree moment) of the release moment distribution. The information about the rupture extent, the characteristic duration and the direction of rupture propagation correspond to the variance of the moment distribution in the spatial, temporal and spatio-temporal domain (second-degree moments). Seismic moments are calculated from apparent durations measured from apparent source time functions (ASTF) for each station after removal of path effects. The ASTF is thus the projection of the rupture process onto the seismic ray path, and its properties also depend on the azimuth and take-off angles (e.g. McGuire, 2004). For a unilateral rupture, the ASTF observed from stations in the direction of propagation would be significantly shorter than the ASTF from stations in the opposite direction.

A major advantage of the second moments method is that it can theoretically be applied to all earthquakes, regardless of their magnitude and complexity, and without requiring the assumptions of an a priori source model (e.g. McGuire 2004; Meng et al., 2020; Cuius et al., 2023). It is also a consistent tool for evaluating scaling relationships between finite source attributes and earthquake magnitudes for large and small earthquakes and for resolving fault plane ambiguity.

However, the elimination of the path effect is crucial, and a biased ASTF calculation would lead to inaccurate calculations of the second seismic moments. However, there may also be other factors that influence the results of the second moments, even if the propagation effects have been correctly removed.

The aim of this study is to implement and test an efficient method for estimating source parameters and rupture directivity in near real-time for medium and small earthquakes. To achieve our goal, we implemented an approach developed by McGuire et al. (2004), which consists of calculating the second-degree seismic moments (Meng et al., 2020; Cuius et al., 2023). In this paper, we first perform a study with some synthetic tests to evaluate the influence of uncertainties related to our prior knowledge and observations on the resulting source parameters (Cuius et al. 2023). We then apply the method to a real earthquake in Italy and present the result.

Analysis of the sensitivity of the second moments tensor resolutions

To evaluate the sensitivity of the second moment solutions, we used synthetic ASTFs computed for a rectangular plane fault discretized by a grid of cells, each assigned a specific slip value. Full details can be found in Cuius et al. 2023. The input parameters used to model the ASTF for a magnitude Mw 4.6 earthquake source are listed in Tab. 1. We assumed that the epicenter was located in central Italy and approximated the fault as a 3.0 km box model (Fig. 1). The rupture area was divided into 12x12 cells, and the slip distribution and rupture time for the unilateral (Fig. 1a; 1b) and bilateral (Fig. 1d; 1e) scenarios were taken from a previous study of a similar magnitude earthquake (SRCMOD database - Mai and Thinbgaijam, 2014), with a focal mechanism of 247° strike, 46° dip and 40° dip. Using the actual station configuration, we calculated the ASTFs with a sampling frequency of 100 Hz and a source time function of 3 seconds. A uniform propagation of the rupture front with a rupture velocity of 2.75 km/s was assumed, which corresponds to 0.9 times the S-wave velocity in the source region. A simplified 1-D velocity model for central Italy was used to model the ASTF (Cuius et al., 2023).

	Unilateral rupture					*Bilateral rupture*				
	(km)	*(km)*	*(sec)*	*| (km/s)*	*Dir*	*(km)*	*(km)*	*(sec)*	*| (km/s)*	*Dir*
Input parameters	1.39	1.21	0.42	2.64	0.80	1.39	1.21	0.31	1.13	0.25

Tab. 1. Input parameters used to model the unilateral and bilateral scenarios for the characteristic rupture size (and), characteristic rupture duration ( ), centroid rupture velocity ( ) and directivity (dir).

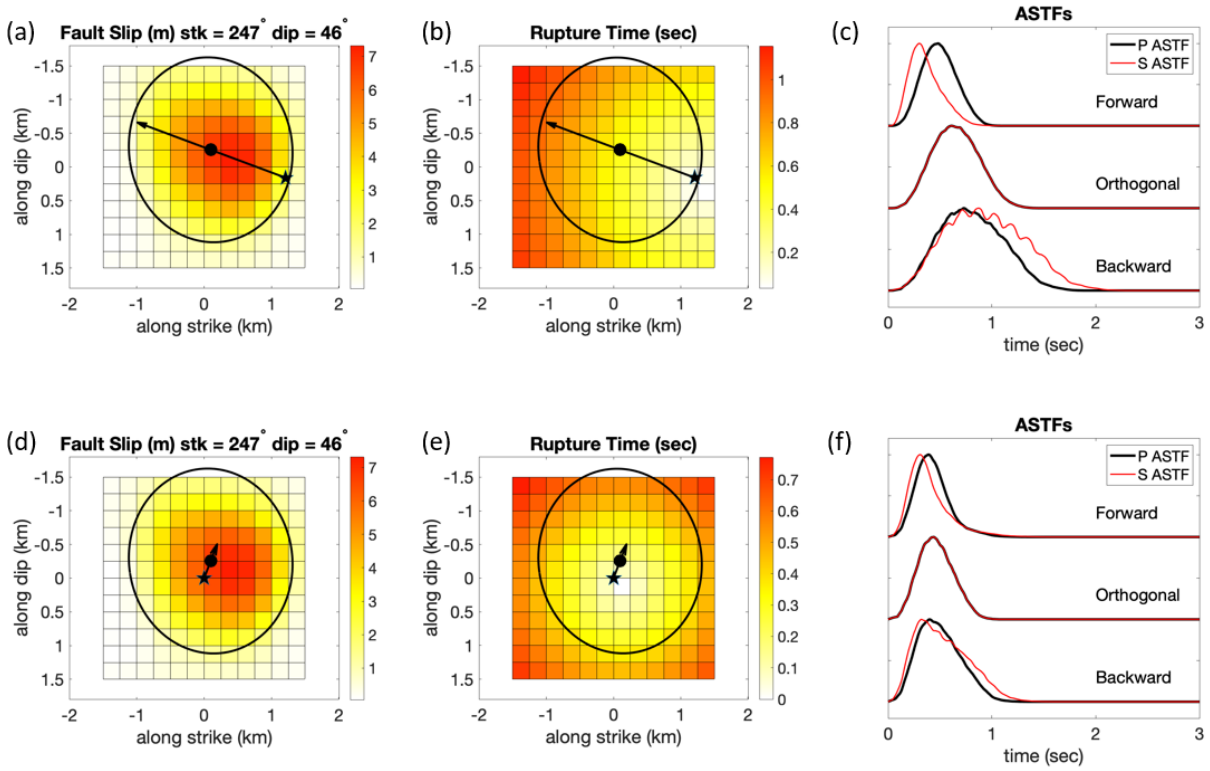

Fig 1. Input source for unilateral (A,B) and bilateral (D,E) scenarios. The star represents the hypocenter, the dot represents the centroid location, and the arrow indicates the rupture direction. Panels (C,F) show the ASTFs calculated from the respective models for three different azimuth directions.

To investigate how the uncertainties introduced by the input data may affect the solutions of the resolved second seismic moments, we used the bootstrap approach. In this technique, perturbations are introduced for each input parameter to be analyzed by generating 1000 variations around the mean value. An inversion is then performed to assess the impact on the mean and standard deviation of the resulting data. The workflow is summarized in Fig. 2.

We investigated the uncertainties associated with the ASTF, the location of the hypocenter, the station distributions around the source, the focal mechanism, and the velocity model used for ray tracing. Some of these tests are interrelated. For example, the uncertainties in the position of the hypocenter and the velocity model affect the calculated ray path, and both the different focal mechanism and station coverage affect the resolution of the fault plane. The uncertainties in the epicenter estimates were not investigated because they have negligible effects on the slowness vectors in the inversion of the second moments.

Results of the synthetic tests

The sensitivity analysis performed in this study shows that the uncertainties in the input data have different effects on the calculation of the source parameters and that an accurate measurement of the ASTF as well as the velocity model play the most important role in influencing the inversion process. The results of our tests (Tab. 2 and Fig. 3) show that the main source parameters, i.e. fracture size, swelling duration and centroid velocity, are generally well reproduced within the standard deviation. The source duration resulting from the inversion process is strongly influenced by the duration of the input ASTF, and even 10 % influences the inversion of the second moment tensor. In the case of dense instrumentation, the horizontal location of the earthquake can be well resolved, but the resolution of the earthquake depth is largely determined by the velocity model, and an inaccurate earthquake location can lead to uncertainties in the resolved second moments. Care must also be taken to avoid artifacts due to the discretization of the velocity model when the hypocenter is located at an interface between two layers with high velocity contrast.

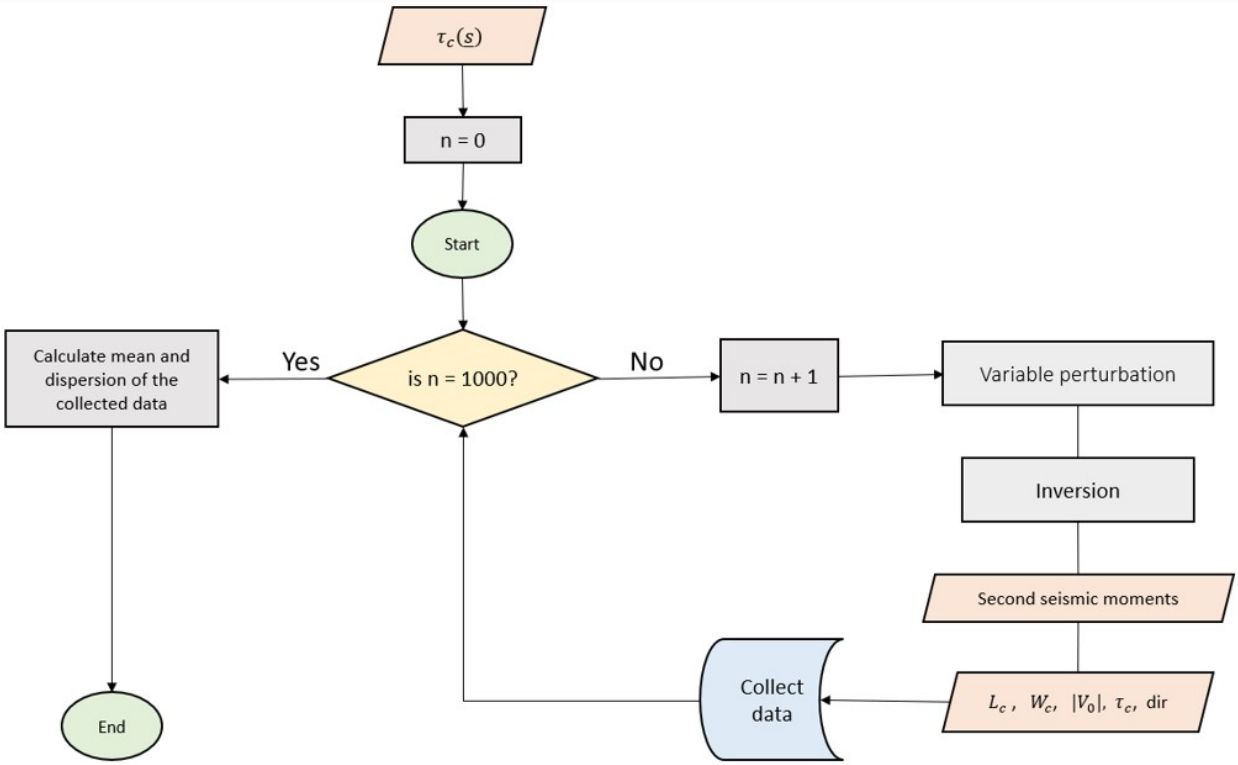

Fig. 2 Flowchart of the perturbation test. For each test, we computed 1000 random station configurations or perturbed input variables (depth, velocity model, focal mechanism, or observed c) with a given standard deviation. Then we performed the inversion and calculated the source parameters and directivity. Finally, we calculated the mean and dispersion of the output variables of the 1000 scenarios.

The values of the directivity depend on the ASTF duration, the choice of velocity model and the focal mechanism (Fig. 3). To ensure good resolution of the fault plane, good coverage of the ray path is critical for both upward and downward waves (McGuire, 2004). The component of rupture directivity along the dip can only be well determined if stations directly above the hypocenter are available, as the seismic rays are nearly horizontal at most other stations.

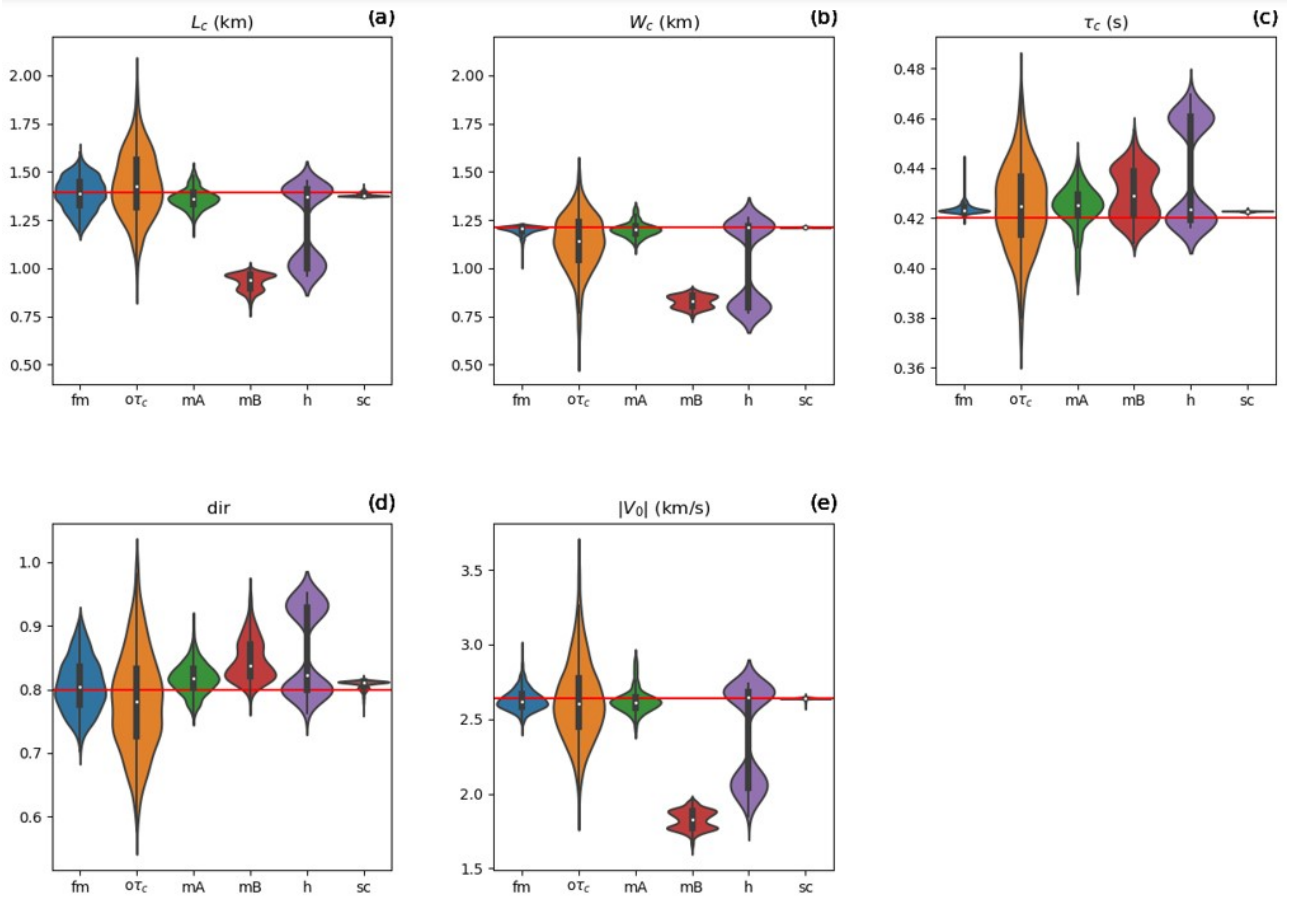

Fig. 3 Violin plots showing the Mean values and dispersions of each output variable resulting from each perturbation test given on the x-axis, i.e., focal mechanism (fm), observed τc (οτc), velocity models (mA and mB, respectively), hypocentral depth (h), and station configuration (sc) for the unilateral scenario. (A–E) represent the solutions for the characteristic length, characteristic width, source duration, directivity and centroid rupture velocity respectively. The y-axis indicates the value of the output variable. The shape of each violin graph reflects the numerical counts of the resulting value. The red line serves as reference, indicating the input value.

	Unilateral rupture					*Bilateral rupture*				
Output variables	*(km)*	*(km)*	*(sec)*	*| (km/s)*	*Dir*	*(km)*	*(km)*	*(sec)*	*| (km/s)*	*Dir*
not perturbed	1.39	1.21	0.42	2.48	0.8	1.38	1.21	0.31	1.13	0.25
Observed (sd = 10%)	1.4	1.13	0.42	2.63	0.78	1.41	1.18	0.31	1.14	0.25
Depth (sd = 1 km)	1.22	1.02	0.44	2.38	0.86	1.20	1.02	0.33	0.81	0.22
Stations' configuration	1.38	1.21	0.4	2.64	0.81	1.39	1.21	0.31	1.12	0.25
Focal Mechanism (sd str = 5°, sd dip = 5°)	1.39	1.20	0.42	2.63	0.81	1.38	1.20	0.31	1.11	0.25
A model (sd = 0.3 km/s)	1.36	1.20	0.42	2.62	0.82	1.37	1.21	0.31	1.10	0.25
B model (sd = 0.3 km/s)	0.93	0.83	0.43	1.83	0.85	0.96	0.84	0.32	0.48	0.15

Tab. 2. Results of the mean of each outcome variable calculated by the perturbation test for the unilateral and bilateral scenarios. For each test case, we report between brackets the standard deviation (sd) applied to the true value.

Application to real case: the Mw 4.6 Central Italy earthquake

The method was then applied to study the Mw 4.6 event of March 2023 in central Italy, using data from the Italian seismic network (RSN (Amato et al., 2008) and the Italian accelerometry network (RAN (Costa et al., 2022)). We compute the ASTFs through the EGF deconvolution using the P and S waves.

We calculated the second seismic moment to obtain information about the directivity and source parameters. The main parameters calculated with this method are the following = 1.16 km, = 0.615, = 0.14 s, = 1.86 m/s, dir = 64, stress drop = 7.37 MPa). The relatively small value of is possibly due to the poor resolution of the vertical component and can be explained by the interaction of two factors: the vertical rupture plane and the small number of stations in the immediate vicinity of the epicenter (< 5 km).

Conclusions

The use of second-moment tensors to determine the source parameters, including directivity, of moderate-magnitude earthquakes could be a valuable tool to improve our understanding of the source dynamics in a given area and to the risk mitigation. One possible application of the second-moments method to small earthquakes would be to identify portions of large faults that produce super-shear ruptures and correlate them with the geology of the fault zone. The second moments method also provides lower constraints on rupture velocity, which can be particularly useful for unilateral ruptures. However, before the results can be interpreted, the resolution limits of the method need to be known due to the possible uncertainties of the parameters used as inputs to the computational procedure.

To overcome the difficulties related to the analysis of noisy signals in the time domain, which can be an important limitation in the calculation of ASTFs and consequently the source duration for low magnitude events, an experimental approach based on the frequency domain is currently being developed. Although the frequency domain deconvolution-based method is currently more time consuming than time domain deconvolution, it can be used in situations where the determination of reliable ASTFs is difficult due to noise, which is often the case for low magnitude earthquakes.

Acknowledgements

We are deeply grateful to the Italian Department of Civil Protection – Presidency of the Council of Ministers for funding this research.

References

Amato, A., & Mele, F. (2008). Performance of the INGV National Seismic Network from 1997 to 2007. Annals of Geophysics.

Calderoni, G., and Abercrombie, R. E. (2023). Investigating spectral estimates of stress drop for small to moderate earthquakes with heterogeneous slip distribution: Examples from the 2016-2017 Amatrice earthquake sequence. J. Geophys. Res.: Solid Earth., 128, e2022JB025022, doi: 10.1029/2022JB025022

Costa, G., Brondi, P., Cataldi, L., Cirilli, S., Ertuncay, D., Falconer, P., ... & Turpaud, P. (2022). Near-Real-Time Strong Motion Acquisition at National Scale and Automatic Analysis. Sensors, 22(15), 5699.

Cuius, A., Meng, H., Saraò, A., & Costa, G. (2023). Sensitivity of the second seismic moments resolution to determine the fault parameters of moderate earthquakes. Frontiers in Earth Science, 11.

Mai, P. M., and Thingbaijam, K. K. S. (2014). SRCMOD: an online database of finite-fault rupture models. Seismol. Res. Lett. 85, 1348–1357. doi:10.1785/0220140077

McGuire, J. J. (2004). Estimating finite source properties of small earthquake ruptures. Bulletin of the Seismological Society of America, 94(2), 377-393.

Meng, H., McGuire, J. J., & Ben-Zion, Y. (2020). Semiautomated estimates of directivity and related source properties of small to moderate Southern California earthquakes using second seismic moments. Journal of Geophysical Research: Solid Earth, 125(4), e2019JB018566.

Corresponding author: arianna.cuius@ingv.it

A natural pump-probe experiment reveals nonlinear elastic properties along the Irpinia Fault, Southern Apennines

N. D'Agostino[1], S. Tarantino[1], P. Poli[2], M. Vassallo[1], G. Ventafridda[3], G. Festa[4], A. Zollo[4]

[1] Istituto Nazionale di Geofisica e Vulcanologia, Italy
[2] Dipartimento di Geoscienze, Università di Padova, Italy
[3] Acquedotto Pugliese SpA, Italy
[4] Dipartimento di Fisica, Università di Napoli Federico II, Italy

The conventional picture of the earthquake cycle implies that rupture is reached by progressive stress buildup until reaching fault's failure strength. Alternatively the failure strength may be altered by changes in pore pressure and/or properties of fault rocks driven by hydrologically-driven strain/stress transients. This scenario may be associated with significant modifications of the elastic properties of the crust potentially detectable with seismological tools. Natural oscillatory stress sources (tides, seasonal and multiannual hydrological stress variations) can thus been exploited to probe the time-dependent response of active fault zones to stress variations at various temporal and spatial scales and investigate time-dependent variations of its elastic properties (Delorey et al., 2021). In the framework of the INGV Pianeta Dinamico project MYBURP (Modulation of hYdrology on stress BUildup on the IRPinia Fault) a multidisciplinary (seismology, geodesy, geochemistry) study is carried out along the Irpinia Fault (Southern Apennines) to investigate the response of the crust to hydrological forcing associated to phases of recharge/discharge of karst aquifers in terms of time-dependent variations of its elastic and hydraulic properties. Charge/discharge phases of the karst aquifers in the Apennines cause significant seasonal and multi-annual strain transients (Silverii et al, 2019), that modulate the secular, tectonic deformation (~3 mm/yr extension across the Apennines). It has been previously observed that these seasonal and multi-annual transients correlate with the seismicity rate (D'Agostino et al, 2018) and seismic velocity variations (Poli et al., 2020). Recent studies (Silverii et al., 2016; D'Agostino et al., 2018) have shown the high sensitivity of the Irpinia Fault System (IFS) volume to hydrological stresses reflected in a complex, time-dependent response of deformation and seismicity. We performed a natural pump-probe experiment to assess the non-linear behavior of the seismogenic volumes in response to non-tectonic deformations. Seasonal horizontal strains associated with discharge and recharge of karst aquifers are used as the "pump". Coda wave interferometry demonstrates to be a powerful tool to probe time-dependent crustal

elastic properties. We computed seismic velocity variations using empirical Green's functions reconstructed by autocorrelation on continuous 14-year-long time series of ambient noise. We analyzed two different sites (co-located GPS and seismic stations), near and afar the IFS. We found that velocity variations are significant (~0.2%) nearby IF (shallow carbonates rocks), rather than far away from it. We compared the velocity variations near IF with the time series of Caposele spring discharge, temperature, horizontal deformation and seismicity rate (computed thanks to dense geodetic and seismic networks). Our observations are coherent at seasonal and multi-annual scales and can be explained with the same mechanism. At the time of the maximum peak of the discharge spring, representing a proxy of the hydraulic head, the seismic wave velocity is minimum, the dilation of crust is maximum and related to the opening of pre-existing cracks' system. The background microseismicity occurrence is favored by the hydrologically-related dilatation, superimposed to the ongoing tectonic extension. From the comparison between hydrological strain variations and velocity changes, we estimate a strain sensitivity of velocity change of ~-10^3 typical of worn crustal material and in good agreement with laboratory experiments. This non-linear elasticity regime suggests the presence of a multi-fractured and damaged crust subject to periodic seasonal phases of weakening/healing, potentially affecting earthquake nucleation processes.

References:

D'Agostino, N. *et al.* Crustal Deformation and Seismicity Modulated by Groundwater Recharge of Karst Aquifers (2018), *Geophys Res Lett* 45, 10.1029/2018GL079794.

Delorey, A. A., Guyer, R. A., Bokelmann, G. H. R. & Johnson, P. A. Probing the Damage Zone at Parkfield (2021), *Geophys Res Lett* 48, 10.1029/2021GL093518.

Poli, P., Marguin, V., Wang, Q., D'Agostino, N. & Johnson, P. Seasonal and Coseismic Velocity Variation in the Region of L'Aquila From Single Station Measurements and Implications for Crustal Rheology (2020), *J Geophys Res Solid Earth* 125, 10.1029/2019JB019316.

Silverii, F., D'Agostino, N., Métois, M., Fiorillo, F. & Ventafridda, G. (2016) Transient deformation of karst aquifers due to seasonal and multiyear groundwater variations observed by GPS in southern Apennines (Italy). *J Geophys Res Solid Earth* 121, 10.1002/2016JB013361.

Corresponding author: nicola.dagostino@ingv.it

Source parameter estimation by using Q tomography: the potentiality of exploiting large sequence of aftershocks

P. De Gori[1], F. P. Lucente[1], C. Chiarabba[1]

[1] *Istituto Nazionale di Geofisica e Vulcanologia (INGV), Rome, Italy*

The determination of seismic source parameters (seismic moment, source dimension, stress drop) play an important role in studying earthquake physics, for example to define fault interaction or to predict the ground shaking. However, the measurement of earthquake source parameters is affected by large uncertainties, and different approaches lead to large variability in results. One crucial aspect is the trade-off between attenuation (Q) and corner frequency (fc) in spectral fitting. Here we describe a method to solve the trade-off based on the fit of displacement spectra to find the source characteristics (corner frequency, fc, and the signal moment, Ω0) and the single-station attenuation operator (t), in addition to the site response. We follow a parametric approach based on the use of 3D Q seismic tomography and a bootstrap-based method for selecting the best spectra fit. The correction of attenuation with synthetic values derived by 3D attenuation tomography efficiently deals with the trade-off between source and path terms, leading to small uncertainties in the determination of source unknowns (fc and signal moment, Ω0), thus yielding constrained estimates of source parameters for low- to medium-magnitude earthquakes. We show an application to the Emilia 2012 seismic sequence, for which we computed the source parameters for 1240 aftershocks (from an initial dataset of 1748) with local magnitude ranging from 2.0 to 4.7 using the spectral fit from P and S waves. This approach gives the opportunity to infer the mechanical state of a complete fault system by taking advantage of the larger number of low-magnitude events (with respect to the largest ones) that always follow a major earthquake.

Corresponding author: pasquale.degori@ingv.it

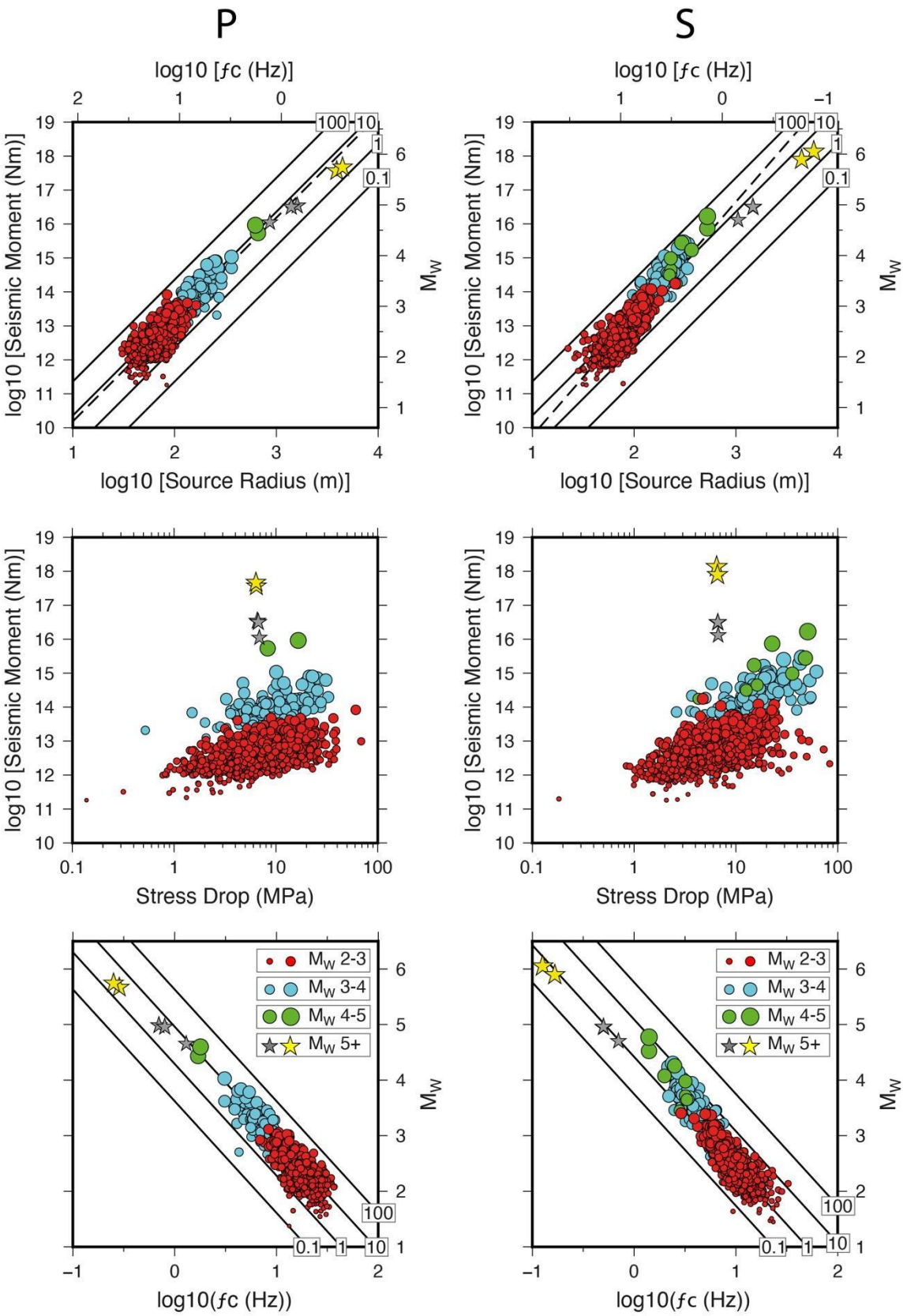

Fig. 1 – Source parameters determined from the fit of (a) P and (b) S spectra. For each phase, the seismic moment versus source radius (top), seismic moment versus stress drop (middle), and moment magnitude versus corner frequency (bottom) are reported. Aftershocks are drawn by circles sized and colored on the basis of their magnitude according to the legend on the bottom panels. Stars are M 5+ events. On the upper and bottom panels, black lines refer to constant stress-drop values expressed in MPa.

Calibration of the local magnitude scale (M_L) for eastern Cuba

E. Diez[1], D. Sandron[2], M. Cutie[1], M. Guidarelli[2]

[1] *Centro Nacional de Investigaciones Sismológicas (CENAIS), Santiago de Cuba, Cuba.*
[2] *Istituto Nazionale di Oceanografia e di Geofisica Sperimentale — OGS, Sgonico, Italy.*

The first attempt to create an international standard for quantifying earthquake energy was made by Richter (1935), who introduced the local magnitude (M_L) as the logarithm of the maximum amplitude from zero to the maximum peak measured with a Wood-Anderson (WA) instrument (with 2800 amplification and a natural period of 0.8 s [Anderson and Wood, 1925]), as follows:

$$M_L = log_{10}A(R) - log_{10} A_0(R)$$

where A(R) is the zero-to-peak amplitude in mm in a WA seismogram; R is the epicentral distance in km, and A_0(R) is the distance correction. The "calibration point" was determined by setting M_L=0 for a displacement amplitude of 1 thousandth of a millimeter at 100 km of epicentral distance. Recently, one hundredth of a millimeter at 17 km was chosen as an alternative anchor point (Hutton and Boore, 1987) and Uhrhammer and Collins (1990) corrected the static gain value for the WA instrument to 2080 (confirmed by Sandron et al. (2015) using data from an original WA instrument still in operation). In 2013, the International Association of Seismology and Physics of the Earth's Interior Magnitude Working Group (IASPEI, 2013) proposed the following general equation:

$$M_L = log_{10}(A) - nlog_{10}(R) - KR - C - S$$

in where A is the maximum amplitude in nanometers recorded by a simulated instrument such as WA with a static gain of 1; R is the hypocentral distance in kilometers; C is a constant; and S is the correction per station due to local conditions (Bormann and Dewey, 2012). The parameters n and K represent the geometric dispersion and the anelastic attenuation, respectively (Bakun and Joyner, 1984).

Several studies have been carried out to calibrate the M_L equation coefficients for different geographical areas around the world. In Cuba, in particular, different approaches have been used to determine local earthquake magnitudes since the establishment of seismological stations in 1964. Álvarez and Bune (1977) and Álvarez et al. (1999, 2000) estimated the parameters for magnitude calculation based on the results obtained from the evaluation of energy class K or K-class, a measure of earthquake strength or magnitude of local and regional earthquakes used in the countries of the former Soviet Union, Cuba and Mongolia. The first equation of M_L,

corresponding to the Richter magnitude scale for the Cuban territory, was proposed by Moreno and González (2001) and was based on the analysis of earthquake records using data from the old short-term stations installed at that time, which were quite limited in quantity and quality. Later, the seismic network was upgraded and converted to digital technology with the installation of broadband stations, which increased the station density in southeastern Cuba and enabled the calculation using digital recordings. With the new database, Moreno (2002) updated the parameters of the M_L considering a new data set. This equation is currently used by the Centro Nacional de Investigaciones Sismológicas (CENAIS). However, in the last 20 years, new stations with new instruments with higher amplification and wider frequency response and dynamic range have been established in the same study region (Diez Zaldívar et al., 2014 and 2022). To date, no comprehensive method has been developed in Cuba to estimate the parameters of the ML equation using many seismic stations and many years of recorded data. For this reason, it was necessary to carry out a study to recalibrate the parameters of the M_L equation with high accuracy and with a focus on the southeastern part of Cuba.

This study covered a geographical area between 19°–22° N and 73°–79° W. In this area, the predominant seismicity is characterized by an "interplate" behavior related to the Oriente fault zone, with a higher frequency of earthquakes that can reach a large magnitude (Mw > 6.0) and a depth of more than 20 km. More than 90% of the earthquakes that strike the country occur in this southeastern area of Cuba (Álvarez and Menendez, 1969; Álvarez and Bune, 1977; Moreno et al., 2002). However, moderate seismicity has also been associated with smaller faults in the interior of Cuba, which have caused some moderate earthquakes with significant damage (Chuy, 1999).

The data comes from the general catalog of the Cuban seismological service CENAIS (2023). Between 2011 and 2021, more than 60,000 earthquakes with fairly well-defined parameters were analyzed by CENAIS seismologists and different signal processing methods were applied, such as filtering, deconvolution with the instrument transfer function and simulation of the WA seismometer by the SEISAN software (Havskov and Ottemoller, 2000). Our selection (M_L in a range between 2 and 5 and at least four triggering stations) includes 7750 seismic events, and the final input dataset contains a total of 33 916 records with: Event ID, date, depth, horizontal component amplitudes, calculated epicentral hypocentral distance, and the number of stations recorded for each seismic event.

We set up the whole procedure of linear regression analysis in the Matlab environment, following Chovanová and Kristek (2018), to obtain the formula for the local order of magnitude in the IASPEI form. In a 3-step procedure, we: 1) removed the outliers; 2) searched for the parameters n, K and Si that minimize the unbiased sample standard deviation of the residuals; c) set the anchor point for the parameter C (1/100 millimeter at 17 km). The new formula for the local parameter M_L is thus defined as follows:

$$M_L = log_{10}(A) - 1log_{10}(R) - 0.003R - 1.963$$

The curve determined is somewhat less attenuated than the curve previously determined by Moreno (2002) for this area and lies between this curve and the curve determined by Hutton and Boore (1987) for California.

The correction values (S) found for the stations are consistent with the local geology, and we can conclude that the M_L scale proposed in this study can replace the local magnitude scale currently used in the routine work of CENAIS.

References

Álvarez, H., and A. Menendez (1969). Sismicidad de Cuba, Izv. Akad. Naukk S.S.S.R. Fizika Zemli 1, 74–78 (in Russian).

Álvarez, J. L., and V. I. Bune (1977). Seismic hazard assessment for southeastern Cuba, Izv. Akad. Naukk S.S.S.R. Fizika Zemli 10, 54–67 (in Russian).

Álvarez, L., T. Chuy, J. García, B. Moreno, H. Álvarez, M. Blanco, O. Expósito, O. González, and A. I. Fernández (1999). An earthquake cata- logue of Cuba and neighbour- ing areas, ICTP Internal Rept. ic/ir/99/1, Miramare, Trieste, Italy, 60, available at http:// iohanis.com/~leoalvar/papers/ ICTPcata.pdf (last accessed November 2023).

Álvarez, L., R. S. Mijailova, E. O. Vorobiova, T. J. Chuy, G. N. Zhakirdzhanova, E. R. Perez, L. M. Rodionova, H. Alvarez, and K. M. Mirzoev (2000). Terremotos de Cuba y áreas aledañas, in Sismicidad de Cuba y estructura de la corteza en el Caribe, J. L. Alvarez (Editor) Editorial Academia, La Habana, Cuba, 7–35 (in Spanish).

Anderson, J. A., and H. O. Wood (1925). Description and theory of the torsion seismometer, Bull. Seismol. Soc. Am. 15, no. 1, 1–72, doi: 10.1785/ BSSA0150010001.

Bakun, W. H., and W. B. Joyner (1984). The ML scale in central California, Bull. Seismol. Soc. Am. 74, 1827–1843.

Bormann, P., and J. W. Dewey (2012). The New IASPEI Standards for Determining Magnitudes from Digital Data and Their Relation to Classical Magnitudes, New Manual of Seismological Observatory Practice 2 (NMSOP-2), Deutsches GeoForschungs Zentrum GFZ, Germany, 1–4.

Chovanová, Z., and J. Kristek (2018). A local magnitude scale for Slovakia, Central Europe, Bull. Seismol. Soc. Am. 108, 5A, 2756–2763, doi: 10.1785/0120180059.

Chuy, T. (1999). Macrosísmica de Cuba y su aplicación en los esti- mados de peligrosidad y microzonación Sísmica, Tesis en opción al Grado de Doctor en Ciencias Geofísicas, Fondos del MES y CENAIS, 150 p. (in Spanish).

Diez Zaldívar, E. R., M. C. Mustelier, C. M. Moracén, R. P. Cláres, V. Poveda Brossard, Z. Yinxing, C. Yang, and W. Fengxia (2014). Modernización de la red sísmica cubana, Instalación, calibración y puesta a punto, Rev. Fac. Ing. UCV 29, 69–78 (in Spanish).

Diez Zaldivar, E. R., E. Priolo, D. Sandron, V. Poveda Brossard, M. Cattaneo, S. Marzorati, and R. Palau Clares (2022). Evaluation of the event detection level of the cuban seismic network, Seismol. Res. Lett. 93, 2048–2062, doi: 10.1785/0220220016.

Havskov, J., and L. Ottemoller (2000). SEISAN Earthquake Analysis Software, Seismol. Res. Lett. 70, 532–534, doi: 10.1785/ gssrl.70.5.532.

Hutton, L. K., and D. M. Boore (1987). The ML scale in southern California, Bull. Seismol. Soc. Am. 77, 2074–2094, doi: 10.1785/ BSSA0770062074.

IASPEI (International Association of Seismology and Physics of the Earth's Interior (2013). Summary of magnitude working group recommendations on standard procedures for determining earthquake magnitudes from digital data, available at http://download .iaspei.org/commissions/CSOI/ Summary_WG_recommendations_ 20130327.pdf (last accessed April 2023).

Moreno, B., and O. González (2001). Local magnitude scale for the eastern region of Cuba, in Sismicidad de Cuba y estructura de la corteza, J. L. Alvarez Gómez (Editor), Editorial Academia, La Habana, Cuba, ISBN: 978-959-02-0242-1 (in Spanish).

Moreno, B., M. Grandison, and K. Atakan (2002). Crustal velocity model along the southern Cuba margin. Implications for the tectonic regime at an active plate boundary. Geophys. J. Int. 151, 632–645.

Richter, C. F. (1935). An instrumental earthquake magnitude scale, Bull. Seismol. Soc. Am. 25, no. 1, 1–32.

Sandron, D., G. F. Gentile, S. Gentili, A. Sarao, A. Rebez, M. Santulin, and D. Slejko (2015). The Wood-Anderson of Trieste (northeast Italy): One of the last operating torsion seismometers, Seismol. Res. Lett. 86, no. 6, 1645–1654, doi: 10.1785/0220150047.

Uhrhammer, R. A., and E. R. Collins (1990). Synthesis of Wood– Anderson seismograms from broadband digital records, Bull. Seismol. Soc. Am. 80, 702–716.

Corresponding author: diez@cenais.cu

Insights on the seismotectonics of the Alps-Apennines transition zone, NW Italy, after the 2022 earthquake sequence near Genoa

E. Eva[1], M.G. Malusà[2] and S. Solarino[1]

[1] Istituto Nazionale di Geofisica e Vulcanologia, Osservatorio Nazionale Terremoti, Genoa, Italy

[2] Department of Earth and Environmental Sciences, University of Milano-Bicocca, Milan, Italy

In the years 2021-2022 three seismic sequences located respectively close to Savignone (August - October 2021), Borzonasca (February – March 2022) and Bargagli (September – October 2022) struck the area ENE of Genoa, in the region classically referred to as the transition between the Alps and the Apennines. According to the instrumental catalogues, seismic events in this sector are infrequent and of low magnitude and even the catalogues of historical seismicity do not report major seismic events. Nevertheless, the earthquake of September 22, 2022 in the Bargagli area (red star in Fig.1), reached a magnitude M_w 4.0. It was felt in a large area and caused minor damages to a cemetery and a church in Bargagli and in a nearby village, respectively. Given the low number of seismic events occurred in the area in the past, the three seismic sequences represent a valuable dataset to shade some light on how the convergence between Africa and Europe is presently accommodated across the Alps-Apennines transition zone. They are thus the topic of this study.

It must be remarked that according to the catalogue CPTI15, only few earthquakes with a magnitude comparable with the event in Bargagli have occurred near Genoa but none in the area of the 2022 earthquake. The first step of this study consisted then in a reappraisal of the events of the last century with an approach profiting from the instrumental data for the events of the last century stored at the Sismos database. In particular, historical seismograms and seismic bulletins provided a new location for the September 21, 1924 earthquake originally located offshore about five kilometres from the Ligurian coast (green star in Fig.1). Based on the results obtained, this earthquake locates near Bargagli (blue star in Fig. 1) and deserves attention in that it can provide insights on the relationship between recent and historical seismicity (Solarino and Eva, 2023). Although the new location has no particular implications for the seismic hazard of the area, however it represents an important information to be taken into account in the calculation of the return period.

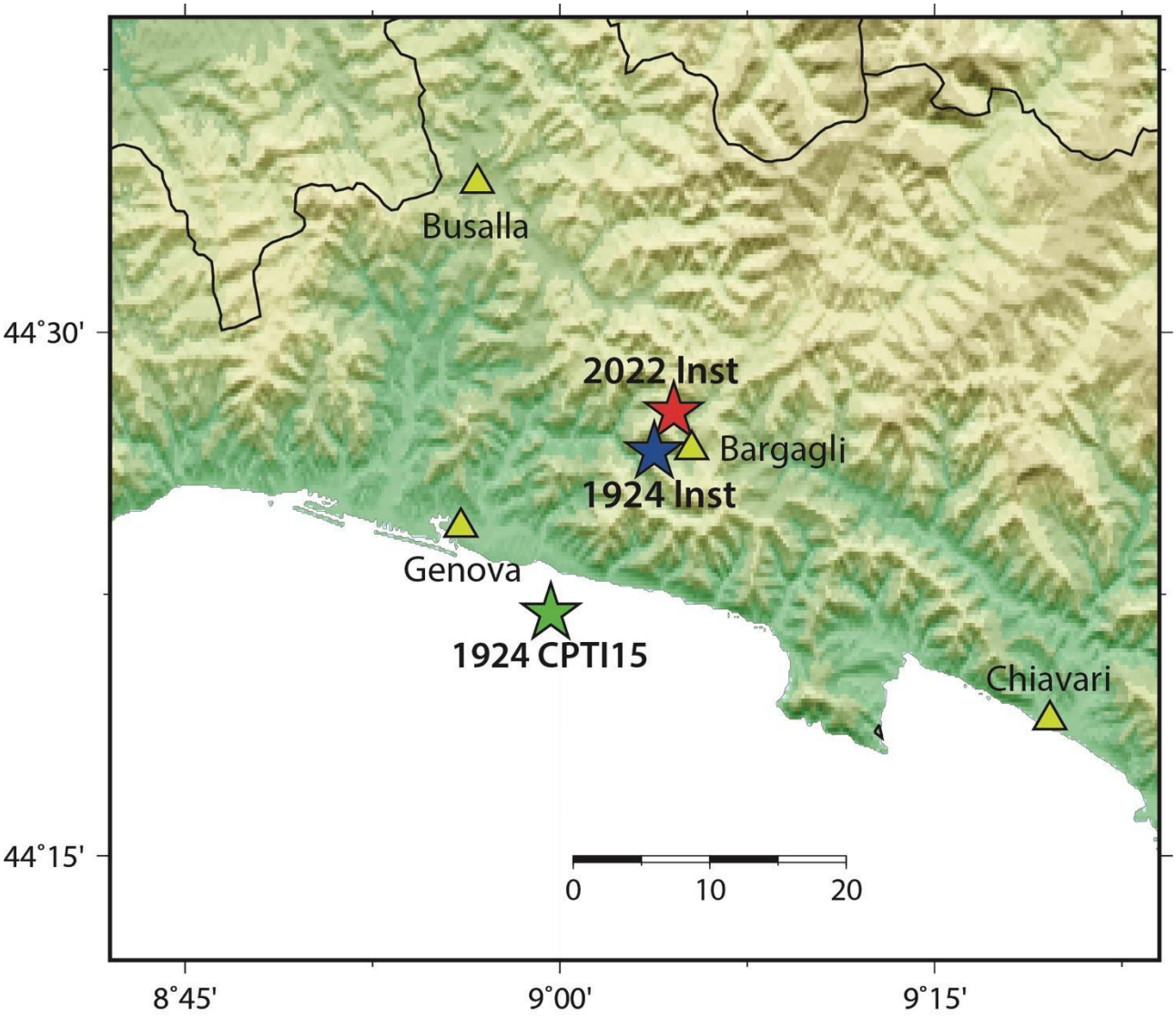

Fig. 1 – Locations of the 2022 and 1924 events. The latter was originally located using macroseismic intensities in the Ligurian Sea, some 5 km from the coast. Instrumental data shifted the event inland, close to Bargagli.

With the double aim of investigating on the seismotectonics of the area and its geodynamic implications, we analysed the events occurred between 1989 and 2022. After relocation using the HypoDD (Waldhauser and Ellsworth, 2000) location code, the events reveal a NE-SW alignment for the Savignone seismic sequence and NNW-SSE alignments for the Borzonasca and Bargagli sequences (Fig. 2). The Borzonasca seismic sequence plots in correspondence of the Villalvernia-Varzi-Ottone Fault, often considered as the transition between the Alps and the Apennines. The seismicity would favour the hypothesis of a kinematic activity in comparison with the Sestri-Voltaggio Fault, along which no seismicity is currently documented. The main-shock focal solutions are invariably strike-slip, with near-vertical NNW-SSE and NE-SW to ENE-WSW nodal planes (Fig. 2). The evident earthquake alignments in the study area mark active, km-scale fault planes in the upper crust, pointing to a scenario of distributed strike-slip deformation in the transition zone between the Alps and the Apennines (Eva et al., 2023). The NE-SW faults are inherited structures that underwent major Neogene rotations and are no longer suitably oriented to accommodate the northward motion of Adria relative to Europe.

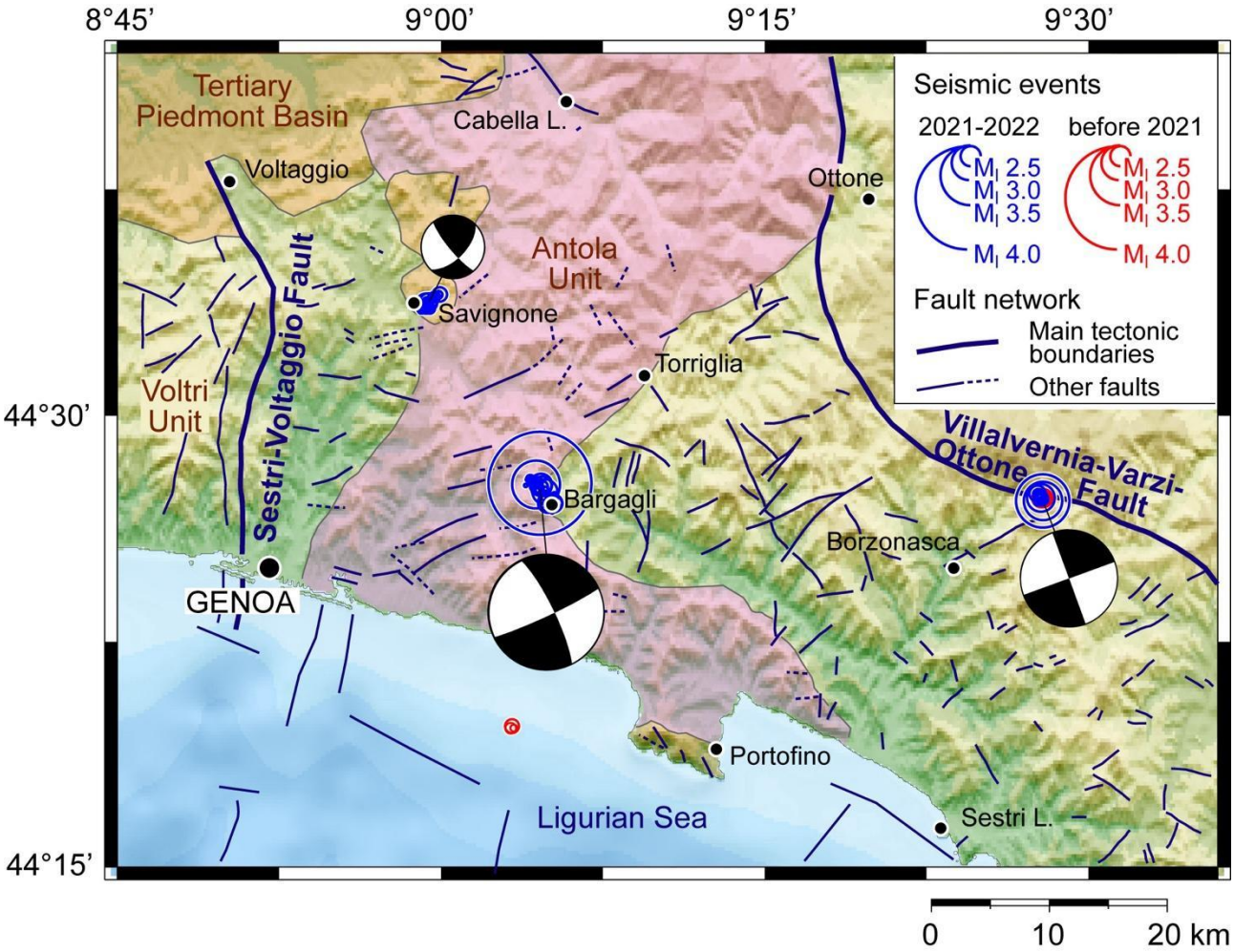

Fig. 2 – Hypo-DD locations of the earthquakes analysed in this study. The focal mechanisms of the main event of the three sequences (Savignone, Borzonasca and Bargagli) are strike-slip. Modified from Eva et al., 2023.

The Bargagli seismic sequence may reflect the formation of new NNW-SSE strike-slip faults in the upper crust that are more suitably oriented to accommodate the present-day stress field, consistent with the seismotectonic framework outlined by recent works in the nearby regions of the Adria-Europe plate-boundary zone (Eva et al., 2020). Our results highlight the important role of strike-slip faulting in the Adria-Europe plate boundary zone not only in the past, but also during its present-day evolution.

Low seismicity areas are often neglected due to the small size of the faults generating low magnitude events. However, our study shows that such areas may contribute to the understanding of the geodynamic evolution putting “a dowel in a larger puzzle”.

References

Eva, E., Malusà, M.G., Solarino, S.; 2020: Seismotectonics at the transition between opposite-dipping slabs (western Alpine region). Tectonics 39. https://doi.org/10.1029/2020TC006086 e2020TC006086.

Eva E., Malusà M.G., Solarino S.; 2023: The 2021–2022 Genoa seismic sequences reveal distributed strike-slip deformation in the Alps-Apennines transition zone, NW Italy Tectonophysics 868. https://doi.org/10.1016/j.tecto.2023.230101.

Solarino, S., Eva, E.; 2023: Il terremoto del settembre 1924 in mar Ligure e la sua relazione con il recente evento sismico a Bargagli (Genova, settembre 2022). Quad. Geofis. 184, 1–24. https://doi.org/10.13127/qdg/184.

Waldhauser, F., Ellsworth, W.L.; 2000: A double-difference earthquake location algorithm: Method and application to the northern Hayward fault, California. Bull. Geol. Soc. Am. 90 (6), 1353–1368. https://doi.org/10.1785/0120000006.

Corresponding author: elena.eva@ingv.it

Single-station ambient noise measurements to detect faults below the ground surface in the Fucino basin.

D. Famiani[1], F. Cara[1], G. Di Giulio[2], M. Vassallo[2], G. Milana[1]

[1] *Istituto Nazionale di Geofisica e Vulcanologia, Rome, Italy.*
[2] *Istituto Nazionale di Geofisica e Vulcanologia, L'Aquila, Italy.*

Microzonation studies generally focus their attention to the characterization of urban areas distinguishing stable zones from those prone to seismic amplification or unstable in general, including also those related to the presence of faults. In order to face this last task, the classical approach in the first-level of microzonation studies is based on geological evidence and information coming from previous studies which allows us to hypothesize the location of the seismic fault line. However, geological evidence or previous studies are often missing but there may be clues of the presence of hidden active faults that it is important to define for urban development or assessment. In all cases, the exact localization of the fault traces is preliminary to perform reflection profiles and seismic trenches to establish whether the faults are active or not.

In this study, we propose and illustrate a procedure that we applied in the Fucino basin (Central Italy) and that has been published in Famiani *et al.* (2022). The procedure is based on single-station microtremor recordings. In particular, in Famiani *et al.* (2022) we performed 88 single-station ambient noise measurements (Fig. 1) and used the horizontal-to-vertical spectral ratio (HVNSR) technique to investigate hidden faults in the Trasacco municipality located in the southern part of the Fucino basin, where microzonation studies pointed out hypothetical fault lines crossing the urban area with the Apennine orientation. The noise survey consisted of two steps: first, the measurement points were set in a regular grid geometry; second, we individuated areas where increasing the spatial density of measurements.

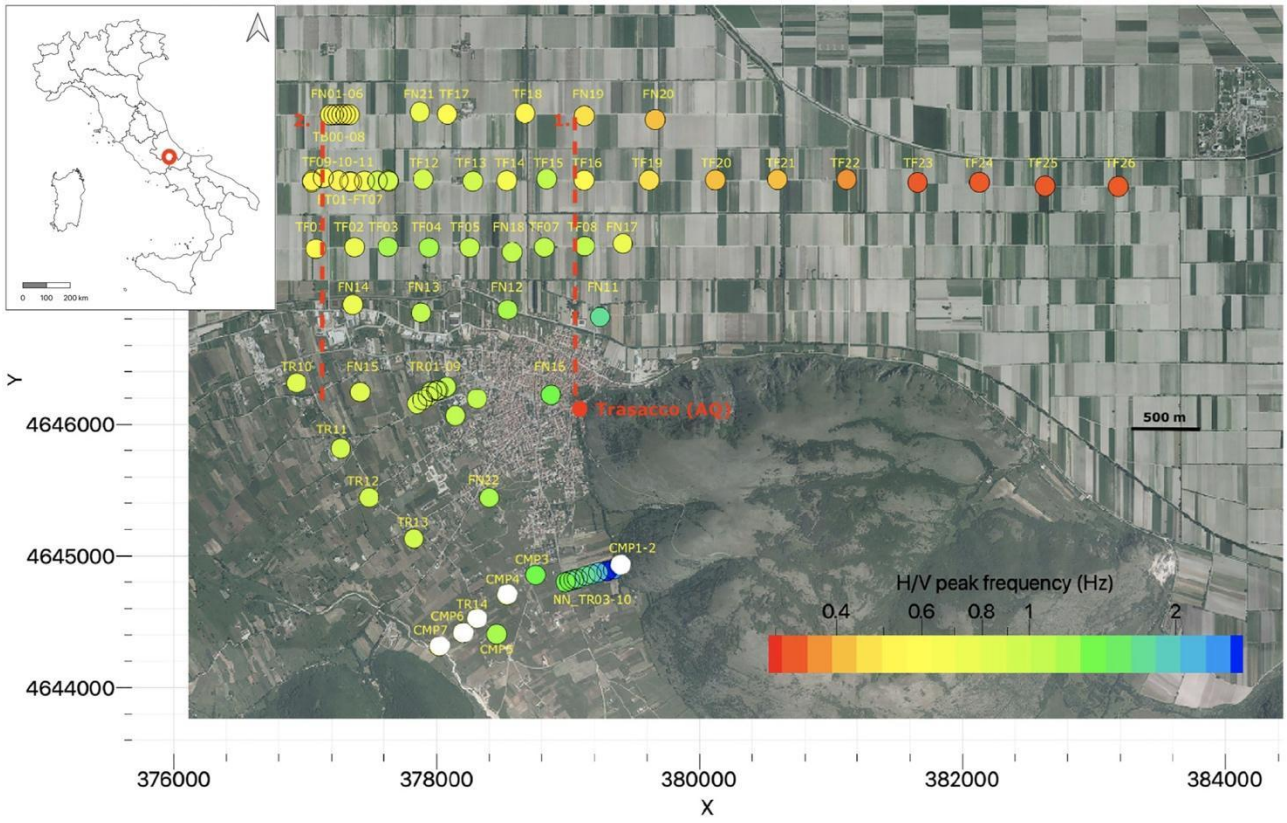

Fig. 1 - f0 results of the 88 HVNSR performed in the Trasacco municipality (modified from Famiani et al. 2022). The trend of the results suggests a deepening of the Quaternary Fucino basin towards east and the presence of a horst structure included between Section 1 and 2 in red dashed lines.

Results of HVNSR for all the measurements highlighted spatial variation of f0 along some transects (Fig. 1) which could also be represented in contour plots (Fig. 2) remarking similar trends of the interpreted seismic lines in Patruno and Scisciani (2021). In consideration of the availability of seismic stations, sometimes it was possible to perform several simultaneous recordings: in these cases the noise surveys acted as seismic arrays. It was then possible also to retrieve the dispersion characteristics of the surface waves, in this case using cross-correlation (CC) and FK analyses.

For some sites with nearby borehole log data availability, the HVNSR curves were inverted around the fundamental resonance (f0) using the aforementioned dispersion curves as constraints. This analysis allowed us to reconstruct some 1D shear wave velocity profiles and interpret results in terms of subsoil setting of geological features. Finally, we performed a rotational analysis of HVNSR for some specific transects of stations, highlighting localized polarization effects that we interpreted as due to the presence of the hidden fault in those positions. This interpretation was supported by available seismic reflection profiles for the area. This case study shows that the low-cost HVNSR technique is able to give preliminary indications of anomalous behaviors when crossing fault lines (Fig. 2).

These results are important for planning specific geophysical surveys, requested to validate the preliminary findings. Therefore, our approach can support microzonation studies, especially in urban areas where fault zones are involved, or in places designated for future developments.

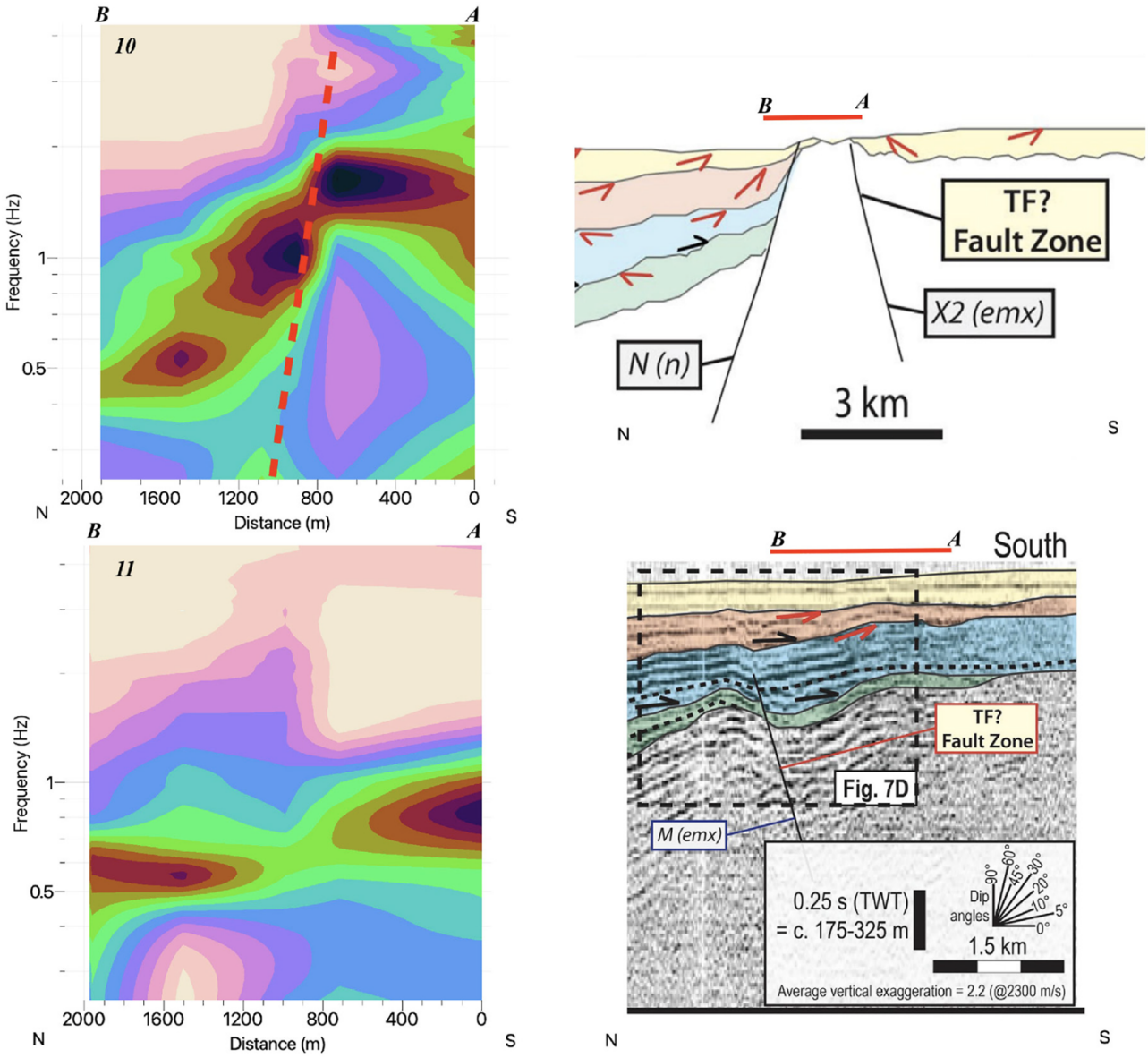

Fig. 2 - Example of HVNSR contour plots of Section 1 and 2 (see Fig. 1 for position) located along seismic lines interpreted in Patruno and Scisciani (2021) (from Famiani et al. 2022).

References

Famiani D., Cara F., Di Giulio G., Vassallo M. and Milana G.; 2022: *Detection of hidden faults within the Fucino basin from single-station ambient noise measurements: The case study of the Trasacco fault system*. Frontiers in Earth Science, 10, p.937848.

Patruno S. and Scisciani V.; 2021: *Testing normal fault growth models by seismic stratigraphic architecture: The case of the Pliocene-Quaternary Fucino Basin (Central Apennines, Italy)*. Basin Research, 33(3), pp.2118-2156.

Corresponding author: daniela.famiani@ingv.it

Early results of a systematic revision of Ferrarese seismicity of the 13th-15th centuries.

A. Faoro[1], R. Camassi[1], V. Castelli[2]

[1] Istituto Nazionale di Geofisica e Vulcanologia - Sezione di Bologna, Bologna, Italy,
[2]Istituto Nazionale di Geofisica e Vulcanologia - Sezione di Bologna, Bologna/Ancona, Italy

Within the PRIN 2020 project NASHA4SHA [Fault segmentation and seismotectonics of active thrust systems: the Northern Apennines and Southern Alps laboratories for new Seismic Hazard Assessments in northern Italy] and in order to improve our general knowledge of the seismic record of the Ferrara area, we are proceeding to examine the ancient local narrative sources, not only to find information on “unknown” or “forgotten" earthquakes, but primarily to improve the understanding of earthquakes already known through a comprehensive study of the original texts which are relied on by the reference studies of the CPTI15 catalogue (Rovida et al., 2022).

Far from limiting ourselves to searching for “earthquake news” and taking them out of context, as we tended to do in the "heroic" days at the dawn of modern historical seismology, we attempted here a more ambitious undertaking. Our aim is to examine original earthquake news in their cultural framework, to check their intrinsic quality and "authoritativeness", and thus to improve the quality of general knowledge on historical earthquake observations. Using data extrapolated from narrative written sources (such as chronicles and annals) to compile earthquake catalogues sometimes risks isolating the data themselves and undermining their evaluation. Indeed, news taken out of the context that reports them, while useful in itself, remain impoverished, like archaeological findings whose site, location and circumstances of discovery are unknown.

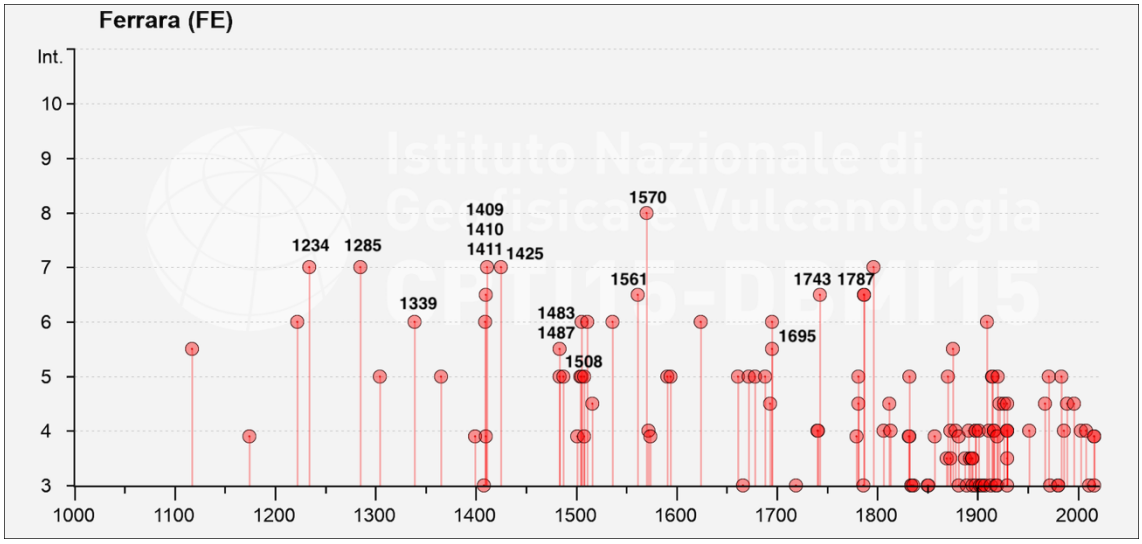

Fig. 1 – Seismic history of Ferrara (1000-2020) from Locati et al. (2022). The dated earthquakes are local ones (i.e. with epicentral location "in" Ferrara or in the "Ferrarese").

Up to now our study has considered some dozen earthquakes with M ≥3.5, dated between 1234 and 1495, of which 11 are located by the CPTI15 catalogue (Rovida et al., 2022) in Ferrara, 3 in Modena, while a couple of cases are unknown to the CPTI15 catalogue. A couple of these earthquakes were never studied at all, in several cases epicentral parameters are derived from reference studies that are almost 20 years old, and in 5 cases even 40 years old. The informative basis for these earthquakes, as summarized in Locati et al. (2022) and Rovida et al. (2022) is rather poor. In many case information on a single locality is available from a single source, whose intrinsic value and reliability are also questionable.

The preliminary results of the revision work are generally an improvement of the intensity estimates. In a few cases, the studied earthquakes turned out to be doubtful or completely fake.

Year	Mo	Da	Ho	Mi	Ax	Ref	**Np**	Imx	Mw	NOTE Prel.
1234	03	20			Ferrara	ENEL85	5	7	5,14	Doubtful
1249	09				Modena	GUAL07	4	7-8	4,93	i.p.
1285	12	13			Ferrara	ENEL85	2	7	5,14	Doubtful
1339	11	16	14	10	Ferrara	GUAL07	1	6	4,72	Doubtful
1346	02	08			Modena	GUAL07	1	5	4,16	i.p.
1379	02	10			Ferrara	-	-	-	-	i.p.
1409	08	17	00	35	Ferrara	GUAL07	1	6	4,72	Pending revision
1410	05	09	22	30	Ferrara	ENEL85	3	6-7	4,93	Doubtful
1411	01	09	02		Ferrara	GUAL07	1	7	5,14	Doubtful
1425	08	10	19		Ferrara	POS85		7	4,72	Pending revision
1474	03	11	20	30	Modena	ENEL85	12	6	4,30	Pending revision
1483	*03*	*03*	*22*		*Ferrara*	*ENEL85*	*1*	*5-6*	*4,51*	Pending revision
1487	01	11	15	40	Ferrara	GUAL07	12	5	3,70	Pending revision
1495	12	5			**Ferrara**	-	-	-	-	Pending revision

Tab. 1 – The list of earthquakes in the Ferrara and Modena currently under revision (time window: 1234-1500; M≥ 3.5).

References

ENEL; 1985: Studi e indagini per l'accertamento della idoneità tecnica delle aree suscettibili di insediamento di impianti nucleari per le Regioni Piemonte, Lombardia e Puglia: indagini di sismica storica. Rapporti tecnici predisposti da ISMES-SGA, Roma.

Guidoboni E., Ferrari G., Mariotti D., Comastri A., Tarabusi G. and Valensise G.; 2007: Catalogo dei forti terremoti 461 a.C.-1997, http://storing.ingv.it/cfti4med/

Locati M., Camassi R., Rovida A., Ercolani E., Bernardini F., Castelli V., Caracciolo C.H., Tertulliani A., Rossi A., Azzaro R., D'Amico S. and Antonucci A.; 2022: Database Macrosismico Italiano (DBMI15), versione 4.0. Istituto Nazionale di Geofisica e Vulcanologia (INGV). https://doi.org/10.13127/DBMI/DBMI15.4

Postpischl D.; 1985: Catalogo dei terremoti italiani dall'anno 1000 al 1980. Progetto Finalizzato Geodinamica. "Quaderni de «La Ricerca Scientifica»", n.114, v.2B.

Rovida A., Locati M., Camassi R., Lolli B., Gasperini P., Antonucci A; 2022: *Catalogo Parametrico dei Terremoti Italiani (CPTI15), versione 4.0*. Istituto Nazionale di Geofisica e Vulcanologia (INGV). https://doi.org/10.13127/CPTI/CPTI15.4

Corresponding author: andrea.faoro@ingv.it

A re-analysis of micro-earthquakes for characterising debated faults in the Esaro valley (Northern Calabria)

H. Fernandez[1,2], G. D. Chiappetta[1], A. Schibuola[1,3], M. La Rocca[4], S. Gentili[1], L. Peruzza[1]

[1] *OGS, Trieste, Italy*
[2] *Università degli Studi "G. d'Annunzio" Chieti - Pescara, Italy*
[3] *Université Gustave Eiffel, Marne-la-vallée, France*
[4] *Università della Calabria, Italy*

The study takes place in the northern part of Calabria, Italy, where a potentially active and capable fault is mapped across the Farneto del Principe's dam, on the Esaro river. A complex set of geological, geophysical and seismological studies performed jointly by the University of Chieti-Pescara (INGEO) and the Istituto Nazionale di Oceanografia e di Geofisica Sperimentale (OGS) are ongoing to estimate the fault seismic activity and its potential surface displacement during major earthquakes.

Our study area lies on the Calabrian Arc that represents the emerging part of the Calabrian accretionary wedge. This region is one of the most seismic-active regions in Italy, with some earthquakes with M ≈ 7.0 (e.g. Feb 1783, *Jacques et al., 2001*). The Esaro valley is located in the Crati Basin in which we find several west-dipping faults with a N-S strike like the Roggiano Fault and the Firmo Fault. As it is reported in the ITHACA database, the Firmo Fault is 16.2 km long, and its surface expression might be crossing the Farneto del Principe's dam but its position, behaviour and activity are debated in the literature. To fill this lack of information and provide more details about the fault, a multidisciplinary study started in 2022, funded by the *Consorzio di Bonifica integrale dei Bacini Settentrionali del Cosentino* .

The historical seismicity around the dam, analysed by mainly 2 historical databases (CPTI15 and ASMI) shows that the 20 km area around the dam seems to be affected only by superficial and moderate earthquakes (M < 5.5); a stronger but more distant earthquake occurred in 1184 earthquake, in the Crati valley, M≈7. Concerning the instrumental seismicity, we collected and compared data from 2 different catalogues: INGV catalogue (1985-2023, 5 events with M > 3.5) and the University of Calabria catalogue (May 2013-Dec 2023, 0 event with M > 3.5). In these 2 datasets, we can notice that events are less frequent in the closest area around the dam; conversely, there is a concentration of shallow events (~10 km deep) in the North (Pollino area) and in the South-East. Furthermore, we find deeper events (> 30 km deep) that are related to the subduction zone, on the west.

As our main goal is to obtain information about the seismicity and the seismic activity of the faults in the surroundings of the Farneto del Principe' dam, we will focus only on events within a constrained area around the dam (Fig. 1). We remove the deep events as they are not related to the same tectonic context of the fault system we are interested in. These criteria give us a list of about 150 events (Fig. 1).

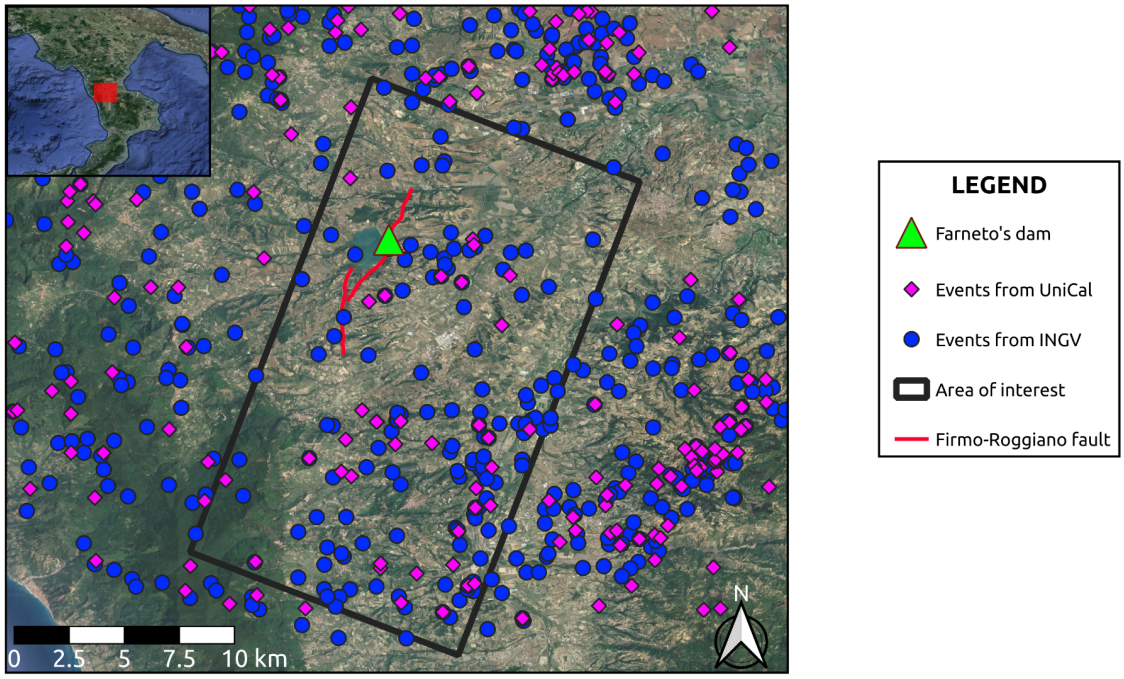

Fig. 1 - Seismic activity on the Esaro valley, Northern Calabria, Italy (1985-2023)

One of the main problems for using different catalogues is that the same event can have a slightly different localisation depending on the catalogue. Since we are studying a very local area, we need to harmonise our list and have the most precise location as possible for each event. Thus, we collect waveforms from the University of Calabria' network, for every event in our new dataset. This will allow us to do, for each station and event, a re-picking of the P- and S- phases, in order to perform a uniform re-localisation of our selected earthquakes.

The re-localisation process is ongoing and is carried out using different codes: Hypo71 (*Lee et al., 1972*), HypoEllipse (*Lahr, 2012*) and Hyposat (*Schweitzer, 2001*). First results show that a small part of the re-localised events has now migrated out of the area of interest, mainly on the west and the northeastern sides. Another interesting feature is a kind of clustering with an E-W trend and 5-20 km deep, just eastwards of the dam.

In our study area, we only have earthquakes with small magnitudes (maximum M≈3) so the focal mechanisms were not released by the national and international agencies. We can now analyse our re-localised events to have indications about the stress regime and the kinematics of the fault.

References

Jacques E.; 2001: Faulting and earthquake triggering during the 1783 Calabria seismic sequence. Geophysical Journal International, Volume 147, Issue 3, December 2001, Pages 499–516.

Lahr J.C.; 1999, revised 2012: HYPOELLIPSE: a computer program for determining local earthquake hypocentral parameters, magnitude, and first-motion pattern: U.S. Geological Survey Open-File Report 99–23, version 1.1, 119 p.

Lee W.H.K., Lahr J.C.; 1972: HYPO71: A computer program for determining hypocenter, magnitude, and first motion pattern of local earthquakes (p. 100). US Department of the Interior, Geological Survey, National Center for Earthquake Research.

Schweitzer J. 2001: HYPOSAT - An enhanced routine to locate seismic events. Pure and Applied Geophysics.

Corresponding author: hfernandez@ogs.it

High-resolution seismic depth imaging challenges across the 1980 (Ms 6.9) Southern Italy earthquake fault scarp at Pantano di S. Gregorio Magno (SA)

G. Ferrara[1], P.P. Bruno[1,2], L. Improta[2]

[1] Dipartimento di Scienze della Terra, dell'Ambiente e delle Risorse, Università degli studi di Napoli 'Federico II', Napoli, Italy
[2] Istituto Nazionale di Geofisica e Vulcanologia, Roma, Italy

In this study, we present initial findings and interpretations derived from an high-resolution seismic dataset, both 3D and 2D, obtained at Pantano di San Gregorio Magno (SA). The data were collected during two field surveys, one in 2005 (the majority of the 2D lines, as detailed in Bruno et al., 2010) and another in 2022, as part of the TESIRA project (i.e., TEst Site IRpinia fAult; Bruno et al., 2023), a collaborative effort involving Istituto Nazionale di Geofisica e Vulcanologia (INGV) and Consiglio Nazionale delle Ricerche (CNR). The seismic surveys focused on the imaging of the basin across a surface scarp resulting from the Ms 6.9, 1980 Irpinia earthquake (Pantosti & Valensise, 1990).

Notably, pre-stack depth migration (PSDM: see Yilmaz, 2001) is crucial for improving the accuracy of shallow seismic reflection images and the measured velocity distribution before stacking, particularly in the presence of complex near-surface conditions (Bradford et al., 2006). However, a comprehensive understanding of the p-wave velocity distribution in the subsurface is crucial for this purpose. In this context, the efficacy of pre-stack migration combined with full-waveform inversion could prove crucial in providing information to iteratively enhance the velocity model and the associated seismic imaging of this complex environment.

We show here the preliminary depth images resulting from pre-stack and post-stack depth migration of the 2D profiles and 3D volume. To enhance PSDM imaging through the refinement of the velocity model, we employed two distinct approaches within SeisSpace ProMAX®: the layer stripping method and the Deregowsky method. Both techniques utilize the Residual Move-Out (RMO) values picked from common image points. In certain instances, PSDM proved effective in enhancing depth image quality compared to post-stack data. Conversely, due to the intricate near-surface conditions characterized by substantial lateral velocity variations, post-stack migration outperformed PSDM in some cases. This implies that our assessment of the background velocity model remains inaccurate.

Even in this early phase of depth imaging, all seismic profiles and the volume clearly depict the intricate splays associated with the 1980 Irpinia fault and its connections to other active segments of the Pantano San Gregorio Magno fault system. The tectonic influence of these faults on basin development and sedimentation is also evident.

References

Bradford, J.H., Liberty, L.M., Lyle, M.W., Clement, W.P., and Hess, S., 2006 Imaging complex structure in shallow seismic-reflection data using prestack depth migration, Geophysics, 71, 6, b175–b181.

Bruno, P.P.G.; Castiello, A.; Improta, L., 2010, Ultrashallow seismic imaging of the causative fault of the 1980, M6. 9, southern Italy earthquake by pre-stack depth migration of dense wide-aperture data. Geophys. Res. Lett., 37.

Bruno, P.P.G., Ferrara, G., Improta, L., Maraio, S., Di Fiore, V., Iacopini, D., Fusco, M., Punzo, M., Paoletti, V., Cavuoto, G., and De Martini, P.M., 2023, High-resolution 3-D geophysical imaging across a seismogenic fault: the TEst Site IRpinia fAult (TESIRA) project, EGU General Assembly 2023, Vienna, Austria, 23–28 Apr 2023, EGU23-11176, https://doi.org/10.5194/egusphere-egu23-11176.

Pantosti, D.; Valensise, G., 1990, Faulting mechanism and complexity of the November 23, 1980, Campania-Lucania earthquake, inferred from surface observations. J. Geophys. Res. Solid Earth, 95, 15319–15341.

Yilmaz, O., 2001, Seismic data analysis (2 volumes), in Investigations in Geophysics; SEG: Tulsa, OK, USA; Volume 10, p. 1000.

Corresponding author: giuseppe.ferrara@unina.it

Linking Seismicity, Geochemical And Environmental Data: The New Frontier Of Multiparametric Networks

E. Ferrari[1], M. Massa[1], A.L. Rizzo[2,1], S. Lovati[1], F. Di Michele[1]

[1] National Institute of Geophysics and Volcanology (INGV), Milano, Italy
[2] Department of Earth and Environmental Sciences, University of Milano-Bicocca, Milano, Italy

Nowadays increasingly consciousness on the interaction between tectonics and crustal fluids dynamics is lacking simultaneous monitoring of the relative key factors. Changes in water chemistry and levels, spring discharges, soil flux regimes (e.g., CO_2, CH_4, radon) and compositions of dissolved gases in water are well documented in the literature (e.g., Italiano et al., 2001, 2004; Wang and Manga, 2021; Chiodini et al., 2020; Gori and Barberio, 2022 and references therein), as being pre-, co- and post-seismic modifications as well as being markers of the local tectonic stress acting in the crust. However, geological differences among sites require specific knowledge of crustal fluids response to seismicity.

For this purpose, multiparametric stations have been set up starting from the end of 2021 and equipped with: (i) sensors installed in water wells measuring water level, temperature, and electrical conductivity; (ii) meteorological sensors measuring atmospheric pressure, temperature, rain, humidity, wind speed and direction; (iii) seismic sensors providing accelerometric and velocimetric datasets; (iv) radon sensors; (v) CO_2 soil flux chamber. Stations are placed on the major seismogenic structures and are widely distributed among the Alps, Apennines and Pianura Padana. Our new multiparametric network is aimed to address this point and, to the best of our knowledge, it is the first network developed in Italy under this philosophy.

Data are transmitted in near real-time to an *ad hoc* developed dynamic relational database and displayed in a dedicated website. The built-in philosophy is to easily compare distinct parameters from the various sensors and possibly recognize cause-effect relationships among them.

A statistic approach is also applied to the time-series to investigate intra-annual and inter-annual trends and correlations among different parameters. Alternative methods (e.g., signal decomposition, spike detection) will be presented and discussed.

References

Chiodini G., Cardellini C., Di Luccio F., Selva J., Frondini F., Caliro S., Rosiello A., Beddini G., Ventura G., 2020: Correlation between tectonic CO_2 Earth degassing and seismicity is revealed by a 10-year record in the Apennines, Italy. Science Advances, https://www.science.org/doi/10.1126/sciadv.abc2938

Gori F., Barberio M.D., 2022: Hydrogeochemical changes before and during the 2019 Benevento seismic swarm in central-southern Italy. Journal of Hydrology, 604:127250

Italiano F., Martinelli G., Nuccio P.M., 2001: Anomalies of mantle-derived helium during the 1997 – 1998 seismic swarm of Umbria-Marche, Italy. Geophysical Research Letters, 28(5):839-842

Italiano F., Martinelli G., Rizzo A., 2004: Geochemical evidence of seismogenic-induced anomalies in the dissolved gases of thermal waters: A case study of Umbria (Central Apennines, Italy) both during and after the 1997–1998 seismic swarm. Geochemistry, Geophysics, Geosystems, 5:11, doi:10.1029/2004GC000720

Wang C.-Y., Manga M., 2021: Water and Earthquakes. Lecture Notes in Earth System Sciences, Springer Cham, 387 pp., https://doi.org/10.1007/978-3-030-64308-9

Corresponding author: elisa.ferrari@ingv.it

OTRIONS seismic network after ten years of operation: the new seismic catalog

A. Ferreri[1], A. Romeo[2], R. Giannuzzi[1], G. Cecere[2], S. de Lorenzo[1], L. Falco[2], M. Filippucci[1,2], M. Michele[2], G. Selvaggi[2], A. Tallarico[1,2]

[1] Dipartimento di Scienze della Terra e Geoambientali, Università degli Studi di Bari Aldo Moro, Bari, Italy
[2]Istituto Nazionale di Geofisica e Vulcanologia, Italy

The OTRIONS seismic network (FDSN network code OT) is a local network installed in the Apulia region (Southern Italy) with the aim of monitoring the seismicity of the Gargano area (Northern Apulia) and the Salento area (Southern Apulia). The OT network is managed by the University of Bari Aldo Moro (UniBa) and by the National Institute of Geophysics and Volcanology (INGV). It started to operate in 2013 and in 2019 the recording stations migrated to EIDA (all details can be found in Filippucci et al., 2021a). In 2021 a first database was collected, with the event detection achieved both manually and automatically with SeisComP3 (Helmholtz-Centre Potsdam), and was released (Filippucci et al., 2021a; Filippucci et al., 2021b).

After ten years of operations, we focus on the microseismicity of the Gargano area with the aim of collecting a new seismic database for the period from April 2013 to December 2022, by using a recently acquired software, CASP (Complete Automatic Seismic Processor), for the automatic detection, picking and location of seismic events (Scafidi et al., 2019). The CASP software is installed on a remote server implemented by RECAS-Bari, the computational infrastructure of INFN and UniBa.

Through an appropriate parameter setting, we adapted CASP and NonLinLoc (Lomax et al., 2000) to the Gargano area and to the seismic stations available, both OT and INGV permanent seismic networks. We used the 1D velocity model of Gargano developed by de Lorenzo et al., (2017).

The recorded seismic events were organized in two catalogs: the first one is the automatic catalog, obtained from the automatic locations of CASP; the second one is the manual catalog, obtained through a manual revision of P and S waves arrival times. To evaluate the reliability of CASP, a comparison between the automatic and manual catalog was performed.

From a comparison of the manual catalog with the already released catalog of the Gargano seismicity (Filippucci et al., 2021b), the number of events detected by CASP increased a lot. Furthermore, the results show that the choice of the CASP parameters allows us to lower the minimum magnitude threshold of the recorded microseismicity in the Gargano area. Preliminary analysis of the earthquake's foci shows that the seismicity pattern retrace, substantially, the same discussed in the work of Miccolis et al., (2021).

References

de Lorenzo S., Michele M., Emolo A., and Tallarico A.; 2017: *A 1D P-wave velocity model of the Gargano promontory (southeastern Italy)*. J. Seismol., 21 (4), 909–919, doi:10.1007/s10950-017-9643-7

Filippucci M., Miccolis S., Castagnozzi A., Cecere G., de Lorenzo S., Donvito G. and Tallarico A.; 2021a: *Seismicity of the Gargano promontory (Southern Italy) after 7 years of local seismic network operation: Data release of waveforms from 2013 to 2018*. Data in brief, 35, 106783, https://doi.org/10.1016/j.dib.2021.106783

Filippucci M., Miccolis S., Castagnozzi A., Cecere G., de LorenzoS., Donvito G., Falco L., Michele M., Nicotri S., Romeo A., Selvaggi G. and Tallarico A.; 2021b: *Gargano Promontory (Italy) microseismicity (2013-2018): waveform data and earthquake catalogue*. Mendeley Data, V3, doi: 10.17632/7b5mmdjpt3.3

Helmholtz-Centre Potsdam - GFZ German Research Centre for Geosciences and gempa GmbH (2008). The SeisComP seismological software package. GFZ Data Services. doi: 10.5880/GFZ.2.4.2020.003.

Lomax A., Virieux J., Volant P. and Berge-Thierry C.; 2000: *Probabilistic Earthquake Location in 3D and Layered Models*. In: Thurber C.H., Rabinowitz N. (eds) Advances in Seismic Event Location. Modern Approaches in Geophysics, vol 18. Springer, Dordrecht. https://doi.org/10.1007/978-94-015-9536-0_5.

Miccolis S., Filippucci M., de Lorenzo S., Frepoli A., Pierri P., and Tallarico A.; 2021: *Seismogenic Structure Orientation and Stress Field of the Gargano Promontory (Southern Italy) From Microseismicity Analysis*. Front. Earth Sci., Sec. Structural Geology and Tectonics, Volume 9, doi: 10.3389/feart.2021.589332

Scafidi D., Spallarossa D., Ferretti G., Barani S., Castello B., and Margheriti L.; 2019: *A complete automatic procedure to compile reliable seismic catalogs and travel-time and strong-motion parameters datasets.* Seismological Research Letters, 90(3), 1308-1317, doi: 10.1785/0220180257

University of Bari Aldo Moro. (2013). OTRIONS [Data set]. International Federation of Digital Seismograph Networks. https://doi.org/10.7914/SN/OT

Corresponding author: Andrea Pio Ferreri (andrea.ferreri@uniba.it)

Monitoring tectonic environments with DAS: the case study of the Irpinia Near Fault Observatory

G. Festa[1,2], C. Strumia[1], F. Scotto di Uccio[1], A. Trabattoni[3]

[1]Department of Physics 'Ettore Pancini', University of Napoli Federico II, Italy.
[2]Istituto Nazionale di Geofisica e Vulcanologia, Italy.
[3]Université Côte d'Azur, Observatoire de la Côte d'Azur, CNRS, IRD, Géoazur, France.

DAS systems are interrogators connected to a termination of a fiber optic dark cable, that sense the fiber by sending a laser pulse and recovering the back-scattered light. When the fiber is at rest, the pattern of the light is the same after each pulse; during the occurrence of an earthquake, because of the deformation of the cable, the backscattered light changes its pattern and the resulting phase difference can be connected with the strain rate along the direction of the cable (Hartog, 2017). Thus, interferometric analysis provides time series with spatial sampling along the fiber even of few meters, making the DAS recording similar to seismic arrays, with the main advantages of being cheaper, easier to plugin into available dark fibers, and working in harsh environments, such as at the seafloor or in volcanic areas (e.g., Sladen et al., 2019; Currenti et al., 2021). On the other hand, DAS systems collect a huge amount of data that require proper management and advanced processing tools.

We tested the DAS system along a short cable in the Irpinia Near Fault Observatory (INFO), an on-field laboratory of 31 seismic stations that monitors the seismicity along the Campania-Lucania Apennines (Iannaccone et al., 2010; Chiaraluce et al., 2022), across the fault system that generated the 1980, M 6.9 Irpinia earthquake. INFO has been operational in the last 15 years and has recorded more than 3000 earthquakes, with magnitude of completeness of 1.1 (Vassallo et al., 2011). We performed a DAS survey lasting 5 months along a 1.1 km-long fiber, buried in a dry lake at depths ranging from 30 cm to 1.5m, collecting continuous strain rate data at a spatial sampling of 2.4 m and sampling frequency of 200 Hz. The system recorded several earthquakes spanning different magnitude and location, providing an initial dataset to investigate DAS records and related source parameters (Trabattoni et al., 2022). This experiment also provided the basis for the future installation of a long-term monitoring system, grounded on 3 DAS interrogating fibers of different extent across the near-fault observatory.

Seismic phases related to earthquakes were analyzed with the help of seismic refraction experiments and numerical simulations. In this particular context, DAS records appear to be mainly sensitive to waves guided horizontally by the low-velocity structure beneath the site. Because of the near-to-vertical incidence of waves, seismograms appear to be depleted of P waves, and dominated by low velocity S and surface waves. Moreover, the wave pattern is similar for all

earthquakes irrespective of the event azimuth, due to the high velocity contrast between the bedrock and the basin, the main difference being in the P to S differential time owing to the distance between the fiber and the event hypocenter. The high impedance contrast at the base of the dry lake leads to considerable site amplification and allows to detect local microearthquakes without stacking.

We developed an integral approach for converting strain-rate data into kinematic quantities (Trabattoni et al., 2023), based on moving average filters, that allows retrieving the high-pass displacement from DAS records. Using converted data, we performed automatic arrival phase identification using ML based detectors (e.g., EQTransformer, Mousavi et al., 2020; PhaseNet, Zhu et al., 2019). We found phase picking consistent with manual measurements, and an enhanced sensitivity when compared to strain rate data, in terms of number and quality of picks. This approach also enables for event detection when information is integrated across the whole fiber.

We used displacement converted data for local magnitude (ML) computation. The final magnitude was estimated as the median value of the ML distribution at all the usable channels, while uncertainties have been quantified by the standard median absolute deviation (SMAD). Magnitude estimates provided by the DAS are compatible with those computed from the INFO network showing that using DAS recovered velocity enables simple and accurate ML estimation.

We also investigated the correlation between the elastic energy release rate estimated at the fiber and the kinetic energy release rate from the closest station (< 2 km) and we used this scaling to retrieve the energy magnitude from the integral of elastic energy. We found that our observations are compatible with the detection threshold as a function of the distance associated with the signal to noise level of the DAS recordings. Finally, we evaluated seismic moment and source size by inverting the spectral amplitude of DAS records, after removal of site effects, according to the Anderson and Hough (1984) model.

In conclusion, this workflow enables for automatic event detection and characterization from DAS records, even in presence of longer cables and larger bunches of data.

References

Anderson, J. G., Hough, S. E.; 1984: A model for the shape of the Fourier amplitude spectrum of acceleration at high frequencies, *Bulletin of the Seismological Society of America*, 74(5), 1969-1993.

Chiaraluce, L., Festa, G., Bernard, P., Caracausi, A., Carluccio, I., Clinton, J., et al.; 2022: the near fault observatory community in Europe: A new resource for faulting and hazard studies, *Annals of Geophysics*, 65(3), DM316. https://doi.org/10.4401/ag-8778.

Currenti, G., Jousset, P., Napoli, R., Krawczyk, C., & Weber, M.; 2021: On the comparison of strain measurements from fibre optics with a dense seismometer array at Etna volcano (Italy), *Solid Earth*, *12*(4), 993–1003. https://doi.org/10.5194/se-12-993-2021

Hartog, H.A.; 2017: An introduction to distributed optical fibre sensors (A. H. Hartog, Ed.). CRC Press.

Iannaccone, G., Zollo, A., Elia, L., Convertito, V., Satriano, C., Martino, C., et al.; 2010: A prototype system for earthquake early-warning and alert management in southern Italy, *Bulletin of Earthquake Engineering*, 8(5), 1105–1129. https://doi.org/10.1007/s10518-009-9131-8.

Mousavi, S. M., Ellsworth, W. L., Zhu, W., Chuang, L. Y., Beroza, G. C.; 2020: Earthquake transformer—an attentive deep-learning model for simultaneous earthquake detection and phase picking, *Nature communications*, 11(1), 3952.

Sladen, A., Rivet, D., Ampuero, J. P., De Barros, L., Hello, Y., Calbris, G., Lamare, P.; 2019: Distributed sensing of earthquakes and ocean-solid Earth interactions on seafloor telecom cables, *Nature Communications*, 10(1). https://doi.org/10.1038/s41467-019-13793-z.

Trabattoni, A., Festa, G., Longo, R., Bernard, P., Plantier, G., Zollo, A., Strollo, A.; 2022: Microseismicity monitoring and site characterization with distributed acoustic sensing (DAS): The case of the Irpinia fault system (Southern Italy), *Journal of Geophysical Research: Solid Earth*, 127(9), e2022JB024529.

Trabattoni, A., Biagioli, F., Strumia, C., Van Den Ende, M., Scotto Di Uccio, F., Festa, G., Rivet, D., Sladen, A., Ampuero, J. P., Métaxian, J.-P., & Stutzmann, É.; 2023: From strain to displacement: using deformation to enhance distributed acoustic sensing applications, *Geophysical Journal International*, 235(3), 2372–2384. https://doi.org/10.1093/gji/ggad365

Vassallo, M., Festa, G., Bobbio, A.; 2012: Seismic ambient noise analysis in southern Italy, *Bulletin of the Seismological Society of America*, 102(2), 574-586.

Zhu, W., Beroza, G. C.; 2019: PhaseNet: A deep-neural-network-based seismic arrival-time picking method, *Geophysical Journal International*, 216(1), 261-273.

Corresponding author: Gaetano Festa (gaetano.festa@unina.it)

ML *vs* semi-automatic seismic catalogues: the L'Aquila 2009 earthquake sequence example

R. Fonzetti [1, 2], L. Valoroso [1], A. Govoni [1], P. De Gori [1], C. Chiarabba [1]

[1] *Istituto Nazionale di Geofisica e Vulcanologia (INGV), Rome (RM)*
[2] *Università degli Studi Roma Tre , Rome (RM)*

Nowadays the use of neural networks and artificial intelligence in seismology delivers high-resolution seismic catalogues including very small magnitude events that remained undetected by human analysts and standard monitoring room procedures. Here, we test the performance of such ML methods for their reliability in the high-seismic hazard area of the Central Apennines, Italy.
In this work, we apply the QuakeFlow (QF) workflow (Zhu et al., 2023), based on the PhaseNet (Zhu et al., 2019) and GaMMA (Zhu et al., 2022) modules for event detection and association respectively, to the L'Aquila 2009 seismic sequence involving 90 seismic stations and we benchmark our new catalogue against the high-resolution seismic catalogue of Valoroso et al., (2013) that used a semi-automatic procedure including detection and an automatic picking procedure for P and S waves (i.e., Manneken Pix algorithm, Aldersons et al., 2009).
We analysed the earthquakes that occurred during the entire 2009 year and obtained approximately 336,000 events vs the 182,000 from Valoroso et al., (2013) catalogue, obtaining about 85% more earthquakes. Thus, our new catalogue detected 154,452 more events (~ 85%) with respect to the Valoroso et al., (2013) catalogue.
We selected all events having at least 6 P- and 4 S- arrival times (i.e. about 222,000 earthquakes) and we computed 1D-locations using Hypoellipse (Lahr, 1999) with an ad-hoc velocity models for the Central Apennines (Fig. 1). The 1D-locations clearly highlight the geometric characteristics of the seismogenic faults activated during the sequence: the Paganica fault with its set of synthetic and antithetic minor faults (sections 13-19) and the Campotoso fault (sections 1-9). Finally, in the last sections (sections 19-23) a low-angle fault was activated during the sequence.
The comparison with the Valoroso et al., (2013) catalogue was obtained by using only those seismic stations which were in common between the two datasets (purple triangles in Fig. 2) and selecting the common earthquakes (i.e., events having P- and S- waves arrival times at a common station within 2 seconds, Fig. 2a-c). The ML- catalogue presents a larger number of phases with respect to the Valoroso et al., (2013) catalogue and lower GAP (°) values (Fig. 2d).
The application of this new methodology could speed up the time to analyse seismic sequences even in real time. Our findings are expected to help scientists to understand the earthquake generation mechanisms of the 2009 L'Aquila earthquake sequence in terms of nucleation processes, the underlying physical triggering processes leading to a richer aftershock catalogue, and revealing any hidden faults in the vicinity of well-known and mapped structures that remain unseen for the last two decades.

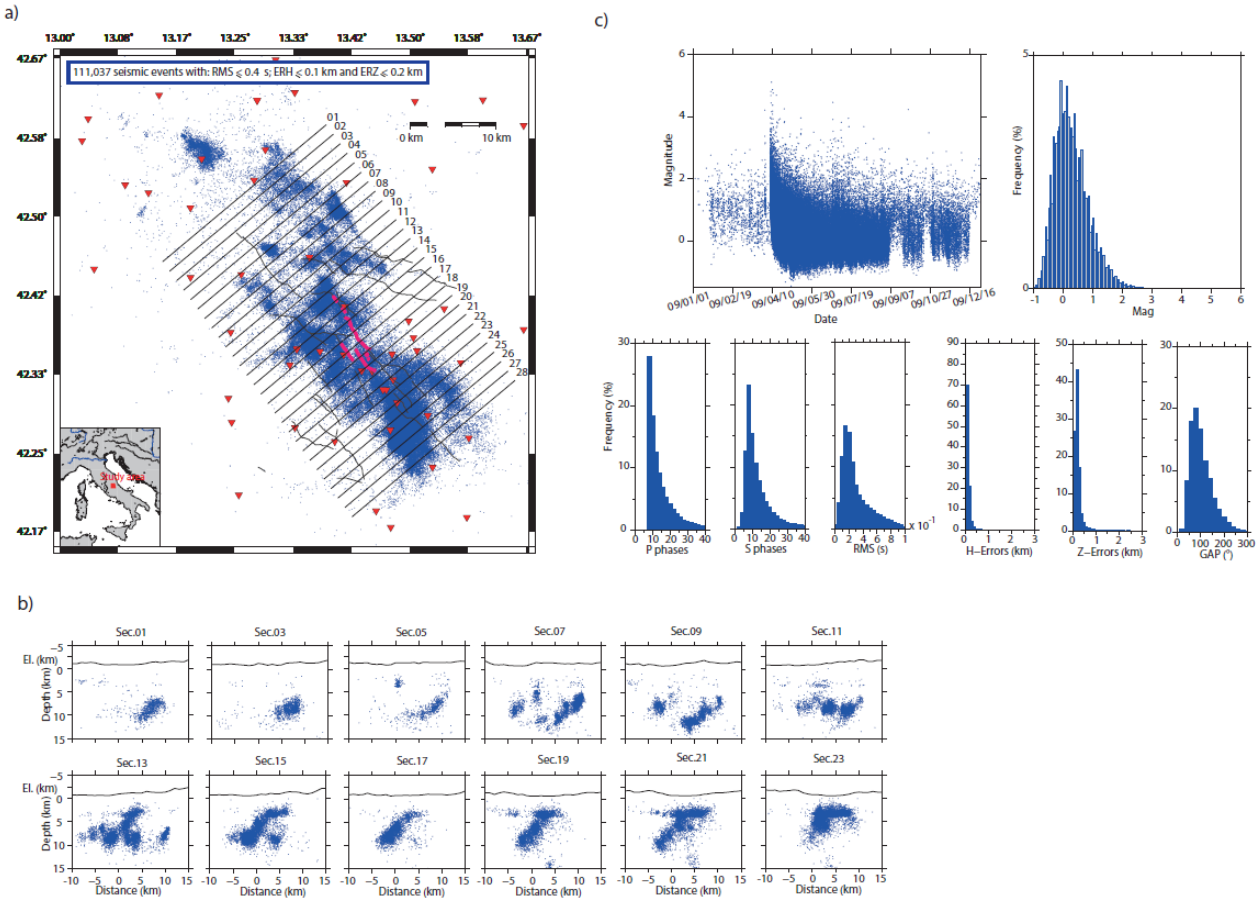

Fig.1 – a) The entire 2009 QF seismicity with at least 6 P- and 4 S arrival times (blue dots) relocated by using Hypoellipse with an optimised 1D-velocity model. The best locations (selecting criteria are specified in the upper left corner of the map) are shown. Red triangles are the seismic stations used by QF for the locations. Dark grey lines represent the main faults of the area. Pink lines are the evidence of surface rupture during the L'Aquila 2009 seismic sequence. Black straight lines are traces of vertical cross sections; b) some of the most interesting vertical sections (strike N°50E) showing the depth distribution of the seismic events occurred within ± 0.8 km distance from the sections; c) above, the magnitude vs time diagram and histogram of magnitude values; bottom) histograms showing the number of P- and S- waves, RMS (s), ERH (km), ERZ (km) and GAP (°).

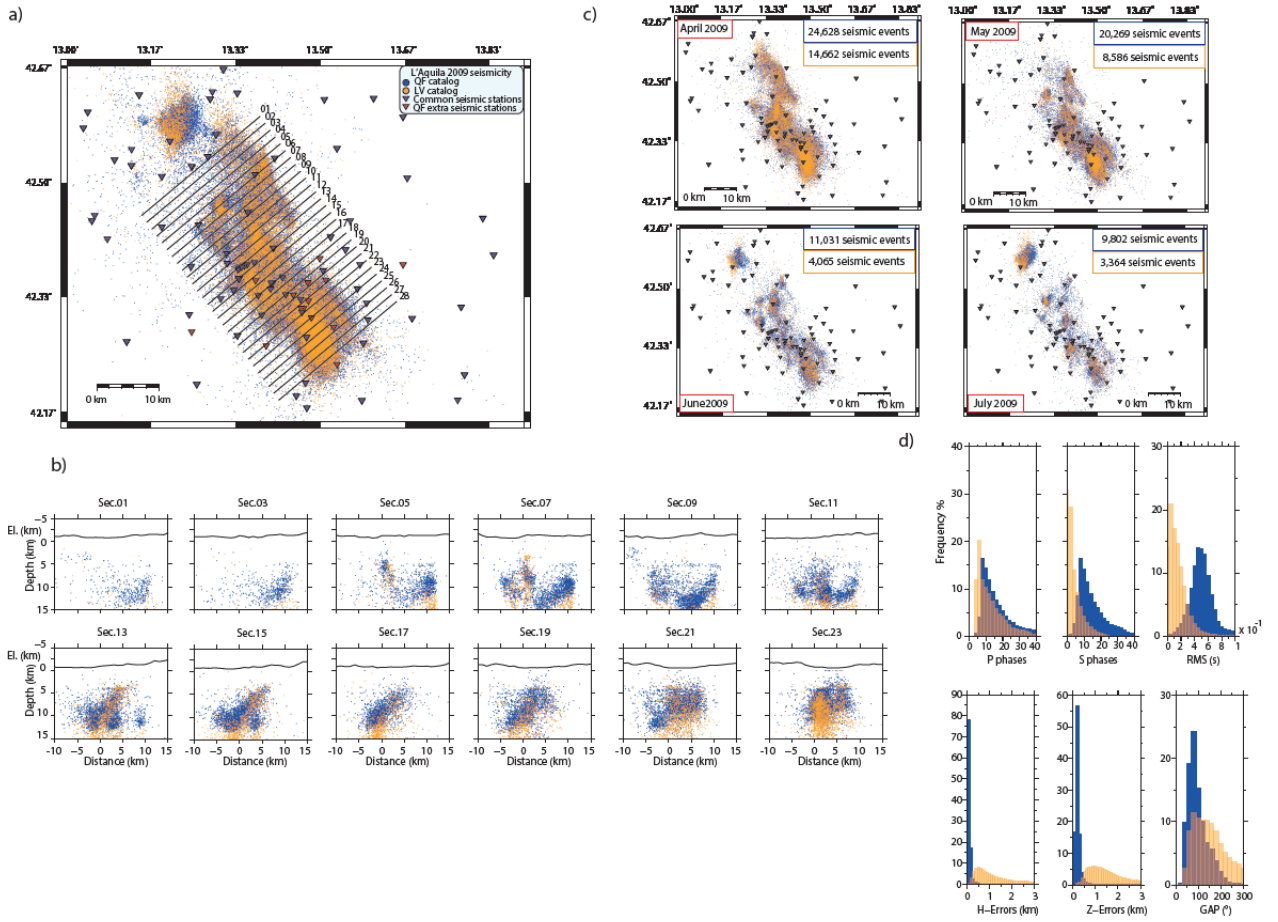

Fig.2 - a) Map view of the common seismic events from QF and Valoroso et al. (2013) catalogues. The best locations (the filters are specified in the boxes) are plotted. The purple triangles are the common seismic stations while the red ones are the extra seismic stations used by QF (not used for the LV processing). The black straight lines are traces of vertical cross sections; b) some of the most interesting vertical sections (strike: N°50E) which show the depth distribution of the seismic events occurring within ± 0.8 km distance from the sections; c) Snap-shot of the seismicity distribution during time (from April to July 2009); d) histograms showing the number of P- and S-waves, RMS (s), ERH (km), ERZ (km) and GAP (°).

References

Aldersons F., Di Stefano R., Chiaraluce L., Piccinini D. and Valoroso L.; (2009). Automatic detection and P- and S-wave picking algorithm: an application to the 2009 L'Aquila (Central Italy) earthquake sequence. http://adsabs.harvard.edu/abs/2009AGUFM.U23B0045A; https://zenodo.org/records/1471534.

Lahr, J. C. (1999). HYPOELLIPSE: A computer program for determining local earthquake hypocentral parameters, magnitude, and first motion pattern (p. 119). Reston, VA: US Geological Survey.

Valoroso, L., Chiaraluce, L., Piccinini, D., Di Stefano, R., Schaff, D., & Waldhauser, F. (2013). Radiography of a normal fault system by 64,000 high-precision earthquake locations: The 2009 L'Aquila (central Italy) case study. Journal of Geophysical Research: Solid Earth, 118(3), 1156-1176.

Valoroso, L., Chiaraluce, L., & Collettini, C. (2014). Earthquakes and fault zone structure. Geology, 42(4), 343-346.

Zhu, W., & Beroza G. B. (2019). PhaseNet: A Deep-Neural-Network-Based Seismic Arrival Time Picking Method. Geophysical Journal International, 216(1), 261-273.

Zhu, W., McBrearty, I. W., Mousavi, S. M., Ellsworth, W. L., & Beroza, G. C. (2022). Earthquake phase association using a Bayesian Gaussian mixture model. Journal of Geophysical Research: Solid Earth, 127(5), e2021JB023249.

Zhu, W., Hou, A. B., Yang, R., Datta, A., Mousavi, S. M., Ellsworth, W. L., & Beroza, G. C. (2023). QuakeFlow: a scalable machine-learning-based earthquake monitoring workflow with cloud computing. Geophysical Journal International, 232(1), 684-693.

Corresponding author: rossella.fonzetti@uniroma3.it

Do parallel active fault systems dream of Coulomb Stress Transfer?

A. Galderisi[1,2], P. Galli[3,2], E. Peronace[2]

[1]Dipartimento di Scienze della Terra, dell'Ambiente e delle Risorse, Università degli Studi di Napoli, Federico II, Italia

[2]CNR-IGAG, Roma, Italia

[3]Dipartimento Protezione Civile, Roma, Italia

Introduction. In this work, we have applied different analytical methodologies in order to explore the modes of frontal transfer of static Coulomb stress between various seismogenic fault systems. We started from the observation of a series of surface ruptures formed along the Norcia fault system (NFS) following the Mw 6.6 event of 30 October 2016. The 2016 sequence was not generated by the NFS, but from the Monte Vettore fault system (MVFS). Since the seismological data relating to this sequence (Chiaraluce et al, 2017; Improta et al, 2019) did not highlight any significant event associable to the NFS, we questioned the nature of these ruptures and the possible interaction between these two parallel fault systems. Firstly, a geological-structural survey was conducted along the entire NFS, mapping the coseismic ruptures and calculating the slip-vector. Then we calculated the change in Coulomb stress produced by the MVFS following the October 30 event. As a result, part of the static Coulomb stress was transferred from the MVFS to the NFS. We then compared paleoseismological data coming from the two fault system trying to understand whether these flange systems also interact over time. Finally, the same analysis methodology was applied to the seismogenic fault systems of the Gran Sasso (GSFS) and the Upper Aterno Fault System (UAFS).

Geological and seismotectonic framework. The MVFS and the NFS are two seismogenic normal fault systems that extend parallel for over 30 km in the N160° direction, at a distance of ~10 km from each other. Both are active in historical times, with evidence of surface ruptures at least throughout the Holocene (Galli et al, 2018 and 2019). Similarly, the GSFS and the UAFS are two seismogenic fault systems, located ~14 km distant. The GSFS shows a N120° direction, in the north and central sector, while NNW-SSE in the southern sector. Differently, the UAFS shows a unique master fault direction N160° (Galli et al, 2010; 2011 and 2022). The return times calculated from paleoseismological studies are ~1.8 kyr for the MVFS and NFS (Galli et al, 2018; 2019; Tab. 1), with a slip rate of 1.3 mm/yr and 1.2 mm/yr respectively. While the return times of the GSFS is 2.8 + 0.5 ky and of the UAFS 1-2 kyr (for large magnitude events), with a slip rate of 1.8 mm/yr for GSFS and 0.58 mm/yr for UAFS (Galli et al, 2010; 2011 and 2022, Tab. 1).

Tab. 1. Archaeo-paleoseismological records.

NFS	MVFS	GSFS	UAFS
1859	2016 CE.	1349 CE	2009 CE
1703 CE	443 CE	~2800 BP	1703 CE
1328	~4000 BP	~6100 BP	1461 CE
99 BCE	~5600 BP		801 CE
~3900 BP	~7400 BP		~3500 BP
~5300 BP			~6300 BP
~7600 BP			

Seismic sequence of 2009 and 2016. The disastrous earthquakes of 2009 and 2016 both involved central Italy, affecting the Abruzzo and Lazio-Umbria regions, respectively. The 2009 seismic sequence recorded a mainshock of Mw 6.3 (Chiarabba et al, 2009), with approximately 64k aftershocks (Valoroso et al, 2013). The arrangement of the aftershocks suggests that, beside the activation of the UAFS - which generated the main mainshock and the greatest number of aftershocks - the nearby GSFS fault system was also involved, without evidence of coseismic rupture along the fault planes of the GSFS (Galli et al, 2022, Fig. 1). Differently, the 2016 seismic sequence was produced first by the joint activation of the MVFS and the Laga Fault System on 24 August, Mw 6.2 (RCMT, 2016) and then only by the MVFS, first in the northern sector, 26 October, Mw 6.1 (RCMT, 2016) and later entirely on 30 October Mw 6.6 (RCMT, 2016). Following the 30 October event, ~2 km of coseismic ruptures were observed along the main fault planes of the NFS (Galderisi and Galli, 2019; 2020), although no aftershocks were observed along the NFS (Improta et al, 2019; Galderisi and Galli, 2020).

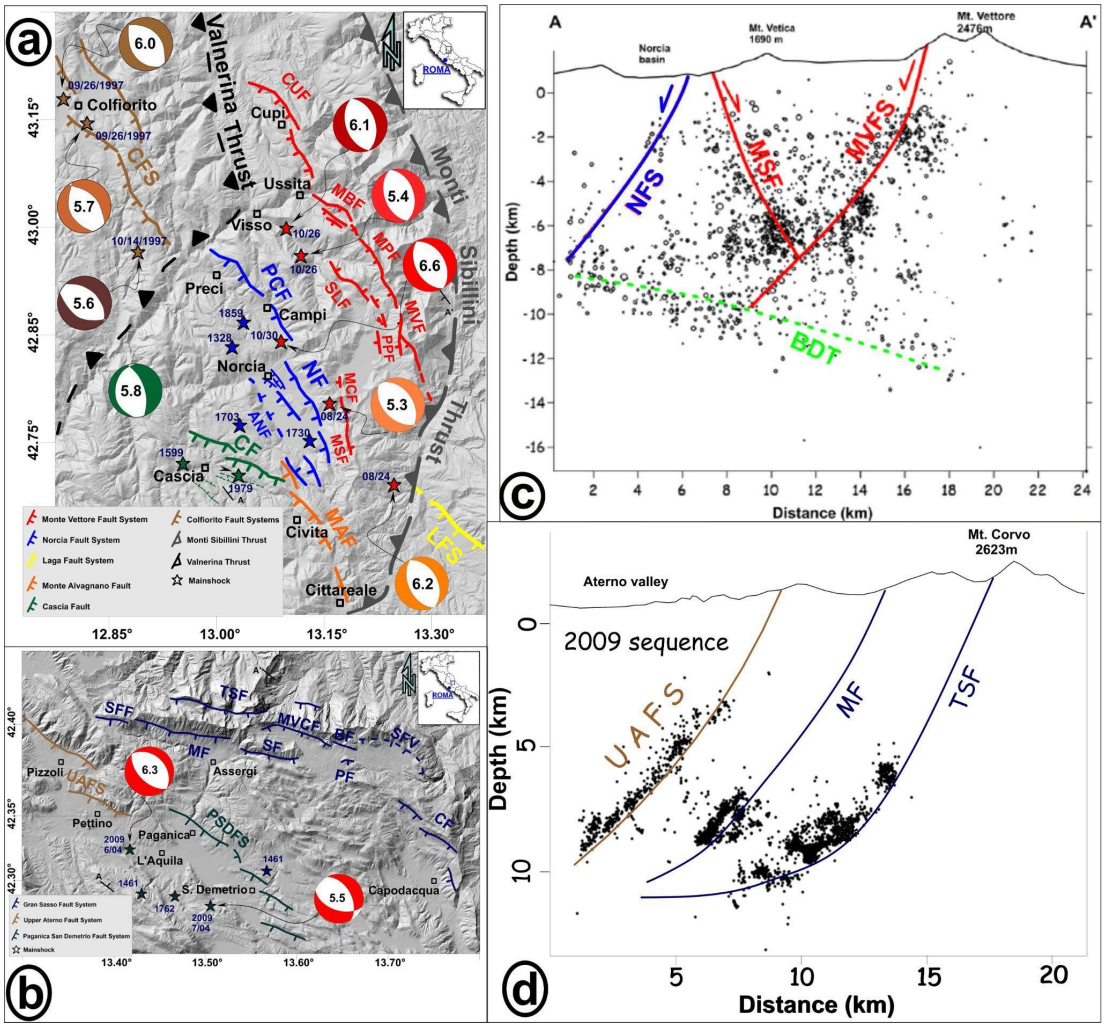

Fig. 1 – (a) Digital Terrain Model of the 2016 epicentral area with the main active fault segments. (b) Digital Terrain Model of the 2009 epicentral area with the main active fault segments. (c) Hypocentral distribution of the 2016 seismic sequence. (d) Hypocentral distribution of the 2009 seismic sequence.

Coseismic ruptures in the Norcia basin. The coseismic ruptures observed in the Norcia basin reflect the emergence of the master fault and the synthetic and antithetical splays already known and recognized as active in Galli et al. (2005; 2018; 2023). Following the earthquake of 30 October 2016, in total, over 2 km of coseismic ruptures with a maximum vertical offset of ~12 cm were measured. In December 2017, Galli et al. (2018) excavated a trench for paleoseismological studies along the coseismic rupture, where it was found that this rupture occurred in correspondence with the surface expression of the main splay observed on the walls of the trench.

Coulomb stress transfer. According to Coulomb stress change theory, following a seismic event part of the static stress can be transferred to nearby fault systems (King et al, 1994). Some authors have already analysed the variation in the static Coulomb stress produced by the 30 October event (Improta et al, 2019), with particular reference to the lateral interactions that occur between neighbouring seismogenic systems (Mildon et al, 2019). In our case, however, it is observed that part of the Coulomb stress is transferred frontally from the MVFS to the NFS. We then calculated the Coulomb stress changes generated on 30 October by the MVFS using the Coulomb 3.3 software (Toda et al, 2011). To define the Coulomb stress variation the software uses this equation:

$$\Delta CSC = \Delta\tau s + \mu\Delta\sigma n$$

where ΔCST is the change in Coulomb stress (Coulomb Stress Change – CSC), Δτs is the variation of shear stress, μ is the friction coefficient and Δσn is the variation of normal stress. The fault parameters entered into the software are:

• strike N160°; dip 70°; rake -90°; kinematic dip-slip; Mw 6.6; maximum slip -2 m for MVFS and -2.5 for NFS (INGV, 2016); friction coefficient μ=0.6 (typical of carbonate rocks). Two simulations were conducted, one activating the MVFS fault (S1), the other that of the NFS (S2) (Fig. 2).

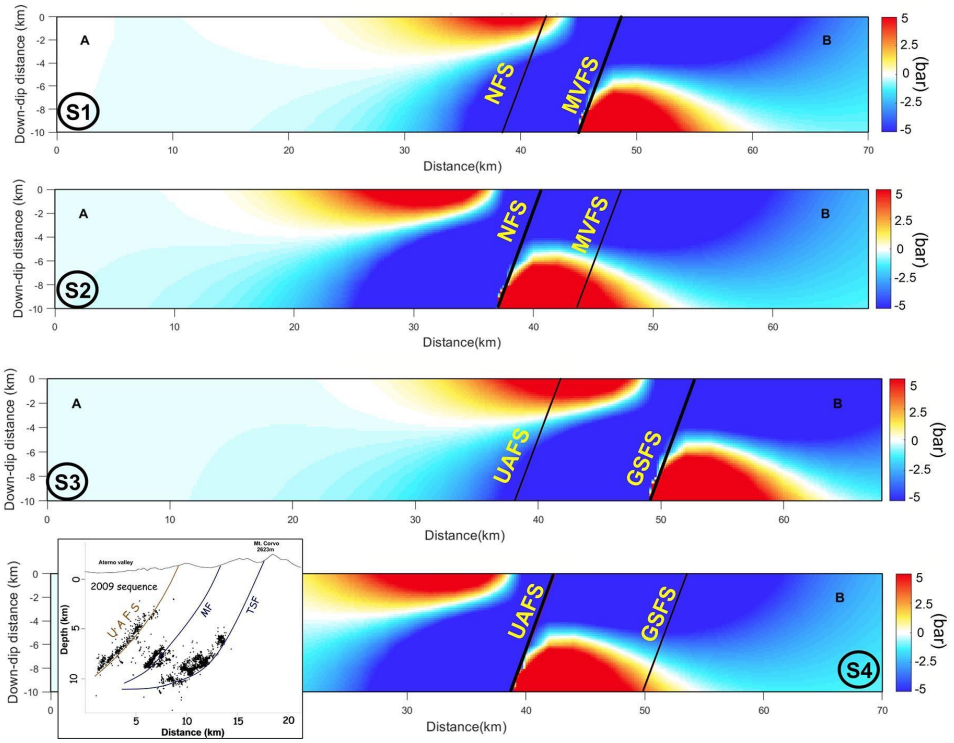

Fig. 2 – Simulation results for the calculation of the CST with the Coulomb 3.3 software. (S1) Cross-section with the activation of the MVFS. (S2) Cross-section with the activation of the NFS. (S3) Cross-section with the activation of the GSFS. (S4) Cross-section with the activation of the UAFS, with comparison of 2009 seismic sequence. Coulomb stress increase countering (red), Coulomb stress decrease countering (blue).

Similarly, two simulations were conducted for the GSFS (S3) and for the UAFS (S4), with parameters entered the software are:

• strike N160°; dip 70°; rake -90°; kinematic dip-slip; Mw 6.6; maximum slip -2.5 for both fault systems; friction coefficient μ=0.6 (Fig. 2).

Discussions and conclusions. The combination of all these analyses allowed us to hypothesize why the NFS was activated on the surface and how it interacts with the MVFS. The results obtained from the simulations for the calculation of the variation of the static Coulomb stress show that, in simulation S1, the formation of a stress growth lobe is observed in the first 2 km in the hanging-wall of the MVFS, corresponding to the superficial part of the NFS (Fig. 2). In simulation S2, however, a Coulomb stress increase lobe is observed at ~6.5 km depth in the footwall of the NFS,

corresponding to the deep part of the MVFS (Fig. 2). This suggests that, when the MVFS is activated, the static Coulomb stress is increased only in the most superficial portion of the crust crossed by the NFS, while when the NFS is activated, it is the static stress in the deep portion crossed by the MVFS that increases.

Considering that the 1) vector slips observed on the field along the coseismic breaks indicate pure dip-slip kinematics, while the slickenlines measured on the border fault planes indicate left oblique kinematics (Galderisi and Galli, 2020), and that 2) any significant seismicity has been detected at depth along the NFS (Improta et al., 2019), it is likely that the 30 October 2016 surface slip of the NFS cannot be attributed to deep deformation dynamics induced by Apennine tectonic stress release. Thus, excluding shaking-induced phenomena, as differential compaction or slope movements, both impossible in the splays of the plain, we hypothesize that the sudden increase in Coulomb stress induced by the activation of MVFS have triggered a slight passive slip along the pre-existing fault planes of the NFS, which accommodated also the abrupt, 12 cm uplift of the Norcia block (GSI, 2016; Bignami et al., 2019). Probably, due to the lack of sufficient lithostatic weight, friction was low and slip occurred seismically.

Considering the long paleoseismic history of the two fault systems (Galli et al., 2018; 2019; 2023), it is possible that the MVFS and the NFS have been interacting for thousands of years, mutually inducing variations in the Coulomb stress in the hanging wall of the other (Fig. 3). But while the activation of the MVFS seems to favour only the formation of superficial passive ruptures along the NFS, the activation of the NFS, which seems to precede that of the MVFS by 100-500 years, could act as a trigger for the complete rupture of the latter.

The same analysis methodology was applied for the GSFS and the UAFS. The results obtained from the simulations for the calculation of the variation of the static Coulomb stress show what was observed in the MVFS and NFS simulations (S3 and S4 in Fig. 2). This evidence suggests that the GSFS and the UAFS also interact by mutually inducing variations in the Coulomb stress in each other's hanging walls. The analysis of the aftershocks of the 2009 seismic sequence (Valoroso et al, 2013) unequivocally shows that the GSFS recorded seismicity, where the Coulomb stress growth lobe is created (Fig. 2). In fact, according to King et al, (2004) the increase of even just 1 bar would be sufficient to trigger slip on a fault system. In our case, the transfer of Coulomb stress from MVFS to NFS may reach 2–3 bars only in the upper lobe (Fig. 2). What is shown by the arrangement of the aftershocks of the 2009 seismic sequence, linked to the evidence of the 2016 coseismic ruptures observed along the NFS, shows that there is indeed an interaction between the parallel fault systems of the MVFS-NFS and the GSFS-UAFS, with possible Coulomb stress transfer.

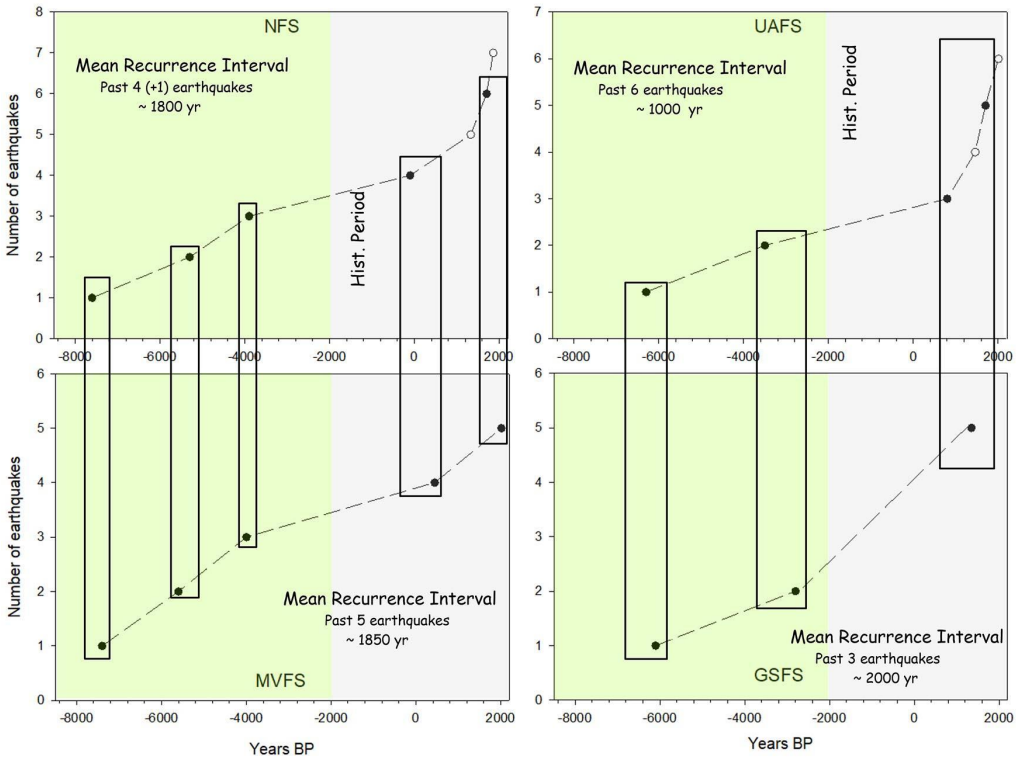

Fig. 3 – Comparison between the age of paleoearthquakes sourced by the NFS-MVFS and UAFS-GSFS. The white dots indicate seismic events known from historical bibliography but not recognized in the trenches.

The analysis of paleoseismological data shows that both the NFS-MVFS and the UAFS-GSFS recorded events at close times (Fig. 3). Differently, historical records show that the NFS and UAFS had greater activity, compared to the MVFS and GSFS (Fig. 3). In fact, the MVFS and the GSFS were classified as silent faults, as they did not show instrumental seismicity and even correlated historical seismic events. On the other hand, the seismic events of 1328 and 1859 for the NFS and 1461 for the UAFS were not observed in trenches. Even the 2009 seismic event didn't produce important surface coseismic ruptures, probably because not all the UAFS was activated. Considering only the earthquakes observed in the trenches, even in historical times a close activity is observed between the NFS-MVFS and UAFS-GSFS.

References

Bignami C., Valerio E., Carminati E., Doglion, C., Tizzani P., Riccardo Lanari R.; 2019. Volume unbalance on the 2016 Amatrice - Norcia (Central Italy) seismic sequence and insights on normal fault earthquake mechanism. Sci. Rep. 9, 4250.

Chiarabba C., et al; 2009. The 2009 L'Aquila (central Italy) Mw 6.3 earthquake: main shock and aftershocks. Geophys. Res. Lett. 36, 1–6.

Chiaraluce L., et al; 2017. The 2016 Central Italy seismic sequence: a first look at the mainshocks, aftershocks, and source models. Seismol. Res. Lett. 88, 757–771.

Galderisi A., Galli P.; 2020. Offset components and fault-block motion during the 2016 Central Italy earthquake (Mw 6.6, Monte Vettore Fault System). J. Struct. Geol. 134, 104014.

Galderisi A., P. Galli; 2020. Coulomb stress transfer between parallel faults. The case of Norcia and Mt Vettore normal faults (Italy, 2016 Mw 6.6 earthquake), Results Geophys. Sci. 1–4, 100003.

Galli P., Giaccio B., Messina P.; 2010. The 2009 central Italy earthquake seen through 0.5 Myr-long tectonic history of the L'Aquila faults system. Quat. Sci. Rev. 29, 3768–3789.

Galli P., Giaccio B., Messina P., Peronace E., Maria Zuppi G.; 2011. Palaeoseismology of the L'Aquila faults (central Italy, 2009,Mw 6.3 earthquake): implications for active fault linkage. Geophysical Journal International 187 (3), 1119–1134.

Galli P., Galderisi A., Ilardo I., Piscitelli S., Scionti V., Bellanova J., Calzoni F.; 2018. Holocene paleoseismology of the Norcia fault system (Central Italy). Tectonophysics 745, 154–169.

Galli P., Galderisi A., Peronace E., Giaccio B., Hajdas I., Messina P., Pileggi D., Polpetta F.; 2019. The awakening of the dormant Mt Vettore fault (2016 central Italy earthquake, Mw 6.6). Paleoseismic clues on its millennial silences. Tectonics 38, 687–705.

Galli P., A. Galderisi P. Messina, E. Peronace; 2022. The Gran Sasso fault system: Paleoseismological constraints on the catastrophic 1349 earthquake in central Italy, Tectonophysics, 822, 1–29.

GSI [Geospatial Information Authority of Japan] 2016. The 2016 Cen- tral Italy Earthquake: Crustal Deformation Detected by ALOS-2 Data.

King G.C.P., Stein R.S., Lin J.; 1994. Static stress changes and the triggering of earth- quakes. Bull. Seismol. Soc. Am. 84 (3), 935–953.

Improta L., et al, The Bollettino Sismico Italiano Work- ing Group; 2019. Multi-segment rupture of the 2016 Amatrice-Visso-Norcia seismic sequence (central Italy) constrained by the first high-quality catalog of Early After- shocks. Sci. Rep. 9, 6921.

INGV Working Group "Terremoto in centro Italia". Summary report on the October 30, 2016 earthquake in central Italy Mw 6.5; 2016.

Mildon Z.K., Roberts G.P., Faure Walker J.P., Toda S.; 2019. Coulomb pre-stress and fault bends are ignored yet vital factors for earthquake triggering and hazard. Nat. Commun. 10, 2744 .

RCMT., 2016: European-Mediterranean RCMT Catalog, web page: http://www.bo.ingv.it/RCMT/

Toda S., Enescu B.; 2011. Rate/state Coulomb stress transfer model for the CSEP Japan seismicity forecast. Earth Planets Space 63 (3), 171–185.

Valoroso L., Chiaraluce L., Piccinini D., Di Stefano R., Schaff D., Waldhauser F.; 2013. Radiography of a normal fault system by 64,000 high-precision earthquake locations: the 2009 L'Aquila (Central Italy) case study. J. Geophys. Res. Solid Earth 118, 1156–1176.

Corresponding author: a.galderisi92@gmail.com

Multidisciplinary analysis of 3D seismotectonic modelling: a case study of Serre and Cittanova faults in Southern Calabrian Arc (Italy).

S. Giuffrida[1*], F. Brighenti [1-4], F. Cannavò[3], F. Carnemolla[1-2], G. De Guidi[1-2], G. Barreca[1-2], S. Gambino[1], G. Barberi[3], L. Scarfì [3], C. Monaco[1-2-3]

1 Department of Biological, Geological and Environmental Sciences, University of Catania, Italy.
2 CRUST-Interuniversity Center for 3D Seismotectonics with territorial applications. U.R. Catania, Italy.
3 INGV-OE, National Institute of Geophysics and Volcanology-Etnean Observatory, Catania, Italy.
4 Department of Physics and Earth Sciences, University of Ferrara, Italy.

Introduction

The Calabrian Arc (CA hereinafter), in Southern Italy (Figure 1a,b,c), is an active structural domain where high-intensity historical and instrumental earthquakes with magnitude higher than 7 were recorded. In particular, some earthquakes in southern Calabria such as the seismic sequence of 1783, with the mainshock on February 5 (M 6.9–7.1; Jacques et al., 2001 (Figure 1a) have been regarded as the strongest seismic events of the Italian Peninsula. The seismogenic sources of major earthquakes occurred in the area are still debated, for instance, different interpretations were proposed regarding the location and the geometries of the causative faults responsible for the 1783 historical seismic sequence. In this work, a multidisciplinary approach has been followed to reconstruct, in the MOVE Software Suite environment (granted by Petroleum Experts Limited; www.petex.com), the 3D geometry of the Cittanova fault (CF) and Serre fault (SRF), the longest tectonic structures occurring in southern Calabria. These faults, belonging to the A2 category of the DISS (Database of Individual Seismogenic sources, https://diss.ingv.it/) (Fig.1 a), are defined by Jacques et al. (2001) and recently, starting from macroseismic data, by Andrenacci et al. (2023) as the seismogenic sources of the 5 and 7 February 1783 seismic events, whereas other authors (e.g., Cucci et al., 1996 and reference therein) consider the Gioia Tauro and Mesima faults, belonging to the A1 category, as the most likely sources for the same seismic events. The open debate between different geometric interpretations (E-dipping vs. W-dipping) reported in DISS and different schools of thought on the sources of the 1783 seismic sequence proves that the development of a 3D model for these faults may be crucial to better characterize the seismotectonics of the area and evaluate its seismic potential. Being characterized by clear surface evidence and seismic cluster at depth, we choose the CF and SRF for our analysis.

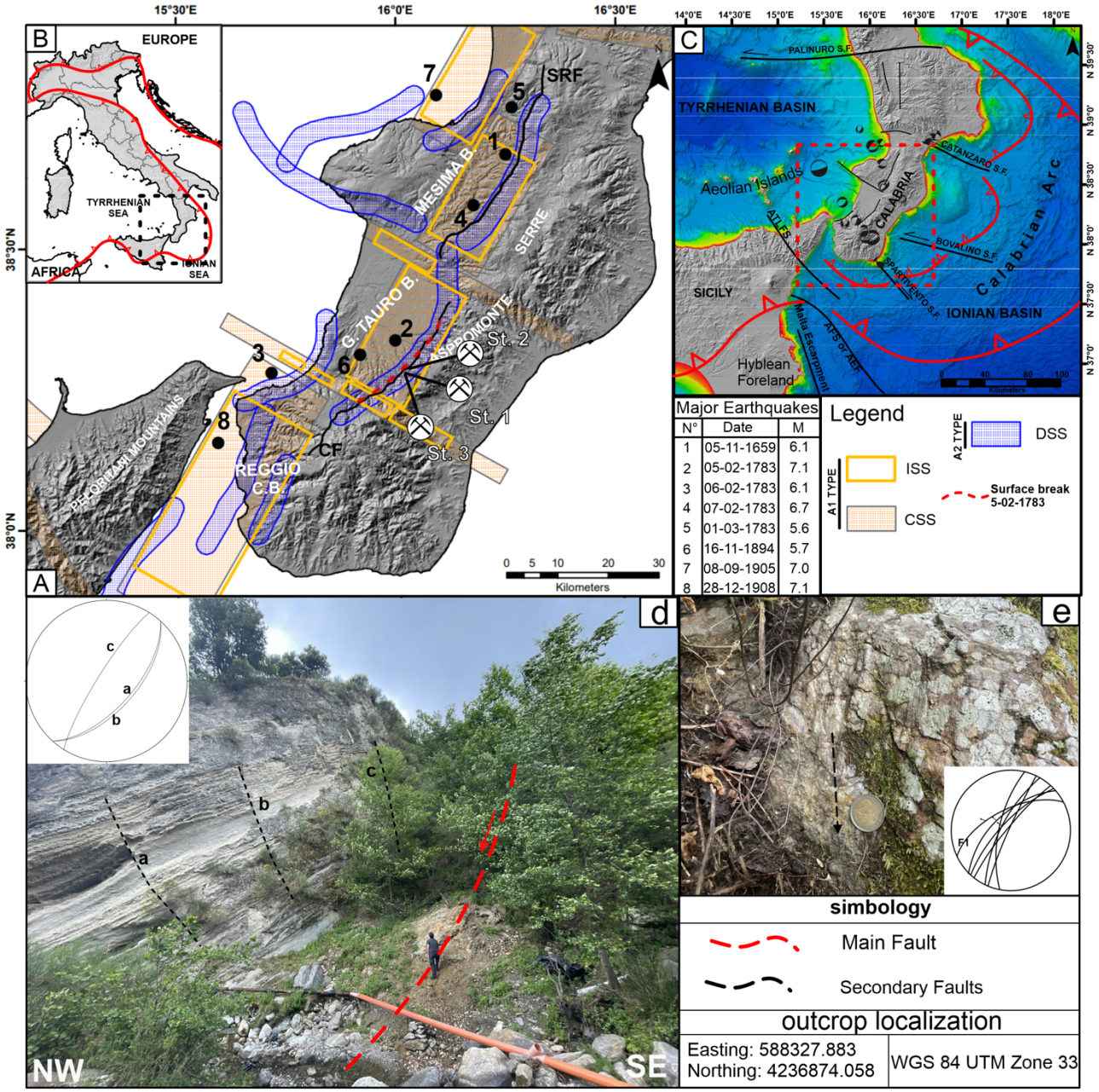

Figure 1: a) Map of seismogenic source types in southern Calabria and major historical earthquakes; The red dashed line represents the coseismic evidence of the 5 February seismic event. b) Front of the Appenninic–Maghrebian Orogen (red line) in the context of the Europe–Africa plate convergence. c) Simplified structural map of the Calabrian Arc domain; d) Upper Pleistocene deposits, tilted by the main fault activity. The main fault (red line) juxtaposes the Pleistocene sediments with the basement rocks. e) Slickenlines on the main fault plane (F1).

Previous seismic source models for the 1783 seismic sequence

The 1783 seismic sequence was characterized by the five events which the main occurred on February 5 that destroyed towns and villages located at the western foot of the northern Aspromonte (i.e., S. Cristina D'Aspromonte and S. Giorgio Morgeto). According to de Dolomieu (1784), after the 5 February mainshock, a 20-km-long scarplet that developed at the western foot of the Aspromonte Mountain between the village of S. Cristina and S. Giorgio Morgeto (red dashed

line in Figure 1a) was observed. Jacques et al. (2001) interpreted this as the coseismic reactivation of the west dipping CF during the 5 February mainshock. Concerning the seismic source models of 5 February, 7 February, and 1 March events, some authors proposed the CF and SRF west-dipping normal faults as responsible sources (Jacques et al., 2001) (Figure 1a, DSS; Debated Seismic Source). This hypothesis was supported by field geologic and morphotectonic data and observation by the distribution of the high-damage sites as exploited by the mesoseismal areas of the 1783 sequence (Baratta, 1901) and revisited macroseismic data (Andrenacci et al., 2023), the observed coseismic fracturing (de Dolomieu, 1784), and also by paleoseismological studies. Conversely, other authors inferred ruptures along the Gioia Tauro and the Mesima east-dipping blind low angle (~30°) normal faults for the same events (Loreto et al., 2013 and reference therein) (see also Figure 1a, ISS: Individual Seismic Source).

Structural data

The CF and SRF border the western sectors of the Aspromonte and Serre mountains, respectively. These NNE-SSW-oriented, west-dipping, and 40-km-long faults (Figures 1A, C) develop cumulative scarps of up to 450 m in height. In order to investigate the surface expression and the kinematic of the faults, a geological–structural survey was carried out. Unfortunately, due to the poorly conservative rock types cropping out in the investigated area, the kinematic indicators are difficult to observe (particularly in the SRF area). Structural data were collected in a few selected outcrops along the CF near Oppido Marmertina Village. Here we reported only the structural station 2 (Fig. 1d, e) (for further information please refer to Giuffrida et al., 2023). The outcrop is located southwest of Oppido Mamertina, along the Spilinga River where the fault meets the Aspromonte gneisses in the footwall and the Middle–Upper Pleistocene deposits in the hanging-wall. Pleistocene deposits are faulted and tilted toward the west (layer attitude 310/35). Minor faults are parallel to the master fault and show steep eastward dips (see also Jacques et al., 2001). The master fault (F1 in stereoplot in Fig. 1e and red line in Fig. 1d) is NE-SW-oriented and shows a set of slickenlines consistent with normal-oblique sinistral kinematics.

Seismological data: 3D fault modelling from earthquakes distribution

To investigate the recent kinematics of the faults affecting the studied area, we analysed the available focal solutions from ISC (http://www.isc.ac.uk/iscbulletin/search/fmechanisms/) and ISIDe (http://iside.rm.ingv.it/tdmt) databases (see Figure 1c). Moreover, earthquakes that have been instrumentally recorded since the early 1980s were used to infer the geometry of the studied faults at depth. We selected the seismic events occurred in the Calabrian Arc from the INGV databases (https://istituto.ingv.it/it/risorse-e-servizi/archivi-e-banche-dati.html) in order to enhance the picture derived from the seismic dataset (refer to Giuffrida et al., 2023 for further information). The final locations (approximately 8,500 seismic events with magnitudes ranging from 1 to 5.7) resulted with an average uncertainty of 0.20 ± 0. 15 km in both horizontal and vertical coordinates and an average root-mean-square travel-time residual of 0.02 s.

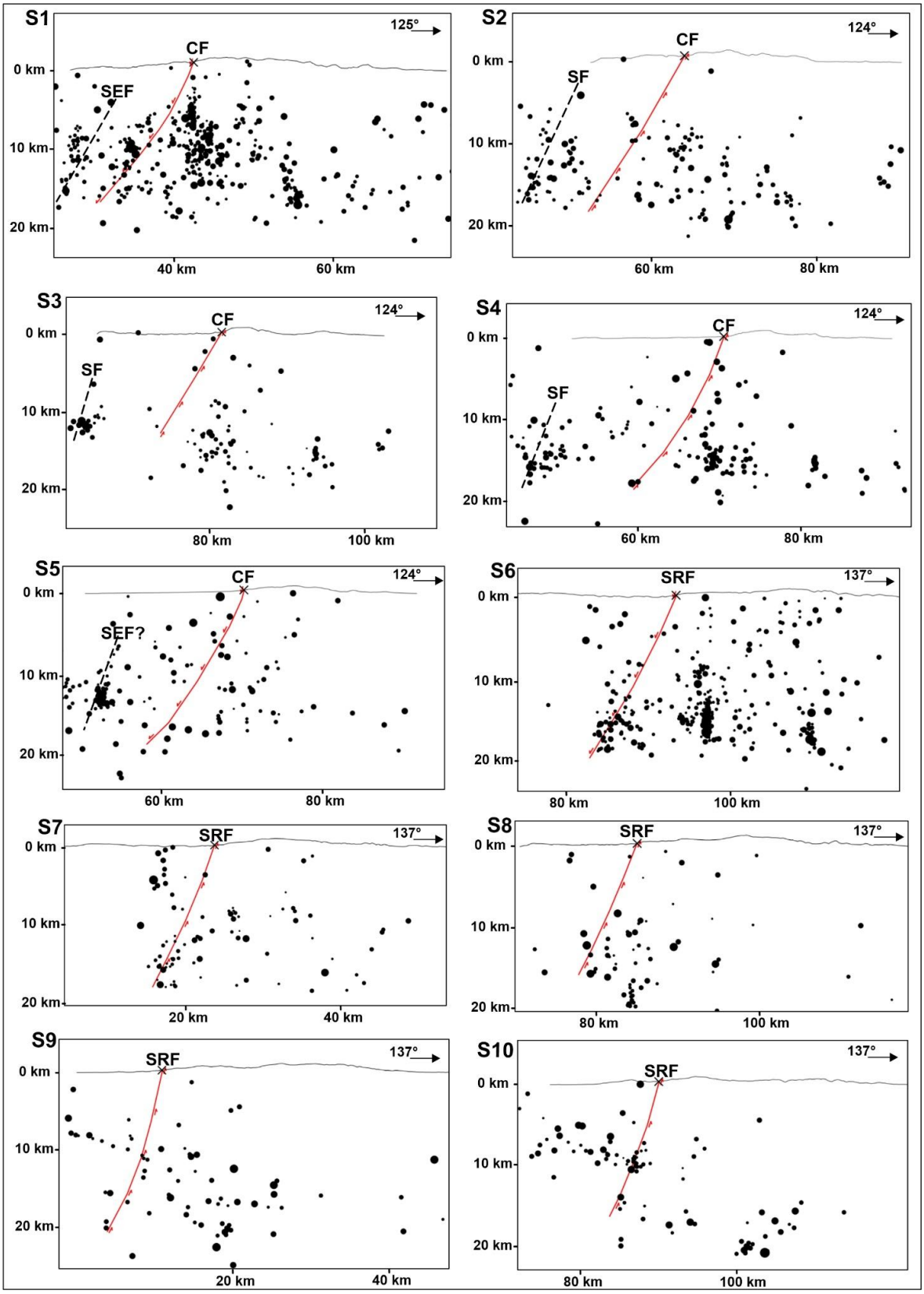

Figure 2: Seismological sections orthogonal to the Cittanova fault (S1–S5) and Serre fault (S6–S10). Crosses are the location of the studied faults at the surface. Black dashed lines are the inferred traces of other faults (SF, Scilla Fault; SEF, S. Eufemia Fault) slicing along the sections.

To constrain the depth geometry of Serre and Cittanova faults, a set of 10-km spaced seismological sections (five sections for each fault) with a buffer projection of 5 km was created (Fig. 2). the geometry at depth of the considered faults (red lines) was traced following earthquake clustering starting from the intersection of the fault on the surface (black crosses in Figure 2). Clusters are visible, especially in S1 and S6 corresponding to the southern tip areas of the CF and SRF, respectively. Despite the other sections that do not exhibit clear clusters useful to infer the attitude of the studied faults at depth, we traced their geometry considering the same trend of S1 and S6 and the earthquakes with the highest magnitude for each section. Subsequently, using a trial-and-error approach, we geometrically tested the modelled planes with the known empirical scaling in order to find a reliable solution for fault planes capable of generating events with a magnitude of 7.

Fault response modelling of the Cittanova and Serre faults

We combined the field structural data, literature data, and kinematics observed at surface with the seismic dataset in order to develop a reliable 3D model of the fault planes. According to the proposed fault model (Figures 3 a), the CF is an almost 44-km-long fault, roughly N40E-oriented with a plane dipping toward NW, whereas the SRF is a N30E-striking, 40-km long fault with a plane dipping toward NW. The average dip of the CF is 57°, while the SRF exhibits an average dip of approximately 60°. All geometric parameters are summarized in Table 1. The parameters derived from the 3D model were used to estimate the expected magnitude for each plane, assuming an activation of the faults for their entire length and using empirical relationships. We used the surface rupture length (SRL) and the rupture area (RA) vs. magnitude empirical scaling both for Wells and Coppersmith (1994) and Leonard (2010). The resulting magnitudes for the given faults are comparable (see Table 1). Moreover, the Fault Response Modelling (FRM) module was applied to kinematically test the model and verify the maximum vertical displacement and its spatial distribution associated with the activation of the fault planes for their entire length (which is consistent with a maximum expected magnitude of approximately 6.8 – 7). The first simulation (Figure 3c) shows the displacement field for the activation of both faults. The simulated vertical displacement ranges from 0.5 to 1.7 m (with a maximum value equal to 2.2 m). The correspondence of the mesoseismal areas of 5 and 7 February and for the 1 March shocks, macroseismic data and simulated coseismic displacement (Figure 3c) confirms the choice of the CF and SRF faults, respectively, as the most likely causative sources for the considered events. The second simulation (Figure 3d) shows the cumulative displacements ranging from −354 m to 112 m. In this case, the displacement values exhibit an abrupt change across the fault traces; the vertical cumulative displacement of CF and SRF reaches almost 450 m (see also the vertical displacement dz profiles shown in Figure 3f), which is consistent with the minimum vertical offset estimated for these faults (see also Jacques et al., 2001).

Geometric parameters and empirical relations								
		CF				SRF		
Av. Dip. Azimuth		313.96°				301.9°		
Av. Dip		57.73°				63.53°		
Dep. range and width (m)		min	Width	max		min	Width	max
		-19767	21070	1303		-21697	22305	608
Wells & Coppersmith (1996)	M vs SRL	6.98				7.14		
	M vs RA	6.99				7.02		
Leornad, (2010)	M vs SRL	6.9				6.93		
	M vs RA	6.98				7.01		
Tmax vs Lmax Manighetti et al., 2001		664m				697m		

Table 1

Slip Tendency

The slip tendency analysis (Figure 3 a, b) shows that both SRF and CF are under an almost unstable mechanical condition in the given remote stress state. Concerning the SRF, Ts ranges from 0.35 to 0.85, with the most frequent values ranging from 0.6 to 0.7, while CF exhibits Ts ranging from 0.45 to 0.80, with the most frequent values ranging from 0.62 to 0.68. Moreover, Ts value distribution for CF is more clustered than that for SRF which exhibits Ts spreading on its overall plane with another highly frequent minor distribution between 0.48 and 5.4, located especially near its northern and deepest portions. Note that the calculation was performed considering the saturated condition of the surrounding medium in order to take into account the worst condition for a potential reactivation of the fault planes.

Conclusion

The instrumental seismicity, merged with structural field investigation and literature data, provided useful constraints to infer the geometry on surface and at depth of SRF and CF. The geometric parameters obtained through the model of these faults are compatible with the empirical relationships (magnitude vs. rupture area and magnitude vs. fault length; Wells and Coppersmith, 1994; Leonard, 2010). Accordingly, we achieved the expected magnitude for CF and SRF and confirmed that these faults can be the probable sources of the mainshocks of the 1783 seismic sequence (5 February, 7 February, and 1 March, M = 6.9–7; Jacques et al., 2001). From the slip tendency analysis, we found that both fault planes are astride under the stable and unstable mechanical conditions in the given regional stress state. The response of the modelled fault planes

indicates that the simulated coseismic and cumulative vertical displacement fields agree with the historical observation of the slip along the fault planes and with actual height of the morphological scarps, respectively. Considering the lack of seismic profiles onshore, the proposed model can represent an important starting point for seismotectonic modelling.

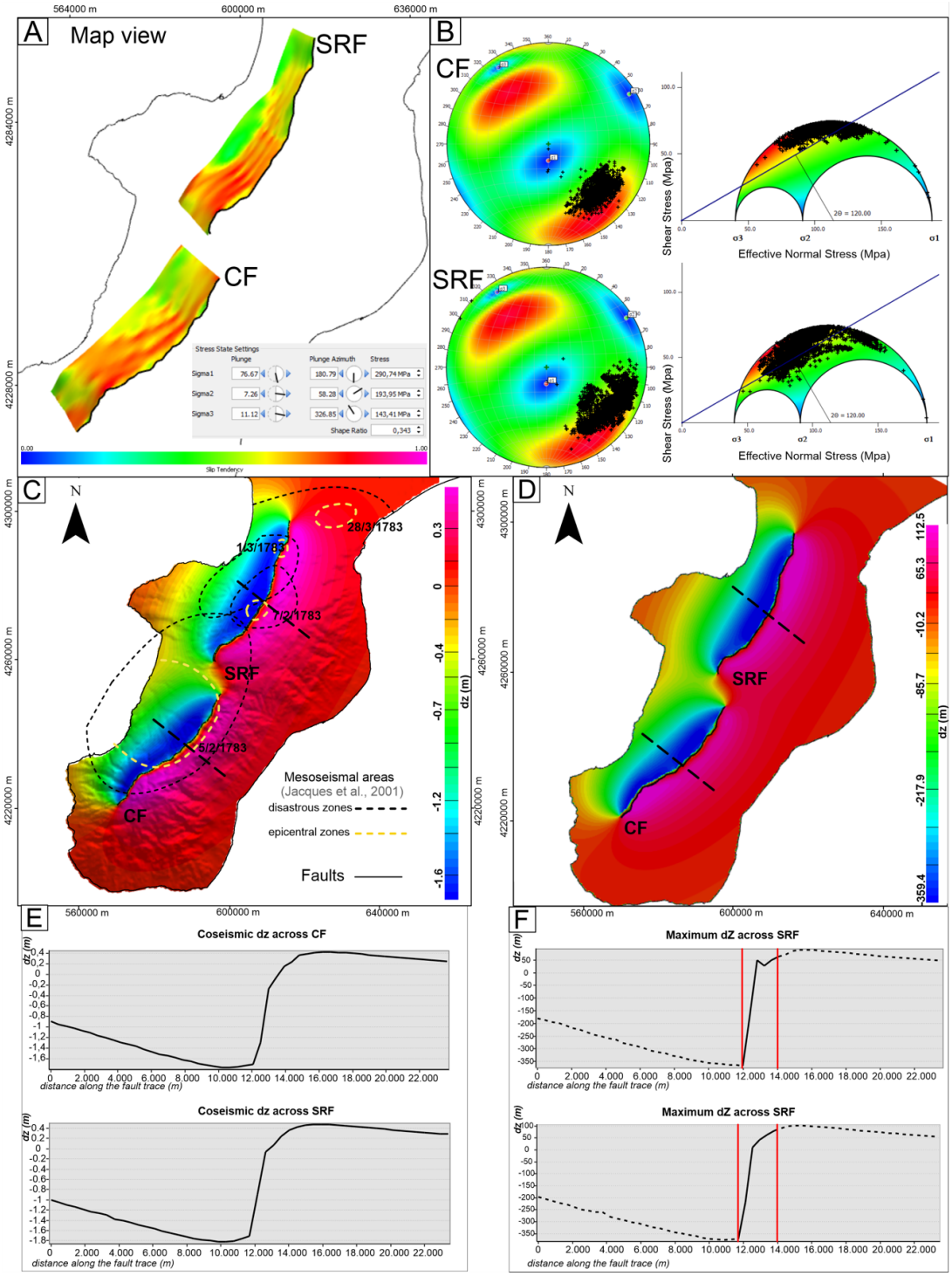

Figure 3: a) Map view of the 3D model of SRF and CF, fault planes are coloured in function of the Slip tendency (Ts). b) Confining stress state resolved at 10 km of depth. c) Vertical displacement (dz) computed for 3 m of uniform slip on the fault planes. Black and yellow dashed lines show the mesoseismal areas for the shocks of the 1783 seismic (see also Baratta, 1901; Jacques et al., 2001 for further information). d) Vertical displacement (dz) computed for Tmax values of 664 m and 697 m. e) Coseismic dz profile across CF and SRF. f) Cumulative dz profile across CF and SRF.

References

Andrenacci, C., Bello, S., Barbano, M. S., de Nardis, R., Pirrotta, C., Pietrolungo, F., et al. (2023). Reappraisal and analysis of macroseismic data for seismotectonic purposes: the strong earthquakes of southern Calabria, Italy. Geosciences 13, 212. doi:10.3390/ geosciences13070212.

Baratta, M. (1901). I terremoti d'Italia. Torino: Arnoldo Forni.

Cucci, L. (2022). NW-Dipping versus SE-dipping causative faults of the 1783 M7.1 southern Calabria (Italy) earthquake: the contribution from the analysis of the coseismic hydrological changes. Front. Earth Sci. 10, 987731. doi:10.3389/feart. 2022.987731.

de Dolomieu, D. (1784). Me´moire sur les Tremblemens de Terre de la Calabre Pendant l'Anne´e 1783. Rome: Fulgoni.

Jacques, E., Monaco, C., Tapponnier, P., Tortorici, L., and Winter, T. (2001). Faulting and earthquake triggering during the 1783 Calabria seismic sequence. Cambridge: Cambridge University Press.

Giuffrida S, Brighenti F, Cannavò F, Carnemolla F, De Guidi G, Barreca G, Gambino S, Barberi G, Scarfi L and Monaco C (2023), Multidisciplinary analysis of 3D seismotectonic modelling: a case study of Serre and Cittanova faults in the southern Calabrian Arc (Italy). Front. Earth Sci. 11:1240051. doi: 10.3389/feart.2023.1240051.

Loreto, M. F., Fracassi, U., Franzo, A., Negro, P., Zgur, F., and Facchin, L. (2013). Approaching the seismogenic source of the Calabria 8 September 1905 earthquake: new geophysical, geological and biochemical data from the S. Eufemia gulf (S Italy). Mar. Geol. 343, 62–75. doi:10.1016/ j.margeo.2013.06.016.

Corresponding author: salvatore.giuffrida@phd.unict.it

Integration of 3D P and S velocity model in SeisComP real time monitoring: an application to Northern Italy

F. Grigoli[1], C. Rossi[2], C. Cocorullo[2]

[1] *University of Pisa, Italy*
[2] *Seismix s.r.l., Italy*

The real-time microseismic monitoring represents a fundamental point in evaluating and managing the risks associated with industrial activities for geo-resources exploitation. SeisComP (Helmholtz Centre Potsdam GFZ German Research Centre for Geosciences and gempa GmbH 2008), a software package developed by the German Research for Geosciences (GFZ), stands out as one of the most extensively utilized tools for seismic monitoring: it facilitates automatic data acquisition and real-time or post-processing.

In this study, we illustrate a SeisComP optimization for real-time data processing applied to microseismic monitoring of an Underground Gas Storage field in Northern Italy. Our analysis encompasses two years of continuous seismic data obtained from a seismic network consisting of 15 stations, including both surface and borehole sensors. To better constrain the earthquakes' location, first, we applied a Joint Hypocenter and Velocity technique (Thurber, 1992; Kissling, et al. 1994) to compute a new P and S 1D velocity model for the gas storage field area.

Then, we derived a 3D P-wave velocity model at the reservoir scale by using migration velocity data from a 3D seismic reflection survey. To obtain the 3D S-wave velocity model, we used an average Vp/Vs value derived from the 1D velocity model and well-logs.

In the concluding phase, the different velocity models are compared by examining the earthquakes' locations obtained with each model. The results indicate a consistent enhancement in location accuracy (both in terms of RMS and waveform coherence) for events within the inner area when using the 3D model. For the other events, the earthquakes' locations computed with the optimized 1D velocity model are improved compared to those obtained by using the initial velocity model.

This seismic processing routine represents a pioneering application in Italy, demonstrating how a 3D velocity model can be fully integrated into real-time microseismic monitoring operations, in agreement with the recommendations of the Italian Guideline for Microseismicity Monitoring in Industrial Activities (Dialuce et al., 2014).

References

Dialuce, G., Chiarabba, C., Di Bucci, D., Doglioni, C., Gasparini, P., Lanari, R., . . . Zollo, A. (2014). Indirizzi e linee guida per il monitoraggio della sismicità, delle deformazioni del suolo e delle pressioni di poro nell'ambito delle attività antropiche.

Helmholtz Centre Potsdam GFZ German Research Centre for Geosciences and gempa GmbH. (2008). *The SeisComP seismological software package.* doi:10.5880/GFZ.2.4.2020.003

Kissling, E., Ellsworth, W., Eberhart-Phillips, D., & Kradolfer, U. (1994). Initial reference models in local earthquake tomography. *Journal of Geophysical Research, 99*(B10), 19635-19646. doi:10.1029/93JB03138

Thurber, C. (1992). Hypocenter-velocity structure coupling in local earthquake tomography. *Physics of the Earth and Planetary Interiors, 75*(1-3), 55-62. doi:10.1016/0031-9201(92)90117-E

Corresponding author: c.rossi@seismix.it

InSAR data analysis to investigate the 2009 post-seismic deformation in L'Aquila downtown

V. Guerriero[1], A. Sciortino[1], R. Marini[2], P. Mazzanti[2, 3], M. Tallini[1]

1 Dipartimento di Ingegneria Civile, Edile-Architettura e Ambientale, Università degli Studi dell'Aquila
2 NHAZCA S.r.l., start-up Università degli Studi di Roma "La Sapienza"
3 Dipartimento di Scienze della Terra & centro di ricerca CERI, Università degli Studi di Roma "La Sapienza"

Introduction

A statistical analysis of time series of A-DInSAR post-seismic data, acquired in the time range 2010-2021 from the Cosmo-SkyMed and Sentinel-1 missions, has been carried out. This has allowed analysing the relationships between ground deformations and geological, hydrogeological, and geomorphological features of the study area, located in L'Aquila (Italy) historical centre (LAHC). The correlation analysis between predisposing factors and SAR deformation has highlighted that subsidence is substantially controlled by the shalow lithology, showing how compositional variations within lithology can significantly influence ground deformations. Furthermore, hydrogeological features, such as water table depth and its seasonal fluctuations exhibit correlation with subsidence rates.
The analysis of these data is still ongoing and offers promising research perspectives in the field of geomechanical/geotechnical subsoil characterization, based on satellite ground deformation data, also useful in seismic hazard characterization and mitigation.

A-DInSAR Displacement Data by means of Multi-Satellite technology

The data set involved in the present study has been achieved by Advanced Differential Synthetic Aperture Radar Interferometry (A-DInSAR) technique, by integrating of ground displacement values from two active satellite SAR missions, namely Sentinel-1 (by ESA) and Cosmo-SkyMed (by ASI).
The resulting data sets consist of time series of 158 values of ground displacement, one for each monitored ground point, detected in the time range from April 14, 2010, to November 30, 2021. Figs. 1, 2 and 3 illustrate A-DInSAR data involved in this study, with their comparison with local geology.

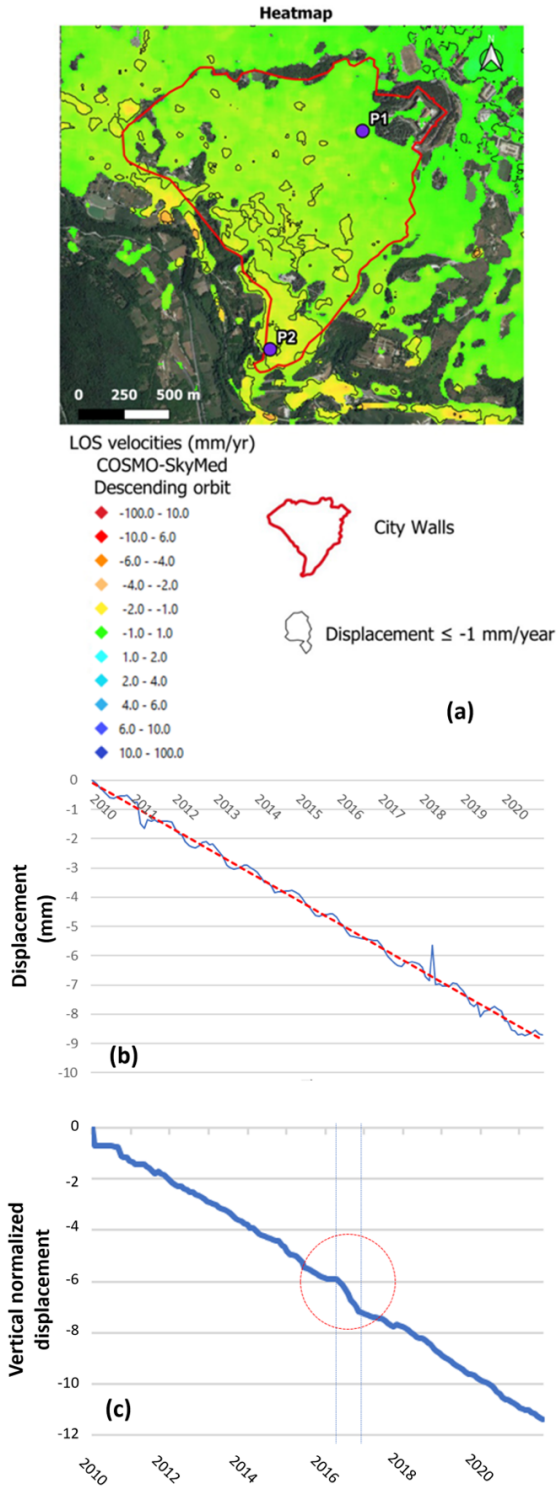

Figure 1 – a) A-DInSAR map resulting from the processing of April 14, 2010, to November 30, 2021, descending orbit images; b) time series of average displacements (i.e., spatially averaged over the studied area, within city walls) showing seasonal fluctuations around the trendline; c) time series of opportunely selected, normalized vertical displacement values in which seasonal oscillations have been removed. Each monthly value is calculated as the average of the values recorded in the previous and following six months. The red circle outlines an observed anomaly in the subsidence trend. The two vertical lines highlight the time range August-November 2016, in which the Amatrice-Norcia seismic sequence occurred.

The study area

L'Aquila downtown is placed in the L'Aquila-Scoppito intermontane basin (ASB) which is a half-graben bordered by SW-dipping normal mostly active faults located in its northern border, which are responsible for the historical and present seismicity. ASB is filled with approximately maximum 600 meters of Plio-Quaternary continental slope, colluvial and alluvial deposits which overlie unconformably the carbonate bedrock formed by Jurassic to Miocene marine carbonate units (Antonielli et al., 2020; Fig. 3).

Heterometric breccias with clayey-silty matrix (S. Demetrio-Colle Cantaro Unit) represent the first Plio-Quaternary detrital sedimentation in the ASB. These lithologies and the underlying bedrock are unconformably overlain by alluvial and marshy deposits composed by silt, clay, and sands (Madonna della Strada Unit – MDS, Early Pleistocene) (Tallini et al., 2019). The Fosso di Genzano Unit (FGS), incised into the earlier deposits, is composed by gravel and sand, pertaining to Middle Pleistocene alluvial fans.

The shallow part of the gently S-dipping hill, in which L'Aquila downtown is located, is mainly composed by 20-100 m-thick of L'Aquila Breccia Unit (LAB). LAB lays unconformably upon FGS and MDS and consists of heterometric poorly sorted carbonate clasts, sometimes with sandy-clayey calcareous matrix sedimented during the Middle Pleistocene with rock-avalanche process (Antonielli et al., 2020). In the southern part of L'Aquila hill, alluvial lens of sand and gravel (ALE) is interlayered within LAB (Fig. 3). The Red Soil Unit (RS) covers unconformably LAB (Tallini et al., 2020). RS includes reddish clayey colluvial sediment and epikarst deposits and exhibits highly variable thickness, reaching up to 30 meters. RS formed during a humid and warm interglacial phase of the Upper Pleistocene at the expense of LAB.

Data about geological features potentially controlling subsidence processes

To perform a geological and seismic characterization of the study area, a total of 142 Shear Wave Velocity (Vs) in-situ measurements, pertaining to the shallow lithologies within LAHC, were acquired from bibliographic sources (e.g., Amoroso et al., 2018). Furthermore, logs from an extensive dataset of 573 boreholes, many of which were drilled after the 2009 earthquake to facilitate the reconstruction of LAHC buildings, were integrated with geological data from the literature (e.g., Tallini et al., 2020).

The collected data formed a substantial database that facilitated numerous GIS-based processing, aimed to assess the surface geology and the RS thickness (Sciortino et al., 2023). Due to their high compressibility, RS have been recognized in various studies as lithology responsible for site-specific seismic amplifications (e.g., Tallini et al., 2020).

The produced geological map was rasterized, assigning a Vs (Shear Wave Velocity) value to each lithology based on literature data from Downhole (DH) and MASW in situ measurements (e.g., Amoroso et al., 2018).

Geomorphological and hydrogeological characterization of the LAHC area were carried out through the analysis of a digital terrain model (DEM) and of the piezometric level.

Results of the correlation analysis

To assess the relationship between the geological-geomorphological and hydrogeological study area features and ground deformation in LAHC, a correlation analysis has been carried out. We compared the vertical deformation, with slope maps, RS thickness, depth of regional aquifer and Vs of the outcropping lithologies. For each of these factors, the Pearson correlation coefficient with ground vertical average velocity has been calculated (Tab. 1).

Predisposing factor	Pearson coefficient
Depth of regional aquifer	-0.52
Ground slope	-0.22
Red Soil thickness	0.13
Vs of outcropping geology	0.46

Table 1 – Values of the Pearson coefficients calculated between the considered geological predisposing factors and subsidence velocities.

Furthermore, seasonal fluctuations of subsidence velocity, as evidenced in Fig 1b, have been analysed. To this end, the cross-correlation between quarterly average rainfall (mm/d) and detrended average subsidence rate (mm/y), has been analysed, in the time range 2010-2021. A statistically significant correlation value, equal to 0.56, has been individuated.

Discussion and perspectives for subsoil characterization by means of A-DInSAR displacement data

The correlation values in Tab. 1 are statistically significant, nevertheless, it is presumable that the subsidence process is mainly controlled by the kind and thickness of lithologies involved. The above illustrated correlation analysis provides a first result, which may be improved by a multivariate approach, as described below.

Fig.3 illustrates the velocity values associated with monitored points, falling in the strip (width: 50 m), indicated in semi-transparent red in Fig.3a, to achieve a more accurate comparison of ground displacement data with the subsurface structure. This band surrounds an accurate geological section accomplished by Antonielli et al. (2020; Fig. 3b). Subsidence velocities decrease going from LAB 3 (with abundant fine and more deformable fraction) to LAB 2 and LAB 1 (Fig. 2), whereas, local variations seem to be predominantly controlled by the RS thickness, as the trend of the point cloud in the diagram faithfully follows the thickness of the RS units (Figs. 3c and 3d).

The results illustrated in Fig. 3d lead to conclude that a significant contribution to the observed subsidence phenomenon is provided by the consolidation of Quaternary units. In In granular soils, seismic shaking produces well-known phenomena of variation in porosity, such as compaction or dilatancy. In the case of saturated fine-grained soils (even above the water table) a first phase of porosity variation occurs slowly, associated with fluid expulsion (Terzaghi consolidation), followed by a second phase of secondary consolidation, due to creep phenomena.

Therefore, the post-seismic velocity and displacement values of the monitored PS are given by the sum of effects of primary and/or secondary consolidation in saturated soils and the only secondary consolidation of non-saturated ones.

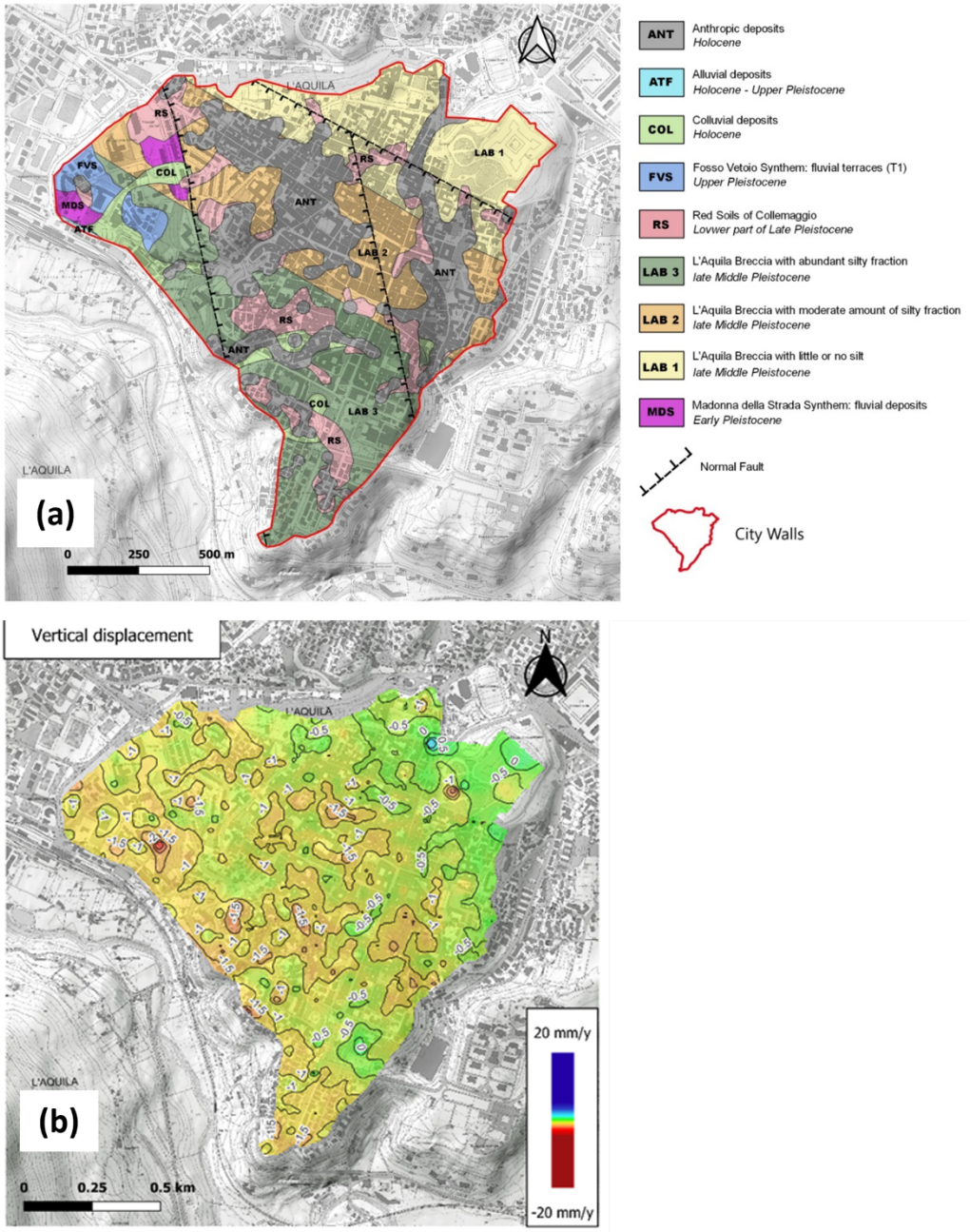

Figure 2 – a) Geological map with an internal division of LAB based on the abundance of the muddy-limestone matrix. From LAB 1 to LAB 3 the silt fraction increases; b) vertical velocity map achieved by means of interpolation of values calculated by combining Cosmo-SkyMed descending and Sentinel-1 ascending orbit data. Green colour, denoting velocity lesser tha 0.5 mm/y (in absolute value), is prevalent over LAB1, light green (velocity in the range 0.5-1 mm/y) over LAB2 and yellow (velocity >1 mm/y) over LAB3.

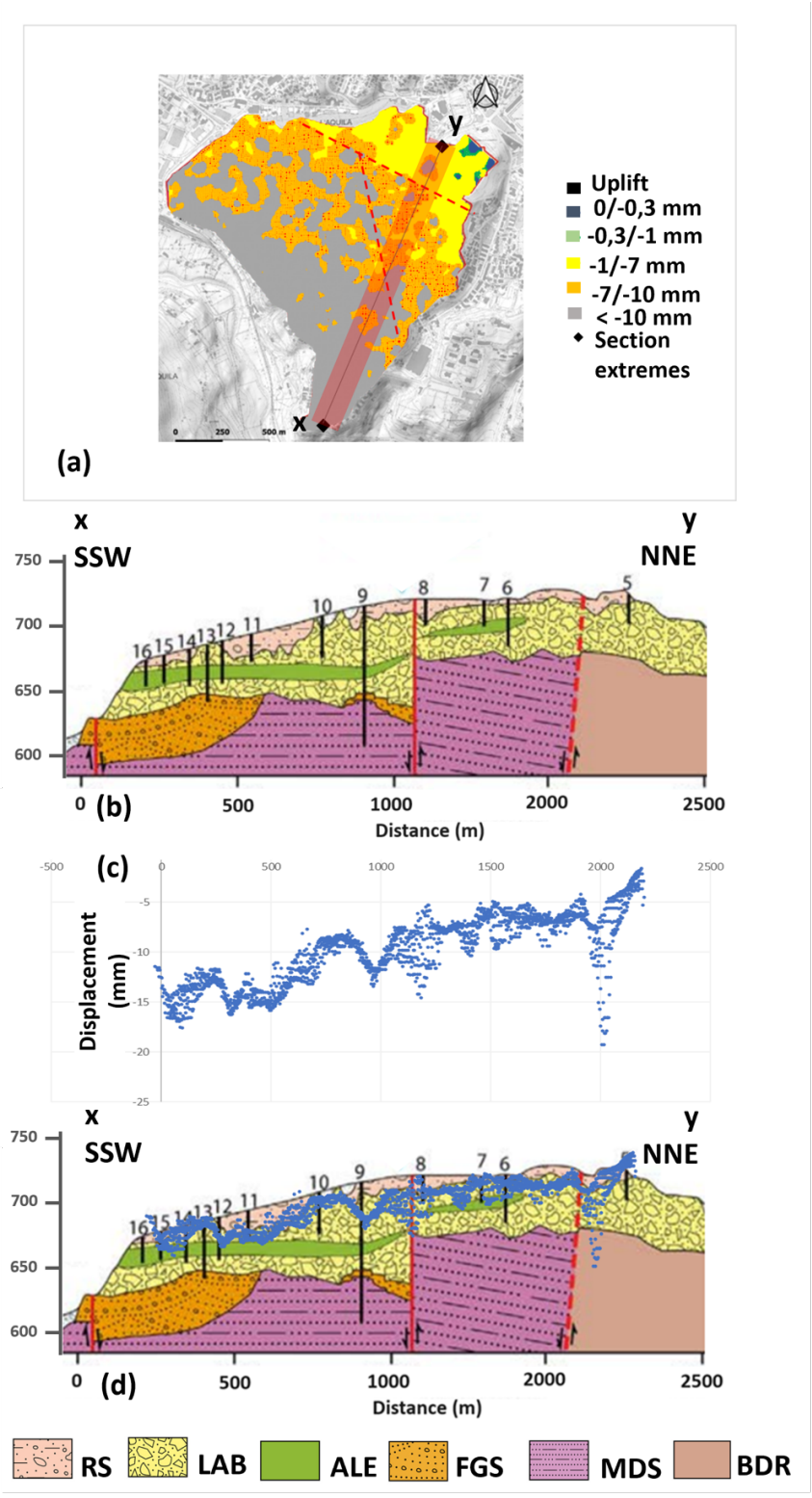

Figure 3 – a) Monitored points grouped in cumulative displacement classes (time range 2010-2021) in L'Aquila downtown; x-y: geological section reported in b and d; b) geological section; RS: Red Soil (Upper Pleistocene); LAB: L'Aquila Breccia (late Middle Pleistocene); ALE: Alluvial lens (sand and gravel, Middle Pleistocene); FGS: Fosso di Genzano Synthem (sand and gravel, Middle Pleistocene); MDS: Madonna della Strada Synthem (silt, clay and sand, Early Pleistocene); BDR: carbonate bedrock (Jurassic to Miocene); c) cumulative displacement values (mm) of the monitored points, falling in the red 50 m width semi-transparent band in panel a; d) the comparison of deformation and geology is shown through the superposition of the cumulative displacement of panel c and the geological section in panel b. Note the good matching between displacement with the Red Soil bottom boundary.

Let us consider a simple vertical strain model, made up of overlying layers (e.g., RS, LAB, etc.) in the consolidation phase. According to such a model, the subsidence velocity (or cumulated displacement in a given time interval) at a point is given by sum of contributions by the N layers under such point. Denoting by v such velocity value and by h_j the thickness of the j-th layer, then:

$$v = \sum_{j=1}^{N} C_j \bullet h_j, \quad (1)$$

where C_j are constants depending on the mechanical properties of the considered layers, which can be viewed as the contribution provided by each thickness unit (e.g., 1 m) of layer. If for M wells the thicknesses h_j are known, we have M equations like (1) in which v and h_j are known. Then, the constants C_j can be calculated by means of multivariate statistical analysis, e.g., by adopting a Least Squares or a Maximum Likelihood approach. Once C_j values have been evaluated, the thickness of shallow lithologies can be calculated for whatever point of the study area.

This may provide a promising powerful method of geotechnical characterization at urban scale and at a relatively low cost. This model may also be adapted to study variations in subsidence velocity over time, according to a multi-layer Terzaghi consolidation model. In this case, Eq. 1 would be nonlinear and, therefore, the analysis would follow a nonlinear multivariate approach.

Conclusion

- The A-DInSAR post-seismic data, recorded in the time range 2010-2021, revealed a subsidence phenomenon, still ongoing, due to the concurring effect of variation in pore pressures and secondary consolidation of shallow and deep rocks. The correlation analysis and the evidence illustrated in Fig. 3d allow us to conclude that subsidence velocities are mainly controlled by the properties and thicknesses of shallower rock layers, such as RS and LAB.
- The cross-correlation analysis highlighted a significant correlation between seasonal fluctuations in subsidence rate and rainfall variations.
- The seasonally adjusted A-DInSAR time series highlighted an anomaly in the subsidence trend, observable during the Amatrice-Norcia seismic sequence of 2016. The study of this anomaly deserves attention and will be the subject of future research.
- Ground deformations detected by means of A-DInSAR technology may provide a promising inversion criterion, enabling us to perform a geotechnical characterization of shallow rock layers, over large areas, at relatively low costs.

References

Amoroso, S.; Gaudiosi, I.; Tallini, M.; Di Giulio, G.; Milana, G. 2018: 2D site response analysis of a cultural heritage: the case study of the site of Santa Maria di Collemaggio Basilica (L'Aquila, Italy). Bull. Earthq. Eng., 16, 4443–4466, doi:10.1007/s10518-018-0356-2.

Antonielli B., Della Seta M., Esposito C., Scarascia Mugnozza G., Schilirò L., Spadi M., Tallini M. 2020: *Quaternary rock avalanches in the Apennines: New data and interpretation of the huge clastic deposit of the L'Aquila Basin (central Italy)*. Geomorphology, 361, 107194, doi: 10.1016/j.geomorph.2020.107194

Sciortino A., Guerriero V., Marini R., Spadi M., Mazzanti P., Tallini M. 2023: *Satellite A-DInSAR pattern recognition for seismic vulnerability mapping at city scale: insights from the L'Aquila (Italy) case study*. GIScience & Remote Sensing. https://doi.org/10.1080/15481603.2023.2293522

Tallini, M.; Lo Sardo, L.; Spadi, M. 2020: *Seismic site characterisation of Red Soil and soil-building resonance effects in L'Aquila downtown (Central Italy)*. Bull. Eng. Geol. Environ., 79, 4021–4034, doi:10.1007/s10064-020-01795-x.

Tallini, M.; Spadi, M.; Cosentino, D.; Nocentini, M.; Cavuoto, G.; Di Fiore, V. 2019: *High-resolution seismic reflection exploration for evaluating the seismic hazard in a Plio-Quaternary intermontane basin (L'Aquila downtown, central Italy)*. Quat. Int. 2019, 532, 34–47, doi:10.1016/j.quaint.2019.09.016.

Corresponding author: vincenzo.guerriero@univaq.it

Supervised and unsupervised machine learning approaches for identifying the preparatory process of moderate earthquakes at The Geysers, California

A.G. Iaccarino[1], M. Picozzi[1,2]

[1]Università degli Studi di Napoli "Federico II", Dipartimento di Fisica "Ettore Pancini", Napoli, Italy
[2]National Institute of Oceanography and Applied Geophysics, OGS, Sgonico, Italy

Earthquakes prediction is considered the holy grail of seismology. After almost a century of efforts without convincing results, the recent raise of machine learning (ML) methods in conjunction with the deployment of dense seismic networks has boosted new hope in this field. Even if large earthquakes still occur unanticipated, recent laboratory, field and theoretical studies support the existence of a preparatory phase preceding earthquakes, where small and stable ruptures progressively develop into an unstable and confined zone around the future hypocenter (Dresen et al., 2020; Kato & Ben-Zion, 2020; Mignan, 2012).

Here, we present two works focused on the induced seismicity at The Geysers geothermal field in California. Due to its complex geological structure, the industrial operations for energy production and the existence of a dense seismic network, the Geysers area represents a natural laboratory for seismicity studies (Bentz et al., 2019; Holtzman et al., 2018; Martínez-Garzón et al., 2020; Trugman et al., 2016).

We address the preparatory phase of Mw≥3.5 earthquakes identification problem by developing ML approaches to analyze time-series of physics-related features extracted from catalog information and estimated for events that occurred before the mainshocks. Specifically, we study the temporal evolution of the *b-value* from the Gutenberg-Richter (b), the magnitude of completeness (Mc), the fractal dimension (Dc), the inter-event time (dt), and the moment rate (Mr).

In a first work (Picozzi & Iaccarino, 2021), we use a supervised technique (Recurrent Neural Network, RNN) to reveal the preparation of 8 Mw≥3.9 earthquakes. In the second one (Iaccarino & Picozzi, 2023), we apply an unsupervised K-means clustering technique on 19 Mw≥3.5 events.

The results of the first work show that the preparatory phase for the three testing Mw≥3.9 earthquakes lasted from few hours to few days, in agreement with the short-time preparation process (~1 day) observed for a similar magnitude natural earthquake (De Barros et al., 2020).

In the second work, we show that out of 19 moderate magnitude events considered, a common preparatory phase for 11 events is clearly identified, plus other 5 events for which we can guess a preparatory phase but with different characteristics from the previous ones. The latter result confirms that even within the same tectonic context different possible activation behavior may exist. The duration of the preparatory process ranges between about 16 hours and 4 days. We observe that also for the retrieved preparatory process a decrease in b, and Dc, and an increase of Mr, as found by many authors (Gulia & Wiemer, 2019; Mignan, 2011; Picozzi et al., 2023). Finally, we find a clear spatial correlation (Fig. 1) between events with a preparation phase and the location of injection's wells, suggesting an important role of fluids in the preparatory process.

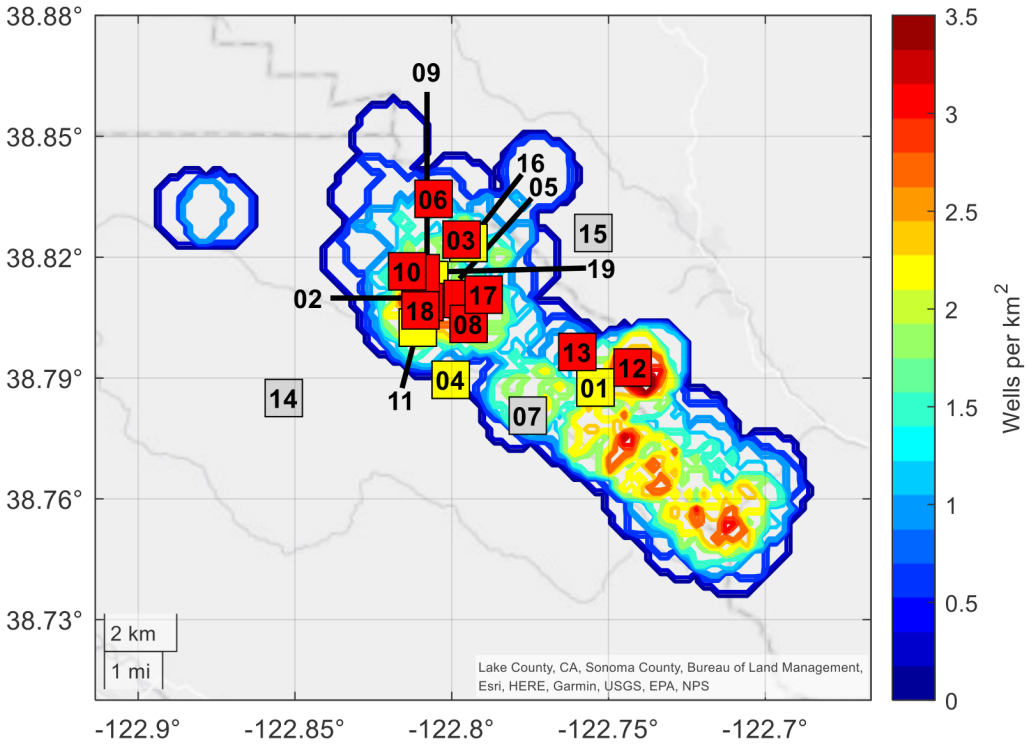

Fig. 1 – Maps of the M3.5 events compared to the areal well density (contour plot). The events with a preparatory phase are shown as red squares; yellow squares refer to the events with an unclear preparatory phase; the other M3.5 events as grey squares.

References

Bentz, S., Martínez-Garzón, P., Kwiatek, G., Dresen, G., & Bohnhoff, M. (2019). Analysis of Microseismicity Framing ML ' 2.5 Earthquakes at The Geysers Geothermal Field, California. Journal of Geophysical Research: Solid Earth, 124(8), 8823–8843. https://doi.org/10.1029/2019JB017716

De Barros, L., Cappa, F., Deschamps, A., & Dublanchet, P. (2020). Imbricated Aseismic Slip and Fluid Diffusion Drive a Seismic Swarm in the Corinth Gulf, Greece. Geophysical Research Letters, 47(9), e2020GL087142. https://doi.org/10.1029/2020GL087142

Dresen, G., Kwiatek, G., Goebel, T., & Ben-Zion, Y. (2020). Seismic and Aseismic Preparatory Processes Before Large Stick–Slip Failure. Pure and Applied Geophysics, 177(12), 5741–5760. https://doi.org/10.1007/s00024-020-02605-x

Gulia, L., & Wiemer, S. (2019). Real-time discrimination of earthquake foreshocks and aftershocks. Nature 2019 574:7777, 574(7777), 193–199. https://doi.org/10.1038/s41586-019-1606-4

Holtzman, B. K., Paté, A., Paisley, J., Waldhauser, F., & Repetto, D. (2018). Machine learning reveals cyclic changes in seismic source spectra in Geysers geothermal field. Science Advances, 4(5). https://doi.org/10.1126/SCIADV.AAO2929/SUPPL_FILE/AAO2929_SM.PDF

Iaccarino, A. G., & Picozzi, M. (2023). Detecting the Preparatory Phase of Induced Earthquakes at The Geysers (California) Using K-Means Clustering. Journal of Geophysical Research: Solid Earth, 128(10), e2023JB026429. https://doi.org/10.1029/2023JB026429

Kato, A., & Ben-Zion, Y. (2020). The generation of large earthquakes. Nature Reviews Earth & Environment 2020 2:1, 2(1), 26–39. https://doi.org/10.1038/s43017-020-00108-w

Martínez-Garzón, P., Kwiatek, G., Bentz, S., Bohnhoff, M., & Dresen, G. (2020). Induced earthquake potential in geothermal reservoirs: Insights from The Geysers, California. The Leading Edge, 39(12), 873–882. https://doi.org/10.1190/TLE39120873.1

Mignan, A. (2011). Retrospective on the Accelerating Seismic Release (ASR) hypothesis: Controversy and new horizons. Tectonophysics, 505(1–4), 1–16. https://doi.org/10.1016/J.TECTO.2011.03.010

Mignan, A. (2012). Seismicity precursors to large earthquakes unified in a stress accumulation framework. Geophysical Research Letters, 39(21), 21308. https://doi.org/10.1029/2012GL053946

Picozzi, M., & Iaccarino, A. G. (2021). Forecasting the Preparatory Phase of Induced Earthquakes by Recurrent Neural Network. Forecasting, 3(1), 17–36. https://doi.org/10.3390/forecast3010002

Picozzi, M., Iaccarino, A. G., & Spallarossa, D. (2023). The preparatory process of the 2023 Mw 7.8 Türkiye earthquake. Scientific Reports 2023 13:1, 13(1), 1–10. https://doi.org/10.1038/s41598-023-45073-8

Trugman, D. T., Shearer, P. M., Borsa, A. A., & Fialko, Y. (2016). A comparison of long-term changes in seismicity at The Geysers, Salton Sea, and Coso geothermal fields. Journal of Geophysical Research: Solid Earth, 121(1), 225–247. https://doi.org/10.1002/2015JB012510x: Title. Journal.

Corresponding author: antoniogiovanni.iaccarino@unina.it

Detection capability of earthquakes by a hydraulic pressure device in the Gran Sasso aquifer (central Italy)

D. Isaya[1], G. De Luca[2], M. Tallini[1]

1 Dipartimento di Ingegneria Civile, Edile-Architettura e Ambientale, Università degli Studi dell'Aquila
2 Istituto Nazionale di Geofisica e Vulcanologia

1. Introduction

The Gran Sasso aquifer (GSA) can be considered paradigmatic of the fissured-karst carbonate ones of the Mediterranean domain as concerns also the Earthquake Hydrology topic because (*i*) it is crossed by several active faults, (*ii*) it is placed in central Italy characterized by high Seismic hazard and (*iii*) it hosts the INFN underground laboratory (UL). UL is a strategic site for studying aquifer versus earthquakes because it represents a unique "window" within the deep saturated zone located in the GSA core which has above a very thick unsaturated zone (more than a thousand of meters). Therefore, UL rock mass volume is not involved by shallow hydrological processes and this opportunity generally it is very rare to find. For these considerations, UL was used to monitor groundwater parameters in the inter-, co- and post-seismic period above all of the recent 2009 L'Aquila earthquake and the 2016-2017 Central Italy seismic sequence (Adinolfi Falcone et al., 2012; De Luca et al., 2016; 2018; Petitta and Tallini, 2002).

As stated, we present further data concerning the estimation of the detection capacity of earthquakes by a hydraulic pressure device (in the following HPD) installed in the boreholes S13 and S14 (for their location see Fig. 1) by comparing earthquake detected by the INGV seismic station GIGS, placed in UL. The HPD measures at very high frequency (20 Hz) the hydraulic pressure and the boreholes S13 and S14 are located very near to UL. Moreover, the detection capability of earthquakes by the HPD installed in the boreholes S13 and S14 was compared to that due to earthquake-induced hydrological phenomena (liquefaction, stream discharge increase, mud

volcanoes) in worldwide sites (Galli, 2000; Manga and Wang, 2015).

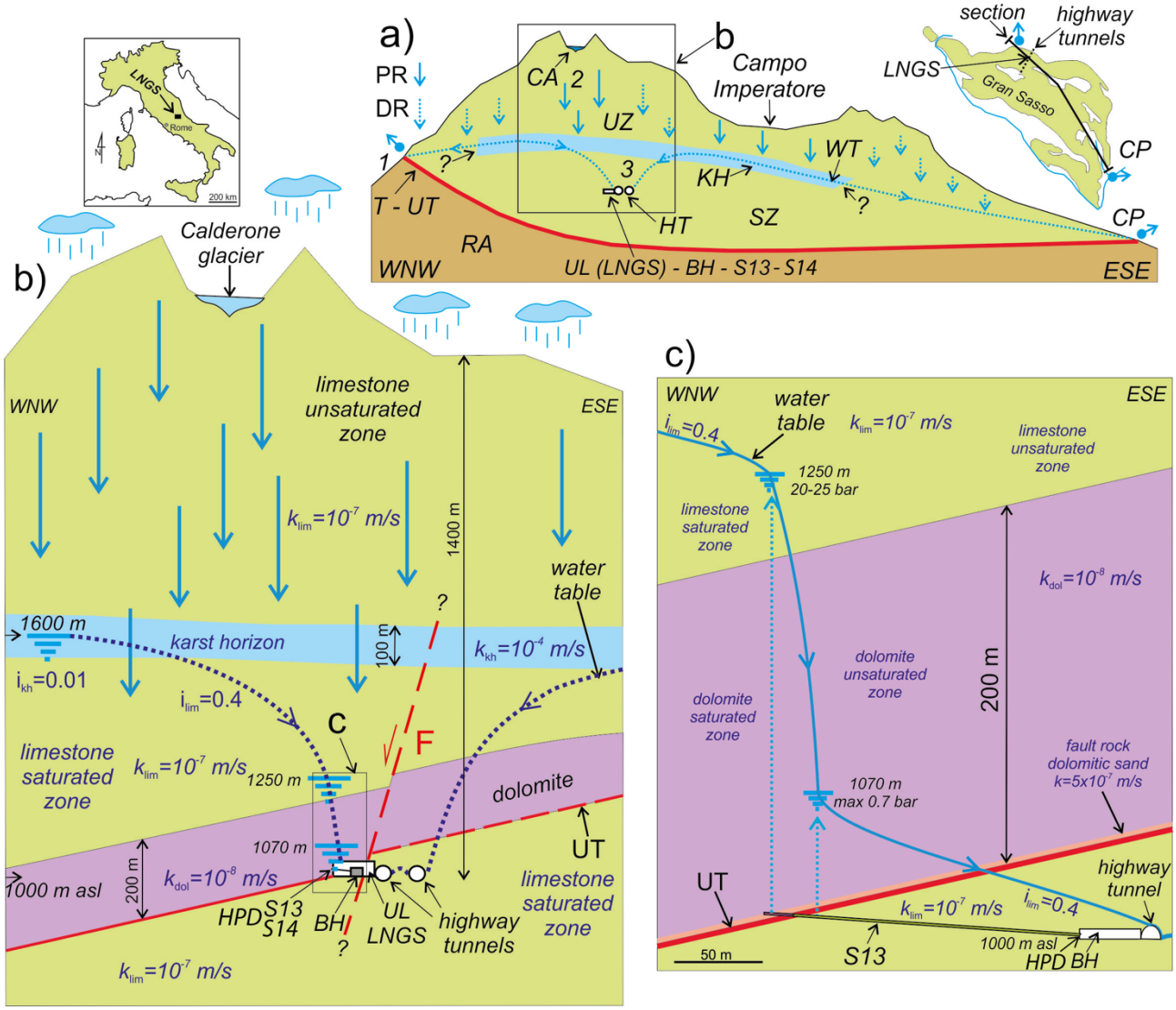

Figure 1 – (a) Sketch of GSA transversal to the highway tunnels and passing through UL and borehole S13 area. UZ: Unsaturated Zone; SZ: Saturated Zone; KH: Karst Horizon; RA: Regional Aquiclude; T: permeability boundary (regional Thrust); UT: local thrust named Upper Thrust; WT: Water Table; HT: Highway Tunnels; UL LNGS: Underground Laboratories; BH: Borehole Hall; CA: Calderone glacier (high elevation water reservoir – preferential recharge area); 1: overflow spring (CP: Capo Pescara spring); 2: preferential groundwater flowpath area; 3: preferential groundwater flowing toward the UL; PR: Preferential Recharge; DR: Diffuse Recharge; S13, S14: monitored horizontal boreholes, S14 is located very near to S13 (HPD). The hydrogeological relationships in the square are showed into details in (b). (b) Detailed hydrogeological relationships between Calderone glacier acting as a water reservoir for the carbonate aquifer down below; i: hydraulic gradient; k: hydraulic conductivity (m/s) (kh: karst horizon; lim: limestone; dol: dolomite). The hydrogeological relationships in the square are showed in detail in (c) (De Luca et al., 2018).

2. The water pressure device (HPD) and the INGV seismic station GIGS

The Borehole Hall (BH of Fig. 1), placed near UL at 965 m asl, hosts six horizontal boreholes (among which S13 and S14) and UL hosts the INGV seismic station GIGS located at around 250 m from BH. For the purposes of this work, boreholes S13 and S14, adjacent to each other, were monitored.

The borehole S13, has a horizontal length of 190 m, slopes gently upwards by ~5° and intercepts a fault near its end (UT of Fig. 1). The first 175 m of S13 are intubated, while the last 10 m drain

within the Upper Triassic dolomite (Fig. 1). The borehole S14, the same is 170 m long and drains within the same rocks as the borehole S13.

The boreholes S13 and S14 were equipped with a 3-channel, 24-bit analog-digital converter ADC (model SL06 by SARA Electronic Instrument company, http://www.sara.pg.it/), with a very high hydraulic pressure sampling frequency (20 Hz).

The hydraulic scheme of the experimental apparatus (showed in Fig. 5 in De Luca et al. 2018) is composed by (a) the horizontal boreholes; (b) an old analogic manometer; (c) a hydraulic valve always open during the data acquisition periods; (d) hydraulic pressure sensor; (e) hydraulic valve not completely close to enable the measurement of temperature and electrical conductivity in a container (h); (f) temperature sensor; (g) electrical conductivity sensor; (h) transparent plastic container housing the temperature and electrical conductivity sensors. Water is expelled when reaching about three quarters of the volume of the container.

The hydraulic pressure measured at the head of the 150-200 m long horizontal boreholes was about 0.5-0.7 MPa (piezometric height of 50-70 m), except for borehole S13, where a much higher pressure was recorded, about 2.0-2.5 MPa (piezometric head of 200–250 m).

Inside UL, the INGV seismic station GIGS, which was also adopted as part of the GINGER experiment used also to study the Rotational seismology (Belfi et al., 2017; Di Virgilio et al., 2017), is equipped with two broadband seismometers (Nanometrics Trillium 240 s and Guralp CMG 3T 360 s). This instrumentation is used both for continuous microseismic monitoring of GSA and for recording global seismicity (Italian seismicity and teleseismic events).

The main objective of the work was to identify and correlate the coincidences between earthquakes on a global, regional and local scale to the variations in hydraulic pressure within GSA detected by the HPD installed in the boreholes S13 and S14. To this end, we proceeded by comparing the hydroseismograms obtained from the hydraulic pressure values recorded in the HPD of the boreholes S13 and S14 and the seismograms recorded by the INGV seismic station GIGS.

The time interval for data acquisition, observation and analysis was between May 1st, 2015 and December 31st, 2022 and the monitoring is still going on.

3. Hydraulic pressure versus seismic data discussion

In the period May 2015 and December 2022, the HPD recognized 130 earthquakes compared to the 974 analysed. The event recognition by HPD means that (i) the hydraulic pressure signal recorded by the sensors is attributable to a hydroseismogram and, (ii) the time coincidence of the hydroseismogram with the seismogram of the same event recorded by the seismic station GIGS (Fig. 2).

Based on the elaboration of the above-mentioned hydraulic pressure versus seismic data it was possible to plot the diagrams of Fig. 3 which summarize the results.

The top plot of Fig. 3 shows two dotted lines: the grey line represents the sensitivity limit for the detection of seismic events reported by Manga and Wang (2015), as a result of a review of all similar studies until 2015; the blue line, obtained from the observation in the time interval of 15 months (May 2015-September 2016) by De Luca et al. (2016), is more sensitive, regardless of distances, with respect to that of Manga and Wang (2015). The slope of the blue line by De Luca et

al. (2016) is compatible with the results obtained with this study, despite the observation of a greater number of events due to a significantly longer observation period. However, approximately 20 events detected by the HPD with epicentral distances greater than 2000 km are located below the blue line (top plot, Fig. 3). On the other hand, 5 events with a Mw of 6.5 are superficial. Therefore, with the same magnitude and distance, deep events are not detected by the HPD.

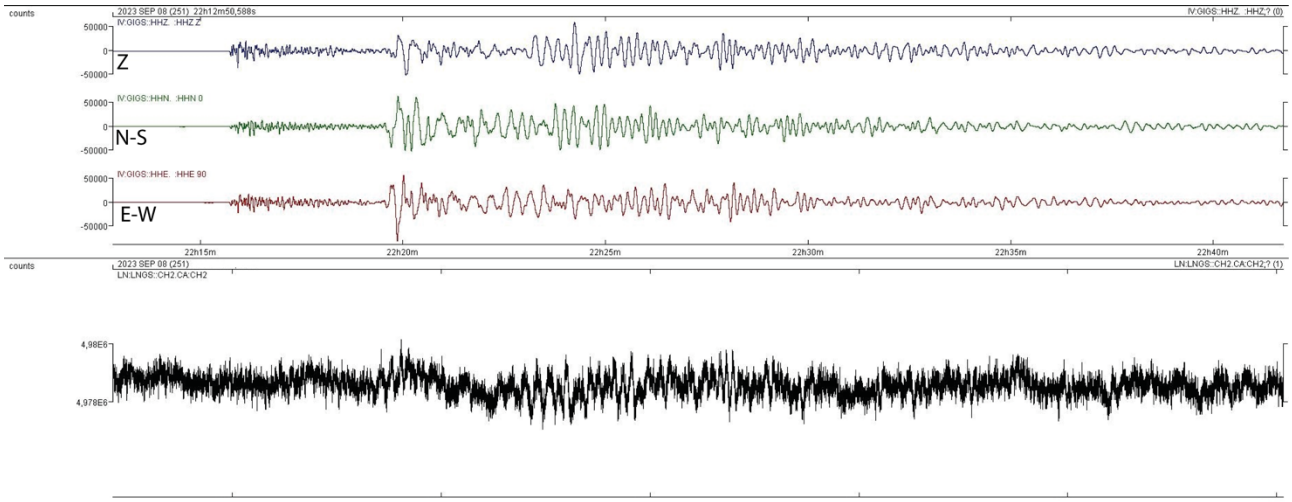

Figure 2 – Mw 6.8 earthquake occurred in Morocco on 9 September 2023 at 22:11:00 UTC. Top panel: The blue (Z), green (N-S) and brown (E-W) seismic traces refer to the vertical, N-S and E-W components, respectively, recorded by the INGV seismic station GIGS. Bottom panel: black trace is the hydraulic pressure signal recorded in the borehole S13 (i. e., hydroseismogram).

Events with an epicentral distance of less than 200 km, the hypocentral depth is low (about 5-20 km, shallow earthquakes). Beyond 200 km of epicentral distance, the first deep earthquakes that are identified with distances just over 200 km are those in the Tyrrhenian area, which however are not detected by the HPD system (bottom panel, Fig. 3). In accordance with the top plot in Fig. 3, HPD is more sensitive to surface events. Instead, the events detected with hypocentral depth greater than 80 km are significantly reduced.

Also note in the cluster at the top right (top plot of Fig. 3: A) as among the events at greater depth, i.e. greater than approximately 500 km, the HPD detected only two events (Mw 7.6 event located in the Sea of Japan at a depth of 675 km and epicentral distance of 10527 km, and the Mw 8.1 event located in the sea of Fiji Islands at a depth of 574 km and an epicentral distance of 17089 km).

In the most populous cluster (top plot of Fig. 3: B), consisting of events with a hypocentral depth between approximately 5 km and 20 km, HPD detectability is instead correlated to epicentral distance and magnitude.

Generally, events with a magnitude less than 3 and with an epicentral distance and hypocentral depth less than 20 km are not detected by the HPD.

Instead, most of the events detected by the HPD, regardless of the epicentral distance, have hypocentral depths generally less than 20 km as perhaps with the same magnitude the deep events generate smaller amplitudes of the surface waves which are normally particularly evident in the hydroseismograms.

Among the earthquakes with greater depth, i.e. greater than 80 km, only those of high magnitude greater than Mw 7.3 are detected by HPD (bottom plot, Fig. 3).

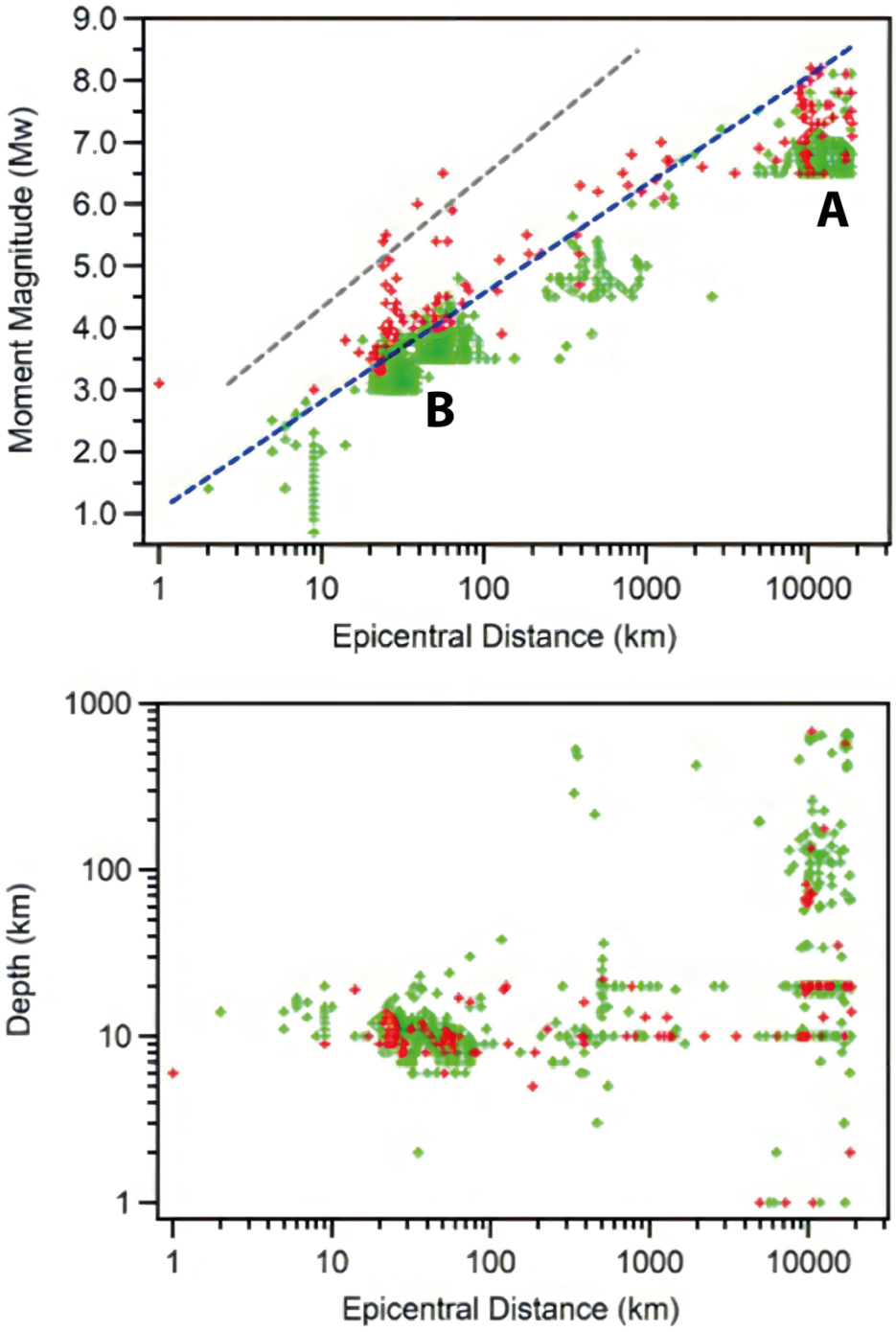

Figure 3 – Top: M_W versus epicentral distance (km) of earthquakes detected by HPD installed at boreholes S13 and S14 from May 2015 to December 2022. The blue line is the detection level obtained from De Luca et al. (2016), while the gray line refers to the detection level obtained from Manga and Wang (2015). A and B refer to the main cluster (see the text). Bottom plot: hypocentral depth (km) vs epicentral distance (km) of the same events population reported in the top plot. Red and green crosses represent earthquakes observed and not observed by the HPD, respectively.

4. Conclusions

We present further data concerning the estimation of the detection capacity of earthquakes by a hydraulic pressure device (HPD) (boreholes S13 and S14 in De Luca et al., 2018, Fig. 1) placed very near to UL, by comparing earthquakes detected by the INGV seismic station GIGS, located in UL.
The detection capability of the HPD was compared to the currently published bibliography (e.g., Galli, 2000; Manga and Wang, 2015).
In the period May 2015 and December 2022, the HPD recognized 130 earthquakes compared to the 974 analysed.
The results confirm the sensitivity of the HPD higher than the known values and recorded so far on a global scale (Manga and Wang, 2015).
Considering (i) the hydrogeological versus seismotectonic importance of GSA, (ii) the hydrological sensitivity to earthquakes of the HPD, which is placed in the GSA core, so that in a unique and strategic location, and (iii) the encouraging and significant results, the hydrological versus seismic monitoring of the HPD is continuing.

References

Adinolfi Falcone R., Carucci V., Falgiani A., Manetta M., Parisse B., Petitta M., Rusi S., Spizzico M., Tallini M.; 2012: *Changes on groundwater flow and hydrochemistry of the Gran Sasso carbonate aquifer due to the 2009 L'Aquila earthquake*. Ital. J. Geosci. (Boll. Soc. Geol. It.), 131, 459-474, doi: 10.3301/IJG.2011.34.

Belfi J., Beverini N., Bosi F., Carelli G., Cuccato D., De Luca, G., et al.; (2017): *Deep underground rotation measurements: Gingerino ring laser gyroscope in Gran Sasso*. Rev. Sci. Instrum. 88:034502, doi: 10.1063/1.4977051.

De Luca G., Di Carlo G., Tallini M.; 2016: *Hydraulic pressure variations of groundwater in the Gran Sasso underground laboratory during the Amatrice earthquake of August 24, 2016*. Annals of Geophysics 59, Fast Track 5, doi: 10.4401/AG-7200.

De Luca G., Di Carlo G., Tallini M.; 2018: *A record of changes in the Gran Sasso groundwater before, during and after the 2016 Amatrice earthquake, central Italy*. Scientific Reports, G:15982, doi: 10.1038/s41598-018-34444-1.

Di Virgilio, A.D.V. et al.; 2017: *GINGER: A feasibility study*. Eur. Phys. J. Plus, 132, 157, https:// doi.org/10.1140/epjp/i2017-11452-6.

Galli P.; (2000): *New empirical relationships between magnitude and distance for liquefaction*. Tectonophysics, 324, 169–187, doi: 10.1016/S0040-1951(00)00118-9.

Manga M., Wang C.-Y.; (2015): *Earthquake Hydrology*. In: Gerald Schubert (editor-in-chief), Treatise on Geophysics, 2nd edition, Vol 4. Oxford: Elsevier, 305–328, https://doi.org/10.1016/ B978-0-444-53802-4.00082-8.

Petitta, M., Tallini, M.; 2002: *Idrodinamica sotterranea del massiccio del Gran Sasso (Abruzzo): indagini idrologiche, idrogeologiche e idrochimiche (1994–2001)*. Boll. Soc. Geol. It., 121, 343–363.

Corresponding author: isayadomenico@live.it

Fault (re)activation, fluid-induced seismic activity and seismogenic potential in the Val d'Agri (southern Italy).

A. Lavecchia[1], V. Serlenga[2], M. Filippucci[1,3], T.A. Stabile[2], G. Prosser[4], A. Tallarico[1,3]

[1] University of Bari, Italy
[2] National Research Council of Italy, Institute of Methodologies for Environmental Analysis, Tito Scalo, Italy
[3] National Institute of Geophysics and Volcanology, Rome, Italy
[4] University of Basilicata, Potenza, Italy

The Val d'Agri is one of the regions around the globe where the relationship between fluids and earthquakes has been suggested. In this basin, wastewater reinjection led to the reactivation of the Costa Molina blind fault and the generation of a microearthquakes cluster. In addition, another cluster is observed within the basin and is related to seasonal variations of the Pertusillo Lake. The factors that led to the generation and reactivation of the fault systems responsible for both the Costa Molina and Pertusillo seismic clusters are still a matter of debate. Consequently, the characteristics of the seismic potential in the basin is largely uncertain. Therefore, we have built a 2D thermo-mechanical model to address the main mechanisms promoting the present-day tectonic setting of the Val d'Agri and assess the seismic hazard in the basin. Our findings suggest that deformation is mostly led by mechanisms of thin-skinned tectonics and the Burano Formation acts as a décollement layer between the sedimentary cover and the crystalline basement. Based on the quantification of the stress field in the region and estimations of the crust's Coulomb stress values, we suggest that the Val d'Agri sedimentary cover is characterized by a high seismic hazard, and therefore a careful approach is advisable when fluids injection and storage activities are programmed.

Corresponding author: alessio.lavecchia@uniba.it

From field geology to strain and stress inversion: multi-scale variations throughout peninsular Italy

G. Lavecchia[1,2], C. Andrenacci[1,2], S. Bello[1,2], F. Pietrolungo[1,2], D. Cirillo[1,2], A. Carducci[1,2], F. Ferrarini[1,2], F. Brozzetti[1,2], R. de Nardis[1,2]

[1] DiSPuTer, Università degli Studi "G. d'Annunzio" Chieti-Pescara, Chieti, Italy
[2] CRUST - Centro inteRUniversitario per l'analisi Sismotettonica Tridimensionale, Chieti, Italy

Exploring the complexities of stress field variations in regions beyond tectonic plate boundaries has become a central focus in innovative geodynamic and seismotectonic research. Traditional methodologies in this field encompass examining focal mechanisms and in situ stress data enriched by geological features and Quaternary fault-slip data. The formal inversion of stress, a critical step in establishing precise principal stress orientations and magnitudes, necessitates a wealth of input data, a resource more commonly abundant in seismological studies than geological investigations.

Italy has recently seen an increase in geological data availability by introducing two comprehensive databases containing Quaternary fault/striation pairs (FSP) records. These are represented by the QUIN 1.0 and 2.0 databases, collecting a total of ~8000 FSP in Lavecchia et al. (2022 and 2024) for Northern-Central and Southern Apennines, respectively. Together, the databases span the extensional intermountain seismogenic Province of the entire Peninsular Italy, encompassing approximately 2,500 kilometers along its strike length.

In the present study, we integrate the information from the two QUIN databases with additional data, forming a unified TOTOQUIN database. The latter serves as foundational input for conducting detailed strain analysis and formal stress inversion at three scales: 1) Structural site scale, 2) Fault system scale, and 3) Regional domains scale.

The multi-order principal stress attitudes and relative magnitudes obtained through TOTOQUIN inversion are analyzed and interpreted in light of the geometry and multi-scale segmentation pattern of the outcropping intra-Apennine fault system and the associated crustal structure. The analysis is further enriched by comparison with deformation trends derived from earthquake and geodetic data. Through this examination, the study validates the complete consistency between Italy's long-term and current stress fields, effectively bridging a crucial gap in the seismotectonic puzzle.

Beyond its evident applications in seismic hazard, seismotectonics, and geodynamics, the TOTOQUIN stress database holds the potential to optimize resource exploration strategy and

ensure the resilience of engineered structures in the intra-Apennines region. In general, the comprehensive insights derived from this study contribute to the scientific understanding of regional tectonics and have far-reaching implications for practical and strategic endeavors in the broader geological context.

References

Lavecchia, G., Bello, S., Andrenacci, C. et al. QUaternary fault strain INdicators database - QUIN 1.0 - first release from the Apennines of central Italy. Sci Data 9, 204 (2022). https://doi.org/10.1038/s41597-022-01311-8

Lavecchia, G., Bello, S., Andrenacci, C. et al. QUIN 2.0 - new release of the QUaternary fault strain INdicators database from the Southern Apennines of Italy. Sci Data (2024).

Corresponding author: glavecchia@unich.it

Analysis and preliminary results of the Mw 4.9, Marradi seismic sequence (September 18th, 2023), in the northern Apennines, carried out by the BSI working group.

A. Lisi, L. Arcoraci, P. Battelli, M. Berardi, B. Castello, D. Latorre, A. Marchetti, M. Michele, V. Misiti, A. Nardi, D. Piccinini, A. Rossi, Gruppo di lavoro del Bollettino Sismico Italiano*

*** A. Battelli, B. Cantucci, C. Castellano, D. Cheloni, M.G. Ciaccio, L. Colini, M. De Caro, A. Frepoli, L. Improta, A.M. Lombardi, A. Malagnini, L. Margheriti, M.T. Mariucci, G. Mele, C. Melorio, L. Miconi, G. Modica, C. Montuori, N.M. Pagliuca, M. Pastori, S. Pinzi, L. Pizzino, A. Sciarra, T. Sgroi, S. Spadoni, R. Tardini, C. Thermes, A. Bono, I. Carluccio, E. Della Bina, M. Fares, D. Franceschi, V. Lauciani, A. Mandiello, M. Maniscalco, S. Pintore, M. Quintiliani, M. Moretti, R. Di Stefano, L. Scognamiglio**

Istituto Nazionale di Geofisica e Vulcanologia, Roma, Italy

On September 18, 2023, an earthquake with a magnitude of M_L=4.8 (Mw=4.9) occurred a few kilometers SW of Marradi (FI) at a depth of about 8 kilometers. The computed TDMT solution of the mainshock suggests a normal fault oriented NW-SE (Scognamiglio et al., 2006).

The earthquake, preceded by a foreshock with a magnitude of M_L=3.3 (Mw=3.4), triggered a seismic sequence characterized, in the first two months, by approximately 700 aftershocks localized by the staff on duty in the Seismic Monitoring Room of the INGV in Rome, including 6 events with a magnitude of $M_L \geq 3.0$ occurred in the first two days.

The sequence occurred in a high seismic hazard region. The two closest historical earthquakes occurred in the Mugello area about 30 km SW of Marradi (and about 25 km north of Florence): one, whose magnitude (Mw) is estimated to be about 6.0, occurred on June 13, 1542 while the other with estimated magnitude (Mw) of about 6.4 occurred on June 29, 1919. The second one is among the strongest (most significant) Italian earthquakes of the 20th century, and also one of the strongest known to date with its epicentre in the northern Apennines. The affected area was that of Mugello, with extensive damage both in the province of Florence and on the Romagna side of the Apennines.

The analysts of the BSI (Italian Seismic Bulletin) reviewed the initial three days of the sequence, paying special attention to the hours directly following the mainshock. The BSI work mainly consists in revising the picking of P and S phases and assigning them appropriate weights, retrieving previously unused phases, and evaluating the maximum amplitudes necessary for calculating the value of M_L. The latter is a critical aspect of the initial phases of a seismic sequence; in fact, the occurrence of events is very close in time, making it challenging to estimate the

maximum amplitudes and, consequently, the magnitude automatically. Through this analysis, they have identified an earthquake with a magnitude of M_L=3.4, occurring approximately one minute after the mainshock and overlooked during the surveillance service. Furthermore, a comprehensive effort to recover smaller seismic events not initially analyzed in the Seismic Monitoring Room resulted in the localization of 498 earthquakes, nearly a 30% increase within the first three days. In Figure 1(a-d), hypocentral parameters and time readings of the 352 earthquakes detected in the Seismic Monitoring Room have been compared with those of the same events revised by the BSI. It is evident as both the horizontal and vertical errors, as well the seismic gap associated with the location decrease for the dataset analyzed from the BSI, while the number of P and S phases increases for the same dataset. Subsequently, the events revised from BSI were initially relocated by applying the NonLinLoc code (Lomax et al., 2000) using a 1D regional velocity model from Pastori et al. (2019). Following this, a double-difference technique (Waldhauser and Schaff, 2008) was applied to improve the geometries of the activated structures (see Figure 2).

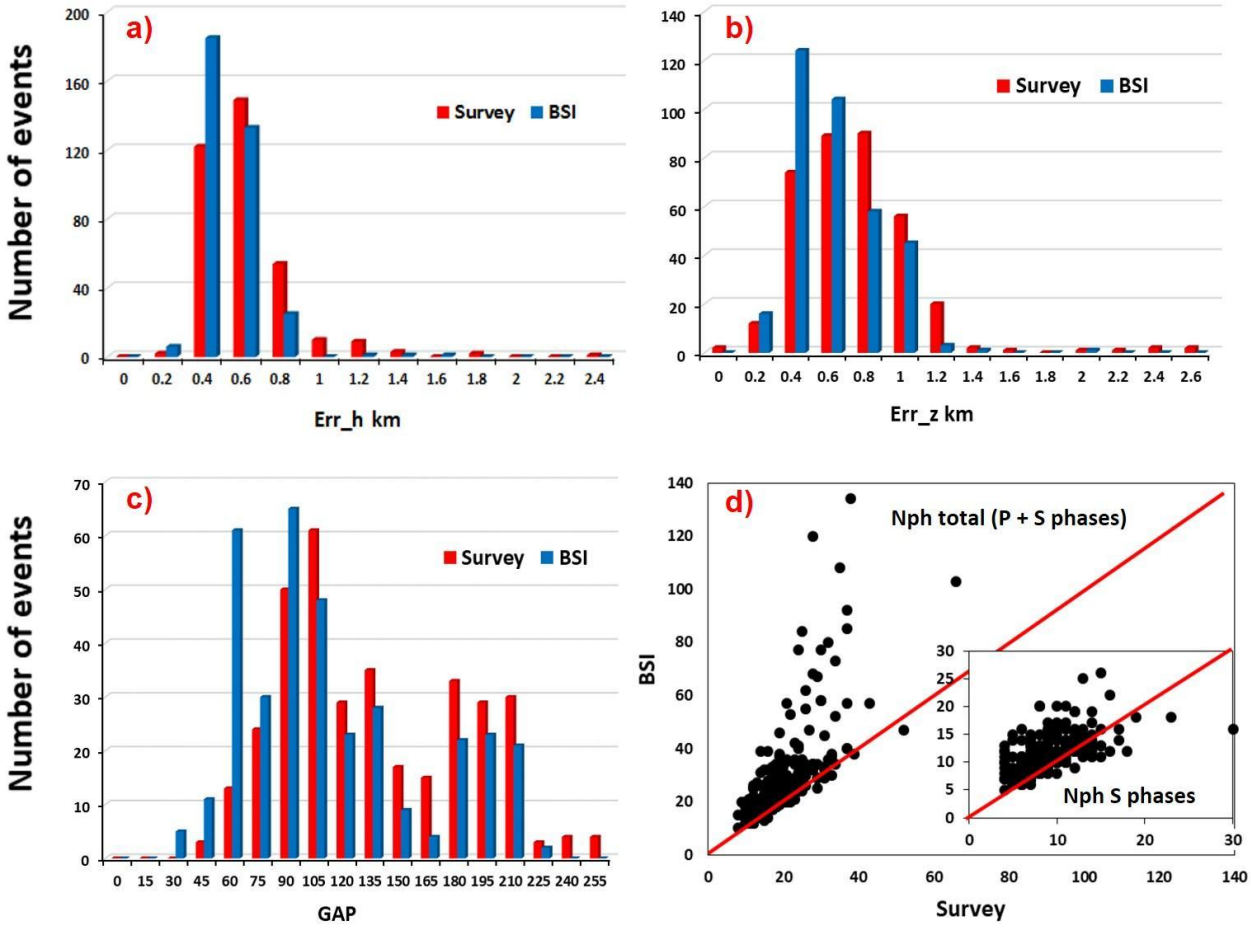

Fig.1 – Comparison between hypocentral parameters (a,b,c) and used time readings (d) for the same 352 earthquakes detected, during the first 3 days of the sequence, from seismic monitoring room and revised from BSI.

Concomitantly, an analysis using the *template-matching* technique was applied, for the period from September first to October 10th, to identify events overlooked by the Earthworm system in the Seismic Monitoring Room. The results are shown in Figure 3. It was found that the number of detections increased by approximately 60%. Furthermore, Figures 3c and 3d put in evidence as the

larger number of new detected earthquakes is characterized by lower magnitude. This result highlights the value of integrating this type of analysis to complement the efforts of the Italian Seismic Bulletin (BSI).

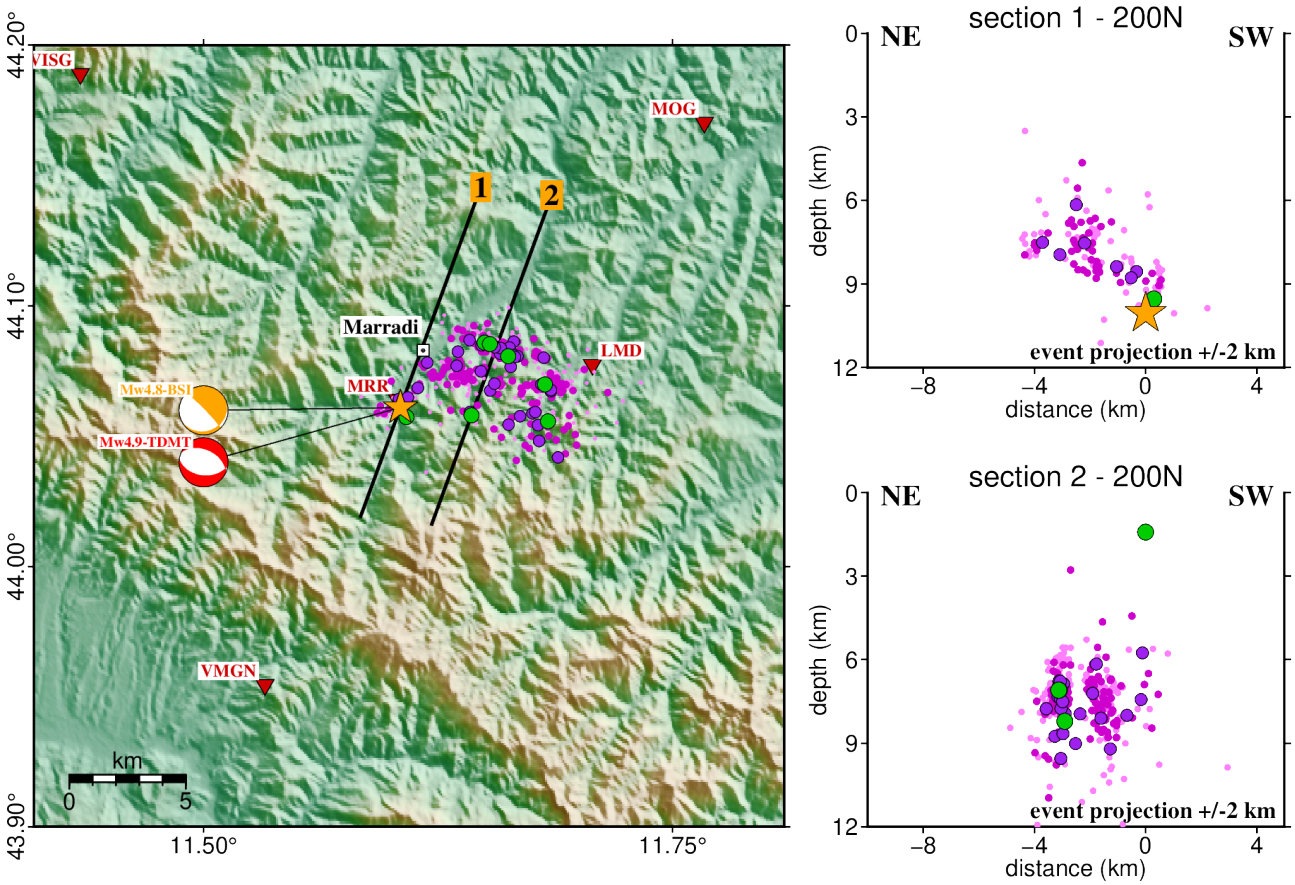

Fig.2 – Map view: Earthquakes recorded in the first 3 days of the sequence and revised by the BSI working group. Events are initially relocated using the NonLinLoc code (Lomax et al., 2000) and the local 1D velocity model from Pastori et al. (2019). Subsequently, a double-difference code (Waldhauser and Schaff, 2008) is applied to improve the geometries of the activated structures. The two vertical cross-sections are oriented perpendicular to the strike of the computed TDMT solution of the Mw=4.9 event (Scognamiglio et al., 2006).

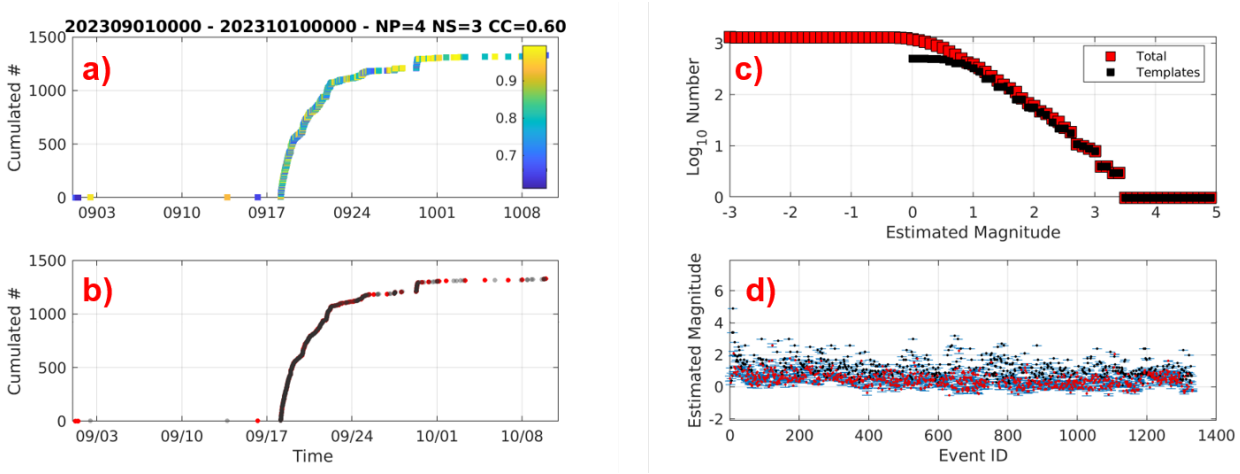

Fig.3 – Cumulative number of events over the time and relative magnitude distribution until October 10th. (a)The colours represent the average cross-correlation (CC) of each detected event. (b) New detected events are shown in red colour while the templates are in grey. (c) The Gutenberg - Richter relationship. (d) The magnitude of matched events (in red with their respective error bars) and that of the templates (in black).

References

Lomax, A., J. Virieux, P. Volant and C. Berge, 2000. Probabilistic earthquake location in 3D and layered models: Introduction of a Metropolis-Gibbs method and comparison with linear locations, in Advances in Seismic Event Location Thurber, C.H., and N. Rabinowitz (eds.), Kluwer, Amsterdam, 101-134.

Pastori M., Latorre, D., (2021). Report del Progetto DPC-B2-2019-2021, WP1-Task4.

Scognamiglio, L., Tinti, E., Quintiliani, M. (2006). Time Domain Moment Tensor (TDMT) [Data set]. Istituto Nazionale di Geofisica e Vulcanologia (INGV). https://doi.org/10.13127/TDMT

Waldhauser, F. and D.P. Schaff (2008), Large-scale relocation of two decades of Northern California seismicity using cross-correlation and double-difference methods. J. Geophys. Res., 113, B08311, doi:10.1029/2007JB005479.

Corresponding author: arianna.lisi@ingv.it

Studying the Viability of Kinematic Rupture Models and Source Time Functions with Dynamic Constraints

M.E. Locchi[1], F. Mosconi[1], M. Supino[2], E. Casarotti[2], E. Tinti[1,2]

[1] Sapienza Università di Roma, Rome, Italy;
[2] Istituto Nazionale di Geofisica e Vulcanologia, Rome, Italy;

Earthquakes are one of the greatest natural hazards and a better understanding of the physical processes causing earthquake ruptures is required for appropriate seismic hazard assessment. Progresses on the knowledge of the seismic source have been made in both modelling the increasingly dense geophysical data and through laboratory experiments. Kinematic modelling is a standard tool to provide important information on the complexity of the earthquake rupture process and for making inferences on earthquake mechanics.

Despite recent advances, kinematic models are characterized by uncertainties and trade-offs among parameters (inherent non-uniqueness of the problem). It has been documented that, for the same earthquake, source models obtained with different methodologies can exhibit significant discrepancies in terms of slip distribution, fault planes geometry and rupture time evolution.

Prescribing the slip velocity on causative faults (source time function) is one of the crucial components in the models because it contains key information about the dynamics and prescribes how fast each point on the fault reaches its final slip (Tinti et al, 2005). Such function is nonetheless one of the most poorly observationally constrained characteristics of faulting.

Recently, slip velocity time histories have been studied with laboratory earthquakes and a systematic change of mechanical properties and traction evolution has been observed to correspond with a change in the shape of slip velocity (Scuderi et al., 2020). However, this function is assumed a-priori following two different approaches: in the single window approach an analytic function is assumed; while in the multi window approach the complexity and heterogeneity of the process is simulated through the linear sum of cumulative slip at different time windows. The final effect is a heterogeneous function over time that accumulates the slip until it reaches the final slip. Multiple-window inversions impose the smoothness of the slip distribution, introduce a sort of causality but at the same time heterogeneity of the rupture front prescribed by the different time windows, solve for the evolution of rupture, allow the slip at each point to be determined by multiple time window functions with no predetermined shape, and observe the slip functions a posterior (Konca et al., 2013). Nevertheless, the limited resolution of the kinematic models prevents reliable constraints on the slip velocity time history.

To investigate the effect of the slip velocity function on the ground motion and on the inverted slip history on the fault we run a series of forward and inverse models. We generate spontaneous

dynamic models and use their ground motion as real events and we invert the data with kinematic models (Fig. 1).

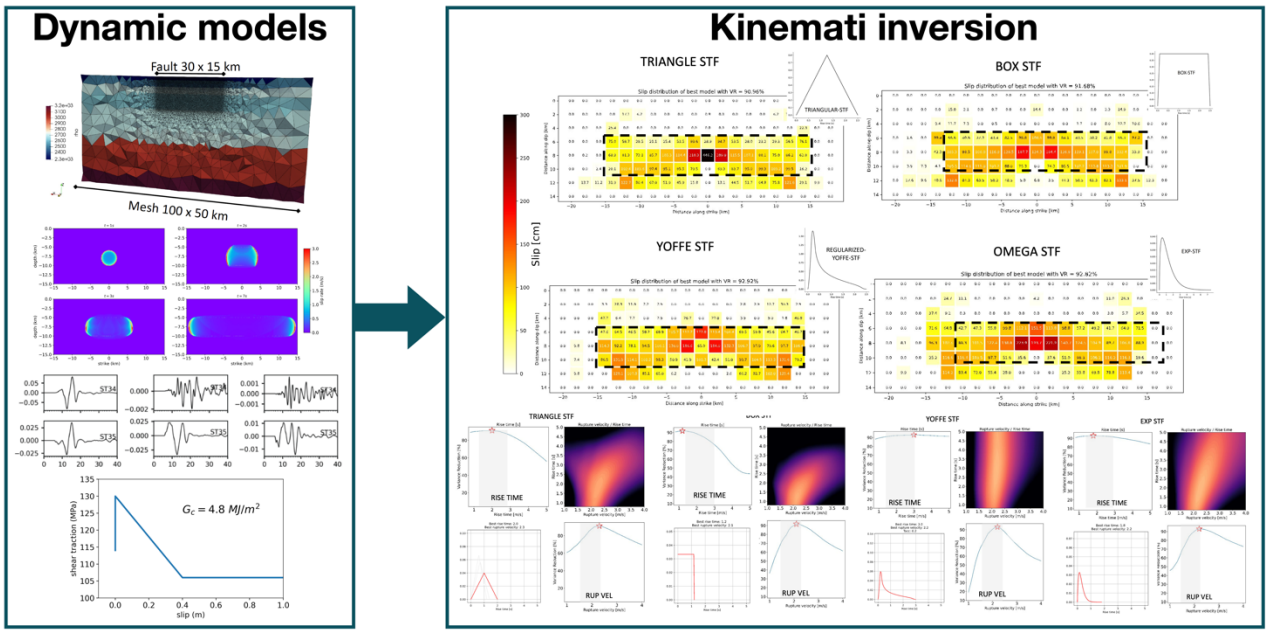

Fig. 1: Workflow for one model: results from spontaneous rupture of a bidirectivity model on the left; kinematic inversions results using ground-motion from dynamic model. For each source time function different rise time and rupture velocity were tested. The slip distribution from best models of each source time function.

The kinematic inversion has been conducted utilizing both single-time and multi-time windowing and to mitigate the uncertainties we adopt four different source time functions on the fault plane (triangular, box, regularized-yoffe and exponential). In this way we could examine how the slip velocity function influences the slip distribution on the fault plane and test if the inferred kinematic parameters are consistent with the dynamic models. We also examine the variability of the peak ground velocity (PGV) from forward modelling of synthetic seismograms up to 1 Hz, for a dense grid of phantom received, assuming the same slip distribution, rise time and rupture velocity, but changing the source time functions. Those results provide a glimpse of the variability that kinematic source time functions (dynamically consistent or not) might have when used as a constraint to model the earthquake dynamic.

Finally, we use the retrieved kinematic history on the pseudo-dynamic models to examine how different kinematic assumptions lead to a variability in the shear stress evolution. We focus on some dynamic parameters such as the breakdown work, the stress drop, and the Dc parameter. Those results provide a glimpse of the variability that kinematic source time functions (dynamically consistent or not) might have when used as a constraint to model the earthquake dynamic.

References

Ozgun Konca, A., Kaneko, Y., Lapusta, N., & Avouac, J. P. (2013). Kinematic inversion of physically plausible earthquake source models obtained from dynamic rupture simulations. *Bulletin of the Seismological Society of America*, *103*(5), 2621-2644.

Scuderi, M. M., Tinti, E., Cocco, M., & Collettini, C. (2020). The role of shear fabric in controlling breakdown processes during laboratory slow-slip events. *Journal of Geophysical Research: Solid Earth*, *125*(11), e2020JB020405.

Tinti, E., Fukuyama, E., Piatanesi, A., & Cocco, M. (2005). A kinematic source-time function compatible with earthquake dynamics. *Bulletin of the Seismological Society of America*, *95*(4), 1211-1223.

Corresponding author: mariaeugenia.locchi@uniroma1.it

Recalibration of the intensity prediction equation in Italy using the Macroseismic Dataset DBMI15 V2.0

B. Lolli[1], P. Gasperini[2,1], G. Vannucci[2]

[1]Istituto Nazionale di Geofisica e Vulcanologia, Sezione di Bologna
[2]Dipartimento di Fisica e Astronomia, Università di Bologna

We re-compute the coefficients of the intensity prediction equation (IPE) in Italy using the data of the DBMI15 V2.0 intensity database and the instrumental and combined (instrumental plus macroseismic) magnitudes reported by the CPTI15 V2.0 catalog. We follow the same procedure described in a previous article, consisting of a first step in which the attenuation of intensity *I* with respect to the distance *D* from macroseismic hypocenter is referred to the expected intensity at the epicenter I_E and a second step in which I_E is related to the instrumental magnitude M_i, the combined magnitude M_c, the epicentral intensity I_0 and the maximum intensity I_{max}, using error-in-variable (EIV) regression methods.

The main methodological difference with respect to the original article concerns the estimation of the uncertainty of I_E to be used for EIV regressions, which is empirically derived from the standard deviation of regression between I_E and M_i and also used for the regressions of I_E with M_c, I_0 and I_{max}.

In summary, the new IPE determined from DBMI15 V2.0 is

$$I = I_E - 0.0081\left(D - h\right) - 1.072\left[ln(D) - ln\left(h\right)\right]$$

where $D = \sqrt{R^2 + h^2}$, h=4.49 km and I_E can be calculated from the intensity data distribution of the earthquake. If the intensity data distribution is not available, I_E can be calculated from the following relationships

$$I_E = -2.578 + 1.867M_w$$

$$I_E = I_0$$

*Corresponding author: barbara.lolli@ingv.it

What is in the INGV ISIDe online database before 16 April 2005?

B. Lolli[1*], G. Vannucci[1] and P. Gasperini[2,1]

[1]Istituto Nazionale di Geofisica e Vulcanologia, Sezione di Bologna
[2]Dipartimento di Fisica e Astronomia, Università di Bologna

Abstract

The Italian Seismological Instrumental and Parametric Data-Base (ISIDe) is the recipient of earthquake data collected in real time by the Istituto Nazionale di Geofisica e Vulcanologia (INGV). When it went online, following a significant improvement of the seismic acquisition system of INGV, it was including only data since the second fortnight of April 2005. About ten years later, the data since the beginning of 1985 suddenly appeared without any other notice than the updating of the starting date of the dataset. However, the characteristics of the added data appeared clearly different from the following period both in terms of numbers of located earthquakes and of types of magnitudes provided. After having analyzed the numerical consistency and the calibration of magnitudes of ISIDe as a function of time from 1985 to 15 April 2005, we can say that such dataset is incomplete and poorly calibrated with respect to other catalogs of Italian seismicity (CSTI, CSI and HORUS) available for the same period. Hence, we suggest not to use it as it is for statistical analyses of Italian seismicity. However, it provides some magnitudes which are missed by other catalogs and thus might be used for improving such catalogs.

*Corresponding author: barbara.lolli@ingv.it

The implementation of the paleoseismological sites database into ITHACA Catalogue in the framework of the GeoScienceIR project

D. Maceroni[1], A.M. Blumetti[1], L. Bonadeo[2], M.P. Congi[1], V. Comerci[1], P. Di Manna[1], L. Guerrieri[1]

[1] ISPRA, Geological Survey of Italy, Roma, Italy
[2]Università degli Studi dell'Insubria, Dipartimento di Scienza ed Alta Tecnologia, Como, CO, Italy

The ITHACA (ITaly HAzard from CApable faults) Catalogue aims at collecting and summarising available information on capable faults affecting the national territory. ITHACA implementation started in the nineties, taking advantage from the knowledge deriving from siting studies of critical infrastructures (i.e., nuclear power plants, gas and oil pipelines, chemical plants, etc.). The first version was released for the 31st session of the International Geological Congress headed in Rio de Janeiro, Brazil, on August 6–17, 2000. Since then, the Catalogue has been continuously maintained and updated by the Geological Survey of Italy (ITHACA Working Group, 2019) and its present-day version is accessible through the following link: https://sgi.isprambiente.it/ithaca/viewer/index.html.

A capable fault is defined as an active fault able to produce permanent ruptures or deformation at or near the ground surface (surface faulting) during strong or moderate earthquakes (e.g. IAEA, 2015, 2022). The occurrence of surface faulting may cause serious damage to buildings and infrastructures and, therefore, it represents a geological hazard to be taken into due consideration at the local scale, particularly in the most densely populated and industrialised areas of the Italian territory. Consequently, the identification of capable faults and their characterization can provide useful information both for scientific research, aiming at seismotectonic studies, and for engineering purposes, intended for land use planning and management.

In this regard, in agreement with the "Guidelines for the management of territories affected by Active and Capable Faults" (Commissione Tecnica per la Microzonazione Sismica, 2015), the deepest degree of knowledge and insight achievable on capable faults require to perform paleoseismological investigations, site levels survey that allows to reconstruct the geological history of a given fault by analysing its past movements over the last few thousand years, providing useful information to define the seismogenetic and surface faulting potential of the fault.

For the same reason, since the very beginning of its implementation, the ITHACA Catalogue has included an information layer dedicated to paleoseismological sites (or paleosites). At that time, the compilation of the paleoseismological data in the Catalogue was in line with the available literature. Later, the collection of paleoseismological data has become insufficient and sparse in

comparison to the number of faults. As a result, it was decided not to include them in the public version of ITHACA.

However, in the last decade, also following the introduction of specific regulatory guidelines for fault displacement hazard assessment, paleoseismological studies have seen a significant increase, making available a large set of new data.

Given the relevance of this data for a better characterization of capable faults and, more broadly, to support the research aiming at minimising the risk associated with active and capable faults, it has become essential to make paleoseismological information again available within the ITHACA Catalogue. This choice will thus allow to improve the set of information associated with the archived faults, taking into account both the published studies on single faults and the already published inventories of paleoseismological data in Italy (e.g. Galli et al., 2008 and Cinti et al., 2021), and what is in the Catalogue, enriching the basket of information associated with the collected faults.

The paleoseismological sites database is implemented in the framework of the GeoSciencesIR project by collecting the information available from the published paleoseismological studies (Fig. 1a). The collected data are spatialized through GIS tools and organised in a relational database developed as a relational branch of the ITHACA Catalogue (Fig. 1a). The database consists of two main tables: the “Paleosites” attribute table and the “Paleoevent” related table. The first table refers to the identification of the paleoseismological site and provides geographic, geometric and descriptive attributes, including photographs and sketches of the trenches and evidence. The identification code (PaleoSiteCode) is linked to the FaultCode of the ITHACA fault, to which the paleoseismological study refers. Additional information is reported regarding the reference of the study and the location reliability of the site (Location Scale) (Fig. 1b). The second table provides a description of the paleoseismological evidence pointed out in the study, summarising the sequence of the faulting events and their characterization in terms of offset values and chronology, together with information on the type of sampled material and the dating methods applied for the age determination (Fig. 1c). To ensure a standardised compilation of field content, specific and detailed codelists have been arranged for each key domain. This enables driving and simplifying the compilation procedure and the dataset implementation, as well as ensuring that a certain field may only be populated with a list of preset attributes (Fig. 1d).

The paleosites database implementation in ITHACA enhances the set of information about capable faults collected in the Catalogue. The semantic and geographic link between the datasets in the Catalogue facilitates data access and cross-examination by offering an interactive view of fault traces and related paleoseismological evidence. This could be a useful tool for seismic hazard assessments, providing quick view of areas and faults where paleoseismological data is already accessible and, more importantly, facilitating access to the information for assessing the seismic and faulting potential of the mapped faults.

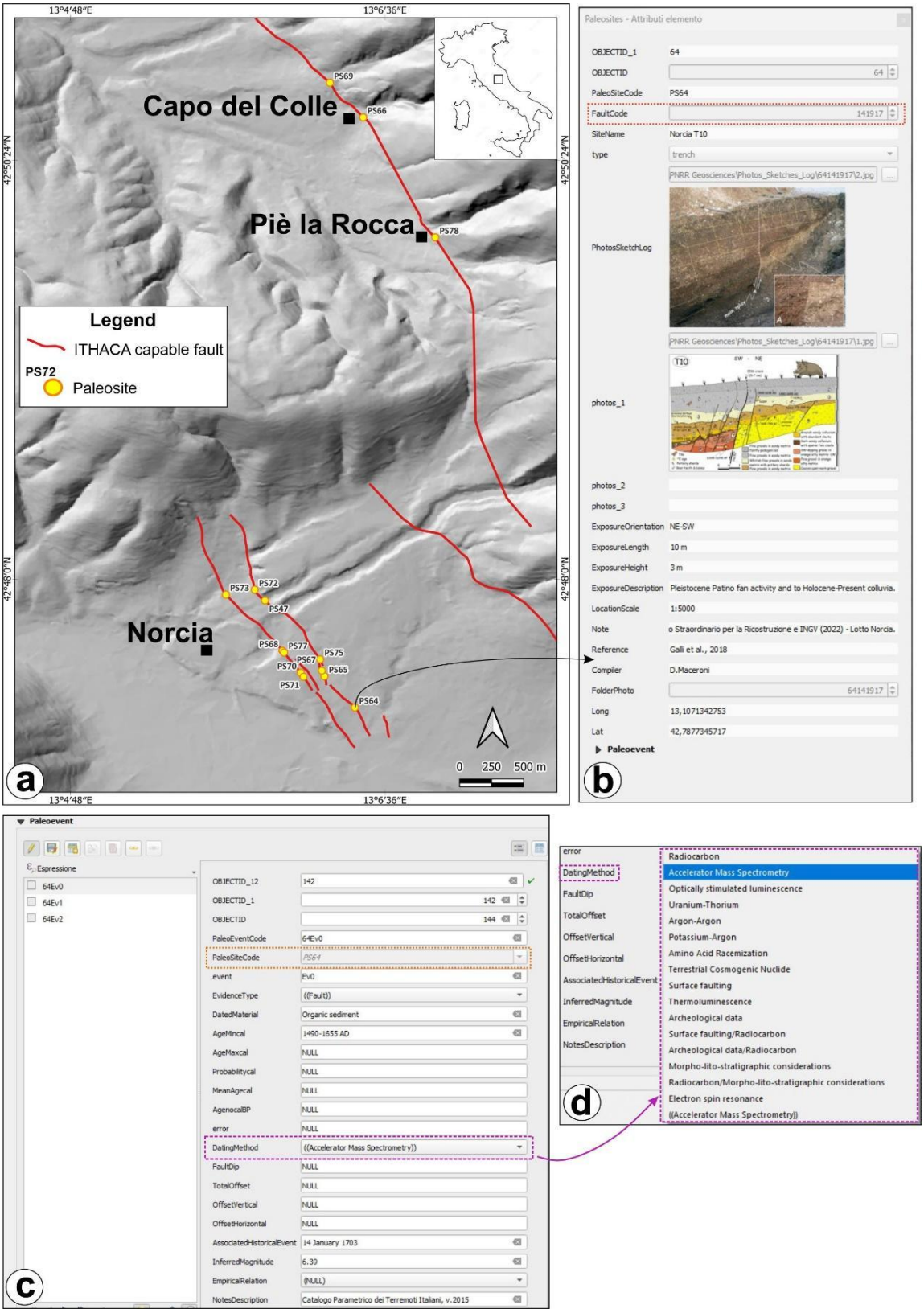

Fig. 4 – An example of a view of the ITHACA Catalogue that shows the geographic relations and architecture of the paleosites database, where each paleosites is connect to its respective ITHACA fault. a) View of the database for the Norcia-Campi basin, showing the traces of capable faults and the location of paleoseismological sites, labeled with specific identification codes (PaleoSiteCode); b) The "Paleosites" attribute table, which refers to the PS64 site. The link between the paleosite and the related capable fault is ensured by the "FaultCode" (dotted red box); c) The "Paleoevent" related table for the PS64 site. The connection is based on "PaleoSiteCode" (dotted orange box); d) A preset codelist for the "DatingMethod".

Finally, following the philosophy of open data fully adopted within the GeoSciencesIR project, the application of FAIR (Findable, Accessible, Interoperable and Reusable) principles to the entire ITHACA dataset has been promoted. Interoperability and data sharing will be ensured through the publication of OGC standard services (WMS, WFS and OFAPI). To simplify the resource reuse, the dataset will also be available in GeoPackage format with open licence attribution (CC BY 4.0).

Acknowledgments

The research activity described in this work is funded by European Union - NextGenerationEU programme- Mission 4 “Education and Research” - Component 2 “From Research to Business” – Investment 3.1 “Fund for the realisation of an integrated system of research and innovation infrastructures” - Project IR0000037 - GeoSciences IR. The Authors thank the Department of Earth, Environment and Resources Sciences of the University Federico II of Naples (Italy) for their help in collecting available paleoseismological data for the capable faults in central-southern Apennines.

References:

Cinti, F.R., Pantosti, D., Lombardi, A.M. & Civico, R. (2021). Modeling of earthquake chronology from paleoseismic data: Insights for regional earthquake recurrence and earthquake storms in the Central Apennines. Tectonophysics, 816, 10.1016/j.tecto.2021.229016

Dipartimento della Protezione Civile (2015). Microzonazione sismica. Linee guida per la gestione del territorio in aree interessate da faglie attive e capaci (FAC). http://www.protezionecivile.gov.it/media-comunicazione/pubblicazioni/dettaglio/-/asset_publisher/default/content/microzonazione-sismica-linee-guida-per-la-gestione-del-territorio-in-aree-interessate-da-faglie-attive-e-capaci-fac-

Galli, P., Galadini, F. & Pantosti, D. (2008). *Twenty years of paleoseismology in italy.* Earth-Science Reviewes 88 (2008) 89-117.

IAEA (2015). *The Contribution of Paleoseismology to Seismic Hazard Assessment in Site Evaluation for Nuclear Installations*. IAEA-TECDOC-1767. http://www.pub.iaea.org/MTCD/Publications/PDF/TE-1767_web.pdf

IAEA (2022). *Seismic Hazards in Site Evaluation for Nuclear Installations. Specific Safety Guide. IAEA Safety Standards*. Series SSG-9 (Rev.1) http://www.iaea.or/publications/14665/seismic-hazards-in-site-evaluation-for-nuclear-installations

ITHACA Working Group (2019). *ITHACA (ITaly HAzard from CApable faulting), A database of active capable faults of the Italian territory*. Version December 2019. ISPRA Geological Survey of Italy. Web Portal https://sgi.isprambiente.it/ithacaweb/Default

Corresponding author: deborah.maceroni@isprambiente.it

Seismic attenuation and stress on the San Andreas Fault at Parkfield: are we critical yet?

L. Malagnini*[1,2], R. M. Nadeau[2], and T. Parsons[3]

[1]Istituto Nazionale di Geofisica e Vulcanologia, Rome, Italy
[2]Berkeley Seismological Laboratory, University of California Berkeley, USA
[3]U.S. Geological Survey, Moffett Field, CA, 94035, USA

The Parkfield transitional segment of the San Andreas Fault (SAF) is characterized by the production of frequent quasi-periodical M6 events that break the very same asperity. The last Parkfield mainshock occurred on September 28th 2004, 38 years after the 1966 earthquake, and after the segment showed a ~22 years average recurrence time. The main reason for the much longer interevent period between the last two earthquakes is thought to be the reduction of the Coulomb stress from the M6.5 Coalinga earthquake of May 2nd1983, and the M6 Nuñez events of June 11th and July 22nd 1983.

Plausibly, the transitional segment of the SAF at Parkfield is now in the late part of its seismic cycle and current observations may all be relative to a state of stress close to criticality. This study aims at the recognition of the precritical state of the transitional segment of the SAF at Parkfield, in the hypothesis that the fluctuations of the attenuation parameter represent a proxy for the stress conditions in the crustal volume crossed by an active fault, even though the behaviour of the attenuation parameter in the last few years seems substantially different from the one that characterized the years prior to the 2004 mainshock.

A few questions arise from this study: (i) Does a detectable preparation phase for the Parkfield mainshocks exist, and is it the same for all events?; (ii) How dynamically/kinematically similar are the quasi-periodic occurrences of the Parkfield mainshocks? (iii) Are some dynamic/kinematic characteristics of the next mainshock predictable from the analysis of current data? (e.g., do we expect the epicenter of the impending failure to be co-located to that of 2004?) (iv) Should we expect the duration of the current interseismic period to be close to the 22-year “undisturbed” average value?

We respond to the questions above by analyzing the non-geometric attenuation of direct S-waves along the transitional segment of the SAF at Parkfield, in the close vicinity of the fault plane, between January 2001 and November 2023. Of particular interest is the preparatory behaviour of the attenuation parameter as the 2004 mainshock approached, on both sides of the SAF. We also show that the non-volcanic tremor activity modulates the seismic attenuation in the area, and possibly the seismicity along the Parkfield fault segment, including the occurrence of the mainshocks. The hypothesis is that the non-geometric attenuation is directly related to the bulk permeability of crustal rocks, which in turn is driven to crack density and interconnection.
Figure 1 shows a map of the investigated region, with the locations of the earthquakes in our dataset and more information of interest. An interesting observation is the 10-day smoothed rate of non-volcanic tremor (NVT) collected along the transitional segment of the SAF (Guilhem and

Nadeau, 2012). The long-term NVT rate (~8500 days, updated through November 15 2023) is plotted in red in Figure 2A, the cumulative NVT is plotted in black, and its detrended version is shown in Figure 2B. About 30-days prior to the 2004 Parkfield event a significant NVT fore tremor was observed (Nadeau and Guilhem, 2009; Guilhem and Nadeau, 2012). Prior to this fore tremor, a relatively quiescent period of ~120-days of NVT activity was also observed (Figure 2C).

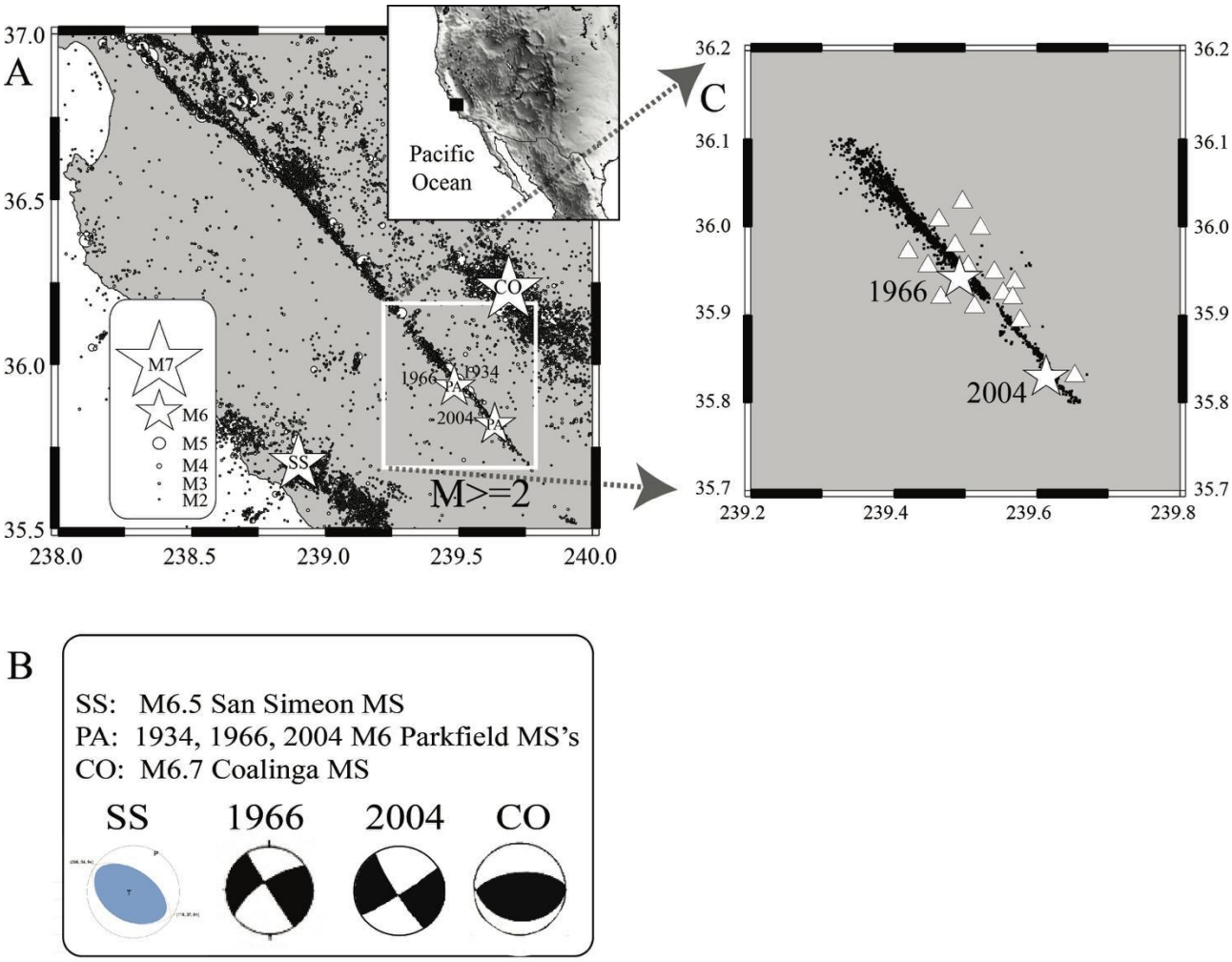

Figure 1. A: map of the region, showing the background seismicity and four mainshocks of specific interest in this study (white stars), whose focal mechanisms are indicated in B. C: i) epicentral locations of the SAF earthquakes used in this study; white triangles indicate the seismic stations of the HRSN.

A similar quiescent period also precedes the proposed foretremor of the next possible Parkfield M6 (Figure 2D). This 120-day quiescence is unusual for the majority of NVT episodes throughout the long-term NVT catalog (Figure 2A). The two pairs of dashed red vertical lines in Figures 2A,B correspond to the time windows of Figures 2C,D. Figure 2A suggests the presence of an anomaly in the tremor rate at Parkfield, which we call foretremor, between 15 and 30 days before the 2004 mainshock. A similar anomaly (another foretremor?) seems to characterize the tremor rate in

recent weeks (Figure 2B). Observations shown in Figure 2 are intriguing, although we can not produce solid proof of the recent anomaly being a foretremor.

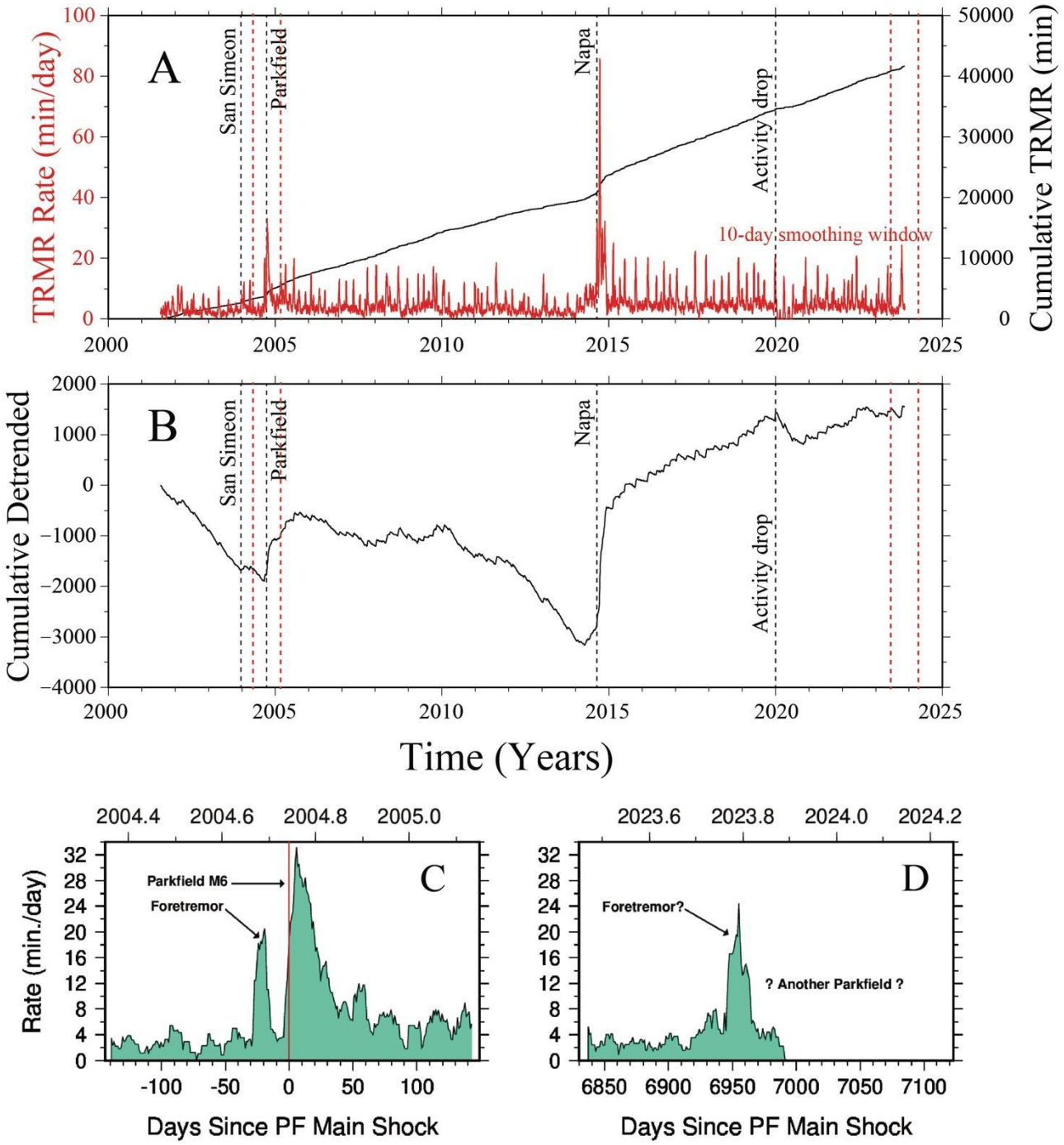

Figure 2. A) In red, the long term rate of non-volcanic tremor NVT (~8500 days) smoothed using a 10-day window (min/day); in black, the cumulative tremor activity (min). B) The detrended cumulative tremor activity. C) Rate of tremor 10-day smoothed (minutes/day) in the 293-day (9.7-month) 7-month time windows: May 7, 2004 - February 24, 2005. D) Rate of tremor 10-day smoothed (minutes/day) in the time window Jun 13, 2023 - April, 1, 2024. Bracketing dates of the two time windows of C and D are indicated in A and B by vertical dashed red lines.

The behaviour of the attenuation parameter during the latest portion of the earthquake cycle that ended with the mainshock of 28 September 2004 is shown in Figure 3, where are the logarithms of the ratios between spectral amplitudes taken at two specific hypocentral distances of 12 and 4 km

(the more such logarithms are negative, the stronger the attenuation). Spectral amplitudes are estimated through peak values of narrowband-filtered time histories: if *fc* is the central frequency, the bandpass filter is obtained by an eight-pole Butterworth low-pass filter with corner at $\sqrt{2}f_c$, followed by an eight-pole high-pass filter with a corner at $\frac{1}{\sqrt{2}}f_c$. After filtering, Random Vibration Theory (RVT) is applied to peak values to produce an estimate of spectral amplitude, given the time duration of the analyzed signal. Details can be found in Malagnini and Dreger (2016), and references therein.

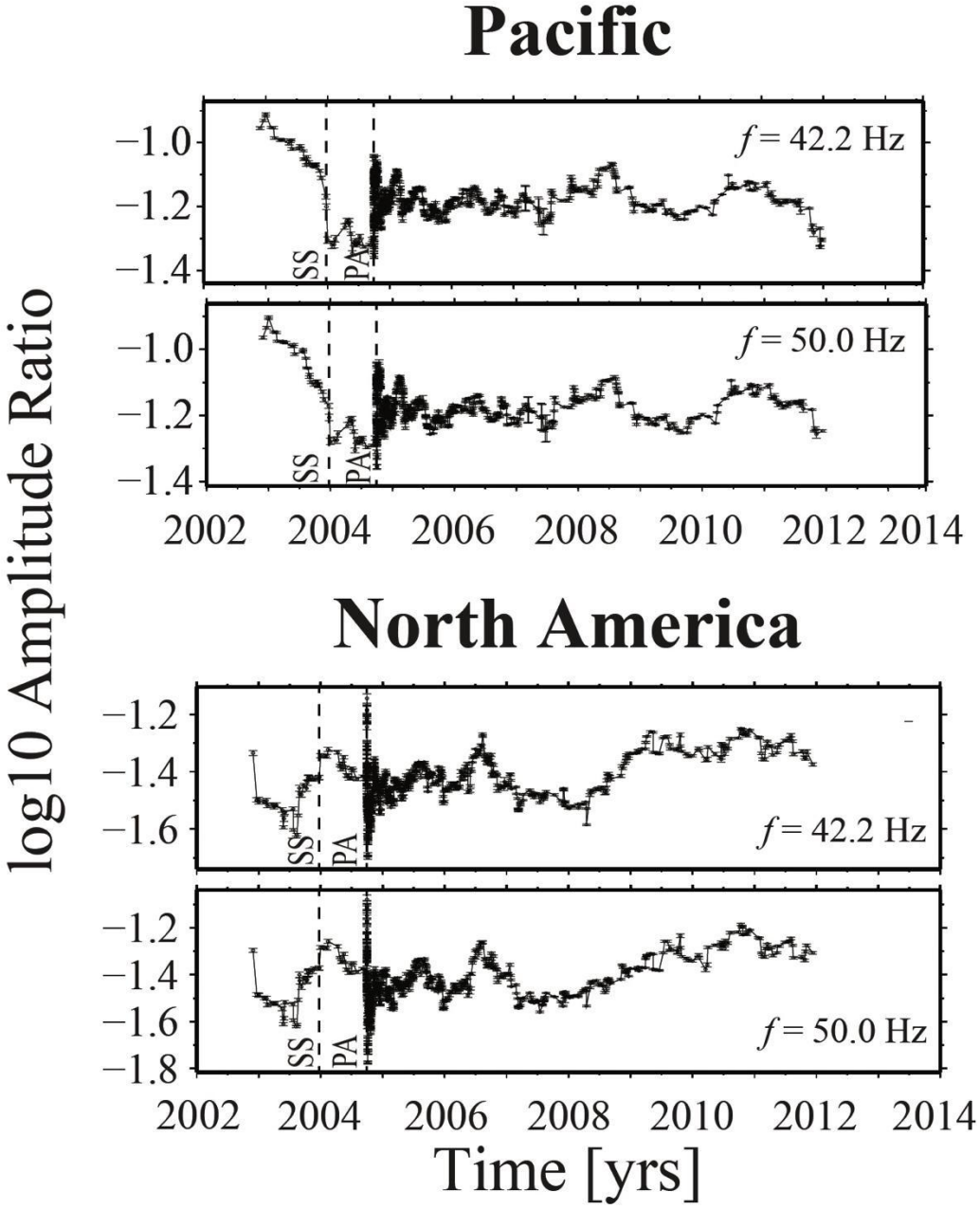

Figure 3. Logarithms of total attenuation experienced by direct S waves along the transitional segment of the SAF at Parkfield, between 4 and 12 km of hypocentral distance, at the indicated central frequencies of 42.2 and 50.0 Hz.

With Figure 4 we try to extract more specific information on two frequency bands at the two ends of the investigated spectrum: 2-5 Hz and 30-50 Hz. The quantities shown in Figure 4 are the stacked attenuation values that were calculated in the central frequencies contained in the

mentioned bands. Of great interest is the bifurcation of the stacked attenuation time histories that can be observed starting 6-8 weeks before the September 28, 2004 Parkfield mainshock. No bifurcation characterizes intermediate frequency bands.

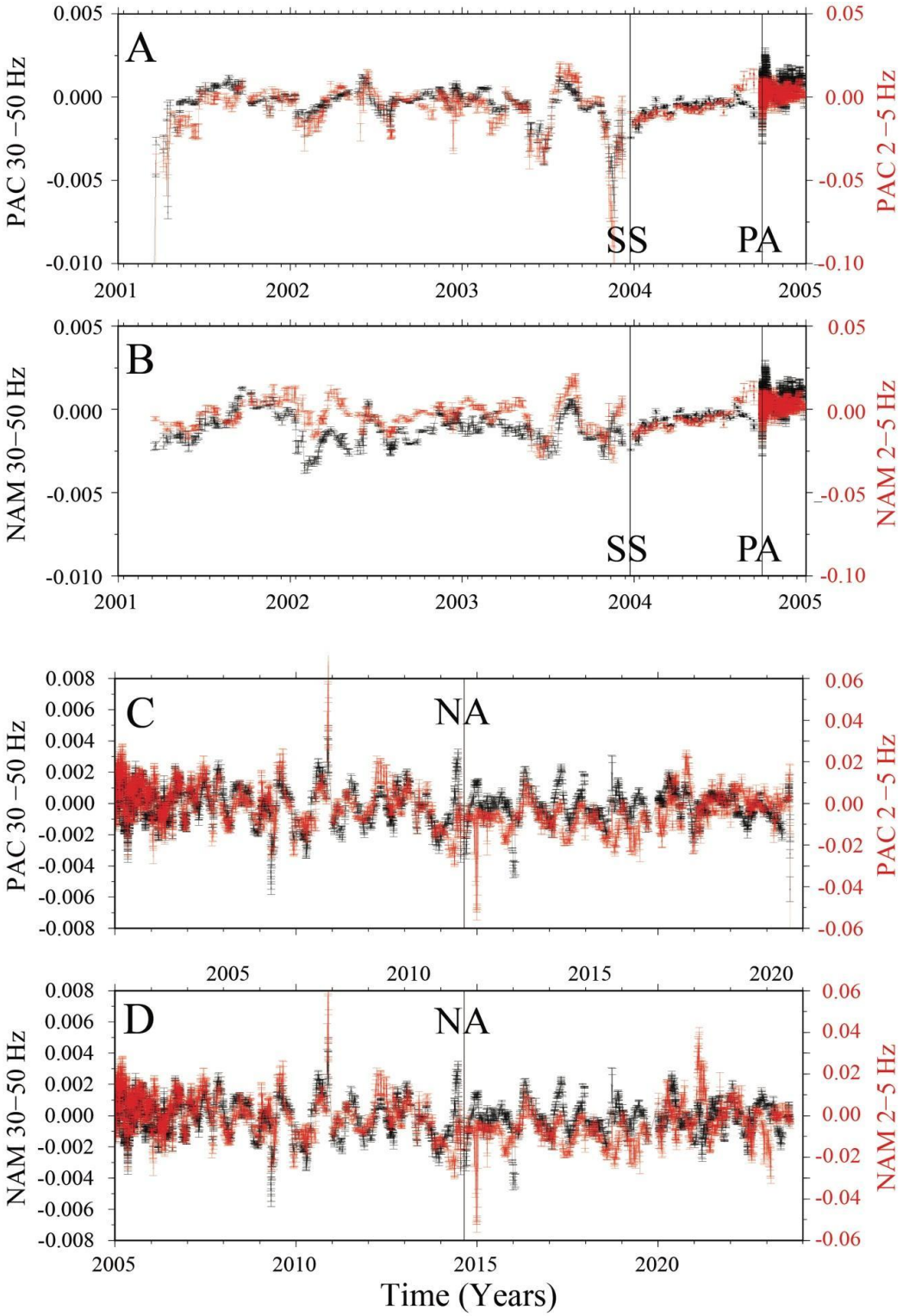

Figure 4. Stacked-averaged estimates of time histories of the variation of the attenuation parameter $\left(\delta\left(Q_S^{-1}(t,f)\right)\right)$ in two frequency bands: 2.0-5.0 Hz (black, left scale) and 30-50 Hz (red, right scale). In A and B the stacked-averaged values of the attenuation parameter are plotted in a three-year time window (01/01/2002 through 01/01/2005), whereas C and D show the stacked-averaged attenuation time histories between 01/01/2005 and the fall of 2023.

Following Sebastiani & Malagnini (2020), who provided a forecast for the next Parkfield mainshock via the analysis of the variability of the variance of the daily center of the seismic activity along the transitional segment of the SAF in the time window between 1973 and late 2019, we look at the variability of the variance of the attenuation anomalies as a function of time. Variances are computed over subsequent subsets of attenuation anomalies, and the latter are obtained as follows: after a number of samples is chosen (e.g. 40) , we look at the longest time window needed to gather 40 subsequent data points, then we apply that length to all the time windows that we analyze.

In each time window we randomly choose a subset of 40 data points to be used to compute the variance. We randomly choose 10% of data points to be eliminated from each subset and do multiple estimates of variance by looping through this bootstrap step of the analysis a number of times (10). We finally average all variance determinations. Time windows are moved, one data point at a time, toward more recent times. The analysis done without applying the bootstrapping/ averaging technique yields very similar results. In Figure 5 we plot the average variances, normalized by the length of the time window. We also point out that a single estimate of variance does not differ much from what we present here. Finally, Figure 6 shows the average attenuation parameter $\left(Q_S^{-1}(f) \right)$ calculated for the North American side (black) and for the Pacific side of the SAF (red), in the indicated time windows (2001-2004 and 2005-2019).

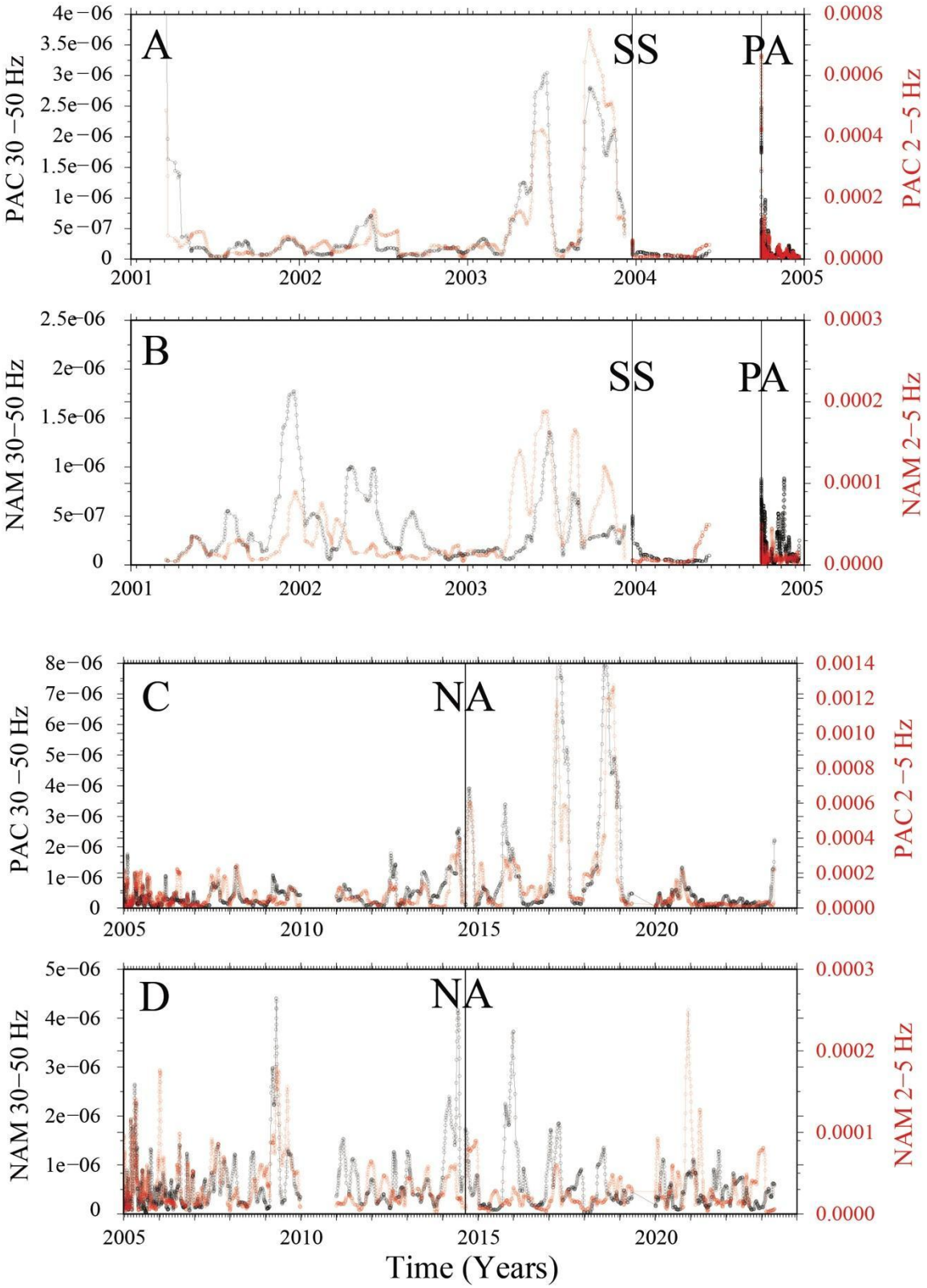

Figure 5. Variance of the stacked attenuation time histories of Figure 5 calculated on adjacent subsets of 40 data points. Note that, at the end of the previous seismic cycle, the San Simeon earthquake completely shuts off the variance of the attenuation time histories on both sides of the fault. Before being shut-off, variance shows an increasing trend on the Pacific side of the fault. During the current cycle, in the decade 2010-2020, a similar increasing trend is observed on the variance on the Pacific side of the SAF. SS, PA and NA indicate, respectively, the occurrences of the San Simeon, Parkfield, and Napa earthquakes. Comparing this Figure with Figure 2 we see a correspondence between the variance drop and a significant reduction of tremor activity in 2020, suggesting that the seismic attenuation (and possibly the main seismic activity) is modulated by the NVT rate.

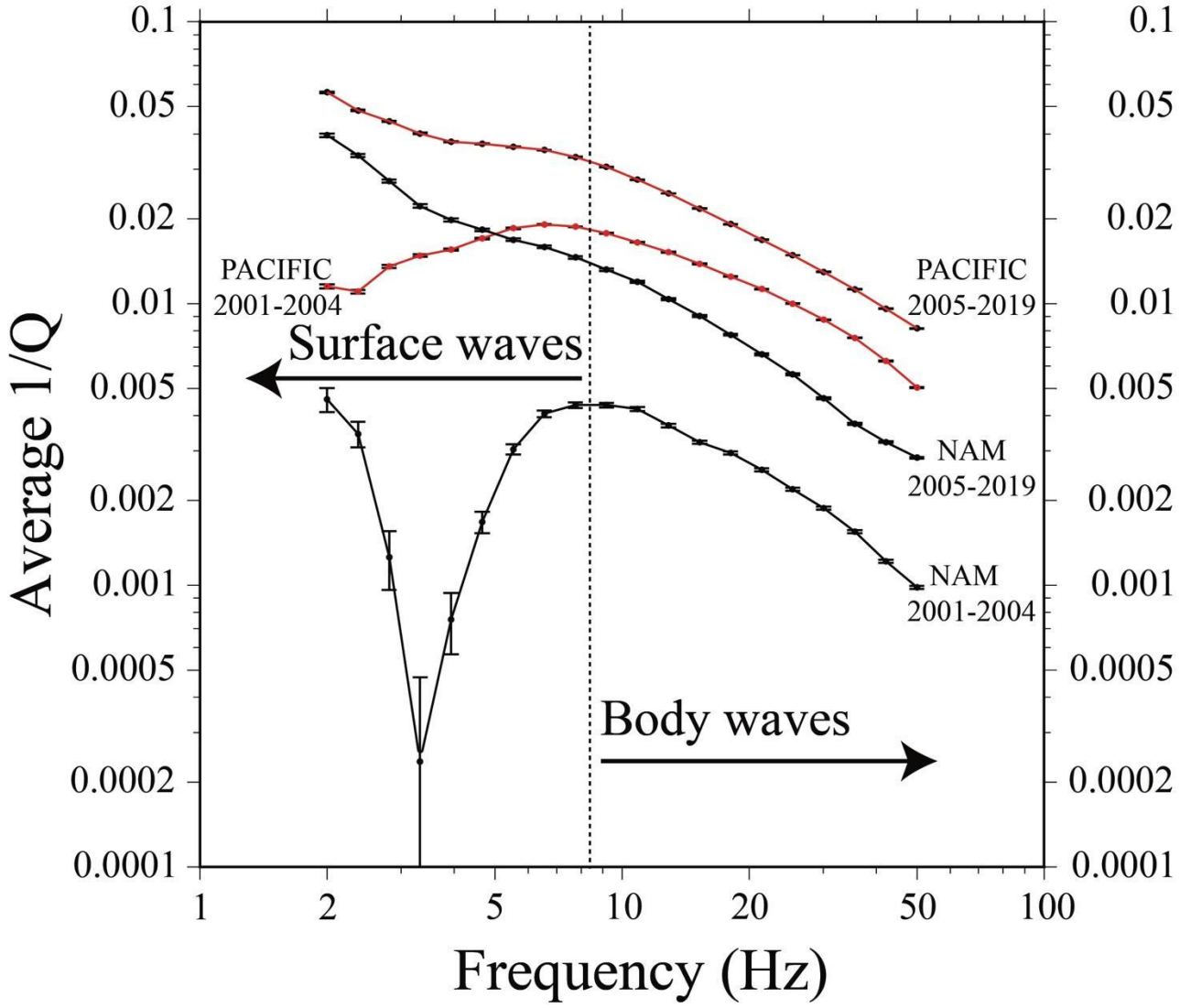

Figure 6. Average attenuation parameter $\left(Q_S^{-1}(f)\right)$ calculated for the North American side (black) and for the Pacific side of the SAF (red), in the indicated time windows (2001-2004 and 2005-2019). Below 8-10 Hz, all curves show a flattening that is stronger for the attenuation parameter calculated on both sides of the SAF in the 2001-2004 time window. Such behavior is consistent with the fact that the ground motion in the 2-8 Hz band is rich with surface waves, if not dominated by them.

Our study shows that, along the fault segment under scrutiny, the signature of the precritical state of the 2004 mainshock is represented by the variations in opposite directions of the low- and the high-frequency attenuation parameters as a function of time (low-frequency attenuation increases sharply, high-frequency attenuation decreases). The bifurcations are observed on both sides of the fault, and last 6-8 weeks. The precritical state of the Parkfield asperity emerges after a period of smooth variability of the attenuation parameter that lasts for about one year.

The bifurcation of the stacked seismic attenuation is the result of the different trends followed by the populations of cracks in the two ranges of frequency at both ends of the available spectrum: 2-5 Hz and 30-50 Hz. In order to interact with the seismic energy, cracks' lengths must form permeability structures with dimensions comparable to the wavelengths carried by the seismic radiation: 400-1500 m for the 2-5 Hz band, and 60-100 m for the 30-50 Hz band. The cracks in the

permeability structures with dimensions comparable to the short-wavelength radiation tend to close because crack coalescence causes strain localization into the macroscopic fracture, and compaction and stress relaxation in the surrounding volume. The long-wavelength radiation, on the contrary, gets more attenuated because the longer cracks that dominate the coalescence process increase the bulk permeability in the volume immediately around the fault plane by enhancing their aperture and interconnection. Finally, we observe that the 2-5 Hz band is dominated by surface waves that sample a shallower crustal structure than the direct S-waves of the 30-50 Hz band (see Figure 6).

About the intertwined behaviour of $\delta\left(Q_S^{-1}(t,f)\right)$ and the NVT activity, it is possible that the increased permeability along the very fault plane under subcritical conditions allows pore pressure to diminish at NVT depth (in our case, this would correspond to the observed decrease in NVT activity that starts in 2020), and to an upward pore fluid migration along the fault plane. In turn, the latter may weaken the fault and facilitate the occurrence of the mainshock. Within the limits of this hypothesis, monitoring the fluctuations of NVT activity along the SAF would be useful in recognizing the precritical state of the fault.

In the next few months (or years) the Parkfield segment of the SAF will provide most of the answers to our questions. In the meantime, it may be worthwhile applying our technique on different tectonic settings characterized by more complex fault geometries and ongoing NVT activity. Aside from more advanced theoretical developments and laboratory experiments on seismic attenuation under increasing differential stress, the most important ingredient for a successful use of non-geometric attenuation and NVT information would be the use of data from dense(r) seismic networks equipped with borehole sensors recording at high sampling rate.

References

Guilhen, A. and Nadeau, R.M. (2012), Episodic tremors and deep slow-slip events in Central California, EPSL, 357-358, 1-10.

Malagnini, L., Dreger, D. S., Bürgmann,R., Munafò, I., & Sebastiani, G. (2019). Modulation of seismic attenuation at Parkfield, before and after the 2004 M6 earthquake. Journal of Geophysical Research: Solid Earth,124, 5836–5853. https://doi.org/10.1029/2019JB017372.

Malagnini, L., & D.S. Dreger (2016). Generalized Free-Surface Effect and Random Vibration Theory: a new tool for computing moment magnitudes of small earthquakes using borehole data, Geophys J Int (2016) 206 (1): 103-113. https://doi.org/10.1093/gji/ggw113.

Nadeau, R.M., Guilhem, A. (2009). Nonvolcanic Tremor Evolution and the San Simeon and Parkfield, California, Earthquakes,Science 325, 191, DOI: 10.1126/science.1174155.

Sebastiani, G., & L. Malagnini (2020). Forecasting the Next Parkfield Mainshock on the San Andreas Fault (California), Journal of Ecology and Natural Resources, vol. 4, issue 3, https://doi.org/10.23880/jenr-16000218.

Corresponding author: luca.malagnini@ingv.it

Density values in the shallow crust: analysis and comparison of deep well data in the Adriatic region (Italy)

M.T. Mariucci[1], P. Montone[1], P. Balossino[2]

[1] Istituto Nazionale di Geofisica e Vulcanologia, Rome, Italy
[2] Former ENI S.p.A. Natural Resources, Italy

A detailed knowledge of rock densities helps in constraining the interpretation of crustal structures and their modelling. This work presents the results of a first systematic comparison between two datasets relative to density data of geological formations crossed by 13 deep wells. The wells are located in the Adriatic region and reach depths of over 5000 meters. The main lithologies involved include sedimentary rocks such as clays, sandstones, marls, evaporites, and carbonate rocks. The first dataset concerns density values obtained from the analysis of sonic logs recorded along the wells, by applying the relation proposed by Gardner et al. (1974). The second dataset refers to in situ density log measurements. We calculated the differences among the values in the two datasets. The comparison of the densities obtained from various lithologies and geological formations leads us to draw some initial considerations regarding the applicability and accuracy of Gardner's formula in the area we analyzed. In the Plio-Quaternary formations, characterized by clayey-sandy lithologies, the density values derived from sonic velocities are underestimated by at least 0.1 g/cm^3 with respect to the values measured by density logs. Whereas, densities of the carbonate sequences are overestimated by the same extent. Noteworthy, especially for gypsum units, the density estimates deviate from the real values, overestimating by a factor of approximately 0.3 g/cm^3. The results that we obtained emphasize the differences in density values when using the Gardner formula and suggest the need for taking into account the possible errors in the specific geological context or instead lithologies, such as those explored in this study. Since usually density values have to rely on evaluations and not real measurements, we should try to obtain the best possible estimates. We think that continuing in comparisons with as much data as possible of density log data and velocity-derived density data could produce also a numerical correction to adapt the Gardner rule to the Italian area.

References

Gardner G.H.F., Gardner L.W., Gregory A.R.; 1974: Formation velocity and density—the diagnostic basics for stratigraphic traps. Geophysics, 39, 770–780.

Corresponding author: mariateresa.mariucci@ingv.it

Earthquake swarms frozen in an exhumed hydrothermal system (Bolfin Fault Zone, Chile)

S. Masoch[1], G. Pennacchioni[1], M. Fondriest[1], R. Gomila[1], P. Poli[1], J. Cembrano[2,3], G. Di Toro[1,4]

1. Dipartimento di Geoscienze, Università degli Studi di Padova (Italy)
2. Departamento de Ingeniería Estructural y Geotécnica, Pontificia Universidad Católica de Chile (Chile)
3. Andean Geothermal Center of Excellence (Chile)
4. Sezione di Tettonofisica e Sismologia, Istituto Nazionale di Geofisica e Vulcanologia (Italy)

Earthquake swarms commonly occur in upper-crustal hydrothermal-magmatic systems and activate mesh-like fault networks within zones of fault geometric complexity. How these networks develop through space and time along seismic faults is poorly constrained in the geological record. Here, we describe a spatially dense array of small-displacement (< 1.5 m) epidote-rich fault-veins within granitoids, occurring at the intersections of subsidiary faults with the exhumed seismogenic Bolfin Fault Zone (Atacama Fault System, Northern Chile). Epidote faulting and sealing occurred at 3-7 km depth and 200-300 °C ambient temperature. At distance ≤ 1 cm to fault-veins, the magmatic quartz of the wall-rock shows (i) thin (<10- µm-thick) interlaced deformation lamellae, and (ii) cross cutting quartz-healed veinlets. The epidote-rich fault-veins (i) include clasts of deformed magmatic quartz, with deformation lamellae and quartz-healed veinlets, and (ii) record cyclic events of extensional-to-hybrid veining and either aseismic or seismic shearing. Deformation of the wall-rock quartz is interpreted to record the large stress perturbations associated with the rupture propagation of small earthquakes. In contrast, dilation and shearing forming the epidote-rich fault-veins are interpreted to record the later development of a mature and hydraulically-connected fault-fracture system. In this latter stage, the fault-fracture system cyclically ruptured due to fluid pressure fluctuations, possibly correlated with swarm-like earthquake sequences.

Corresponding author: Simone Masoch simone.masoch@phd.unipd.it

3D Hypocenters relocation in high-resolution central Mediterranean velocity model

I. Menichelli[1*], P. De Gori[1], C. Chiarabba[1]

[1] *Istituto Nazionale di Geofisica e Vulcanologia (Rome, Italy)*

In this study, a new 3D relocated hypocenters catalogue has been built for the Italian region using an updated 3D velocity model computed for the central Mediterranean area (Menichelli et al., 2023). Classical one-dimensional velocity models, due to their limitation in recovering lateral heterogeneous variations in the velocity structure, offer only a simplified depiction of the reality. For this reason, the necessity to use 3-D velocity models in the location of hypocenters, which consider the inhomogeneous structure of the different layers that constitute the earth's interior, has been emerging in recent years.

The 3D tomographic model used has been computed inverting P- and S- arrival times recorded between 2014-2021 by the RSN (Italian Seismic Network) and AlpArray (AlpArray 2015; Hetenyi et al., 2018) seismic network. In particular, the seismic data set includes Pg, Pn, Sg, and Sn, and the related arrival times were manually picked within a maximum epicentral distance of 1000 km.

We used the code Simulps 14 (Thurber 1983, 1999) to locate seismic events with the 3D velocity model. The method uses P and S–P arrival times to solve for hypocentral parameters while keeping fixed the Vp and Vs velocity structure.

We compute the hypocentral parameters for about 170.000 seismic events recorded by the INGV seismic network (RSD) that occurred in the period 2005–2023 starting from 1D absolute locations obtained using the best fit 1D Minimum Velocity Models and procedure presented in Menichelli et al., (2022). The decision to start with an already precise localization was made with the intention of improving the accuracy of localization as much as possible.

In order to determine stable solutions we selected only seismic events with at least 3 P-wave and 2 S-wave arrival times, the closest station within 50 km and *rms* ≤ 0.4 s. A further selection was also performed on the basis of the focal depth extracted from the previous 1D hypocentral locations: seismic events occurring at significant depths (≥ 80 km) were localized using a local model built ad hoc for the southern Tyrrhenian area using the arrival times of intraslab seismicity (Chiarabba et al., 2008). The decision was aimed at achieving accurate localization even at mantle depths.

The preliminary results obtained by the statistical analysis show low errors for the hypocentral coordinates (maximum peak at around 7 km for x and y-coordinates and at around 1-2 km for the z-coordinate) and small *rms* values (< 0.5 s).

The relocation process plays a key role in improving the accuracy of hypocenter determination, thus contributing significantly to the understanding of the intricate seismotectonic framework of the central Mediterranean region. By ensuring accurate relocation of seismic events, this method sheds light on the fundamental and deep crustal processes that define the structural dynamics of the Alpine and Apennine mountain ranges. In this way, the main seismic features, both large- and small-scale, within these regions are effectively highlighted.

In addition, through this work, the variation of the crustal seismogenic layer (CSL) along the Mediterranean area can be thoroughly evaluated. The delineation of the characteristics and variations of the crustal seismogenic layer in this area provides crucial insights into seismic potential and crustal behaviour, offering a comprehensive understanding of seismic hazards in this geologically complex area.

Furtherly, to test the performance of our location procedure, we performed detailed comparisons with the recent seismic catalogues obtained with both 1D (Menichelli et al., 2022) and 3D (CLASS, Latorre et al., 2023; CARS, Michele et al., 2023) velocity models. These kinds of studies turn out to be an important step forward in the assessment of the country's seismic hazard, aiming to improve the associated risk mitigation of the seismic activities.

References

Hetényi, G., Molinari, I., Clinton, J., Bokelmann, G., Bondár, I., Crawford, W. C., ... & AlpArray Working Group. (2018). The AlpArray seismic network: a large-scale European experiment to image the Alpine Orogen. *Surveys in geophysics*, *39*, 1009-1033.

Latorre, D., Di Stefano, R., Castello, B., Michele, M., & Chiaraluce, L. (2023). An updated view of the Italian seismicity from probabilistic location in 3D velocity models: The 1981–2018 Italian catalog of absolute earthquake locations (CLASS). *Tectonophysics*, *846*, 229664. Menichelli, I., De Gori, P., Lucente, F. P., Improta, L., Valoroso, L., Baccheschi, P., ... & Chiarabba, C. (2022). Minimum 1D VP and VP/VS models and hypocentral determinations in the central Mediterranean area. *Seismological Society of America*, *93*(5), 2670-2685.

Menichelli, I., De Gori, P., Lucente, F. P., Improta, L., & Chiarabba, C. (2023). Lithosphere Structure, Processes, and Physical State of the Alpine-Apennine System. Journal of Geophysical Research: Solid Earth, 128(4), e2023JB026411.

Michele, M., Di Stefano, R., Chiaraluce, L., Latorre, D., & Castello, B. (2023). *CARS-Catalog of Relative Seismic Locations of 1981-2018 Italian Seismicity* (No. EGU23-14033). Copernicus Meetings.

Thurber, C. H. (1983). Earthquake locations and three-dimensional crustal structure in the Coyote Lake area, central California. *Journal of Geophysical Research: Solid Earth*, *88*(B10), 8226-8236.

Thurber, C., & Eberhart-Phillips, D. (1999). Local earthquake tomography with flexible gridding. *Computers & Geosciences*, *25*(7), 809-818.

*Corresponding author: irene.menichelli@uniroma3.it

Exploring Italy's Present-Day Stress Field Complexity through Utilisation of Geophysical, Geological, and In Situ Drilling Data

P. Montone and M. T. Mariucci
Istituto Nazionale di Geofisica e Vulcanologia, Roma, Italy

Comprehensive understanding of the shallow crust's present-day stress field in Italy is crucial for enhanced crustal modelling and a more insight into tectonic processes and fault slip behaviour. Adhering to the guidelines of the World Stress Map, this study presents the latest findings on horizontal stress orientations and stress regime in Italy. The analysis is based on recent in situ drilling data and focal mechanisms of significant earthquakes (Figure 1). New borehole breakout analysis was conducted on 14 deep wells along the Adriatic coast and offshore, revealing horizontal stress orientations in nine wellbores. Stress orientations and tectonic regimes were deduced from the analysis of 21 earthquake focal mechanisms with magnitudes equal to or greater than 4, occurring between January 1, 2022, and October 31, 2023. The updated findings from 10 wells in the mid-southern Adriatic Sea, where no borehole ovalization was observed, highlight the absence of breakout zones along these wells.

These new data will be incorporated into the Italian Present-day Stress Indicators (IPSI) database, scheduled for release at the beginning of the year. The IPSI database, managed at INGV (Istituto Nazionale di Geofisica e Vulcanologia), serves as a georeferenced repository containing information on the present-day stress field of the crust.

The database includes horizontal stress orientations accurately analysed and standardised for global reliability and comparability, with 969 entries (all qualities) updated to October 2023. IPSI database consolidates information on contemporary stress within the Earth's crust's upper 40 km, derived from various stress indicators categorised into five main groups.

In the specific context of the Mw 5.5 2022-2023 Adriatic seismic sequence, newly acquired breakout data from deep boreholes exhibit coherent Shmin orientations ranging from N126 to N132, characterised by small standard deviations, indicating their high quality. These results, extending from the surface to approximately 4000 m, fill an information-deficient depth range, because the entire seismic sequence is positioned between 5 and 10 km depth. The seismic sequence, comprising six events with M≥4, yielded four available TDMT focal mechanisms, with three displaying pure thrust faulting and one a strike-slip mechanism. The consistently oriented minimum horizontal stress, evident in the N133 orientation for the Mw=5.5 event at 5 km depth, aligns with the northern Apennines' axis, confirming stress trends inferred from existing datasets in inland and southern sectors.

The intricate plate motions and the presence of multiple subduction zones have given rise to simultaneous and geographically proximate diverse stress regimes.

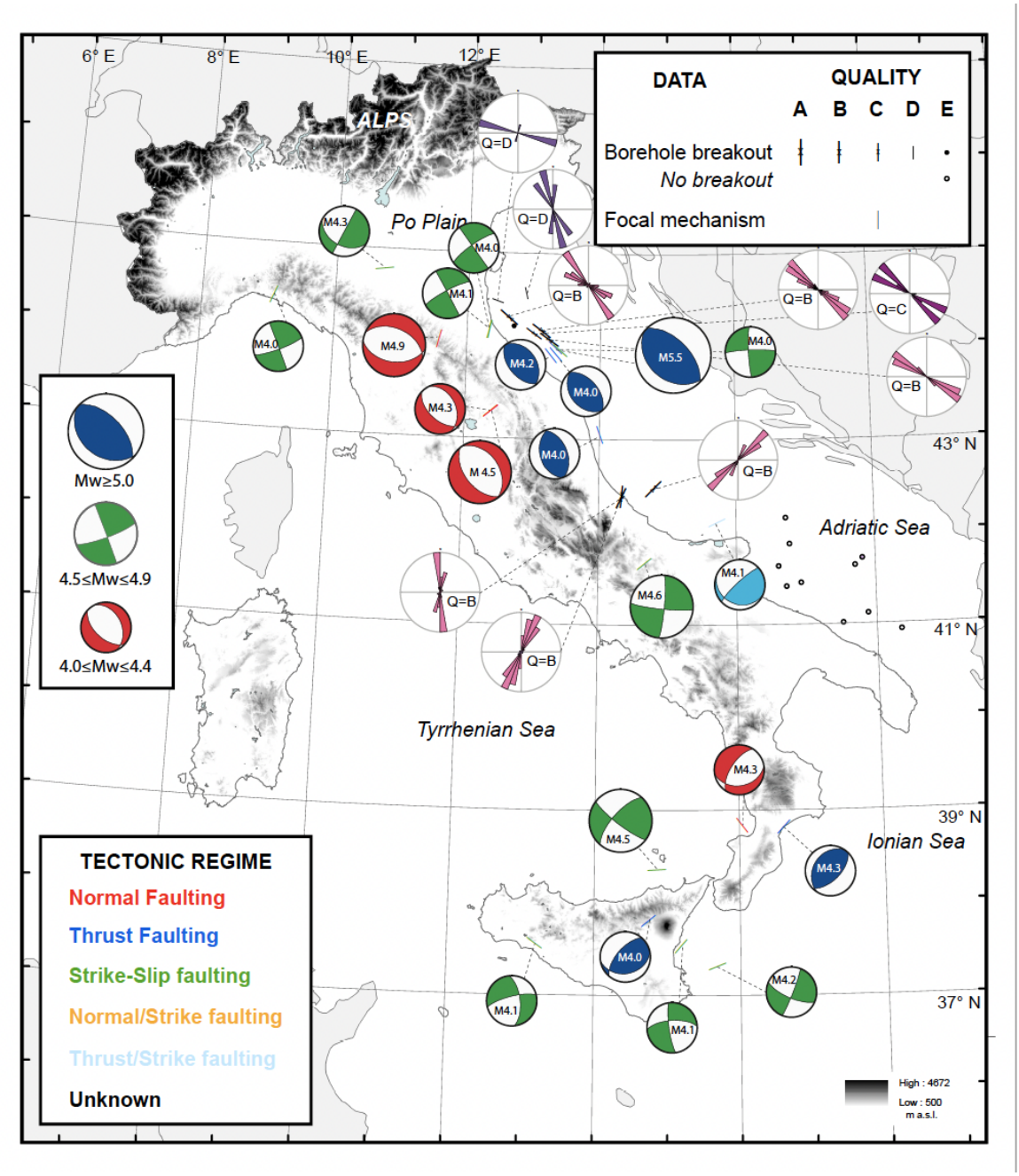

Fig. 1 – New data from 21 earthquake focal mechanisms and 9 breakout directions. Further 10 wells with no ovalization are highlighted with open circles.

Predominantly, extension is observable along the entire Apennine belt with a ~NE–SW orientation, transitioning to NW–SE in the Calabria region, following the curvature of the Calabrian arc. Thrust faulting is constrained to external areas, evident along the northern Apennine front (Adriatic foredeep) with a NE-oriented compression and offshore along the northern Sicilian coast, as well as in the Po Plain and Friuli regions. The stress orientation in the latter areas aligns closely with the ~N–S convergence of ongoing relative crustal motions between the Eurasia and Africa plates. Conversely, there is no apparent compression along the central and southern Apennines' external front based on present-day stress information. The active stress field so far not well defined in the offshore area of

the eastern Calabrian coast, seems to be today finally characterised by a compressive and strike-slip regime with the orientation of the maximum compression in a direction approximately NW-SE. In this area, the new data further highlights the clear separation between the western Tyrrhenian and eastern Ionian margins. Strike-slip faulting, the less prevalent tectonic regime in Italy, is spatially confined to areas along the southern Apennine foredeep and in eastern Sicily, both onshore and offshore in the Tyrrhenian and Ionian regions.

Situated within the broader context of Mediterranean tectonic plate boundary, the Adriatic area holds geological importance as a dynamic region, with the Adriatic microplate assuming a central role. Notably, recent revisions have been made to data from deep wells in the southern sector of the Adriatic Sea, characterised by a lack of seismic activity. The results of the analysis carried out along these wells have not shown borehole ovalization, thus indicating the absence of an anisotropic stress field.

References

ISIDe Working Group; 2007: Italian seismological instrumental and parametric database (ISIDe). Rome, Italy: Istituto Nazionale di Geofisica e Vulcanologia. doi:10.13127/ISIDE.

Mariucci M.T., Montone P.; 2022: IPSI 1.5, database of Italian present-day stress indicators. Rome, Italy: Istituto Nazionale di Geofisica e Vulcanologia. doi:10.13127/IPSI.1.5.

Montone P., Mariucci M.T.; 2023: Deep well new data in the area of the 2022 Mw 5.5 earthquake, Adriatic Sea, Italy: In situ stress state and P-velocities. Front. Earth Sci. 11:1164929. doi: 10.3389/feart.2023.1164929.

Montone P., Mariucci, M.T.; 2016: The new release of the Italian contemporary stress map. Geophys. J. Int. 205, 1525–1531. doi:10.1093/gji/ggw100.

Scognamiglio L., Tinti E., Quintiliani M.; 2006: Time domain moment tensor (TDMT). Rome, Italy: Istituto Nazionale di Geofisica e Vulcanologia. doi:10.13127/TDMT.

Corresponding author: paola.montone@ingv.it

Modeling dynamic ruptures on extended faults for microearthquakes induced by fluid injection

F. Mosconi[1], E. Tinti[1,2], E. Casarotti[2], A. A. Gabriel[3], R. Dorozhinskii[4], L. Dal Zilio[5], A. P. Rinaldi[5], and M. Cocco[2]

[1] Università la Sapienza, Rome, Italy
[2] Istituto Nazionale di Geofisica e Vulcanologia, Rome, Italy
[3] Scripps Institution of Oceanography, UC San Diego, La Jolla, CA 92093, USA
[4] Technical University of Munich, Germany
[5]Seismology and Geodynamics, Institute of Geophysics, Department of Earth Sciences, Swiss Federal Institute of Technology (ETH Zürich), Zürich, Switzerland

Understanding the dynamics of microearthquakes is a timely challenge to solve current paradoxes in earthquake mechanics, such as the stress drop and fracture energy scaling with seismic moment. Dynamic modeling of microearthquakes induced by fluid injection is also relevant for studying rupture propagation following a stimulated nucleation. We study the main features of unstable dynamic ruptures caused by fluid injection on a target pre-existing fault (50m x 50m) generating a $M_w < 1$ event. The selected fault is located in the Bedretto Underground Laboratory (Swiss Alps) at ≈1000m depth and these research activities are performed in the framework of the ERC Synergy project FEAR (Fault Activation and Earthquake Ruptures). We perform fully dynamic rupture simulations coupled with seismic wave propagation in 3D by adopting a linear slip-weakening friction law. We use the distributed multi-GPU implementation of SeisSol on the supercomputer Leonardo (CINECA).

Stress field and fault geometry are well constrained by in-situ characterization, allowing us to minimize the a priori imposed parameters. We investigate the dynamics of rupture propagation and arrest for a target $M_w < 1$ induced earthquake with spatially heterogeneous stress drops caused by pore pressure changes and different constitutive parameters (critical slip-weakening distance, D_c, dynamic friction μ_d). We explore different homogeneous conditions of frictional parameters, and we show that the spontaneous arrest of an unstable rupture is possible in the modeled stress regime (fig.1), by assuming a high ratio between strength excess and dynamic stress drop (the fault strength parameter S), characterizing the fault before the pore pressure change. The rupture arrest of modeled induced earthquakes depends on the heterogeneity of dynamic parameters due to the spatially variable effective normal stress, which controls the on fault G_c spatial increment. Moreover, for a fault with high S values (low rupturing potential), small variations of D_c *(≈0.45÷0.6 mm)* can significantly impact on the final earthquake size, particularly controlling the deceleration and arrest phase. Studying dynamic interactions (stress transfer) among slipping points on the rupturing fault provides insights on the dynamic load and shear

stress evolution at the crack tip. The inferred spatial dimension of the cohesive zone in our models is nearly ~0.3-0.4m, with a maximum slip of ~0.6 cm. Finally, from the generated synthetic waveforms, we examine the differences in the content of high-frequency radiation between self-arresting and run-away earthquakes, also providing an estimation of the source parameters obtained through the spectral inversion. This estimation is then compared with the forward models. Our results suggest that meso-scale processes near the crack-tip during the nucleation and acceleration of the rupture strongly affect dynamics of micro-earthquakes.

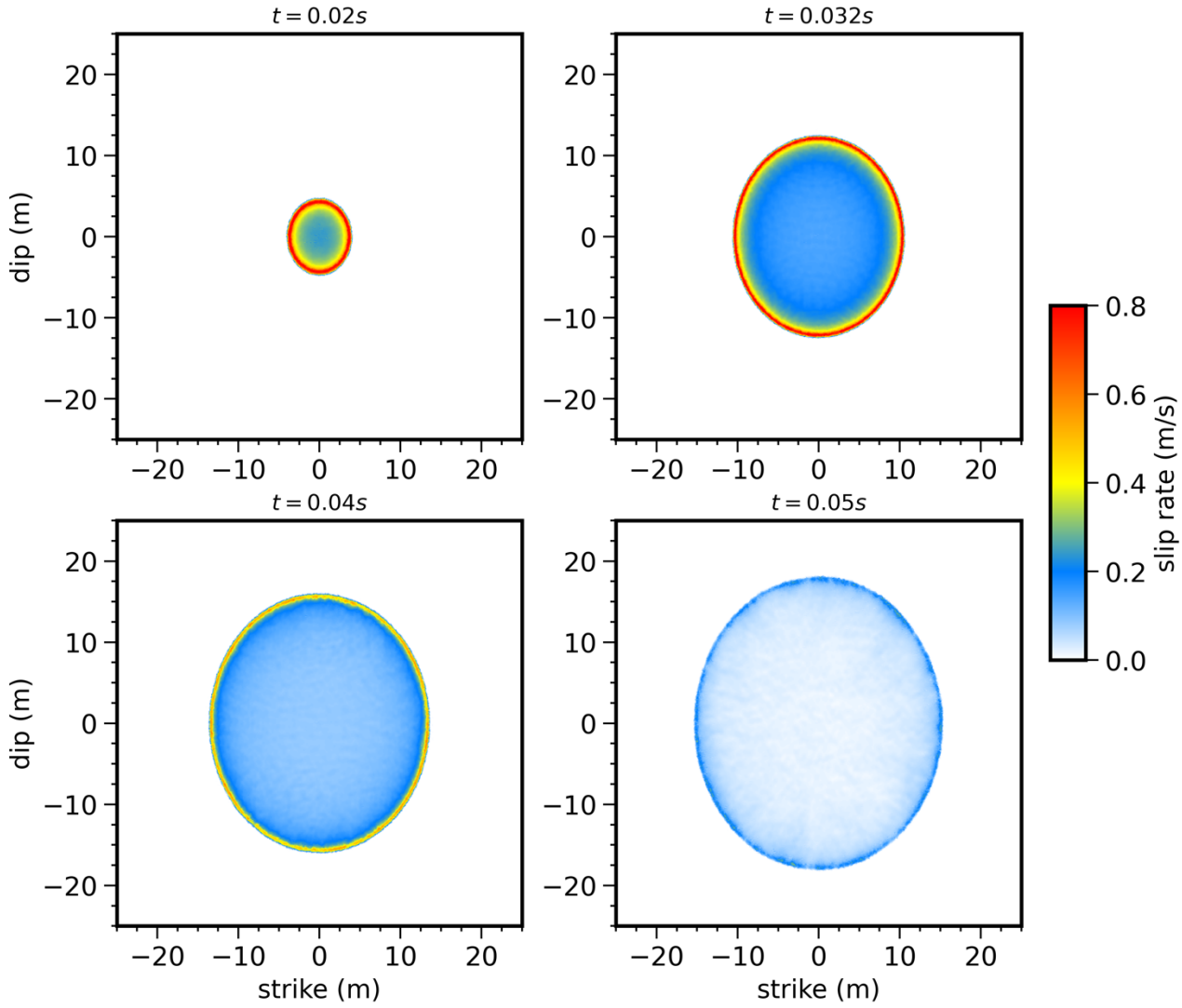

Fig. 1 Snapshot of the slip rate evolution during the rupture propagation of a microearthquakes (M_w = 0.71) in the context of fluid induced seismicity; for the model with D_c = 0.6mm.

Corresponding author: francesco.mosconi@uniroma1.it

Detect and characterize swarm-like seismicity

L. Passarelli [1], S. Cesca[2], L. Mizrahi[3], G. Petersen[2]

[1] INGV - Istituto Nazionale di Geofisica e Vulcanologia, sezione di Bologna, Bologna, Italy.
[2] GFZ – German Research Centre for Geosciences, Potsdam, Germany
[3] SED – Swiss Seismological Service, ETH Zürich, 8092 Zürich, Switzerland

Tectonic earthquake swarms do not follow the classical temporal and spatial pattern observed for mainshock-aftershock sequences. Unlike the typical occurrence of a largest mainshock that initiates the sequence and triggers aftershocks following an Omori-Utsu decay and productivity scaling with the mainshock magnitude, earthquake swarms show a distinctive increase of seismic activity without a clear mainshock. Typically, the largest earthquake(s) occur(s) later in a swarm sequence that often consists of multiple earthquake bursts that show spatial migration. This erratic clustering behavior of earthquake swarms comes from the interplay between the long-term accumulation of tectonic strain and short-term transient forces driving swarm-like seismicity. The detection and investigation of earthquake swarms challenges the community and ideally requires an unsupervised approach, and indeed numerous algorithms have emerged in the last decades for earthquake swarm identification.

In this study, we comprehensively review commonly used techniques for detecting earthquake clusters. We first applied those techniques to thousands synthetic earthquake catalogs produced with state-of-the-art ETAS model, featuring a time-dependent background rate to simulate realistic swarm-like sequences. Our approach enables us to identify boundaries in some parameters commonly used to distinguish earthquake clusters, says mainshock-aftershocks versus swarm sequences. The insights gained from synthetic data contribute to a more accurate classification of seismicity clusters in real earthquake catalogs. We therefore apply the same algorithm to real cases of seismicity where earthquake swarms have already been identified, i.e. the 2010-2014 Pollino seismic sequence; the Húsavík-Flatey transform fault seismicity and the regional catalog of Utah. However, applying these findings to real cases is contingent upon the clustering algorithm used, the statistical completeness of catalogs, and the spatial and temporal distribution of earthquakes. Unfortunately, full automation of swarm detection and characterization remains difficult to attain, necessitating manual verification and investigation of individual swarm-like sequences.

Corresponding author: luigi.passarelli@ingv.it

The Preparatory Process of the 2023 Mw 7.8 Türkiye Earthquake.

M. Picozzi[1,2], A.G. Iaccarino[2], D. Spallarossa[3]

[1] Istituto Nazionale di Oceanografia e di Geofisica Sperimentale - OGS, Italy.
[2]University of Naples Federico II, Italy.
[3]DISTAV, University of Genoa, Genoa, Italy.

To verify the existence of a preparatory process for the 6 February 2023, Mw 7.8 Kahramanmaraş earthquake, southern Türkiye, we analyze the temporal evolution of seismic catalog information for ~7500 earthquakes with magnitudes ML ≥ 1.5, which occurred along the main segments of the East Anatolian Fault (EAF) since 2014. We find the EAF fault segments showing different temporal patterns in the proportion of nonclustered seismicity, which we interpret as temporal variation of coupling. We also study the evolution of the b-value, fractal dimension and energy rate. These seismic features show for the Amanos and Pazarcık fault segments a long-term trend during the period 2020 – 2022 that might correspond to a quiescence phase. The latter is followed by a change in earthquake clustering and characteristics that starts about eight months before the Mw 7.8 Kahramanmaraş event. Our observations confirm the existence of a long-lasting preparatory phase for the 2023, Mw 7.8 Kahramanmaraş earthquake and can stimulate new investigations on the East Anatolian Fault mechanic. Intercepting when a fault starts deviating from its steady behaviour, might be the key for identifying the preparatory phase of large earthquakes and mitigate seismic risk.

Corresponding author: mpicozzi@ogs.it

ML-based workflow for earthquake detection and location: preliminary results from the northern Apennines with a model trained on local waveforms

G. Poggiali[1], S. Bagh[2], L. Chiaraluce[2], C. J. Marone[1], Z. E. Ross[3], E. Tinti[1], W. Zhu[4]

[1] La Sapienza Università di Roma, Rome, Italy

[2] Istituto Nazionale di Geofisica e Vulcanologia, Rome, Italy

[3] Seismological Laboratory, Division of Geological and Planetary Sciences, California Institute of Technology, Pasadena, CA, USA

[4] University of California, Department of Earth & Planetary Science, Berkeley, CA, USA

The analysis of microseismicity has a fundamental role in understanding earthquakes driving processes such as seismic sequences evolution and preparatory phase. Recent advances in machine learning (ML)-based detection and location techniques, coupled with dense seismic networks, have dramatically increased the quantity of low-magnitude earthquakes that can be recorded and properly located. This has led to the development of a new generation of earthquake catalogs illuminating fault systems in unprecedented detail.

We study data from the Alto Tiberina Near Fault Observatory (TABOO-NFO) located in the Apennines of central Italy where earthquake activity is intense. This is an ideal site to apply modern detection techniques and study in detail complex fault systems evolving in a shallow crust surrounded by deep fluid circulation. We build an earthquake catalog for the TABOO area using data from 2010 to present using a ML-based workflow tailored to this area.

We started from an updated version of the deep learning phase picker PhaseNet (Zhu and Beroza, 2019). This version of PhaseNet includes several improvements, such as polarity estimation and better detection of close-in-time events, which were often undetected in the original version. We trained PhaseNet on waveforms collected by the local TABOO seismic network that had been manually labelled by analysts (Cattaneo et al., 2017) with P, S phases and first arrivals polarity. We show that training the model with local data results in a significant improvement mainly in the picking accuracy of S-phases and also in polarity estimation.

The result of the detection step is a massive phase dataset composed of tens of millions of P and S phases making the association (e.g., binding) of events a challenge. For this task we used the Gaussian Mixture Model Association (GaMMA, Zhu et al., 2021) algorithm, which treats earthquake phase association as an unsupervised clustering problem in a probabilistic framework to estimate earthquake (preliminary) locations, origin times and magnitudes. We show the

statistics of associated events and phases as well as some examples that highlight the importance of fine-tuning the parameters, which becomes complex to do in the presence of very large datasets. This first part of the workflow (detection and association) resulted in 1.4M events.

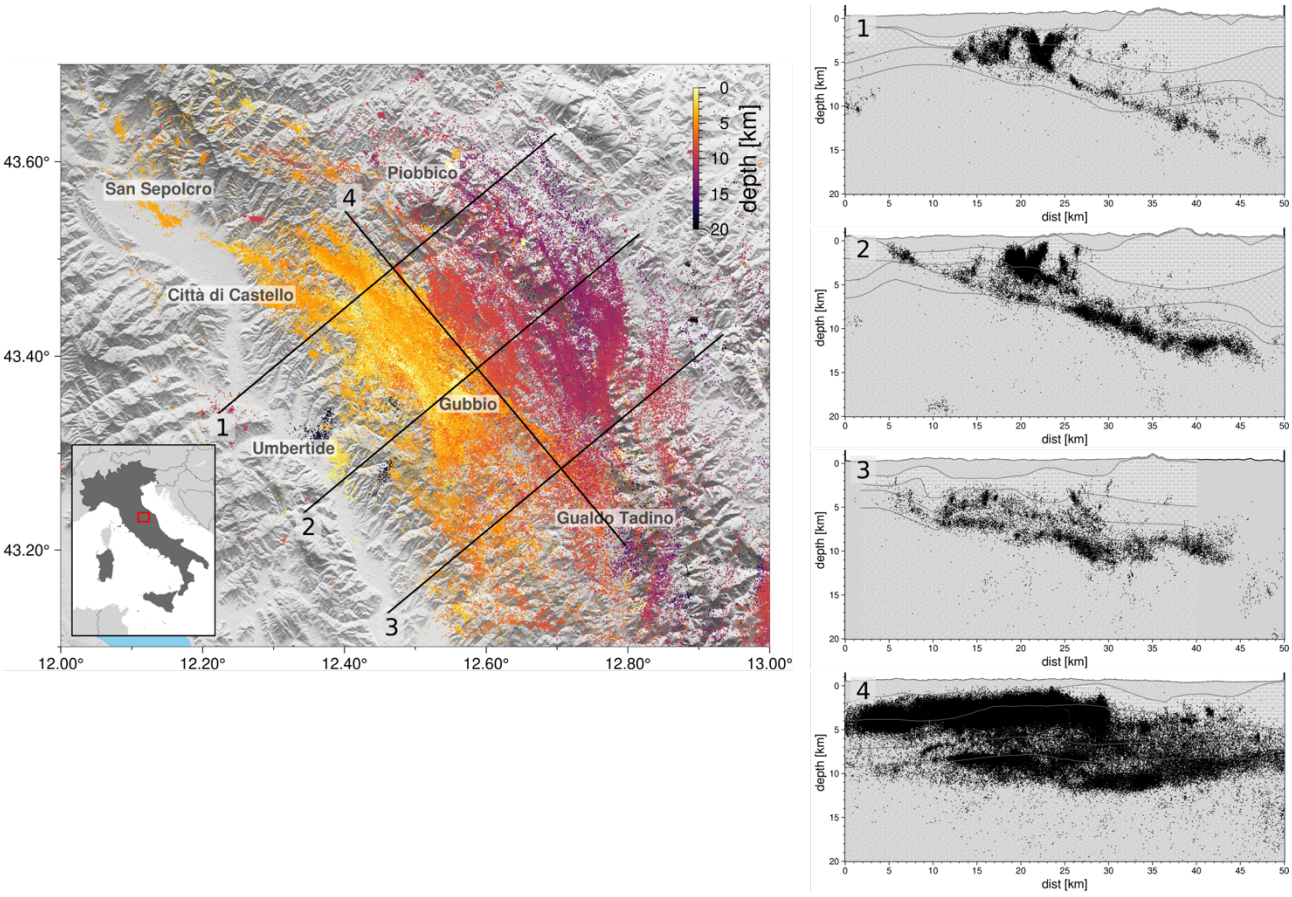

Fig. 1 – Map, cross sections (1-3, width=5km) and longitudinal section (4, width=20km). Cross sections 1 and 2 clearly depict the Altotibernia Fault at depth and the shallower seismicity pertaining to the Pietralunga (1) and Gubbio (2) sequences. The lithological model on the background is from Latorre et al., 2016.

To estimate the absolute hypocentral locations we use an updated version of HypoSVI (Smith et al., 2022), a probabilistic location method in which the forward model is based on a physics informed neural network trained to solve the Eikonal equation. The location procedure makes use of source-specific station terms (SSST) that can vary as a function of source position, allowing better correction for the unmodeled velocity structure with respect to the more classic static station corrections. During the location procedure, outlier picks are filtered out based on the statistics of the residuals. We provide absolute locations for more than 10 times the number of earthquakes recorded by the Italian seismic network, with a spatial distribution of seismicity that illuminates the expected crustal portions and agrees with independent information from a lithological model of the area (Fig. 1).

We are currently in the stage of waveform similarity analysis (cross correlation, CC). The CC refined traveltimes will be used to relocate the catalogue, providing a very detailed picture of the complex seismicity of the area. The similarity values will also be used to start investigating the presence of repeating earthquakes in order to better define the mixed distribution of locked and creeping

patches of The Alto Tiberina Fault and its interactions and coupling with the shallower system of faults. In the final stage we will approach focal mechanisms and moment magnitude estimation.

References

Cattaneo, M., Frapiccini, M., Ladina, C., Marzorati, S., & Monachesi, G. (2017). A mixed automatic-manual seismic catalog for Central-Eastern Italy: analysis of homogeneity. Annals of Geophysics.

Smith, Jonthan D, Zachary E Ross, Kamyar Azizzadenesheli, and Jack B Muir. 2022. "HypoSVI: Hypocentre Inversion with Stein Variational Inference and Physics Informed Neural Networks." Geophysical Journal International 228 (1): 698–710.

Zhu, Weiqiang, and Gregory C. Beroza. 2019. "PhaseNet: A Deep-Neural-Network-Based Seismic Arrival-Time Picking Method." Geophysical Journal International 216 (1): 261–73.

Zhu, Weiqiang, Ian W. McBrearty, S. Mostafa Mousavi, William L. Ellsworth, and Gregory C. Beroza. 2021. "Earthquake Phase Association Using a Bayesian Gaussian Mixture Model." Journal of Geophysical Research: Solid Earth, e2021JB023249.

Corresponding author: giulio.poggiali@uniroma1.it

NEW PALAEOSEISMOLOGICAL EVIDENCE OF COSEISMIC SURFACE RUPTURE ACROSS THE CARNIC PREALPINE FRONT (NE-ITALY): THE BUDOIA-AVIANO THRUST SYSTEM

M.E. Poli[1]; G. Patricelli[2]; E. Falcucci[3]; S. Gori[3]; G. Paiero[1]; E. Rizzo[2]; A. Marchesini[1]; R. Caputo[2]

(1) Università di Udine, Dipartimento di Scienze Agroalimentari, Ambientali e Animali
(2) Università degli Studi di Ferrara, Dipartimento di Fisica e Scienze della Terra
(3) Istituto Nazionale di Geofisica e Vulcanologia

In the framework of the PRIN_2020 “Fault segmentation and seismotectonics of active thrust systems: the Northern Apennines and Southern Alps laboratories for new Seismic Hazard Assessments in northern Italy (NASA4SHA)”, we conducted a palaeoseismological study into the area comprised between the Budoia and Aviano localities (western Carnic Prealps, NE Italy).

The investigated area, which is part of the external Plio-Quaternary front of the Eastern Southalpine Chain, is characterized by the presence of distinct WSW-ENE trending and S-verging reverse fault planes arranged in thrust systems and affecting the Quaternary succession (Poli et al., 2014).

In detail, the geological and morphotectonic survey highlighted many evidence of recent deformation affecting the Last Glacial Maximum alluvial fan of the Artugna Stream, including morphological anomalies of both the topography (scarps) and the hydrography of minor streams.

Following the multidisciplinary and multiscale approach, the preliminary geophysical survey, which included multiscale Electric Resistivity Tomograhy (DERT and ERT) and Ground Penetrating Radar (GPR), allowed us to identify the site for the excavation of two palaeoseismological trenches (Rizzo et al., this session)

The excavated walls intersected a set of medium-to-high angle reverse planes verging towards the North, which displace the alluvial fan stratigraphy and also affect the soil. At about 2 m depth from topography, we identified a paleosoil dividing two alluvial fan units and affected by deformation. The radiocarbon dating of the paleosoil sample revealed an age of about 16 ky BC.

The palaeoseismological analysis allowed us to estimate a cumulative slip, measured on all fault planes, of the order of at least 4.5 m. Moreover, we detected at least three seismic events, the most recent of which is possibly referable to the 1873 M 6.3 Alpago - Cansiglio earthquake (CPTI15, Rovida et al., 2022).

The reverse fault planes identified within the two excavated trenches define an about 20 m wide area of surficial deformation, developed at the hanging-wall of the main S-verging thrust plane and characterized by an ENE-WSW trending. If considering the lateral extension of this deformation area, it clearly affects industrial complexes, urban centres and sensitive structures of Budoia and Aviano localities. Therefore, the paleoseismological evidence collected so far provide implication which are relevant for the seismic hazard estimation of the area, and which must be necessarily considered in the framework of the regional planning.

REFERENCES

M.E. Poli, G. Monegato, A. Zanferrari, E. Falcucci, A. Marchesini, S. Grimaz, P. Malisan, E. Del Pin (2014). Seismotectonic characterization of the western Carnic pre-alpine area between Caneva and Meduno (Ne Italy, Friuli). DPC-INGV-S1 Project “Base-knowledge improvement for assessing the seismogenic potential of Italy” (D6/a2.1).

E. Rizzo, V. Giampaolo, F. Mucchi, P. Boldrin, G. De Martino, M.E. Poli, G. Patricelli, A. Marchesini, R. Caputo (2024). Multiscale geophysical investigation on the Budoia-Aviano thrust system (NE Italy): first results. GNGTS 2024.

A. Rovida, M. Locati, R. Camassi, B. Lolli, P. Gasperini, A. Antonucci (2022). Catalogo Parametrico dei Terremoti Italiani (CPTI15), versione 4.0. Istituto Nazionale di Geofisica e Vulcanologia (INGV). https://doi.org/10.13127/CPTI/CPTI15.4

Corresponding author: eliana.poli@uniud.it

Source parameters of the 2010-2014 Pollino (Italy) seismic sequence and their relationship with structural and geological setting of the area

M. Ponte[1], G. Calderoni[2], R. Di Giovambattista[2], M. La Rocca[1]

[1] Università della Calabria, Dipartimento di Fisica, Rende, Italy

[2] Istituto Nazionale di Geofisica e Vulcanologia, Rome, Italy

Between 2010 and 2014, a seismic swarm of thousands of events (Mwmax= 5.2) occurred in the Mt. Pollino area, between the Calabrian Arc and the Apennines, adjacent to the Ionian Subduction Zone. High resolution source location revealed that seismicity originated from two main clusters with opposite dipping orientations, with the main faults aligned along a NNW-SSE direction. Understanding the source parameters of these seismic events is crucial to get insight on the individual rupture process of the earthquake, the spatial evolution of the seismic sequence and the dynamic properties of the rupture, including the possible involvement of fluids.

We analyzed hundreds of earthquakes of the Pollino seismic sequence in order to investigate the following source parameters: the Brune stress drop ($\Delta\sigma$), the apparent stress (τa) and the Savage-Wood radiation efficiency ($\eta sw= \tau a/\Delta\sigma$). We identified 20 seismic events with $3.1 < Mw < 5.2$ with known TDMT solution and 80 smaller events with $2.4 < M_L < 3.0$ not present in the TDMT archive. For earthquakes not included in the TDMT archive we calculated the seismic moment through spectral scaling of the low frequency plateau in the displacement spectra using the corresponding target event selected on the basis of the distance, larger-magnitude, and greatest number of stations that recorded the event. The two stress parameters depict a similarly scattered trend, with the highest value corresponding to the main shocks. Seismic efficiency is substantially stable versus M0, with values mostly between 0.1 and 0.6, and a mean value of about 0.23, which corresponds to the expectation of the omega square model.

The area affected by the 2010-2014 sequence extends from the Mercure basin to the Campotenese and Morano Calabro basins and it is characterized by a complex system of normal and oblique normal faults (Fig. 1). The area towards the Tyrrhenian side (west) is made up of faults with a NS trend with E/NNE dip and dip-slip kinematics, alternating with segments of faults with WNW-ESE orientation with normal-slip kinematics whose anti-slip component is important. The intramontane area is characterized by NW-SE faults dipping towards the SW that are included in a "western system" and an "eastern" system.

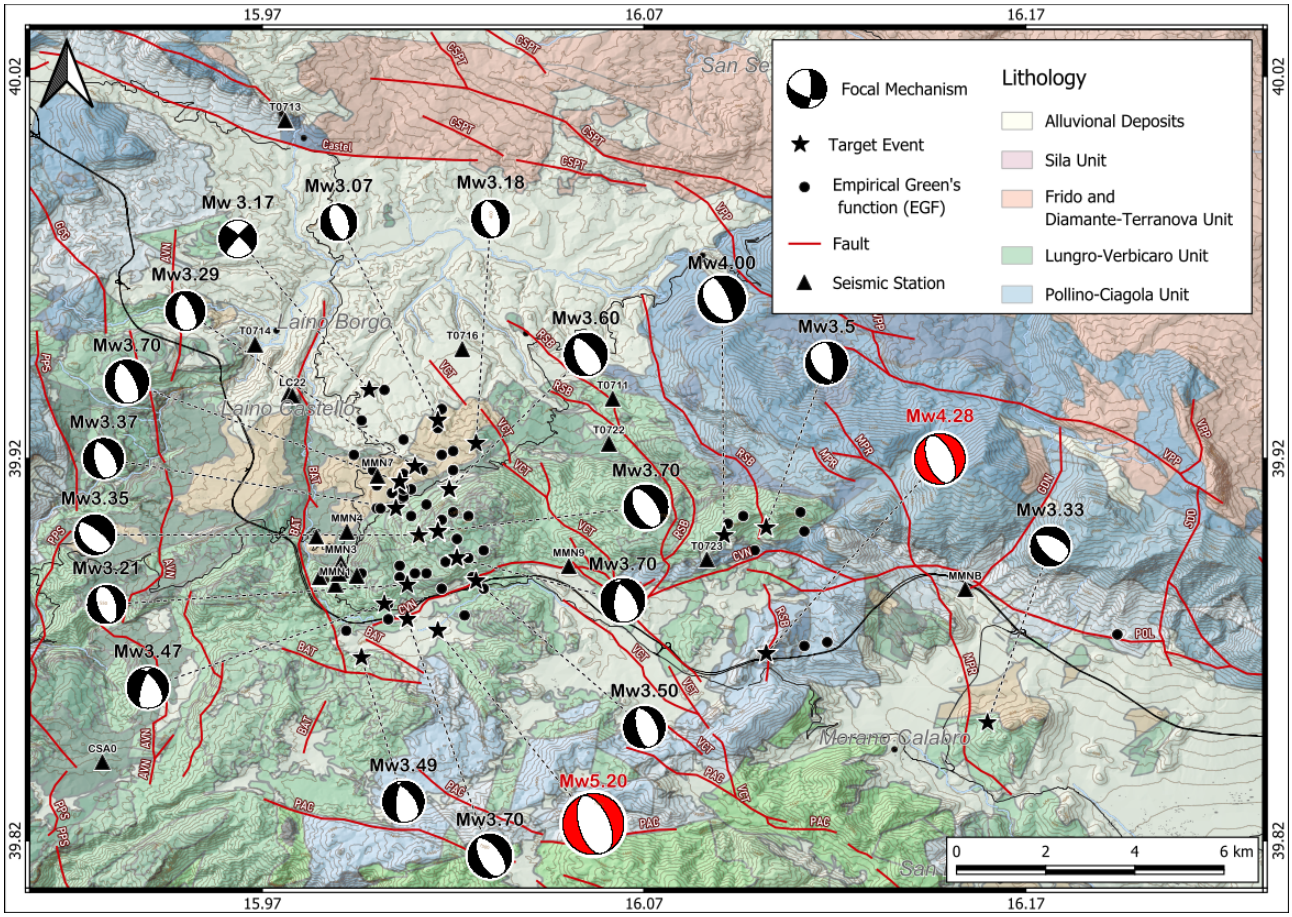

Fig. 1 - Map of the study area showing the main geologic units and structural elements, the seismic stations (black triangle), the seismic events with Mw 3.1 (black star), and 2.4 ML 3.0 (black circle). Beachballs represent the TDMT focal solution of Mw 3.1 and show predominantly normal kinematics with strike oriented in the N-NW/S-SE direction. The red beachballs correspond to the mainshocks (Mw5.20 and Mw4.28) of the seismic sequence nucleated on two different tectonic structures. Red lines represent known normal faults developed following the extensional tectonics during the Plio-Pleistocene. Two main fault systems are identified. The first includes main fault segments with a trend that varies southwards from N-S to WNW-ESE. The other two groups of faults have a NW-SE strike with SW dipping. The lithological basis is taken from the "Carta Geologica dell'area compresa tra Maratea, Castrovillari e Sangineto by A. Iannace; M. D'Errico; S. Vitale - (2004).

Other Quaternary faults are present in the area whose contribution plays an important role on the seismicity of the area. In this region two carbonate platforms, the Apennines Platform and the deeper Inner Apulian Platform, are believed to be overlapped at about 5 km depth. Recent papers describe results obtained from different analyses that indicate the presence of high pressure fluids in the seismogenic volume where the seismic sequence occurred (De Matteis et al., 2021; Pastori et al., 2021; Napolitano et al., 2021, 2023). The fluid moving along the faults causes the lubrification that facilitates the earthquake occurrence. A reduction of the dynamic strength due to high pressure fluid is expected to increase the seismic efficiency ηsw. From our analysis we find the highest ηsw values along the two main faults, reaching their maximum values at the tips of these faults. The concentration of elevated ηsw values at fault tips supports the observations that fluid-related processes play a significant role in the seismic activity within this particular area. The ηsw variability in the target area could be elucidated by considering fluid involvement in controlling

seismicity, a concept invoked by other researchers to explain observed Vp/Vs anomalies and anisotropy variations.

References

De Matteis R., Convertito V., Napolitano F., Amoroso O., Terakawa T., Capuano P.; 2021: Pore fluid pressure imaging of the Mt. Pollino region (southern Italy) from earthquake focal mechanisms. Geophysical Research Letters, 48, e2021GL094552. https://doi.org/10.1029/2021GL094552

Iannace A., D' Errico M., Vitale S.; 2004: Carta geologica dell'area compresa tra Maratea, Castrovillari e Sangineto. Stampa.

Napolitano F., De Siena L., Gervasi A., Guerra I., Scarpa R., La Rocca M.; 2020: Scattering and absorption imaging of a highly fractured fuid-filled seismogenetic volume in a region of slow deformation. Geosci. Front. 11 (3), 989-998. doi:10.1016/j.gsf.2019.09.014

Napolitano F., S. Gabrielli, L. De Siena, O. Amoroso, P. Capuano (2023). Imaging overpressurised fracture networks and geological barriers hindering fluid migrations across a slow deformation seismic gap. Scientific Reports 13:19680, https://doi.org/10.1038/s41598-023-47104-w

Pastori M., Margheriti L., et al.; 2021: The 2011-2014 Pollino Seismic Swarm: Complex Fault Systems Imaged by 1D Re ned Location and Shear Wave Splitting Analysis at the Apennines Calabrian Arc Boundary. Front. Earth Sci. 9:618293.doi: 10.3389/feart.2021.618293

Corresponding author: michela.ponte@unical.it

Geological field survey in the area affected by the 2023 devastating earthquake sequence (Turkey). Part I: the Hahramanmaraş-Pazarcık fault section

S. Pucci[1], M. Caciagli[1], R. Azzaro[1], P. Di Manna[2], A.M. Blumetti[2], V. Poggi[3], P.M. De Martini[1], R. Civico[1], R. Nappi[1], E. Ünsal[4], O. Tatar[5]

[1] Emergeo Working Group, Istituto Nazionale di Geofisica e Vulcanologia (INGV), Italy
[2] Istituto Superiore per la Protezione e la Ricerca Ambientale (ISPRA), Roma, Italy
[3] Istituto Nazionale di Oceanografia e di Geofisica Sperimentale (INOGS), Sgonico (TS), Italy
[4] Disaster and Emergency Management Authority (AFAD), Gaziantep, Turkey
[5] Disaster and Emergency Management Authority (AFAD), General Director of Earthquake and Risk Reduction, Ankara, Turkey

Introduction

Following the devastating M_w 7.8-7.6 earthquakes occurred on 6 February 2023 along the East Anatolian Fault (Fig. 1a), the Italian Civil Protection Department (DPC), in coordination with the Turkish Disaster and Emergency Management Authority (AFAD), set up a team of earthquake geologists belonging to its Competence Centres (INGV – Istituto Nazionale di Geofisica e Vulcanologia; ISPRA - Istituto Superiore per la Protezione e la Ricerca Ambientale; INOGS – Istituto Nazionale di Oceanografia e di Geofisica Sperimentale) to survey the coseismic surface faulting effects. In the period 6-13 May, the Italian team investigated six key-areas along the 140 km-long Nurdagi-Kahramanmaraş-Pazarcık fault section (Fig. 1) in the provinces of Gaziantep, Kahramanmaraş and Adıyaman.

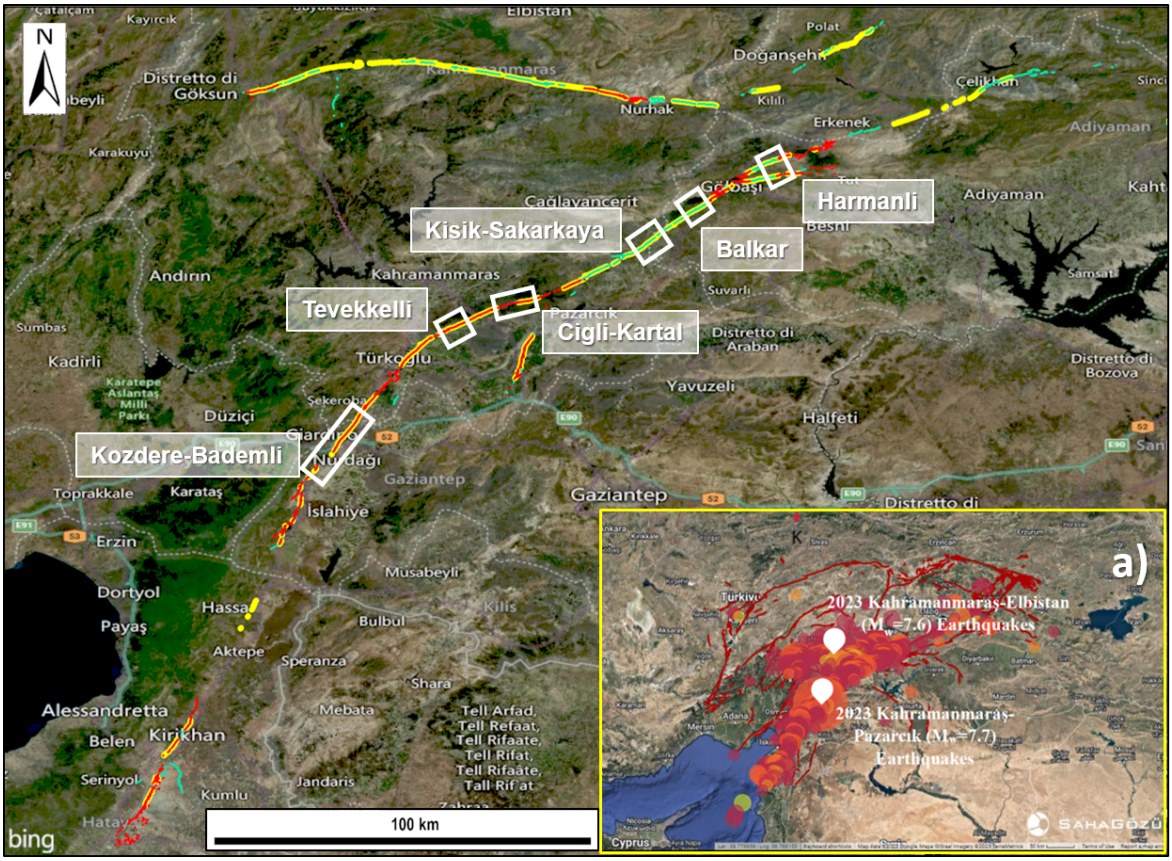

Fig. 1 – Locations of the investigated areas (white boxes) along the Kahramanmaraş-Pazarcık fault. Fault trace colors refer to different sources of data: yellow, AFAD; green, USGS; red, EMERGEO. Inset map (a) shows the regional framework affected by the 2023 seismic sequence (from Middle East Technical University, 2023).

This first mission, carried out within the clearinghouse system, has also allowed us to acquire useful information for planning further investigations, especially in the frame of the presently constituting European Earthquake Geology task force (EuQuaGe).

Methodological approach

The field survey was aimed at collecting data on the coseismic surface geological effects, particularly the primary effects (i.e. surface faulting), in order to contribute to the reconstruction of the near-fault slip distribution through the classical morphotectonic and structural geology approaches. Following the earthquakes, several international research teams began mapping the surface faulting traces by integrating different methodologies (field surveys, high-resolution (<1.0 m/pixel) optical image analysis (WorldView 1, 2, and 3; see Reitman et al., 2023) and remote sensing data processing). Three months after the events, a general overview of fault ruptures was already available, so we preferred to focus on some aspects of particular scientific interest, such as the relationship between coseismic deformation and long-term morphotectonic processes. In this way we concentrated our effort on specific situations that, at the same time, could ensure quickness in the field operations as well as significance of data collected.

First, in the phase of preparation for the mission, we analysed the pattern of fault rupture available on the Internet by different scientific institutions (USGS, METU) through the Google Earth® satellite

images, in some cases also comparing situations documented by both pre- and post-event images. This analysis allowed for the recognition of six key-areas (see labels in Fig. 1) where the interaction between long-term and coseismic deformation was immediately evident, each of them being characterised by different tectonic and morphological features. Then, in the field, we proceeded straight to the previously designated locations; however, it should be noted that in each region only a limited number of measurement points, even 1 km apart from each other, were considered. This operational approach differs significantly from that used in previous seismic emergencies in Italy (Pantosti et al., 2014), where measurement points were mapped extensively and practically in a continuous way along the fault. This strategy is motivated by the huge size of the coseismic phenomena to be mapped, as well as the limited time and personnel available.

In the field, for ground measurements, tapes and Leica DISTO™ laser distance meters have been used, as we have digital mobile devices equipped with Rocklogger® software to determine the position and orientation of the coseismic features. Moreover, in order to map the investigated areas homogeneously and obtain detailed 3D models, we used a DJI Mini 2 drone and tablet featuring a LIDAR scanner system (Polycam®). In addition, a huge amount of photographic documentation has been acquired by professional digital cameras.

Preliminary results

Overall, more than 600 structural and geomorphic data points, along with ca. 4,000 photos, were acquired in the field on orientation, position and dimension of the coseismic features, including the measurements of kinematics and offset components. A part of this dataset was shared in real-time with the MapLab at INGV in Rome, thanks to the tools of the GIS platform (ArcGIS Pro®). These georeferenced data pointed to reconstruct the deformational pattern at the local scale of the six key-areas. Morover, drone surveys provided images to reconstruct eight structure from motion (SfM) high-resolution (5 cm/pixel) digital surface models (DSM) (Fig. 2), and relative ortho-photomosaics. In addition, expeditious LIDAR-derived models representative of the expression of the surface faulting in four key-areas, were also obtained by a handheld device (Fig. 3). In this way it has been possible to derive analytical models of the coseismic mole-track along the fault trace that contain the georeferenced structural and geomorphic data.

In all the investigated key-areas, left-lateral displacements up to 5.0 m were measured and validated through the comparison of the same piercing points on pre-earthquake Google Earth® images through the same piercing points. Similarly, post-earthquake Google Earth® images allowed, at some places, to reproduce a detailed line drawing of the surface faulting in order to integrate the field mapping. This allowed us to highlight the relationships between coseismic surface faulting and tectonic long-term landforms (Fig. 3a).

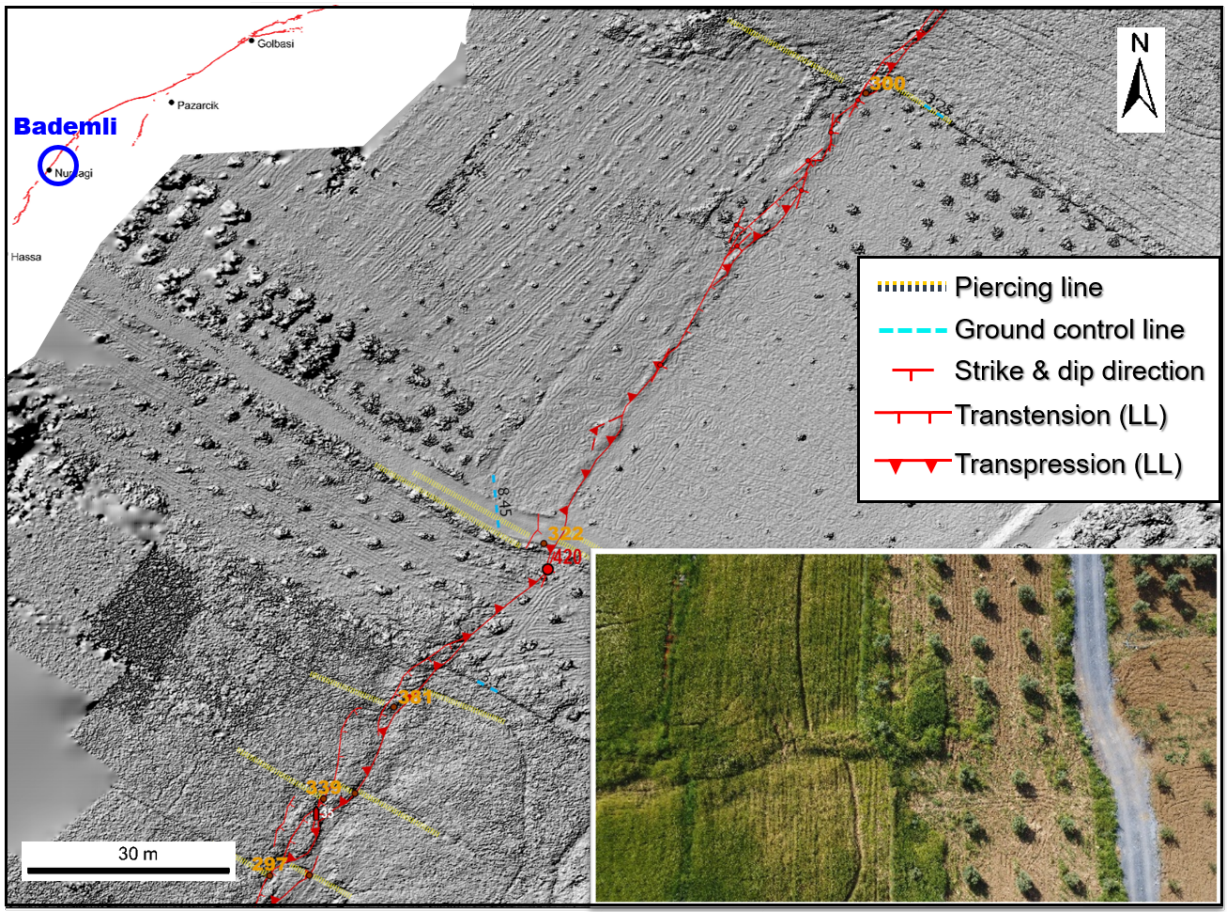

Fig. 2 – Example of a high-resolution digital surface model in the area of Bademli, districts of Nurdağı, and reconstruction of the structural pattern. Single mole-tracks and the horizontal offset component measured in the shifting of the tree rows are shown. The use of a drone represents a powerful tool to save time and resources, provided that control points in the field are calibrated.

The experience of our first mission in Turkey, carried out when national governmental and academic institutions were overwhelmed by the emergency of a devastating earthquake sequence, demonstrated that a relatively small team of experts may also provide external support to acquire detailed field observations and contribute to limiting the loss of data, typically short-lived features. Moreover, the integration of a ground-based traditional survey approach with drone surveys or LIDAR models, if well calibrated by control points in the field, proved to be a very powerful tool to optimise time and resources during a post-earthquake intervention.

Finally, the goal of this first cooperation, promoted by the Italian Civil Protection Department (DPC), was essential in defining a standardized methodology and shared tools for the next mission, held in October 2023 under the umbrella of the international EuQuaGe initiative.

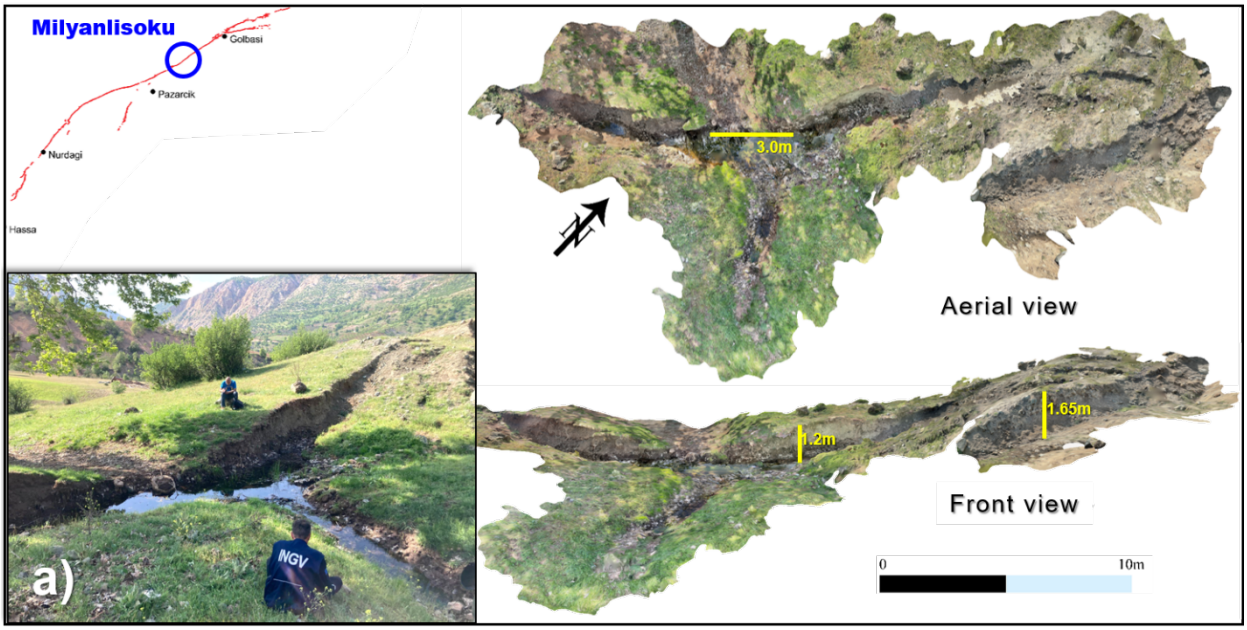

Fig. 3 – Example of speditive terrestrial acquisition by a tablet equipped with LIDAR sensor, in a site near Kartal. a) detail of the earthquake rupture interacting with geomorphological features in a mountain area: here the stream is dammed by the vertical apparent displacement produced by a left-lateral offset of 3 m.

References

Middle East Technical University; 2023: Preliminary reconnaissance report on February 6, 2023, Pazarcık M_w=7.7 and Elbistan M_w=7.6, Kahramanmaraş-Türkiye Earthquakes. Edited by K.Ö. Çetin, M. Ilgaç, G. Can and E. Çakır, Report N° METU/EERC 2023-01, Earthquake Engineering Research Center.

Pantosti D., Azzaro R., De Martini P.M., Moro M., Nappi R. and Pucci S.; 2014: QUI INGV - EMERGEO: un gruppo di lavoro INGV per lo studio degli effetti geologici cosismici. Progettazione Sismica, 2, 137-140.

Reitman N.G., Briggs R.W., Barnhart W.D., Thompson J.A., DuRoss C.B., Hatem A.E., Gold R.D., Akçiz S., Koehler R.D., Mejstrik J.D., Collett C.; 2023: Fault rupture mapping of the 6 February 2023 Kahramanmaraş, Türkiye, earthquake sequence from satellite data. U.S. Geological Survey data release, https://doi.org/10.5066/P985I7U2.

Corresponding author: raffaele.azzaro@ingv.it

The first manually revised catalog of micro-seismicity of Co. Donegal (Ireland): defining baseline seismicity in a region of slow lithospheric deformation.

F. Riva[1,2], N. Piana Agostinetti[2], S. Marzorati[3], C. Horan[4]

1. School of Advanced Studies, University of Camerino, Camerino, Italy
2. Department of Earth and Environmental science, University of Milano-Bicocca, Milan, Italy
3. Osservatorio Nazionale Terremoti, Istituto Nazionale di Geofisica e Vulcanologia (INGV), Ancona, Italy
4. Geophysics Section, Dublin Institute for Advanced Studies, Dublin, Ireland

INTRODUCTION

Ireland is a region of slow lithospheric deformation and at the present Co. Donegal, located in its northwestern part, is the only seismically active area in Ireland, with an average rate of an event every 3–4 years in the range of magnitude between 2-3. Regions of slow lithospheric deformations are characterized by a low seismicity rate and limited accumulation and release of tectonic energy, leaving open the question if such deformation is 'diffusely' accommodated along a wide fault system rather than clusterized along specific faults. Co. Donegal is also the site of post-orogenic radiogenic granites partly exposed along the NW Atlantic coast and potentially buried at shallow depth in the eastern part of the study region. For this reason, the area represents a target for deep (0–5 km depth) geothermal investigation (Goodman et al., 2004). Having a high quality of precisely located micro-seismicity is fundamental before the exploitation of geo-resources for investigating seismicity and rock physical properties in active tectonic and volcanic regions and for the definition of a 'baseline' seismicity, required for a safe future exploitation of georesource areas. For these two reasons, the final aim of our work is the precise location of both human-induced and natural micro seismic events of Co. Donegal, which could give new insights in the tectonic deformation mechanisms and help to find out granite volumes characterized by micro-fractures suitable for fluid circulation.

METHODS

The seismic data provided in this paper have been collected thanks to the SIM-CRUST project*: 'Seismic imaging and monitoring of the upper crust: exploring the potential of low-enthalpy geothermal resources of Ireland*' (https://sim-crust.dias.ie). The SIM-CRUST project provided a seismic network composed of 12 stations installed and maintained in Co. Donegal from August 2012 to June 2015 with the inter-station distance between 5 and 20 km. All stations were equipped

with broadband seismometers (Guralp CMG-40 T), with a flat response between 50 Hz and 60s. Continuous waveform data have been archived as 1-day MSEED files at DIAS (Dublin Institute for advanced Studies).

Our study focuses on the detection and location procedure through a Markov chain Monte Carlo approach of both natural and human-induced seismicity recorded from August 2012 to July 2015 by 12 broadband seismic stations. We compile a first manual-revised catalog of Donegal micro-seismicity, and we integrate it with the location of the seismic events occurred in a small seismic sequence during January 2012 in the study area.

In order to detect the seismic events, we analysed the continuous waveforms by applying a STA/ LTA network coincidence trigger algorithm (Team, 2017). Then, we performed a manual picking of P and S waves first arrival times of the events detected by the trigger algorithm (Goldstein and Snoke 2005) 2005). Finally, a total of 114 earthquakes were located using a hierarchical Bayes Markov chain Monte Carlo (McMC) algorithm, developed on purpose for this study. The Markov chain Monte Carlo method allows us to estimate the realistic uncertainties on the investigated parameters (Lomax et al., 2000). The strength of McMC method lies on the fact that the data uncertainties are also considered as part of the unknowns and are robustly estimated through the McMC sampling following a Hierarchical Bayes approach (Malinverno and Briggs 2004). Moreover, a detailed velocity model of the investigated area does not exist at the moment. This aspect can be easily solved by using our method because we just need to specify the minimum and maximum values of all the priors to define the prior probability distribution (i.e. the velocities of P and S waves).

For a more precise compilation of a seismic catalog, we also calculated the local magnitudes (ML) of the natural seismic events. We decided to use two different approaches for magnitude comparison due to scarceness of local seismicity and the consequent difficult calibration of existing magnitude values with respect to ours. We first used the classical formula for calculating the individual magnitude at each station provided by Richter (1935) that we call “MLRI352” in Table 2. For comparison, we then calculated the magnitude at each station using a calibrated local scale for Ireland, provided in the study of Grannell et al., 2018, where they used a station correction coefficient and a distance-dependant term accounting for geometrical spreading and anelastic attenuation, reported in Table 2 under the name “ML_Donegal”. We added a station correction term for the individual stations used by the Irish Seismic Network for both formulas. We then averaged the individual valued of ML resulted from each station discarding the single values that were more than two standard deviations from the mean ML value and we recalculated the final values of ML for each seismic event, as reported in Table 2.

RESULTS

We tested the performance of McMC algorithm statistically through frequency distribution histograms reported in Figure 1, where we chose a “reference event” from the list of located events. These histograms show the gaussian distribution of the eight parameters used to describe the mathematical model for the geophysical process of seismic wave propagation and thus the

location of each seismic event. Four parameters describe the event location in space and time (X, Y, Z, T0), two parameters represent the elasticity of the rock volume (Vp, Vs) and the last two are used to evaluate the data uncertainties ($\pi_{p,}$ π_s). The X and Y parameters show a Gaussian distribution with a standard deviation of about 1 km. The Z parameter (depth value) shows a Gaussian distribution with a mean value at around − 7 ± 3 km for this event. (Figure 1a–c). The velocity of P waves shows a Gaussian distribution with an average value between 5 and 6 km/s, whereas the velocity of S waves has the highest peak at 3.5 km/s with a standard deviation of about 1 km/s (Figure 1d, e). Both P ($\pi_{p,}$) and S wave uncertainties (π_s) have a Gaussian distribution with a narrow shape meaning that they have been well-constrained. The average value for π_s is 1.2, for π_s is 1.4, both with standard deviation lower than 1 (Figure 1g, h). Finally, the mean value for the Vp ⁄ Vs ratio of 1.69 with a standard deviation of less than 0.1.

The Figure 2 shows the located natural events within the Donegal Granite region. The natural seismicity is gathered between 55.12 and 55.22 N and between −7.59 and − 7.74 E (580–590 Km on the X coordinate and 6110–6120 Km on the Y coordinate) (Figure 2a). In the lower panel (panel b), the events are shown in cross-section along the track line A-B. The majority of the events is clearly aligned, showing a trend towards SE with a high dip angle. Figure 3 shows the distribution of located blast events within the Donegal area. Most of the blast events are concentrated in the proximity of active local quarries in the area. Table 1 resumes the geographical locations for the Donegal's quarries. Quarrie’s locations have been used to cross-validate the location of the recorded blast events. Comparing the position of the quarries and the clusters of localized blast events, the correlation between the two is clearly visible. This means that the majority of the anthropic events in Donegal are quarry blasts and they have been correctly localized by McMC procedure to their correspondent quarry.

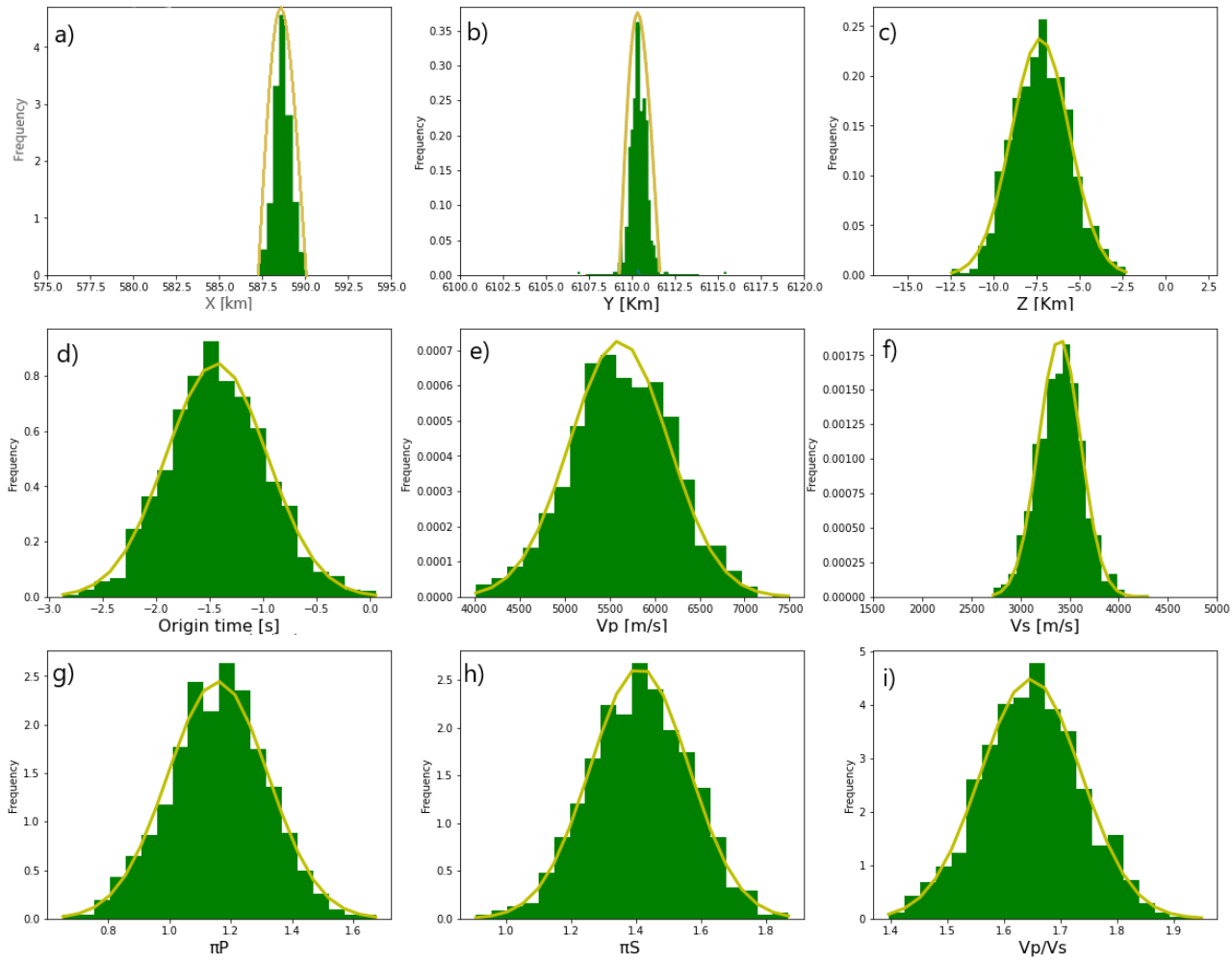

FIGURE 1. Gaussian distributions of (a) longitude [Km] (b) latitude [Km] (c) depth [Km] (d) origin time [s] (e) P-wave velocity [m/s] (f) S-wave velocity [m/s] (g) uncertainty related to the P-wave picking (h) uncertainty related to the S-wave picking (i) P- and S-wave velocity ratio for the “reference” event, chosen from the list of located natural events.

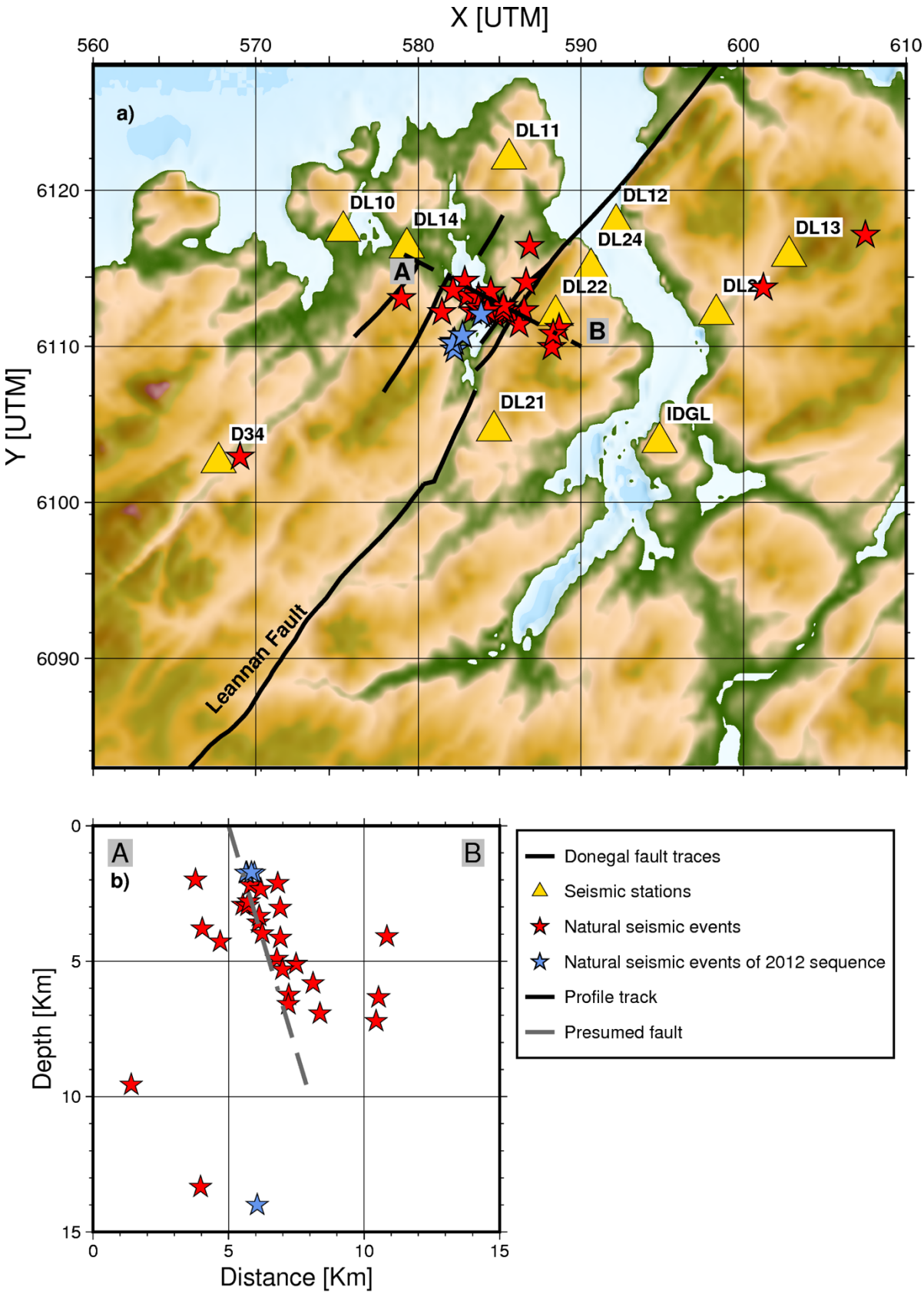

FIGURE 2. Natural seismic events plotted on the X-Y map and on the Z coordinate. Panel (a) shows the seismic stations and the track of the NW-SE profile. Panel (b) shows the natural events projected on depth and the presence of the presumed fault

.

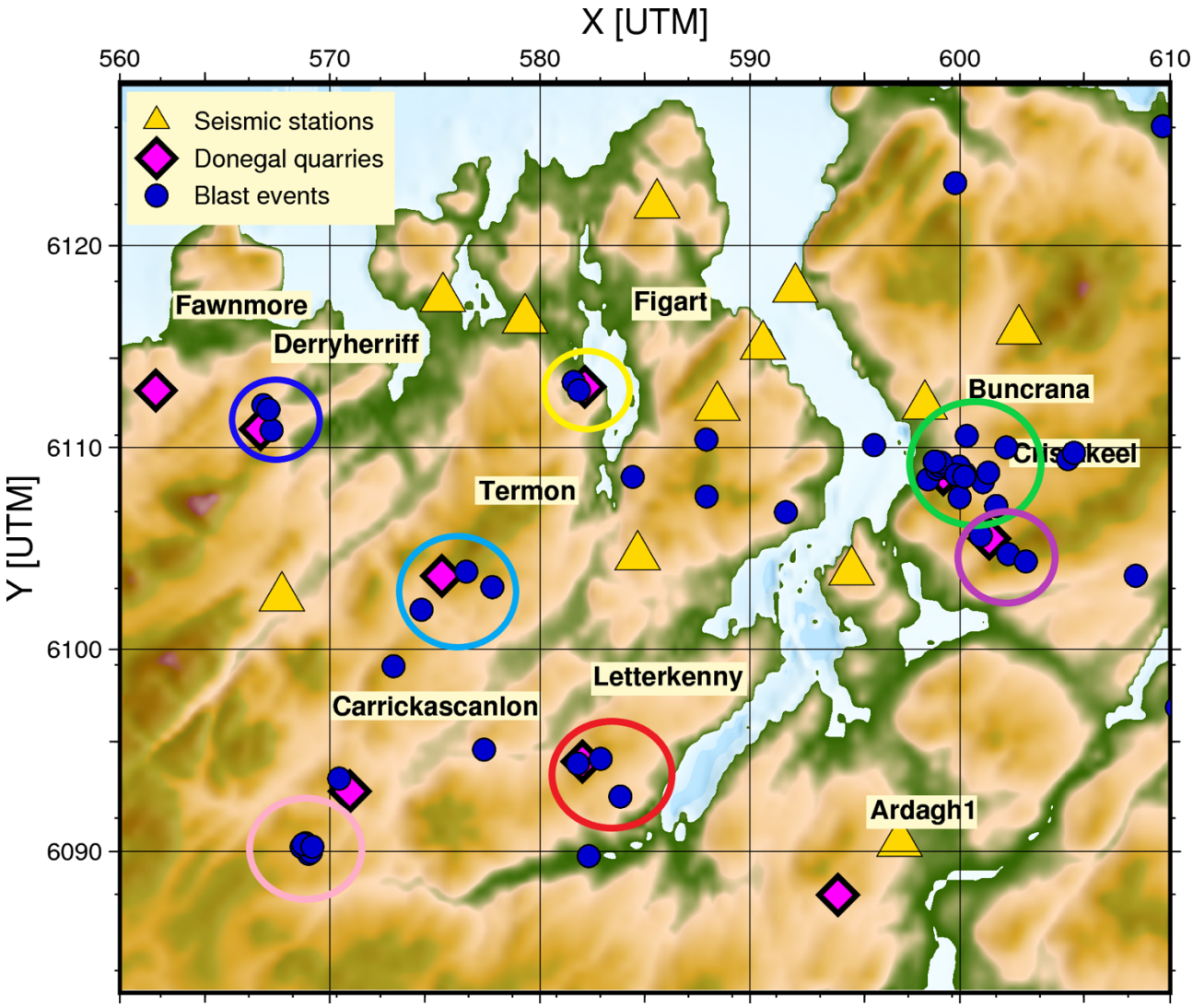

FIGURE 3. Blast events plotted on the X-Y plane. Clusters of events are related to local active quarries.

NAME	LAT	LON
Buncrana Co-Donegal	55,116	-7,440
Termon Co-Donegal	55,072	-7,820
Derryherriff Co-Donegal	55,136	-7,958
Carrickascanlon Co-Donegal	54,978	-7,890
Crislakeel Co-Donegal	55,088	-7,405
Letterkenny Co-Donegal	54,991	-7,714
Figart Co-Donegal	55,154	-7,712

TABLE 1. Donegal quarries' names and coordinates referred to the clusters of blast represented in Figure 3.

Idev num	idev	MLRI35	MLRI35 std	Num sta good	ML Donegal	ML Donegal std	Num sta good
1	20120928062959	1.6	0.3	4	1.2	0.1	4
2	20121024065903	1.5	0.3	6	1.3	0.2	6
3	20121031193817	1.5	0.3	6	1.0	0.6	6
4	20121122194654	1.9	0.4	7	2.3	0.1	6
5	20130210063823	1.5	0.2	6	1.2	0.2	6
6	20130402052503	2.3	0.3	7	1.3	0.3	7
7	20130405004553	2.8	0.3	7	3.7	0.2	7
8	20130405004643	1.4	0.3	7	0.9	0.2	7
9	20130503203415	1.5	0.3	7	1.7	0.3	7
10	20130521101615	1.4	0.3	6	1.5	0.2	6
11	20130523130545	1.4	0.3	6	1.7	0.3	6
12	20130528095326	1.4	0.3	7	1.0	0.4	7
13	20130602025737	1.6	0.4	7	1.2	0.2	7
14	20130608123331	1.4	0.3	7	1.2	0.7	7
15	20130609032716	1.4	0.3	7	0.4	0.1	7
16	20130622075627	1.4	0.3	7	1.2	0.1	6
17	20130625021853	1.4	0.3	7	0.2	0.3	7
18	20130625221351	1.4	0.3	7	0.5	0.5	7
19	20130720051915	1.5	0.2	8	0.5	0.6	8
20	20130925094650	1.8	0.3	7	1.2	0.3	7
21	20131231194717	1.5	0.2	8	1.1	0.4	8
22	20140314011925	1.5	0.3	8	0.7	0.4	8
23	20140401120612	1.5	0.2	8	1.7	0.2	8
24	20140429040202	1.5	0.2	8	1.4	0.3	8
25	20140519061145	1.5	0.2	8	1.1	0.2	7
26	20140611130418	1.5	0.3	8	1.4	0.3	8
27	20140619111118	1.6	0.4	8	1.5	0.3	8
28	20140706122114	1.5	0.2	8	0.6	0.4	8
29	20140706155212	1.5	0.2	8	0.8	0.3	8
30	20140728115302	1.5	0.3	8	1.2	0.3	7
31	20140805055249	1.5	0.2	8	1.8	0.3	8
32	20140818001902	1.5	0.3	8	1.0	0.2	7

33	20141209063409	1.4	0.3	6	1.8	0.2	6
34	20150521215759	1.5	0.3	5	0.9	0.1	5
35	20150701004049	1.4	0.4	3	0.4	0.1	3

TABLE 2. Magnitude values at each station calculated by using the first approach with equation for the magnitude 'MLRI35' and the second approach with equation for 'ML_Donegal', their standard deviations and the corresponding number of stations used to reach the final averaged ML value.

CONCLUSIONS

Our results indicate that the majority of the micro-seismicity is present with magnitudes lower than 2 (the highest magnitude is 2.8). The recorded seismicity is almost clustered along previously mapped NE-SW trending, steeply dipping faults and confined within the upper crust (focal depth less than 10 km). We also recorded anthropogenic seismicity mostly related to quarries' activity in the study area.

REFERENCES

Grannell, J., Arroucau, P., Lebedev, S., Moellhoff, M., & Bean, C. J. (2018). A Local Magnitude Scale for Ireland and its Offshore Regions, Poster Presentation, ESC General Assembly

Goldstein, P., and J. A. Snoke. 2005. "SAC Availability for the IRIS Community." *DMS Electronic Newsletter* 7 (1): 63. www.mathworks.com.

Goodman, R., Jones, G. L., Kelly, J., Slowey, E., & O'Neill, N. (2004). Geothermal energy exploitation in Ireland.

Lomax, A., Virieux, J., Volant, P., & Berge-Thierry, C. (2000). Probabilistic earthquake location in 3D and layered models (pp. 101–134). Springer Netherlands

Malinverno, A., & Briggs, V. A. (2004). Expanded uncertainty quantification in inverse problems: Hierarchical bayes and empirical bayes. Geophysics, 69, 1005–1016.

Richter, C. F. (1935). An instrumental earthquake magnitude scale*. Bulletin of the Seismological Society of America, 25, 1–32.

Team, T. O. D. (2017). Obspy 1.0.3.

Corresponding Author: federica.riva@unicam.it.

Multiscale geophysical investigation on the Budoia-Aviano thrust system (NE Italy): first results

E. Rizzo[1,2], V. Giampaolo[2], F. Mucchi[1], P. Boldrin[1], G. De Martino[2], M.E. Poli[3], G. Patricelli[1], A. Marchesini[3], R. Caputo[1]

[1] Dipartimento di Fisica e Scienze della Terra, University of Ferrara, Italy
[2]Consiglio Nazionale delle Ricerche, Istituto di Metodologie per l'Analisi Ambientale (CNR-IMAA), Tito Scalo (PZ), Italy
[3]Dipartimento di Scienze Agroalimentari, Ambientali e Animali, University of Udine, Italy

The work group is involved in the framework of the PRIN2020 research project (NASA4SHA), which aims to identify the complexity of faults in active thrust systems in Northern Apennines and Southern Alps in Italy. The paper describes the application of a multi-scale geophysical investigations applied on the Budoia-Aviano thrust system, that is part of the Polcenigo–Montereale fault system. The investigated area, which is part of the external Plio-Quaternary front of the Eastern Southalpine Chain, is characterized by the presence of distinct WSW-ENE trending and S-verging reverse fault planes arranged in thrust systems and affecting the Quaternary succession (Poli et al., 2014).

The proposed methodology included deep and shallow geoelectrical and GPR techniques to upscale the buried geological structures and to identify the site for the excavation of paleoseismological trenches. The adopted multiscale geophysical approach was applied in the studied area perpendicularly to the morphotectonic evidence of the Budoia-Aviano fault. The first step of the multiscale approach defined a Deep Electrical Resistivity Tomography (DERT). The DERT was long around 6000m, and it was able to obtain an investigation depth of about 1000m. The used DERT apparatus is a multichannel system designed and implemented by the CNR-IMAA (Rizzo et al.2004; Rizzo and Giampaolo, 2019). The acquired DERT data set was processed and elaborated through a procedure built ad hoc for this type of geoelectric surveys. While the first step highlighted the deep geological structure, several shallow high resolution geophysical surveys were planned close the morphotectonic evidence along the Budoia-Aviano thrust fault. Several shallow Electrical Resistivity Tomographies (ERT) with different electrode spacing were carried out. Three ERTs were carried out with an electrode spacing of about 5m obtaining an investigation depth of about 60m. Consequently, in order to increase the shallow resolution, a high resolution ERT with an electrode spacing of about 1m was acquired. The results of the shallow ERTs highlighted the buried geological structures in terms of subsurface faults and geological formations. Moreover, taking in account the previous results, several GPR profiles were carried out on the investigated area and the obtained results permitted to identify the site for the excavation of two

paleoseismological trenches (Poli et al., at this session 1.1). The GPR results well depicted the high-resolution image of the buried geological deformation, that were highlighted during the excavation phase (Poli et al., 2024). Finally, the multiscale geophysical approach allowed to improve the interpretation of previous geological and morphotectonic studies of the investigated area.

References

Poli M.E., Monegato G., Zanferrari A., Falcucci E., Marchesini A., Grimaz S., Malisan P., Del Pin E. (2014) Seismotectonic characterization of the western Carnic pre-alpine area between Caneva and Meduno (Ne Italy, Friuli). DPC-INGV-S1 Project “Base-knowledge improvement for assessing the seismogenic potential of Italy”.

Rizzo E., Colella, A., Lapenna, V. and Piscitelli, S. (2004). “High-resolution images of the fault controlled High Agri Valley basin (Southern Italy) with deep and shallow Electrical Resistivity Tomographies”. Physics and Chemistry of the Earth, 29, 321-327.

Rizzo E. & Valeria Giampaolo (2019) New deep electrical resistivity tomography in the High Agri Valley basin (Basilicata, Southern Italy), Geomatics, Natural Hazards and Risk, 10:1, 197-218, DOI: 10.1080/19475705.2018.1520150

Poli M.E.; Patricelli G.; Falcucci E.; Gori S.; Paiero G.; Rizzo E.; Marchesini A.; Caputo R. (2024). New palaeoseismological evidence of coseismic surface rupture across the Carnic Prealpine front (NE-Italy): the Budoia-Aviano thrust system. GNGTS 2024 (in this session).

Corresponding author: enzo.rizzo@unife.it

Preliminary results of the Non-Double-Couple seismic sources in the Southern Apennines

P. Roselli[1], L. Scognamiglio[2], F. Di Luccio[1], M. Palano[3], G. Ventura[1]

[1]Istituto Nazionale di Geofisica e Vulcanologia, Roma 1 (Roma, Italy)
[2]Istituto Nazionale di Geofisica e Vulcanologia, ONT (Roma, Italy)
[3]Istituto Nazionale di Geofisica e Vulcanologia, Osservatorio Etneo (Catania, Italy)

The seismic moment tensor analysis is an efficient way to better understand earthquake source processes as well as fault kinematics. Although earthquake sources are assumed to be shear ruptures with associated Double-Couple seismic moment tensors (DCMT), it is widely accepted that the faulting mechanism may include fracture opening and closing, rupture on a non-planar surface or multiple sub-ruptures that, in turn, produce significant Non-Double-Couple components of the moment tensor (Frohlich, 1994). Therefore, the seismic moment tensor can be decomposed into the isotropic (ISO), compensated linear vector dipole (CLVD) and double-couple (DC) components (Knopoff and Randall, 1970). The sum of the ISO and the deviatoric parts (DC and CLVD) constitute the full seismic moment tensor (FMT). DC represents the pure shear motion from two orthogonal vector pairs of equal magnitude but opposite sign; the ISO represents the isotropic volumetric change in the crack closures or implosions; the CLVD represents motion away or toward the earthquake sources with no net volume change and generally complex more physical interpretation (Frohlich, 1994; Julian et al., 1998; Martínez-Garzón et al., 2017). It is known that mixed shear-tensile earthquakes nucleate in geothermal and volcanic zones, where over-pressurized fluids concentrate (Ross et al., 1996; Saraò et al., 2010; Hrubcovà et al., 2021) and in areas of fluid extraction or injection, where hydraulic fracturing processes easily occur (Zoback, 2007; Ellsworth, 2013; Martínez-Garzón et al., 2017; Dost et al., 2020; Roselli et al., 2023). Here we investigate, the DCMTs and FMTs of the earthquakes from seismic sequences occurred in the Southern Apennine chain (Italy); these include the 2013-2014 Sannio-Matese (Di Luccio et al., 2018) and the 2010-2014 Pollino (Pastori et al. 2021; Napolitano et al., 2021) sequences. Our data-set consists of the waveforms ($M_L \geq 2.5$) recorded by both national permanent and local temporary networks operated by the Istituto Nazionale di Geofisica e Vulcanologia (http://www.orfeus-eu.org/data/eida/; Passarelli et al., 2012). To properly cover different magnitude ranges and to compare the results, we apply different approaches and specifically the Time Domain Moment Tensor (Dreger & Helemberger, 1993; Dreger 2003) and Isola (Sokos & Zahradník, 2018) for $M_L > 3.2$, hybridMT (Andersen, 2001; Kwiatek et al., 2016) for $M_L \leq 4$. Our primary goal is to understand the role played by fluids to define type and space-time variability of the source parameters and the behavior of the DC, ISO and CLVD components during the seismic sequences in the Southern Apennines.

References

Andersen L. M.; 2001: *A Relative Moment Tensor Inversion Technique Applied to Seismicity Induced by Mining*. Univ. of the Witwatersrand, Johannesburg, South Africa.

Di Luccio F., Chiodini G., Caliro S., Cardellini C., Convertito V., Pino N.A., Tolomei C., Ventura G.; 2018: *Seismic signature of active intrusions in mountain chains*. Sci. Adv. 4, e1701825.

Dost B., Stiphout A., Kühn D., Kortekaas M., Ruigrok E. and Heimann S.; 2020: *Probabilistic Moment Tensor Inversion for Hydrocarbon-Induced Seismicity in the Groningen Gas Field, the Netherlands*. Part 2: Application. Bull. Seism. Soc. Am., 110 (5): 2112–2123. Doi: https://doi.org/10.1785/0120200076.

Dreger D.S. and Helmberger D.V.; 1993: *Determination of source parameters at regional distances with 3-component sparse network data*. J. Geophys. Res., 98, 8107-8125.

Dreger D.S.; 2003: *Time Domain Seismic Moment Tensor INVersion*. International Handbook of Earthquake and Engineering Seismology, Volume 81(B), pp 1627.

Ellsworth W.L.; 2013: *Injection-induced earthquakes.* Science, 341(6142). doi: 10.1126/science.1225942.

Frohlich C.; 1994: *Earthquakes with Non-Double-Couple Mechanisms*. Science, 264 (5160), 804 -809. doi: 10.1126/science.264.5160.804.

Hrubcova P., Doubravová J., Vavrycuk V.; 2021: *Non-double-couple earthquakes in 2017 swarm in Reykjanes Peninsula, SW Iceland: Sensitive indicator of volcano-tectonic movements at slow spreading rift*. Earth and Planetary Science Letters. 563. 116875. 10.1016/j.epsl.2021.116875.

Istituto Nazionale di Geofisica e Vulcanologia (INGV); 2010-2014: *Rete Sismica Nazionale (RSN)*. doi: https://doi.org/10.13127/SD/X0FXnH7QfY.

Julian B.R., Miller A.D., Foulger G.R.; 1998: *Non-Double-Couple earthquakes 1: Theory*. Rev. Geophys., 36, 525-549.

Knoff, L. and Randall M.J.; 1970: *The compensated linear-vector dipole. A possible mechanism for deep earthquakes*. J. Gephys. Res., 75,1957-1963.

Kwiatek G., Martínez-Garzón P., Bohnhoff M.; 2016: *hybridMT: A Matlab/Shell environment package for seismic moment tensor inversion and refinement*. Seismol. Res. Lett., doi: 10.1785/0220150251.

Martínez-Garzón P., Kwiatek G., Bohnoff M., Dresen G.; 2017: *Volumetric components in the earthquake source related to fluid injection and stress state*. Geophys. Res. Lett., 44(2), 800-809, doi:10.1002/2016GL071963.

Napolitano F., Amoroso O., La Rocca M., Gervasi A., Gabrielli S., Capuano P.; 2021: Crustal Structure of the Seismogenic Volume of the 2010–2014 Pollino (Italy) Seismic Sequence From 3D P- and S-Wave Tomographic Images. Front. Earth Sci., Sec. Solid Earth Geophysics, 9. doi: 10.3389/feart.2021.735340.

Pastori M., Margheriti L., De Gori P., Govini A., Lucente F.P., Moretti M., Marchetti A., Di Giovambattista R., Anselmi M., De Luca P., Nardi A., Piana Agostinetti N., Latorre D., Piccinini D., Passarelli L., Chiarabba C.; 2021: *The 2011–2014 Pollino Seismic Swarm: Complex Fault Systems Imaged by 1D Refined Location and Shear Wave Splitting Analysis at the Apennines–Calabrian Arc Boundary*. Front. Earth Sci., Sec. Solid Earth Geophysics, 9. doi: 10.3389/feart.2021.618293.

Passarelli L., Roessler D., Aladino G., Maccaferri F., Moretti M., Lucente F.P., Braun T., De Gori P., Margheriti L., Woith H., Sebastian H., Eleonora R., Dahm T.; 2012: *Pollino Seismic Experiment (2012-2014)* [Data set]. Deutsches GeoForschungsZentrum GFZ. doi: 10.14470/9N904956.

Roselli P., Improta L., Kwiatek G., Martínez-Garzón P., Saccorotti G., Lombardi A.M.; 2023: *Source mechanisms and induced seismicity in the Val d'Agri Basin (Italy)*. Geophysical Journal International, 234 (3), pp 1617–1627

Ross A., Foulger G.R., Julian B.R.; 1996: *Non-double-couple earthquake mechanisms at The Geysers geothermal area California*. Geophys. Res. Lett., 23(8), 877-880. doi: 10.1029/96GL00590.

Saraò A., Cocina O., Privitera E., Panza G.F.; 2010: *The dynamics of the 2001 Etna eruption as seen by full moment tensor analysis*. Geophys. J. Int., 181(2), 951-965. doi: 10.1111/j.1365-246X.2010.04547.x.

Zahradník J. and Sokos E.; 2018: *ISOLA code for multiple-point source modeling –review. in Moment Tensor Solutions - A Useful Tool for Seismotectonics*. 1–28 (Springer Natural Hazards, 2018). doi:10.1007/978-3-319-77359-9.

Zoback M.D.; 2007: *Reservoir Geomechanics*. Cambridge University Press, 449 pp.

Corresponding author: pamela.roselli@ingv.it

Anatomy of clustering from parametric space-time analysis of seismicity.

G. Rossi[1], G. Bressan [2], C. Barnaba [1], A. Peresan [1]

[1] *National Institute of Oceanography and Applied Geophysics –OGS, Italy*
[2] formerly *National Institute of Oceanography and Applied Geophysics –OGS, Italy*

We propose a multiparametric approach to quantitatively describe the temporal and spatial evolution of seismicity in regions, where the spatial and temporal pattern of seismicity shows no obvious trends and cannot be resolved on well-defined fault planes (Bressan et al., 2021). We consider five different parameters. The spatio-temporal evolution of Shannon entropy quantifies the degree of organization or disorder in the energy distribution of an earthquake population (Telesca et al., 2004). The temporal changes in the classical estimates of the b-value from the Gutenberg-Richter (GR) law (Gutenberg and Richter, 1944) capture the balance between small and large-magnitude events. The temporal variation of the fractal dimension of hypocenters reflects the evolution of the spatial seismicity pattern. The “nearest neighbour" distance (Baiesi and Paczuski, 2004; Zaliapin and Ben-Zion, 2013) further enables characterizing the clustering properties of seismicity (Varini et al., 2021). Finally, the evolution of seismicity can be further investigated with multidimensional principal component analysis (PCA) (Rossi and Ebblin, 1990; Bressan et al. 2018a; 2021). Time adds to the spatial coordinates in the construction of the 4D-correlation matrix, which can be interpreted as a hyper-ellipsoid. The hyper-ellipsoid spatial axes projection onto a 3D space depicts the best-fit plane orientation and the extent of the volume interested by the aftershocks. The fourth axis projection onto space indicates the shock propagation direction and can be used to infer the relationships between the various planes that activate in time (Bressan et al., 2021).
We have focused on an area in northeastern Italy where the maximum interference between the NW-SE oriented Dinaric transpressive structures and the E-W oriented Alpine thrusts occurs, bound to the superposition of three main tectonic phases that affected the area through time (Ponton, 2010). The inversion of the focal mechanisms indicates a dominance of reverse mechanisms but the presence of strike-slip solutions is also relevant (Saraò et al., 2021). Comparison between the stress and strain tensors reveals planes of mechanical weakness that are oriented differently, often unfavourably with respect to the principal stress axes, suggesting heterogeneous crustal strength (Bressan et al., 2018b). This area is characterized by a relatively high seismic hazard and has experienced several destructive earthquakes in the past. The most severe ones occurred in 1700 (I0=VIII-IX MCS on the Mercalli-Cancani-Sieberg scale, Mw=5.7), 1788 (I0=IX, Mw=5.2), 1928 (I0=IX, Mw=6.0), 1959 (I0=VII-VIII, Mw=5.2) (Rovida et al., 2016; Bressan et al., 2019).

For our analysis, we considered a dataset of 1493 earthquakes that occurred between 2015 and March 2020 and whose magnitude M_D is between 0.4 and 4.0. The earthquakes were located

based on the 3D P-wave and S-wave velocity models. The mean values of the standard errors relative to the hypocentral coordinates are 0.07 km for the x- and y-coordinates and 0.23 km for the depth. Four events with a magnitude of more than 3.7 occurred in the time interval investigated: M_D=3.8 on January 19, 2018; M_D=3.9 on August 11, 2018; M_D=4.0 on June 14, 2019; and M_D=3.8 on September 22, 2019 (labelled E1, E2, E3, and E4 in Fig. 1).

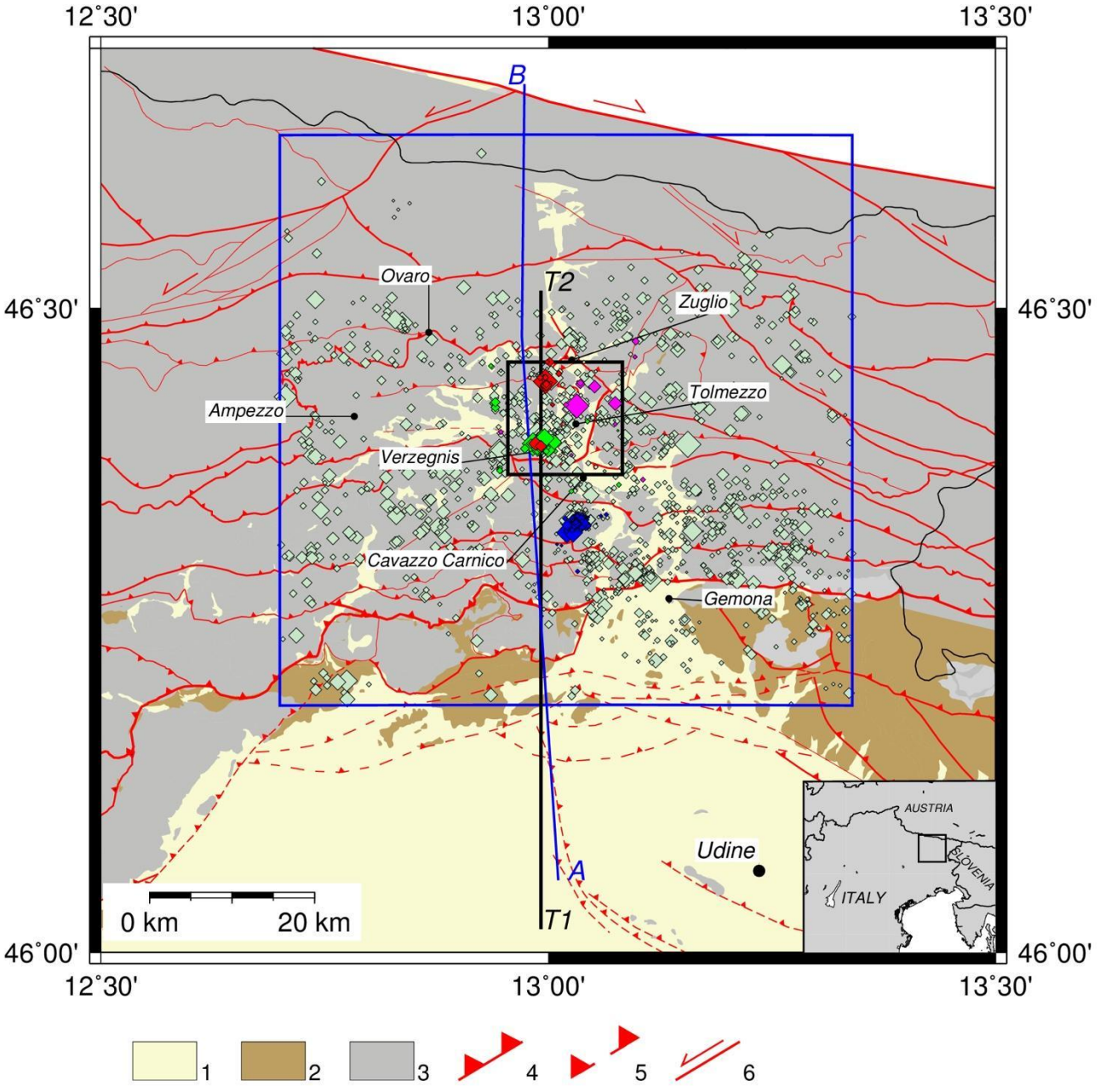

Fig. 1 –Simplified tectonic and geological sketch of the study area. The small black square indicates the central cell of the grid, where the most strongly radiated seismic energy is concentrated and the Shannon entropy was calculated. Light green diamonds: background seismicity from 2015 to March 2020. Magnitude values are given in coda duration magnitude MD. Fuchsia-coloured diamonds: earthquakes of the January 19 2018 MD 3.8 (E1) sequence. Blue diamonds: earthquakes of the sequence of August 11, 2018 MD 3.9 (E2). Green diamonds: earthquakes of the sequence of June 14, 2019 MD 4.0 (E3). Red diamonds: earthquakes of the sequence of September 22, 2019 MD 3.8 (E4). The blue line indicates the trace of the section along which the PCA analysis of Fig. 3 is performed.

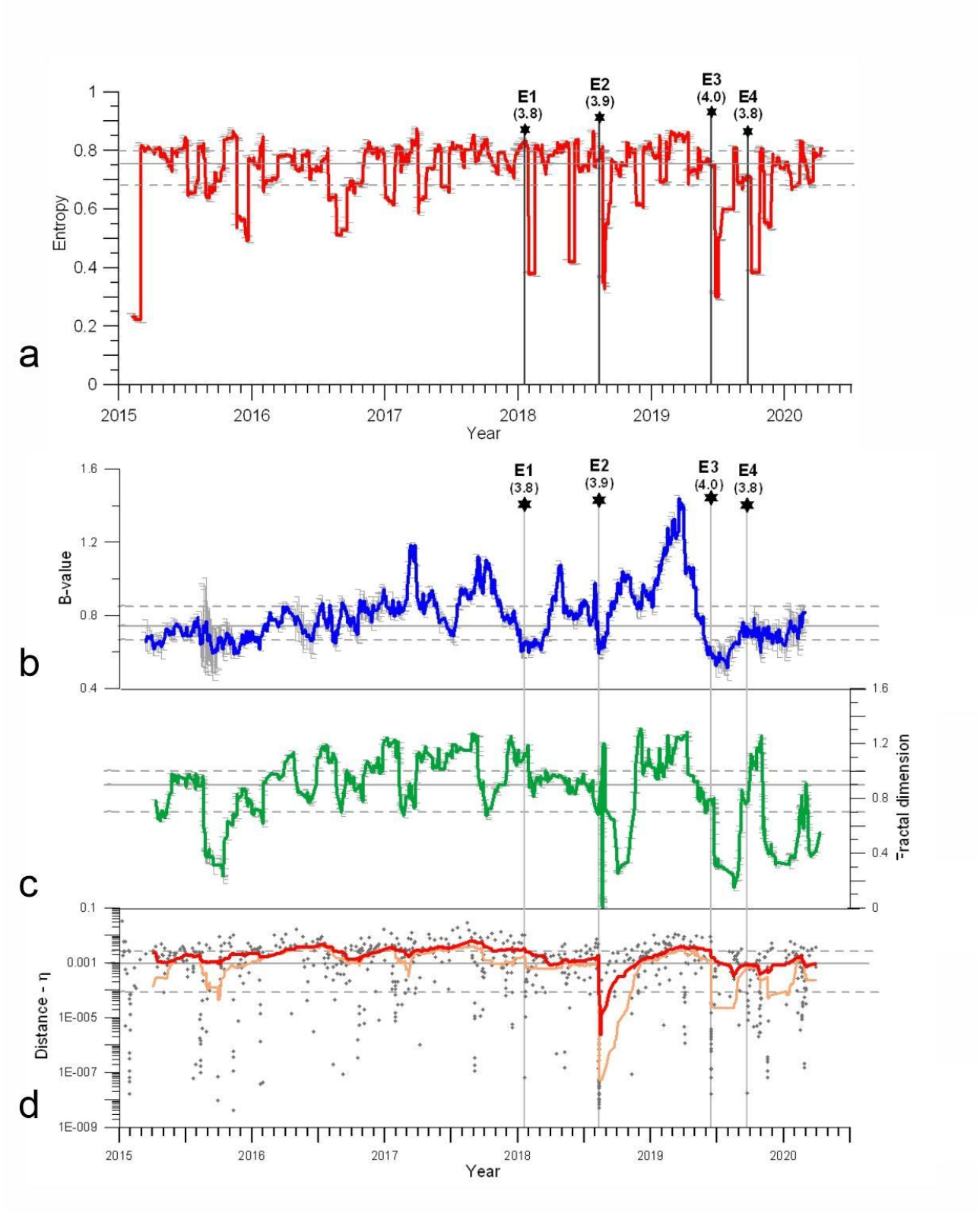

Fig. 2 – Temporal variations of a) Shannon entropy, b) b-value, c) fractal dimension, and d) Nearest-neighbour distances η_{ij}. The four main earthquakes, E1, E2, E3, and E4 are marked by stars with the corresponding magnitudes. For details about parameter computation, see Bressan et al. (2021).

Results

Two distinct periods of the temporal evolution of seismicity appear evident in the curves of Fig. 2: the period between preceding events E1 and E2 and the one following these events, since the beginning of 2017 characterized by marked fluctuations of all the parameters, and in particular b-values and fractal dimension (Fig. 2b, c). The temporal variation of the b-value can be related to crustal stress changes in a medium characterized by different mechanical properties. The fractal dimension time evolution indicates a prevailing clustering of the earthquakes with a tendency to propagate linearly. The temporal variations of the Shannon entropy (Fig. 2a) and η (Fig.2 d) quantify the evolving organization and correlation of seismicity within an area.

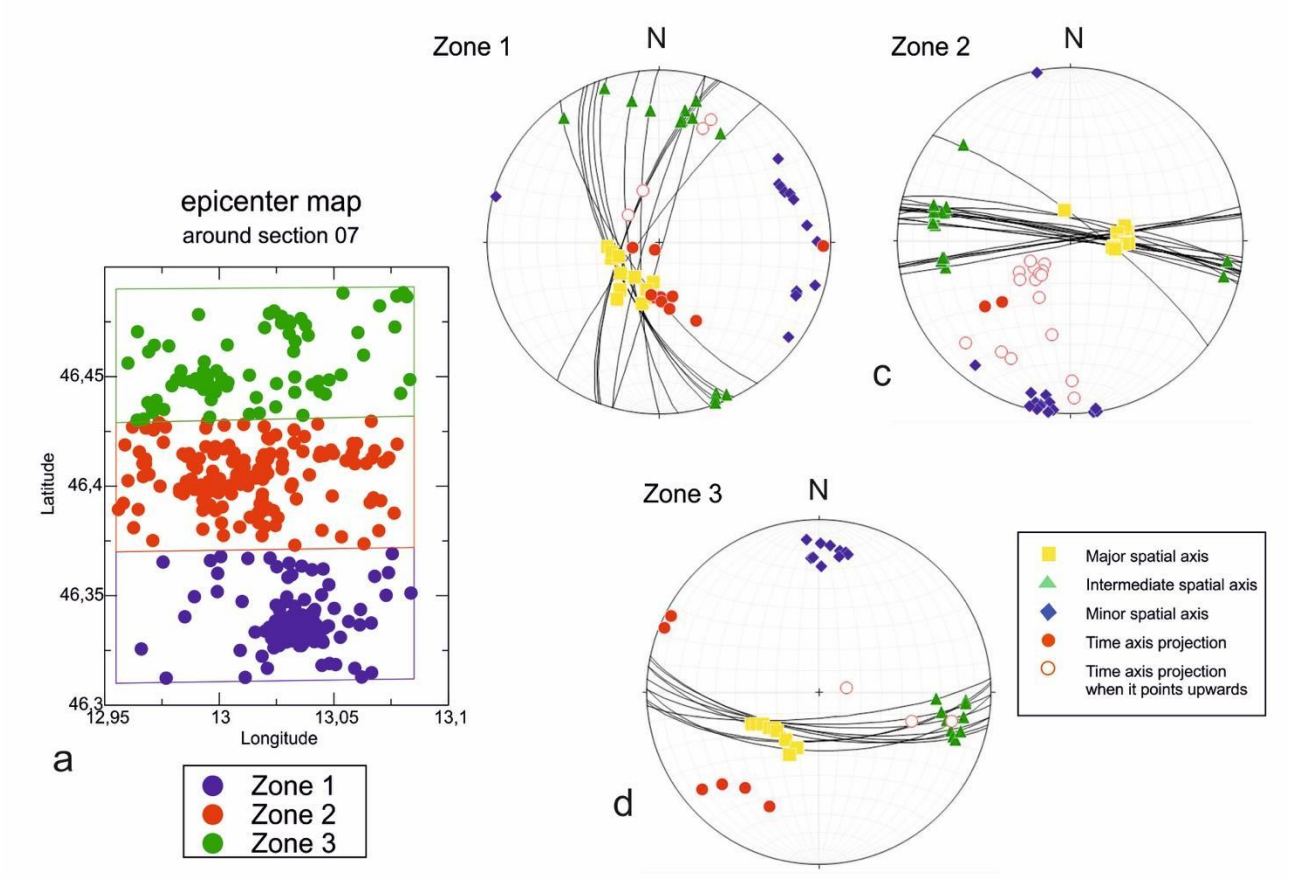

Fig. 3 - a) distribution of the epicentres of the events with M_C = 1 of the catalogue, in the region 10 km wide, centred on the section A-B of Fig. 1, in three spatial windows of about 10 km in longitude and 6.7 km in latitude. The circles are the epicentres of the earthquakes analyzed with PCA: blue circles: zone 1; red circles: zone 2; green circles: zone 3. b) PCA solutions obtained by sliding a 30 events window along the events in zone 1; c) PCA solutions obtained by sliding a 30 events window along the events in zone 2; d) PCA solutions obtained by sliding a 30 events window along the events in zone 3. Yellow square: Maximum spatial axis; green triangle: intermediate spatial axis; blue diamond: minimum space axis; red dot: time axis projection on the space volume: if hollow, the verse is upwards. Black lines: planes normal to the spatial minor axes (blue diamond). (from Bressan et al., 2021, modified).

The spatial distribution of seismicity is not uniform, but local clusters characterize it, as revealed by the fractal analysis and planes changing orientation with time, detected with the PCA method. The PCA solutions (Fig. 3) reveal mostly vertical and sub-vertical planes that fit the seismicity, changing orientation from south to north. The fracture propagates within the fracturing plane in the southern part (zone 1), with the activation of parallel planes in the central part (zone 2) and along weakness lines in the northern part (zone 3). Therefore, the stress concentrations and the localization of seismicity appear to be controlled by the geometric interaction between faults and by sharp variations of rock mechanical characters. Although performed in a narrow area and time span, the adopted procedures and the resulting observations can be applied to other areas of complex tectonics to investigate the time evolution of the seismicity and the damage.

Acknowledgements

The authors thank S. Urban and A. Magrin for help in graphics and critical reading of the manuscript. The local seismic network is managed by the Seismological Research Centre of the National Institute of Oceanography and Applied Geophysics – OGS with the financial contribution of the Regione Friuli Venezia Giulia (Bragato et al., 2021).

References

Baiesi, M., Paczuski, M.;2004: *Scale-free networks of earthquakes and aftershocks*, Phys. Rev. E., 69, 066106, doi:10.1103/PhysRevE.69.066106.

Bragato, P.L., Comelli, P., Saraò, A., Zuliani, D., Moratto, L., Poggi, V., Rossi, G., Scaini, C., Sugan, M., Barnaba, C., Bernardi, P., Bertoni, M., Bressan, G., Compagno, A., Del Negro, E., Di Bartolomeo, P., Fabris, P., Garbin, M., Grossi, M., Magrin, A., Magrin, E., Pesaresi, D., Petrovic, B., Plasencia Linares M.P., Romanelli, M., Snidarcig, A., Tunini, L., Urban, S., Venturini, E., Parolai, S.; 2021: *The OGS–Northeastern Italy Seismic and Deformation Network: Current Status and Outlook*, Seismological Research Letters 92 (3), 1704–1716, doi:10.1785/0220200372

Bressan, G., Barnaba, C., Gentili, S., Rossi, G.;2017: *Information entropy of earthquake populations in northeastern Italy and western Slovenia*, Physics of the Earth and Planetary Interiors, 271, 29–46, doi: 10.1016/j.pepi.2017.08.001.

Bressan G., Barnaba C., Peresan A., Rossi G.; 2021: *Anatomy of seismicity clustering from parametric space-time analysis*. Physics of the Earth and Planetary Interiors 320, 106787, doi:10.1016/j.pepi.2021.106787.

Bressan, G., Barnaba, C., Magrin, A., Rossi, G.; 2018a: *A study on off-fault aftershock pattern at N-Adria microplate*. J. Seismol., 22, 863-881, doi:10.1007/s10950-018-9737-x.

Bressan, G., Barnaba, C., Bragato, P., Ponton, M., and Restivo, A.; 2018b: *Revised seismotectonic model of NE Italy and W Slovenia based on focal mechanism inversion*, J. Seismol., 22, 1563–1578, doi:10.1007/s10950-018-9785-2.

Bressan, G., Barnaba, C., Bragato, P.L., Peresan, A., Rossi, G., Urban, S.; 2019: *Distretti sismici del Friuli Venezia Giulia*, Bollettino di Geofisica Teorica e Applicata, 60, s.3, s1-s74, doi: 10.4430/bgta0300.

Saraò, A., Sugan, M., Bressan, G., Renner, G., and Restivo, A.; 2021: *A focal mechanism catalogue of earthquakes that occurred in the southeastern Alps and surrounding areas from 1928–2019*, Earth Syst. Sci. Data, 13, 2245–2258, doi:10.5194/essd-13-2245-2021.

Ponton, M.; 2010: *Architettura delle Alpi Friulane*. Museo Friulano di Storia Naturale 52, Udine, 80 pp.

Rossi, G., Ebblin, C.;1990: *Space (3-D) and space-time (4-D) Analysis of aftershock sequences: the Friuli (Ne Italy) case*. Boll. Geof. Teor. Appl. 22, 37-49.

Rovida, A., Locati, M., Camassi, R., Lolli, B., Gasperini, P., (eds); 2016: *CPTI15, the 2015 version of the Parametric Catalogue of Italian Earthquakes*. Istituto Nazionale di Geofisica e Vulcanologia. doi:http//doi.org/10.6092/INGV.IT-CPTI15.

Telesca, L., Lapenna, V., Lovallo, M.;2004: *Information entropy analysis of seismicity of Umbria-Marche region (Central Italy)*. Nat. Haz. Earth Syst. Sci. 4, 691–695, doi: 10.5194/nhess-4-691-2004.

Varini, E., Peresan, A., Zhuang, J.; 2020: *Topological Comparison Between the Stochastic and the Nearest-Neighbor Earthquake Declustering Methods Through Network Analysis*. J. of Geophysical Research: Solid Earth, 125 (8), e2020JB019718, doi: 10.1029/2020JB019718

Zaliapin, I., Ben-Zion, Y.; 2013: *Earthquake clusters in southern California I: Identification and stability*, J. Geophys. Res. 118, 6, 2847–2864, doi:10.1002/jgrb.50179.

Corresponding author: grossi@ogs.it

Rheological behaviour along the Hellenic Wadati-Benioff zone

D. Russo[1,2] and R. Caputo[1,2]

[1] Department of Physics and Earth Sciences, University of Ferrara, Italy
[2] Centro Interuniversitario per La Sismotettonica Tridimensionale, CRUST-UR Ferrara, Italy

Following the method and the working flow proposed by Maggini et al. (2023) for reconstructing the 3D thermo-rheological modelling of the broader Aegean Region, the present note is focused on the rheological characteristics in correspondence of the Wadati-Benioff zone of the Hellenic subduction. The geometry of the interface has been reconstructed based on the results of Bocchini et al. (2018) and Halpaap et al. (2018). Figure 1a shows the isobaths, while Figure 1b the slope distribution.

The rheological model of Maggini et al. (2023) is based on a simplified approach, assuming frictional sliding and power-law creep as dominating deformational mechanisms for describing the brittle and the ductile behaviour, respectively. Calculations have been performed by means of several purposedly written MATLAB scripts (Maggini, 2020; Maggini and Caputo, 2020a, 2020b, 2021) allowing to calculate and reproduce the thermo-rheological features. In order to obtain a 3D cover for the whole investigated area, a number of 1D vertical logs were reconstructed in correspondence of the nodes of a horizontal regular grid (115 x 115 pixels) and were than interpolated to reconstruct a pseudo 3D model. Using common GIS tools, all the input parameters considered in the modelling (see Maggini et al., 2023 for details) were properly averaged at the selected pixel size of 10 x 10 km.

Based on the general results and for the purpose of the present note, we investigated a 500 m-thick volume on either side of the modelled slab interface (Figure 1a) conceptually corresponding to the core of the Wadati-Benioff zone separating the two plates. In particular, we implemented a dedicated MATLAB script to analyse the rheological behaviour of the lowermost portion of the upper plate and the uppermost one of the lower plate. Although, four different combinations between brittle versus ductile and upper versus lower plate could in principle occur, the results show that three conditions dominate the whole subduction zone, each uniformly and regularly covering wide sectors of the interface zone.

Figure 1c clearly shows that the most external and shallower zone (blue in Figure 1c), grossly at the base of the active accretionary wedge, is characterised by a brittle behaviour in both sides of the interface. In a progressively deeper sector, the model results indicate the contact between brittle rocks in the upper plate with ductile ones in the lower plate (purple zone in Figure 1c). Further deeper along the Wadati-Benioff zone, the modelled behaviour is ductile on either side (pink area in Figure 1c). Taking into account the resolution of the rheological model (10 x 10 km), only in a

very limited sector (in correspondence of Akarnania and Peloponnesus) the results indicate the contact between ductile rocks overlying brittle ones (yellow in Figure 1c).

Comparing the rheological results with the geometry characteristics of the interface, it is possible observe some peculiarity. For example, the transition from the brittle/brittle to the brittle/ductile behaviour occurs at the depth range between 20 and 25 km (Figure 1a), in a narrow sector where the slope progressively varies from less than 15°, characterizing the upper- and frontal-most portion of the slab, to more than 18°, therefore in correspondence of a dip-angle change along the interface. On the other hand, the deepest sector characterized by brittle rocks overlying the interface occur at 90-100 km in correspondence of a slope increase from less than 35° to more than 40°.

As a very preliminary conclusion of the rheological model, brittle and hence potentially seismogenic activity in correspondence of the Wadati-Benioff zone could occur only down to a depth of ca. 100 km as far as at greater depths the 1 km-thick modelled rock volume embedding the interpolates shear zone is entirely characterized by a ductile behaviour. Accordingly, though rarely recorded deeper seismicity should likely occur due to internal deformation of the subducting slab and not on the interface. This is in accordance with Halpaap et al. (2018); these authors, where the Wadati-Benioff zone was well-imaged, identified earthquake clusters standing out the intraslab seismicity between 40 km and 60 km depth. Also, in Bocchini et al. (2018) the interplate seismicity is imaged at depth shallower than 100 km, while in Meier et al. (2008) the relocated interplate seismicity, plotted on reconstructed profile across the Aegean, generally don't exceed 60 km depth, only few events are located between 80 km and 100 km.

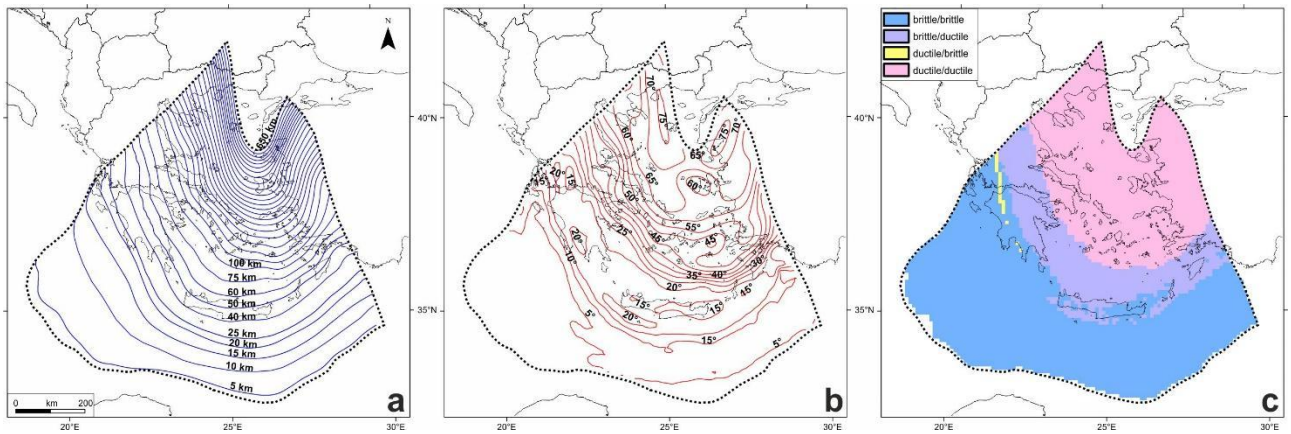

Figure 5: a) modelled Hellenic Subduction Zone (modified from Maggini et al., 2023 and references therein) with isobaths; b) slope distribution of the modelled Hellenic Slab; c) rheological behaviour in correspondence of the HSZ.

References

Bocchini G.M., Brustle A., Becker D., Meier T., van Keken P.E., Ruscic M., Papadopoulos G.A., Rische M. and Friederich W.; 2018: Tearing, segmentation, and backstepping of subduction in the Aegean: New insights from seismicity. *Tectonophysics*, 734-735, 96-118, doi: 10.1016/j.tecto.2018.04.002.

Halpaap F., Rondenay S. and Ottemoller L.; 2018: Seismicity, Deformation, and Metamorphism in the Western Hellenic Subduction Zone: New Constraints from Tomography. *J. Geophys. Res.: Solid Earth*, 123, 3000-3026, doi: 10.1002/2017JB015154.

Maggini M. and Caputo R.; 2020a: Sensitivity analysis for crustal rheological profiles: examples from the Aegean Region. *Ann. Geophys*., 63(3), SE334, doi: 10.4401/ag-8244.

Maggini M. and Caputo R.; 2020b: Rheological behaviour in collisional and subducting settings: inferences for the seismotectonics of the Hellenic Region. *Turk. J. Earth Sci.*, 29, 381–405, doi: 10.3906/yer-1909-4.

Maggini M. and Caputo R.; 2021: Seismological data *versus* rheological modelling: comparisons across the Aegean Region for improving the seismic hazard assessment. *J. Struct. Geol.*, 145, 104312, doi: 10.1016/j.jsg.2021.104312.

Maggini M., Russo D. and Caputo R.; 2023: A 3D rheological model for the Aegean Region: Mechanical layering and seismotectonic implications. *J. Struct. Geol.*, 175, 104956, 1-19, doi: 10.1016/j.jsg.2023.104956.

Meier T., Rische M., Endrun B., Vafidis A. and Harjes H.-P.; 2004: Seismicity of the Hellenic subduction zone in the area of western and central Crete observed by temporary local seismic networks. *Tectonophysics*, 383, 149 – 169, doi: 10.1016/j.tecto.2004.02.004.

Corresponding author: davide.russo@unife.it

Tracking the evolution of seismic sequences in the normal fault environment of Southern Apennines using deep catalogues

F. Scotto di Uccio[1], M. Michele[2], C. Strumia[1], G. Festa[1], M. Supino[2], L. Chiaraluce[2], N. D'Agostino[2], G. C. Beroza[3]

[1]Department of Physics 'Ettore Pancini', University of Napoli Federico II, Italy.
[2]Istituto Nazionale di Geofisica e Vulcanologia, Italy.
[3]Department of Geophysics, Stanford University, USA.

Seismic sequences, featuring events clustered in space and time and generating seismicity with a higher rate than the background, are a powerful tool for investigating the geometry and the mechanical state of faults that may host large magnitude earthquakes in the future. The knowledge about the involved structures and processes achievable from the analysis of the sequences strongly depends on the content and the magnitude of completeness of available catalogues. Enhanced catalogues obtained using advanced techniques, such as machine learning models or similarity-based detectors have contributed to decrease the magnitude of completeness of one point or more, increasing the number of events buried in the noise of more than one order of magnitude, with respect to manual earthquake identification. Furthermore, accurate location and source parameter estimation can provide direct access to mechanical properties of the structures hosting sequences. Earthquake location for deep catalogues can provide a high-resolution imaging of fault structures and their mutual interaction (e.g., Ross et al. 2019, Sugan et al. 2023) and define paths for fluid migration (Vuan et al. 2020), while evolutive models can be constructed accessing to the source parameters (Yoon et al., 2017).

In this study, we generated high resolution catalogues for seismic sequences in the complex normal fault system of Southern Apennines (Italy) by comparing and integrating advanced state of the art detectors (deep learning models and similarity-based detectors, Yoon et al. 2015, Chamberlain et al. 2018, Mousavi et al. 2020). We found that the integration of the machine learning and template matching detectors, the former providing templates for the cross-correlation, largely outperforms techniques based on autocorrelation and machine learning alone, featuring an enrichment of the existing automatic and manual catalogues of factors 21 and 7, respectively (Scotto di Uccio et al., 2023). Using deep catalogues of microseismic sequences, we performed accurate double-difference location, source parameter estimation and stress release modelling, that allows for addressing the spatiotemporal evolution and generation of the sequences. Relocated seismicity clearly identifies local patches on kilometric-scale structures, featuring an orientation coherent with the main faults of the area. When mapping the seismic sequences at depth, their location is generally not compatible with the faults that hosted the 1980, M 6.9 Irpinia event, looking at the fault traces on the Earth surface (Westaway & Jackson 1987), the event dip and the estimated geometry from inversion of seismic and levelling data (Bernard and Zollo, 1989). This indicates that seismic sequences ruptured small patches of secondary segments. When mapping the stress change on the fault plane, the inter-event distance compared to the size of the events suggests that the dominant triggering mechanism within the sequences is the (static) stress transfer, that allows the nucleation of individual events. The distribution of the events is not isotropic around the main events of the sequences, but small events tend to align dominantly along the dip direction, which also corresponds to the slip direction for normal faults. They can be interpreted as the boundary between locked and creeping domains (Rubin et al. 1999, Rubinstein and Beroza, 2007). The occurrence of an aseismic event appears to be more likely in the case of the 3-7 July 2020 Rocca San Felice sequence featuring the activation of two parallel clusters oriented along the dip direction but distant 5 km from each other. Although evident aseismic transients were not detected during the sequence, we evaluated the maximum average slip allowed on a deep dislocation whose displacement on the surface does not emerge within uncertainties from the noise level. We inferred that an aseismic event of Mw ~5.0 could have occurred during the sequence, transferring stress across the two asperities without producing a signal emerging at the GPS stations at the surface

References

Bernard, P., & Zollo, A. (1989). The Irpinia (Italy) 1980 earthquake: detailed analysis of a complex normal faulting. Journal of Geophysical Research: Solid Earth, 94(B2), 1631-1647.

Chamberlain, C. J., Hopp, C. J., Boese, C. M., Warren-Smith, E., Chambers, D., Chu, S. X., Kostantinos, M. & Townend, J. (2018). EQcorrscan: Repeating and near-repeating earthquake detection and analysis in Python. Seismological Research Letters, 89(1), 173-181.

Gualandi, A., Nichele, C., Serpelloni, E., Chiaraluce, L., Anderlini, L., Latorre, D., Belardinelli, M.E. & Avouac, J. P. (2017). Aseismic deformation associated with an earthquake swarm in the northern Apennines (Italy). Geophysical Research Letters, 44(15), 7706-7714.

Kaviris, G., Elias, P., Kapetanidis, V., Serpetsidaki, A., Karakonstantis, A., Plicka, V., ... & Bernard, P. (2021). The western Gulf of Corinth (Greece) 2020–2021 seismic crisis and cascading events: First results from the Corinth Rift Laboratory Network. The Seismic Record, 1(2), 85-95.

Mousavi, S. M., Ellsworth, W. L., Zhu, W., Chuang, L. Y., & Beroza, G. C. (2020). Earthquake transformer—an attentive deep-learning model for simultaneous earthquake detection and phase picking. Nature communications, 11(1), 3952.

Ross, Z. E., Trugman, D. T., Hauksson, E., & Shearer, P. M. (2019). Searching for hidden earthquakes in Southern California. Science, 364(6442), 767-771.

Rubin, A. M., Gillard, D., & Got, J. L. (1999). Streaks of microearthquakes along creeping faults. Nature, 400(6745), 635-641.

Rubinstein, J. L., & Beroza, G. C. (2007). Full waveform earthquake location: Application to seismic streaks on the Calaveras fault, California. Journal of Geophysical Research: Solid Earth, 112(B5).

Scotto di Uccio, F., Scala, A., Festa, G., Picozzi, M., & Beroza, G. C. (2023). Comparing and integrating artificial intelligence and similarity search detection techniques: application to seismic sequences in Southern Italy. Geophysical Journal International, 233(2), 861-874.

Sugan, M., Campanella, S., Chiaraluce, L., Michele, M., & Vuan, A. (2023). The unlocking process leading to the 2016 Central Italy seismic sequence. Geophysical Research Letters, 50(5), e2022GL101838.

Vuan, A., Brondi, P., Sugan, M., Chiaraluce, L., Di Stefano, R., & Michele, M. (2020). Intermittent slip along the Alto Tiberina low-angle normal fault in central Italy. Geophysical Research Letters, 47(17), e2020GL089039.

Westaway, R., & Jackson, J. (1987). The earthquake of 1980 November 23 in Campania—Basilicata (southern Italy). Geophysical Journal International, 90(2), 375-443.

Yoon, C. E., O'Reilly, O., Bergen, K. J., & Beroza, G. C. (2015). Earthquake detection through computationally efficient similarity search. Science advances, 1(11), e1501057.

Yoon, C. E., Huang, Y., Ellsworth, W. L., & Beroza, G. C. (2017). Seismicity during the initial stages of the Guy-Greenbrier, Arkansas, earthquake sequence. Journal of Geophysical Research: Solid Earth, 122(11), 9253-9274.

Corresponding author: francesco.scottodiuccio@unina.it

A preliminary computation of the seismic coupling for Italy

F. Sparacino[1], B. G. Galuzzi[2], M. Palano[1]

1 - Istituto Nazionale di Geofisica e Vulcanologia, Osservatorio Etneo - Sezione di Catania, Catania, Italy.
2 - Istituto di Bioimmagini e fisiologia molecolare, CNR, Milano, Italy.

In the last two decades, the worldwide growth of continuous and episodic GNSS stations as well as the seismic networks allowed the acquisition of extensive geodetic and seismological datasets. This aspect has recently allowed the possibility of comparing geodetic and seismic strain-rates at the scale of regional fault systems. Studies focusing on this topic have provided new insights on the partitioning between fault slip and bulk lithosphere permanent strain (Ferranti et al., 2014; Carafa et al., 2017, 2020). The basic idea is that, for a given region, the moment released by earthquakes mirrors the rate of tectonic deformation (Kostrov, 1974). Achieved results have allowed to identify regions where the crustal deformation budget is entirely released by seismicity (e.g. Mazzotti et al., 2011; Pancha et al., 2006; D'Agostino, 2014; Sparacino et al., 2020), as well as regions where the excess deformation can be released either as aseismic slip across faults or through large future earthquakes (Masson et al., 2005; Palano et al., 2018, 2020, Déprez, et al., 2013; Sparacino et al., 2022).

Here we provided a preliminary computation for Italy by adopting the seismogenic zonation of Meletti et al. (2004). To this aim, we compiled catalogs for both historical (since 1005) and instrumental crustal seismicity occurring in the investigated area (since 1985; http://iside.rm.ingv.it/). These catalogs have been used to estimate the seismic moment-rates along with the expected maximum magnitude, the seismogenic thickness, and the Gutenberg-Richter parameters. In addition, based on an updated GNSS velocity field we derived the geodetic moment-rates.

References

Carafa M.M., Valensise G. and Bird P.; 2017: Assessing the seismic coupling of shallow continental faults and its impact on seismic hazard estimates: a case-study from Italy. Geophys. J. Int., 209(1), 32-47, DOI 10.1093/gji/ggx002.

Carafa M.M., Galvani A., Di Naccio D., Kastelic V., Di Lorenzo C., Miccolis S., Sepe V., Pietrantonio G., Gizzi C., Massucci A., Valensise G. and Bird P.; 2020: Partitioning the ongoing extension of the central Apennines (Italy): Fault slip rates and bulk deformation rates from geodetic and stress data. J. Geophys. Res.: Solid Earth, 125(7), e2019JB018956, DOI 10.1029/2019JB018956.

D'Agostino N.; 2014: Complete seismic release of tectonic strain and earthquake recurrence in the Apennines (Italy). Geophys. Res. Lett., 41(4), 1155-1162, DOI 10.1002/2014GL059230.

Déprez A., Doubre C., Masson F. and Ulrich P.; 2013: Seismic and aseismic deformation along the East African Rift System from a reanalysis of the GPS velocity field of Africa. Geophys. J. Int., 193, 1353-1369, DOI 10.1093/gji/ggt085.

Ferranti L., Palano M., Cannavò F., Mazzella M.E., Oldow J.S., Gueguen E., Mattia M. and Monaco C.; 2014: Rates of geodetic deformation across active faults in southern Italy. Tectonophysics, 621, 101-122, DOI 10.1016/j.tecto.2014.02.007.

ISIDe Working Group 2007: Italian Seismological Instrumental and Parametric Database (ISIDe). Istituto Nazionale di Geofisica e Vulcanologia (INGV). Available online: DOI 10.13127/ISIDE (accessed on 18 December 2023).

Kostrov V.; 1974: Seismic moment and energy of earthquakes, and seismic Row of rock. Izv. Acad. Sci. USSR Phys. Solid Earth, 1, 23-44.

Masson F., Chéry J., Hatzfeld D., Martinod J., Vernant P., Tavakoli F. and Ghafory-Ashtiani M.; 2005: Seismic versus aseismic deformation in Iran inferred from earthquakes and geodetic data. Geophys. J. Int., 160, 217-226, DOI 10.1111/j.1365-246X.2004.02465.x.

Mazzotti S., Leonard L.J., Cassidy J.F., Rogers G.C. and Halchuk S.; 2011: Seismic hazard in western Canada from GPS strain rates versus earthquake catalog. J. Geophys. Res., 116, B12310, DOI 10.1029/2011JB008213.

Meletti C., Galadini F., Valensise G., Stucchi M., Basili R., Barba S., Vannucci G. and Boschi E.; 2004: Zonazione sismogenetica ZS9 [Data set]. Istituto Nazionale di Geofisica e Vulcanologia (INGV), DOI 10.13127/sh/zs9.

Pancha A., Anderson J. G. and Kreemer C.; 2006: Comparison of seismic and geodetic scalar moment rates across the Basin and Range Province. Bull. Seismol. Soc. Am., 96, 11-32, DOI 10.1785/0120040166.

Palano M., Imprescia P., Agnon A. and Gresta S.; 2018: An improved evaluation of the seismic/geodetic deformation-rate ratio for the Zagros Fold-and-Thrust collisional belt. Geophys. J. Int., 213, 194-209, DOI 10.1093/gji/ggx524.

Palano M., Ursino A., Spampinato S., Sparacino F., Polonia A. and Gasperini L.; 2020: Crustal deformation, active tectonics and seismic potential in the Sicily Channel (Central Mediterranean), along the Nubia-Eurasia plate boundary. Scientific Reports, 10, 21238, DOI 10.1038/s41598-020-78063-1.

Sparacino F., Palano M., Peláez J.A. and Fernández J.; 2020: Geodetic deformation versus seismic crustal moment-rates: insights from the Ibero-Maghrebian region. Remote Sensing, 12(6), 952, DOI 10.3390/rs12060952.

Sparacino F., Galuzzi B.G., Palano M., Segou M. and Chiarabba C.; 2022: Seismic coupling for the Aegean-Anatolian region. Earth-Science Reviews, 228, 103993, DOI 10.1016/j.earscirev.2022.103993.

Corresponding author: federica.sparacino@ingv.it

Analysis of the 1982-2016 seismicity of Aswan region (south Egypt)

T.A. Stabile[1], E.R. Fat-Helbary[2], V. Serlenga[1], S. Panebianco[1,3], P. Tizzani[4], R. Castaldo[4], L. Telesca[1], E.M. El-Amin[2], H. Ahmed[2]

[1] *Consiglio Nazionale delle Ricerche (CNR-IMAA), Italy*
[2] *National Research Institute of Astronomy and Geophysics, Egypt*
[3] *Dipartimento di Fisica e Scienze della Terra, Università di Ferrara, Italy*
[4] *Consiglio Nazionale delle Ricerche (CNR-IREA), Italy*

Lake Nasser is the Egypt's largest artificial water reservoir filled behind the Aswan High Dam. In this area a prolonged reservoir induced seismicity has been observed since the November 1981 Ms 5.3 earthquake. The dynamic interplay between loading and unloading operations at Lake Nasser, coupled with the increase of pore fluid pressure within the crustal rocks may lead the faults to go beyond the critical stress for failure (Gahalaut and Hassoup, 2012; Telesca et al., 2017). In response to the seismic concerns and the need for secure reservoir management, a permanent seismic network was established in 1982. This initiative has contributed significantly to the accumulation of an extensive seismological dataset.

From an initial catalogue encompassing 7833 natural and reservoir-induced seismic events recorded in the Aswan region from 1982 to 2016, our objective is to gain insights into the structure and triggering mechanisms of seismogenic faults within this complex tectonic system. To achieve this goal, we obtained a new 1-D velocity model of the area. Then, absolute and relative high-resolution earthquake locations for 2562 events have been determined. This process has enabled us to refine the fault structure in the Aswan region and better comprehend the spatio-temporal evolution of seismicity.

Our analysis revealed previously unmapped fault strands along the Kalabsha fault system and in the Wadi Kalabsha embayment area, enhancing the understanding of fault distribution beyond the original seismic catalogue. The spatio-temporal evolution indicated an eastward migration of seismicity with progressively shallower hypocentres, potentially linked to fluid migration processes and increased pore pressure in the Wadi Kalabsha embayment area. The combination of fluid pore-pressure diffusion and Coulomb stress variation from reservoir loading may also explain the variable faulting styles observed along an NW-SE striking alignment east of the Seyal Fault. We verified such hypothesis through a 3-D poroelastic simulation within a Finite Element (FE) framework. Specifically, we addressed both the time-dependent poroelastic equation and the linear elastic equation, employing a multiphysics approach through the use of the Comsol software package version 6.2.

Furthermore, the projection of earthquakes onto an E-W cross-section identified a seismic gap on the Kalabsha Fault, suggesting a locked fault patch approximately 11 km in length. According to Wells and Coppersmith (1994), such a segment could potentially trigger an earthquake with a magnitude up to Mw=5.9 in the event of a single rupture. Additionally, an earthquake clustering analysis revealed two clusters with prolonged swarm activity, driven by pore pressure diffusion, and four clusters characterized by seismic sequences and repeated earthquakes.

References

Gahalaut K. and Hassoup, A.; 2012: Role of fluids in the earthquake occurrence around Aswan reservoir, Egypt. J. Geophys. Res. 117, B02303.

Telesca L. et al.; 2017: Dynamical characterization of the 1982—2015 seismicity of Aswan region (Egypt). Tectonophysics 712-713, 132—144.

Wells D.L. and Coppersmith K.J.; 1994: New empirical relationships among magnitude, rupture length, rupture width, rupture area, and surface displacement. Bull. Seismol. Soc. Am. 84 (4), 974-1002.

Corresponding author: tonyalfredo.stabile@cnr.it

Synthesis of written, architecture, and geology information sources improving the understanding of seismic sequences in the Ferrara area

M. Stefani[1]

[1] *Università di Ferrara (Italy)*

This contribution is aimed at delving deeper into the impact of historic seismic events on the town of Ferrara and surrounding areas. The paper is based on the integration of the published palaeosismological research with the reconstruction of the architectural history of ancient buildings, and with the results of recent geological and microzonation investigations. The short article is not intended to provide a comprehensive seismological history, but to the interpretations of some significant seismic sequences, often characterized by the migration of the epicentre areas. Given the nature and size of the contribution, provide an exhaustive list of references and historic sources is impossible. The reader is therefore referred to the important contributions of Guidoboni 1984, Locati et al. 2016, Guidoboni et al. 2018 and 2019; Guidoboni and Valensise 2023, and to further references and quotations therein.

12th and 13th centuries earthquakes and the structural reconfiguration of the Cathedral.

The earliest known seismic effects are the local repercussion of the widespread earthquakes of 1117, and an event in 1128. A sequence of shocks occurred during the 1222 Christmas Day, between noon and sunset, within a seismic activity framework affecting large portions of the Po Plain, known as “the Brescia earthquake”. In Ferrara, the shocks induced at least the collapse of chimneys, while more severe damage cannot be ruled out. Another earthquake hit Ferrara on March the 20th 1234, associated with damage to buildings, in town and in the surrounding countryside, evaluated to the VII MCS, but the scantiness of the available documentation again prevents a precise estimation of the damage level. The earthquakes of the first half to the 13th century, together with the poor geotechnical properties of the foundation soils played a major, but previously undetected, role in the architecture evolution of the Cathedral. The building of the Romanesque five-nave church started in 1135 and continued through much of the century. The building was founded on Holocene, mainly cohesive sediments, deposited into interfluvial plain settings, the geotechnical properties of which were investigated through seismic cone penetration and dilatometer tests. The spatially varying load of the building induced differential foundation settlement, which, together with the seismic accelerations, damaged the thin wall structure of the

naves, triforium and clerestory. The analysis of the surviving Medieval structures and of the ancient written and drawn documentation supports a reconstruction of the building evolution. In the second quarter of the 13th century, probably between 1240 and 1250, the Cathedral underwent major structural changes, recording some of the earliest influences of the French Gothic in Italy. The damaged structures of the naves were repaired and reinforced through the building of flying buttresses (Fig. 1A) that conveyed downward the lateral forces pushing aside the nave walls, while the early overhanging façade was supported by two attached buttresses, on both sides of the porch, boasting the Last Judgment sculpture cycle, which is coaeval to the structural modification phase. The 13th century structural reinforcement was to play a major beneficial role during the numerous following seismic events.

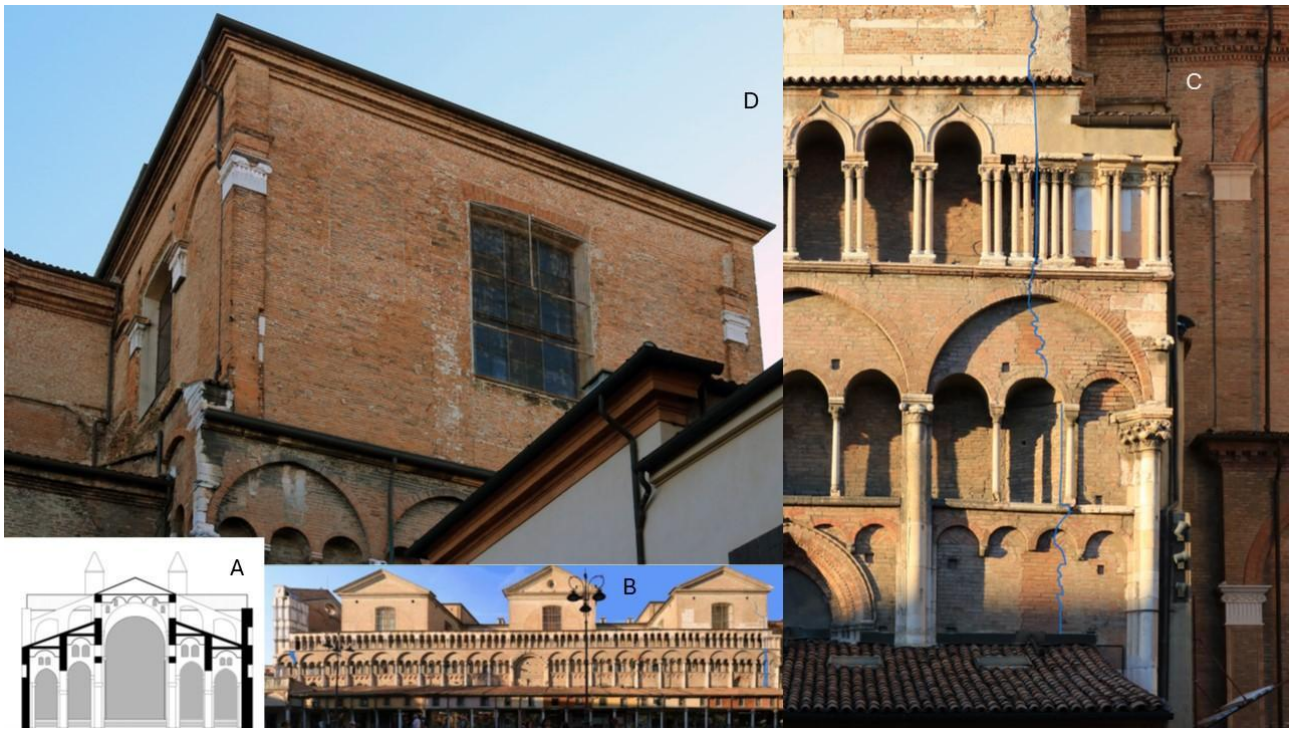

Fig. 1 – **A** reconstructive cross section of the Ferrara Cathedral after the 13th century post-seismic restoration (drawing by A. Toma and V. Vona), **B** southern side of the Cathedral, with the main structural lesions induced by foundation settlement and seismic acceleration depicted in blue, **C** the south-eastern corner, with post-seismic collapse transept reconstruction in a backword position and "wall sewing up restoration" by reddish bricks, **D** the Renaissance transect rebuilt at the end of the 15th century and partially collapsed during the earthquake of 17 Novembre 1570.

Late medieval earthquakes.

Other earthquakes hit the town in 1285, 1339, and 1346. Near the half of the 14th century, likely during the 1346 earthquake, the belltower and roof of the San Nicolò Church and many noble family towers collapsed. At the time, churches were damaged, repaired or rebuilt, as S. Francesco and S. Domenico, but the following transformation makes the damage recognition presently impossible. In the early 15th century, an earthquake sequence affected the town over a 17-month interval, associated with repeated damages in the VII grade MCS range. The sequence started at 9

a.m. August 14th, 1409, with an earthquake epicentre near the town, followed by a stronger shock in the night between the 16th and 17th. Another earthquake is documented the 9th of May 1410, and the strongest of the sequence on the 9th of January 1411. Unspecified damage is reported to buildings; however, the following transformation prevents the present-day recognition of damage. Other earthquakes are known in 1445 and in 1483.

Fig. 2 – The hasty reconstruction of the ducal apartment over the Estense Castle southern barbican, using recycled bricks and limestone fragments, following the large collapse of November 17, 1570.

Early Modern Time earthquakes.

1495, on Sunday the 13th of December (Day of S. Lucia) an earthquake took place, certainly important, even if yet not mentioned in the seismic catalogues. At least a corner (*cantone*) of the cathedral collapsed, certainly in the eastern side, likely the Northeastern one. The upper part of the transept and the large new choir were then rebuilt in Renaissance forms by Biagio Rossetti (Fig. 1D). Post seismic restoration involved the twelfth steps leading from the naves to the raised presbytery area. The steps were previously incorrectly referred to the cathedral entrance. Severe damage and partial collapse also affected some portions of the Estense Castle and the towers of the Ducal Palace (Torre Rigobello) and of the Palazzo della Ragione (Torre Ribelli). The city then experienced the local effects of earthquakes generated in other areas (1505, 1511). In 1532, a seismic sequence, lasting at least 50 days, forced Alfonso I's court to take refuge into the Delizia del Barchetto, at the northeastern corner of the town walls; further seismic damage occurred in 1536. The 1561 earthquakes marked the onset of a long seismic phase that was to last until 1574. A seismic sequence (23.10-16.11.) was followed by a severely damaging earthquake (24.11) and by other shocks (13-14.12). Damage is reported to the Castello Estense, the North-East vaulted chapel

of the Cathedral (*Cappella del Santissimo Sacramento*), the synagogue (*Via dei Sabbioni* = Via Mazzini), and to the Belriguardo Palace, 14 km South-Est of the city. Less violent earthquakes followed in 1562, 1564. In 1569, seismic activity strongly affecting the western area of Pilastri and Bondeno, less so Ferrara.

The 1570-1574 Seismic Sequence and the repeated building damage and destruction.

After a sequence of gentle shocks (1-15.11.70), the city was struck by violent earthquakes on 16th, November and by even stronger shocks on the 17th. Several shocks were then perceived every and each day between the 17th of November and the 27th of February 1571, with possibly a single exception on 28th January. During several days of November, up to ten shock per day were perceived. Due to space limitations, an exhaustive list of damages is not here possible; therefore, attention is focused on some examples; further information is available in the aforementioned references. In the Cathedral, the façade increased its overhang and detached itself form the naves walls, as still partially visible, the south-eastern corner was also severely damaged (Fig. 1B, C). Portions of the transept collapses and its northern tympanum collapsed onto the opposite house, killing several people (17.11.70). In the churches of S. Francesco and S.M. in Vado, the upper portions of the façades and the nave vaults and domes collapsed (Fig. 3). The church of S. Giovanni Battista experienced an almost complete destruction, collapsing through several months of shocks, keeping some surviving walls only in the southern flank. In the Estense Castle, the ducal apartments built over the southern barbican *(rivellino*), internal cross vaults, the upper part of the four towers, and long portions of corbels collapsed (Fig. 2); the western wing was particularly damaged, losing vaults on all floors. Written sources do not clearly report major damage to the Diamanti Palace, which however at the time seems to have lost the porticoes previously built on all four sides of the courtyards. The palace certainly underwent a total reconstruction of the roof and major architecture modification and rebuilt, keeping the original configuration only in part of the lower order of the northern façade. In November 1570. coseismic liquefaction is documented in the granular sediments of the Medieval Po channel, founding the southernmost portion of the city. Liquefaction triggered lateral expansion toward the port basin and Po di Ferrara channel, induced the collapse of Castel Nuovo, and increased the damage to the 13th century fortification walls at the southern side of the city.

Fig. 3 – The upper portion of San Francesco, above the frame of the order, and the internal domes and circular windows rebuilt after the 1570 earthquakes. Italian quotation from Pirro Ligorio's writings, describing the collapse.

Distribution of the seismic sequence damage in time and space.

The reported damage induced by the 1570-1574 seismic sequence normally derived from the summation of the induvial shock effects, but specific damage events can be nevertheless detected. In Ferrara, damage and collapses occurred in the following dates: for the year 1570, 23.11 S. Domenico western façade, Castel Nuovo, portions of the city walls near Porta d'Amore; 3.12 almost complete collapse of S. Giovanni Battista; 13.12 city walls, 14-15.12 S. Andrea, S. Agostino, Palazzo Tassoni; 31.12 Lazzaretto in the Boschetto Island West of town, several churches and palaces; for the year 1571, 8.01. S. Andrea, 11.01 and 7.08 Cathedral, particularly in the transept; 12.01 Palazzo Montecuccoli, 25.08 portions of the new S.M. Angeli building under construction. Further damage took place during two 1574 earthquakes.

The clustering in space and time of the seismic damage and shock perception appears to suggest a migration of epicentres through different seismogenetic structures. Two earthquake cluster areas can be detected on the opposite sides of the city. When damage events in the two countryside clusters can be precisely dated, they are not synchronous with those affecting the city or the opposite cluster area. Areas of severe damage are separated by less affected zones.

(a) Western areas: 24.11.70 at about 8 p.m., deaths and damage in Bondeno and Ficarolo; 1.12.70, 5.03.71, 30.04, strong shocks in Bondeno, Palantone, Stellata and, North to the Po river, Ficarolo and Vico; 4.06, violent shocks inducing building damage in Parma, perceived as strong in Finale Emilia, S. Felice sul Panaro, and Stellata, as light in Ferrara. The destruction of the Castelmassa

church, and the damage to the Melara one, in the western portion of the modern Rovigo Province, respectively 34 and 42 km from the Ferrara epicentre, are noteworthy, considering that many building closer to town experienced only minor damage, as in Ravalle (VI MCS).

(b) South-Eastern Areas: 21-24.11.70 anomalous waves in the Po di Primaro channel; 5.12., 9.12, severe damage in the Belriguardo Palace, particularly in the entrance clock tower and in structures already damaged by the 1561 earthquake; 8.12 shock particularly strong in Montesanto; 14-15.12 the shocks damaging Ferrara were well perceived in S. Pietro in Casale, Bologna and Castelbolognese; 26.12. shocks in Belriguardo and Massa Lombarda, perceived as very light in Ferrara; 2.01.71 damage in Berliguardo and Runco, collapse of canal banks, and possible coseismic liquefaction; 3.01 strong shock perceived in Lugo, Imola, and Faenza; 23.12.71 new structural damage in Berliguardo. In the later area, during the seismic sequence, granular sediments deposited into the main Roman Time channel of the Po (*Eridanus*) were affected by important coseismic liquefaction, possibly associated with the outflowing of salty waters. Damage to churches in the cannot be normally dated with precision, but its areal distribution in the region south-east of Ferrara, is significant. Damage was severe (VII-VIII MCS) in sites surrounding the Belriguardo area, as in the churches of Cona, Masi Torello, Gaibanella, Runco, Gambulaga, S. Nicolò, Santa Maria Codifiume, but it was comparatively reduced in sites closer to the Ferrara epicentre, like Aguscello (3 Km from it), Focomorto, and Francolino.

Conclusions.

The architecture history of all major building in the Ferrara and surrounding area has been severely affected by the intense seismic activity. This is still evident, for instance, in the Cathedral and Estense Castle. A detailed study of the architecture history and of the damage and reparation phases still visible in many buildings can significantly integrate the knowledge generated by written sources, as it is the case of Palazzo dei Diamanti. Documented coseismic liquefaction is confined into the Roman and Medieval fluvial channel and proximal levee sediments. The seismic activity of the area has been often characterized by long seismic sequences, like the 1561-1574 one, recording the epicentre migration, associated to the activation of different seismogenetic fault systems, reflecting the structural intricacy of the buried foredeep external portions of the Apennines Chain.

References

Guidoboni E.; 1984: *Riti di calamità: terremoti a Ferrara nel 1570-74*, Quaderni Storici 55/ a. XIX, n. 1.

Guidoboni E., Valensise G.; 2023: *L'Italia dei Terremoti, l'Azzardo Sismico delle Città*. *Vol. 2, Centro-Nord*. Fondazione CNI, 668 pp.

Guidoboni E., Ferrari G., Mariotti D., Comastri A., Tarabusi G., Sgattoni G., Valensise G.; 2018: *CFTI5Med, Catalogo dei Forti Terremoti in Italia (461 a.C.-1997) e nell'area Mediterranea (760 a.C.-1500).* Istituto Nazionale di Geofisica e Vulcanologia (INGV).

Guidoboni E., Ferrari G., Tarabusi G., Sgattoni G., Comastri A., Mariotti D., Ciuccarelli C., Bianchi M.G., Valensise G.; 2019: *CFTI5Med, the new release of the catalogue of strong earthquakes in Italy and in the Mediterranean area.* Scientific Data 6, Article Number: 80 (2019).

Locati M., Camassi R., Rovida A., Ercolani E., Bernardini F., Castelli V., Caracciolo C.H., Tertulliani A., Rossi A., Azzaro R., D'amico S., Conte S., Rocchetti E.; 2016: *DBMI15, the 2015 version of the Italian Macroseismic Database*. Istituto Nazionale di Geofisica e Vulcanologia (INGV).

Corresponding author: marco.stefani@unife.it

A novel approach to earthquake source characterization using DAS strain rate data acquired along optical fibres

C. Strumia[1], A. Trabattoni[2], M. Supino[3], M. Baillet[2], D. Rivet[2], G. Festa[1]

[1]Università di Napoli Federico II, Physics Department, Complesso Monte S. Angelo, Napoli, Italy.
[2]Université Côte d'Azur, Observatoire de la Côte d'Azur, CNRS, IRD, Géoazur.
[3]Istituto Nazionale di Geofisica e Vulcanologia, Osservatorio Nazionale Terremoti, Roma, Italy.

In recent years Distributed Acoustic Sensing (DAS) is establishing as a powerful tool in seismology, allowing for continuous recordings of earthquakes, with unprecedented spatial sampling. DAS systems are interrogators connected to one end of an optical fibre cable, sending repeated laser pulses, and exploiting measurements of phase variations of the backscattered light with time to infer measurements of the strain rate along the direction of the fibre (Hartog, 2017). The cable, interrogated by the DAS system, behaves as an almost continuous array of single component seismic sensors.

The availability of existing cables deployed for telecommunication purposes and the simplicity of DAS installation opens up the possibility of investigating harsh environments, where deployments of standard instruments could be expensive or unpractical, such as glaciers, remote areas, sea bottoms, volcanic flanks, or geothermal sites (e.g., Walter et al., 2020; Hudson et al.; 2021, Sladen et al., 2019; Currenti et al., 2021; Tsuji et al., 2021). These cables can reach lengths up to hundreds of kilometers and can depict the long-range continuous, shallow propagation of seismic waves when interrogated through DAS. The high potential of these systems has been nowadays exploited in several seismological tasks, from earthquake location (Piana Agostinetti et al., 2022), subsurface characterization (Ajo-Franklin et al., 2019), focal mechanism inversion (Li et al., 2023a), tomography (Biondi et al., 2023), and source back projection (Li et al., 2023b).

Among the several seismological duties, characterizing source parameters allows for interpretation of the rupture process and its effects on the ground motion through the determination of its seismic moment and size. Unlike applications where only time information is needed, consolidated methods based on spectral inversion for the determination of source parameters cannot be directly applied to DAS data, that natively provide strain rate instead of acceleration and/or velocity time series. Using DAS amplitudes for earthquake source characterization leads to two possible alternatives: either converting recordings to kinematic quantities to apply existing physical models (Lior et al., 2021; 2023), or developing a novel forward modelling that directly digests DAS data. Despite conversion techniques have been proposed and validated (Trabattoni et al., 2023), moving to kinematic quantities pollutes the spectral content of the data, especially at low

frequencies. For this reason, we focus here on the development of a new mathematical formulation able to describe the source time function contribution contained in the far field strain domain, leading to forward modelling of time integrated strain spectra and evaluation of source parameters.

We validated the technique on two case-studies, for earthquakes in magnitude range $0.4 - 4.3$, by comparing the results with estimates from standard seismic instruments. When analysing earthquakes recorded on an off-shore, $150km$ long cable during a 1-month DAS survey in Chile, results exhibit scale invariant stress drop distribution between seismic moment and corner frequency estimates, with an average of $\Delta\sigma = (0.8 \pm 0.6)MPa$. Moreover, moment magnitude estimations agree with results from local seismic stations. The second case study involves DAS data acquired on a short cable ($1km$) deployed in the Irpinia region in the Southern Apennines during a 5-month temporary experiment. Here data show a dominance of site effects resulting in an apparent corner frequency around $5Hz$, while the low frequency content of signals gives estimates of moment magnitude in agreement with seismic stations. Nevertheless, the modelling of local site effect through a parametric EGF approach allows to determine corner frequencies for the largest magnitude events in the catalogue.

Overall, results highlight the potential of DAS systems in characterizing the seismic ruptures over different space scales, exploiting the redundancy of information available from the very-high spatial resolution of recordings.

References

Ajo-Franklin, J. B., Dou, S., Lindsey, N. J., Monga, I., Tracy, C., Robertson, M., Rodriguez Tribaldos, V., Ulrich, C., Freifeld, B., Daley, T., & Li, X; 2019: Distributed Acoustic Sensing Using Dark Fiber for Near-Surface Characterization and Broadband Seismic Event Detection. *Scientific Reports*, *9*(1). https://doi.org/10.1038/s41598-018-36675-8

Biondi, E., Zhu, W., Li, J., Williams, E.F., Zhan, Z.; 2023: An upper-crust lid over the Long Valley magma chamber. *Science Advances* https://doi.org/10.1126/sciadv.adi9878

Currenti, G., Jousset, P., Napoli, R., Krawczyk, C., & Weber, M.; 2021: On the comparison of strain measurements from fibre optics with a dense seismometer array at Etna volcano (Italy). *Solid Earth*, *12*(4), 993–1003. https://doi.org/10.5194/se-12-993-2021

Hartog, H.A.; 2017: An introduction to distributed optical fibre sensors (A. H. Hartog, Ed.). CRC Press.

Hudson, T. S., Baird, A. F., Kendall, J. M., Kufner, S. K., Brisbourne, A. M., Smith, A. M., et al.; 2021: Distributed Acoustic Sensing (DAS) for natural microseismicity studies: A case study from Antarctica. Journal of Geophysical Research: Solid Earth, 126, e2020JB021493. https://doi.org/10.1029/2020JB021493

Li, J., Zhu, W., Biondi, E., & Zhan, Z.; 2023a: Earthquake focal mechanisms with distributed acoustic sensing. *Nature Communications*, *14*(1), 4181. https://doi.org/10.1038/s41467-023-39639-3

Li, J., Kim, T., Lapusta, N. *et al.* The break of earthquake asperities imaged by distributed acoustic sensing. *Nature* 620, 800–806; 2023: https://doi.org/10.1038/s41586-023-06227-w

Lior, I., Rivet, D., Ampuero, J. P., Sladen, A., Barrientos, S., Sánchez-Olavarría, R., Villarroel Opazo, G. A., & Bustamante Prado, J. A.; 2023: Magnitude estimation and ground motion prediction to harness fiber optic distributed acoustic sensing for earthquake early warning. *Scientific Reports*, *13*(1). https://doi.org/10.1038/s41598-023-27444-3

Lior, I., Sladen, A., Mercerat, D., Ampuero, J. P., Rivet, D., & Sambolian, S.; 2021: Strain to ground motion conversion of distributed acoustic sensing data for earthquake magnitude and stress drop determination. *Solid Earth*, *12*(6), 1421–1442. https://doi.org/10.5194/se-12-1421-2021

Piana Agostinetti, N., Villa, A., & Saccorotti, G.; 2022: Distributed acoustic sensing as a tool for subsurface mapping and seismic event monitoring: A proof of concept. *Solid Earth*, *13*(2), 449–468. https://doi.org/10.5194/se-13-449-2022

Sladen, A., Rivet, D., Ampuero, J. P., De Barros, L., Hello, Y., Calbris, G., & Lamare, P.; 2019: Distributed sensing of earthquakes and ocean-solid Earth interactions on seafloor telecom cables. *Nature Communications*, *10*(1). https://doi.org/10.1038/s41467-019-13793-z

Trabattoni, A., Biagioli, F., Strumia, C., Van Den Ende, M., Scotto Di Uccio, F., Festa, G., Rivet, D., Sladen, A., Ampuero, J. P., Métaxian, J.-P., & Stutzmann, É.; 2023: From strain to displacement: using deformation to enhance distributed acoustic sensing applications, Geophysical Journal International, 235(3), 2372–2384. https://doi.org/10.1093/gji/ggad365

Tsuji, T., Ikeda, T., Matsuura, R., Mukumoto, K., Hutapea, F. L., Kimura, T., Yamaoka, K., & Shinohara, M.; 2021: Continuous monitoring system for safe managements of CO2 storage and geothermal reservoirs. *Scientific Reports*, *11*(1). https://doi.org/10.1038/s41598-021-97881-5

Walter, F., Gräff, D., Lindner, F, Paitz, P., Köpfli, M., Chmiel, M., Fichtner, A.; 2020: Distributed acoustic sensing of microseismic sources and wave propagation in glaciated terrain. *Nature Communications* 11, 2436 https://doi.org/10.1038/s41467-020-15824-6

Corresponding author: claudio.strumia@unina.it

Comparing Machine Learning to Manual Earthquake Location procedures: evaluating the performance of LOC-FLOW on a microseismic sequence occurred in Collalto area (NE Italy)

M. Sugan[1], L. Peruzza[1], M.A. Romano[1], M. Guidarelli[1], L. Moratto[1], D. Sandron[1], M.P. Plasencia Linares[1], M. Romanelli[1]

[1] National Institute of Oceanography and Applied Geophysics - OGS, Italy

Detecting earthquakes and picking seismic phases are fundamental elements in numerous seismological processes, being crucial in both seismic monitoring and in-depth seismological investigations. The utilization of machine learning (ML) techniques has experienced a notable improvement lately, offering a promising way to face the complexities associated with earthquake detection and localization.

The reliability of ML methods remains an open question in settings with dense and localized seismic networks. In such contexts, fast and accurate detection and localization of earthquakes are essential for decision-making, playing a pivotal role in seismic risk mitigation strategies, even for events of very low magnitude.

In the field of microseismic monitoring, ML applications are similar to those of earthquake monitoring, but have the task of processing weak seismic signals characterized by low signal-to-noise ratios at individual receivers or very short target time signals (Anikiev et al., 2023). Therefore, evaluating the performance of ML models trained on regional datasets in a microseismic sequence is challenging but crucial, especially for applications in the field of induced seismicity (e.g., Mousavi et al., 2016) or for activities of observatories near faults.

This study focuses on evaluating the performance of the PhaseNet algorithm (Zhu and Beroza, 2018), a prominent deep learning model for earthquake phase identification. The evaluation is conducted within the extensive LOC-FLOW workflow for earthquake location proposed by Zhang et al. (2022). The study is performed on the seismic events of the Refrontolo sequence that occurred in August 2021 on an antithetic fault segment of the Montello thrust system in the Pedemontana district of Southeastern Alps (Peruzza et al., 2022).

The seismic sequence displayed remarkable activity despite its low energy release (M_L 2.5 for the main event). The sequence consisted of 374 events occurring at approximately 9 km depth within a confined volume, and was monitored by the permanent Collalto Seismic Network (RSC). This

sequence is a significant case study for testing and refining automated techniques to detect and locate microearthquakes using machine learning.

The RSC is composed of 10 stations and has monitored microseismic activity potentially induced by underground gas storage activities since 2012. Rigorous manual processing conducted by the RSC, involving daily and monthly offline procedures, is undertaken to guarantee data accuracy and metadata reliability. Nevertheless, this approach can be time consuming and demanding, particularly in densely populated seismic sequences where very fast analysis is preferable.

Comparing seismic catalogs derived from associations approved by experienced analysts and revised manual picks with those generated using the PhaseNet integrated with LOC-FLOW provides a unique opportunity to evaluate the performance of ML methods in detecting and localizing local microearthquakes. Our particular focus includes:

1. PhaseNet phase picker performance: we examine the effectiveness of the PhaseNet phase picker in comparison to manual phase picks. This evaluation aims to assess the accuracy and reliability of PhaseNet's automated phase detection.

2. LOC-FLOW-generated earthquake catalogs: we analyse the earthquake catalogs produced by LOC-FLOW, evaluating both origin time and absolute locations. The examination involves comparing catalogs formed with PhaseNet picks against those created with the original RSC manual picks. This analysis offers insights into the coherence and efficacy of PhaseNet in creating the overall earthquake catalog.

3. Contribution of template matching: we assess the influence of template matching on the final catalog and compare it to the dataset obtained from the original RSC procedures. This evaluation aims to clarify the degree to which template matching enhances the accuracy and comprehensiveness of the earthquake catalog within the LOC-FLOW workflow.

4. Spatio-temporal characteristics of seismicity: furthermore, we assess the spatio-temporal characteristics of the acquired seismicity. This examination is useful to check the efficiency of the method in discerning tectonic structures activated during the sequence. Gaining insights into the spatial and temporal patterns of seismic activity offers valuable understanding of the underlying geologic processes.

We find that PhaseNet achieved a detection rate of 79% for manual P arrival times and 90% for S arrival times at the same stations. While P picks exhibited satisfactory accuracy, a noticeable delay was observed for S picks. This delay is presumed to be a common feature, even in other datasets, given the high quality of the manual picking used for comparison.

After integrating events identified by the template matching procedure, the final LOC-FLOW catalog is characterized by an increased number of events compared to the initial manual catalog. However, in our specific case study, PhaseNet did not contribute significantly to the augmentation of the earthquake count during the most active days of the sequence (e.g., 2-3 August), where template matching played a crucial role. Despite the observed lower accuracy in S picks,

PhaseNet's overall performance is commendable, especially when considering the time of processing, significantly reduced compared to manual picking. The seismicity pattern observed vividly depicted the geometry of the activated fault in both temporal and spatial dimensions (Sugan et al., 2023).

References

Anikiev D., Birnie C., bin Waheed U., Alkhalifah T., Gu C., Verschuur D.J., Eisner L.; 2023. Machine learning in microseismic monitoring. Earth-Science Reviews. 239:104371. https://doi.org/10.1016/j.earscirev.2023.104371.

Mousavi S.M., Horton S.P., Langston C.A., Samei B.; 2016. Seismic Features and Automatic Discrimination of Deep and Shallow Induced-Microearthquakes Using Neural Network and Logistic Regression. Geophys J Int. 207(1):29-46. https://doi.org/10.1093/gji/ggw258.

Peruzza L., Romano M.A., Guidarelli M., Moratto L., Garbin M., Priolo E.; 2022. An unusually productive microearthquake sequence brings new insights to the buried active thrust system of Montello (Southeastern Alps, Northern Italy). Front Earth Sci. 10:1044296. https://doi.org/10.3389/feart.2022.1044296.

Sugan M., Peruzza L., Romano M.A., Guidarelli M., Moratto L., Sandron D., Plasencia Linares M.P., Romanelli M.; 2023. Machine learning versus manual earthquake location workflow: testing LOC-FLOW on an unusually productive microseismic sequence in northeastern Italy. Geomatics, Natural Hazards and Risk, 14:1. https://doi.org/10.1080/19475705.2023.2284120.

Zhang M., Liu M., Feng T., Wang R., Zhu W.; 2022. LOC-FLOW: An End-to-End Machine-Learning-Based High-Precision Earthquake Location Workflow. Seismol Res Lett. 93(5):2426-2438. https://doi.org/10.1785/0220220019.

Zhu W., Beroza G.C.; 2018. PhaseNet: A deep-neural-network based seismic arrival-time picking method. Geophys J Int. 216(1): 261–273. https://doi.org/10.1093/gji/ggy423.

Corresponding author: msugan@ogs.it

SUPERSTUDIES: an approach for integrating macroseismic datasets of different nature

A. Tertulliani[1], A. Antonucci[2], F. Bernardini[3], V. Castelli[3], E. Ercolani[3], L. Graziani[1], A. Maramai[1] , M. Orlando[1], A. Rossi[1], T. Tuvè[4]

[1] Istituto Nazionale di Geofisica e Vulcanologia, Roma, Italy
[2] Istituto Nazionale di Geofisica e Vulcanologia, Milano, Italy
[3] Istituto Nazionale di Geofisica e Vulcanologia, Bologna, Italy
[4] Istituto Nazionale di Geofisica e Vulcanologia, Osservatorio Etneo, Catania, Italy

In recent decades, a huge amount of information on Italian seismic history has been produced, contributing to the compilation of the current seismic catalogues, CPTI15 (Rovida et al., 2020 and 2022) and CFTI5Med Guidoboni et al. 2018.). The last version of CPTI15 counts almost 5000 events from 1000 A.D. to 2020.

CPTI15 is fed by DBMI15 (Locati et al., 2022), a macroseismic database that derives its data from approximately 190 studies on single events, produced over time by the scientific community. DBMI15 contains over 120,000 Macroseismic Data Points (MDPs) related to more than 3200 earthquakes. The epicentral parameters and MDPs list of each event in the CPTI-DBMI catalogue are based on a single reference study (the “preferred” one), selected by a criterion based on the quality of the study itself and on the number and distribution of the intensity data it provides. However, in many cases, multiple studies are available in literature for the same event. For this reason, since 2017, the Italian Archive of Historical Earthquake Data (ASMI) has been published and it is continuously implemented (Rovida et al., 2017), collecting many references of interest for the thousands of earthquakes included in the catalogue. At present, ASMI stores about 450 studies dedicated to more than 6000 earthquakes. For many of these earthquakes, multiple studies, by different authors and of various kinds and complexity, are available, ensuring a multiplicity of views and types of information.

A screening of the available studies for different earthquakes showed that the "preferred" studies are not always those with the largest number of MDPs, or the most recent and up to date. In other words, there are cases in which the same earthquake has been investigated by different authors, who produced datasets that can differ in terms of MDPs, geographic coverage, and reference sources. This means that many available and published MDPs, are not included in the catalogue simply because they are not included in the “preferred” studies, and therefore, they cannot be used for any purpose. Earthquakes with multiple studies are particularly numerous in the period from 1985 to the present. A detailed analysis showed that these datasets could be, in many cases, complementary to each other.

In the light of this, we aimed at integrating the different existing datasets for a given event in a unique intensity compilation, thus optimising all the available intensity data. This possible data merging could give, for each studied earthquake, a significant increase both in MDPs number and

in the completeness of the listed localities' seismic histories. This operation could allow to systematize a considerable amount of data that so far has remained under-used or even unused.
We called "superstudy" this approach of integrating, in a single dataset, data derived from several different studies of the same event.
However, to carry out this task is not a straightforward procedure, and some critical issues exist, mainly due to the inhomogeneity of the different intensity dataset. This inhomogeneity is due to different methods of collecting information and assigning intensity, adopted by different research groups, in different "historical" periods, also sometimes using different intensity scales or different kinds of geolocalization (e.g. municipal area or hamlets).
The purpose of this work is to understand whether it is possible to integrate such different datasets into a coherent whole, quickly and efficiently (I.e. without performing a deep revision of each event), without lessening the quality of the resulting intensity assignments. To check this, we made an experiment that started with the selection of a number of earthquakes, occurred in the period from 1985 to 2006, for which several different studies are available.
The selected earthquakes are provided with studies of different kinds, from reports of macroseismic field surveys, to questionnaire data collections and to preliminary reviews.

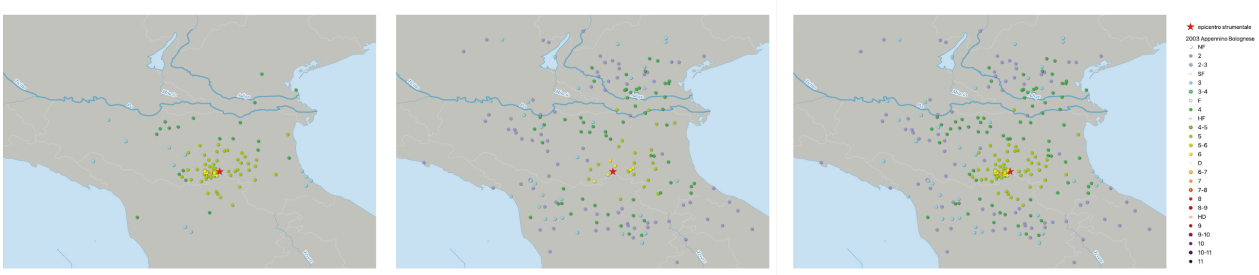

Fig.1 – Example of the superstudy of the September 9, 2003 earthquake. From the left to the right, CPTI15 preferred study (Bernardini et al., 2003) 134 Mdps, the other available source (BMING11, Gasparini et al., 2011) 613 MDPs and the final superstudy, MDPs 693 MDPs.

Integrating macroseismic studies of different nature does not simply mean combining intensity values as they are. On the contrary, it requires first to individuate some homogenization criteria that allow to optimize the quality and quantity of information. As mentioned above, dissimilarities in macroseismic data mostly result from the different practices of data collection followed at different times, according to the methodologies used, and from the kinds of intensity scale used and how they were used. The studies associated with the selected earthquakes provide data sets that differ both in the number of points and in the assessed intensity values. In some cases we find that a given locality is included in all studies, with coincident intensities or sometimes with different intensities. It can also happen that several MDPs are present in one only of the studies of the same earthquake.
To bring our appointed task to completion both efficiently and systematically, it is necessary to establish some criteria and accept some approximations about the nature of data, as for example, considering MCS and EMS intensities <5 to be equivalent. This project, at the moment, involves more than 40 earthquakes with a total of about 4,000 MDPs, which will increase to around 10,000

at the end of the work. The “superstudy” datasets will be compiled both in the MCS scale and in EMS-98. The unquestionable advantages of this operation are quite a number: feeding the catalogue with a great amount of MDPs not previously considered (example in Fig. 1); improving seismic histories with a large number of localities; increasing the knowledge of each event; enriching available datasets in both MCS and EMS-98 scales.

References

Bernardini F., Camassi R., Castelli V., Ercolani E., Frapiccini M., Vannucci G., Giovani L., Tertulliani A.; 2003: Rilievo macrosismico degli effetti prodotti dalla sequenza sismica iniziata il 14 settembre 2003 (Appennino Bolognese). Rapporto tecnico QUEST, Istituto Nazionale di Geofisica e Vulcanologia (INGV), Bologna, 10 pp. https://doi.org/10.13127/QUEST/20030914

Gasparini C., Conte S., Vannucci C. (ed); 2011: Bollettino macrosismico 2001-2005. Istituto Nazionale di Geofisica e Vulcanologia, Roma. CD-ROM

Guidoboni E., Ferrari G., Mariotti D., Comastri A., Tarabusi G., Sgattoni G., Valensise G.; 2018: CFTI5Med, Catalogo dei Forti Terremoti in Italia (461 a.C.-1997) e nell’area Mediterranea (760 a.C.-1500). Istituto Nazionale di Geofisica e Vulcanologia (INGV). doi: https://doi.org/10.6092/ingv.it-cfti5

Locati, M., R. Camassi, A. Rovida, E. Ercolani, F. Bernardini, V., Castelli, C. H. Caracciolo, A. Tertulliani, A. Rossi, R. Azzaro, et al.; 2019: Database macrosismico Italiano (DBMI15), versione 2.0, Istituto Nazionale di Geofisica e Vulcanologia (INGV), doi: 10.13127/DBMI/DBMI15.2 .

Rovida A., Locati M., Antonucci A., Camassi R. (a cura di); 2017: Archivio Storico Macrosismico Italiano (ASMI). Istituto Nazionale di Geofisica e Vulcanologia (INGV). https://doi.org/10.13127/asmi

Rovida, A., M. Locati, R. Camassi, B. Lolli, and P. Gasperini; 2020: The Italian earthquake catalogue CPTI15, Bull. Earthq. Eng. 18, 2953–2984, doi: 10.1007/s10518-020-00818-y

Rovida A., Locati M., Camassi R., Lolli B., Gasperini P., Antonucci A.; 2022: Catalogo Parametrico dei Terremoti Italiani (CPTI15), versione 4.0. Istituto Nazionale di Geofisica e Vulcanologia (INGV). https://doi.org/10.13127/CPTI/CPTI15.4

Corresponding author: andrea.tertulliani@ingv.it

Was the August 26, 1806 earthquake really the largest event in the Roman area ?

A. Tertulliani, C. Castellano

Istituto Nazionale di Geofisica e Vulcanologia, Roma, Italy

The August 26, 1806 earthquake, M_w 5.6 and I_0 8 MCS, with epicenter in the Alban Hills region, is known as the largest one that occurred in the Roman area (CPTI15, Rovida et al., 2020; 2022).

The shock occurred at 7:35 GMT, provoking damage in several localities, particularly severe in the villages of Genzano, Rocca di Papa and Velletri. Some sources have even mentioned the death and injury of some people in Genzano and Rocca di Papa. The earthquake was felt in Naples and caused light damage in Rome.

This is the summary of how the event is known so far in the catalogs (Guidoboni et al., 2018; Rovida et al., 2020).

However, some unique features of this event intrigued us, and motivated us to undertake in-depth research. A dedicated investigation showed that there was still room for improvement in the knowledge about this earthquake, in particular through the examination of archival documents, which had not been consulted by previous studies.

The aim of this work is to present the path of revision and enrichment of the knowledge about the earthquake of August 26, 1806, from which a rather different picture has emerged from what has been known and present in the catalogs so far.

References

Guidoboni E., Ferrari G., Mariotti D., Comastri A., Tarabusi G., Sgattoni G., Valensise G.; 2018: CFTI5Med, Catalogo dei Forti Terremoti in Italia (461 a.C.-1997) e nell'area Mediterranea (760 a.C.-1500). Istituto Nazionale di Geofisica e Vulcanologia (INGV). doi: https://doi.org/10.6092/ingv.it-cfti5

Rovida, A., M. Locati, R. Camassi, B. Lolli, and P. Gasperini; 2020: The Italian earthquake catalogue CPTI15, Bull. Earthq. Eng. 18, 2953–2984, doi: 10.1007/s10518-020-00818-y

Rovida A., Locati M., Camassi R., Lolli B., Gasperini P., Antonucci A.; 2022: Catalogo Parametrico dei Terremoti Italiani (CPTI15), versione 4.0. Istituto Nazionale di Geofisica e Vulcanologia (INGV). https://doi.org/10.13127/CPTI/CPTI15.4

Corresponding author: andrea.tertulliani@ingv.it

Recent activity of the Stradella fault (Emilia Arc, northern Italy) by a multi-scale approach

A. Tibaldi[1,2], R. de Nardis [3,2], P. Torrese [4,2], S. Bressan[1], M. Pedicini[1], D. Talone[2,3], F. L. Bonali[1,2], N. Corti[1], E. Russo[1,2], G. Lavecchia[3,2]

[1] Department of Earth and Environmental Sciences, University of Milan-Bicocca, Milan, Italy
[2] CRUST-Interuniversity Center for 3D Seismotectonics with Territorial Applications, Chieti, Italy
[3] Department of Psychological Sciences, Health and Territory, University of the Studies "G. d'Annunzio", Chieti, Italy
[4] Department of Earth and Environmental Sciences, University of Pavia, Italy

The deformation front of the northern Apennines - Italy - is mostly covered under the alluvial deposits of the Po Plain. Some of the folds and thrusts of this front show geological evidence of Late Quaternary activity, thus posing the need for an accurate seismic hazard assessment due to widespread housing settlements, industries, lifeline infrastructures, and large towns. We present new morphostructural, geophysical, and seismological data to discuss the recent activity of the Broni-Sarmato fault, an 18 km-long outcropping section of the north-verging Stradella thrust, located 50 km south of Milan, along the Pede-Apennine thrust front (PTF) in the rear of the Emilia Arc thrust system. The new geoelectrical surveys across the fault scarp show deformation of the shallow deposits. The outcropping deformations, with a fault scarp ranging up to 25.8 m, are investigated within the seismotectonic framework of the PTF and the Emilia Arc. The analysis of the associated seismicity and new focal mechanisms highlight two seismogenic contractional volumes dipping at low-angle southwest-ward, at upper (<12 km) and lower crustal depths (~20–30 km). The shallow seismicity partially illuminates the Stradella thrust and its alongstrike southeastward prosecution along the extent of the Stradella-Salsomaggiore Arc. Subordinately, it also illuminates some of the Emilia Arc thrust planes. The deeper seismogenic volume shows large patches of the basal thrust of the Emilia Arc fault system. We interpret the above multi-scale data as evidence of ongoing tectonic activity of the outer fronts of the Emilia Arc under a regional NNE-oriented compressional stress field, with some evidence of thrust involvement along the Pede-Apennine front. In our 3D fault-model reconstruction, all the analyzed thrust structures appear as expressions of a thick-skinned deformation that controls earthquake release at different structural levels. The results do not allow to establish if the Broni-Sarmato scarp really represents the emersion of the main fault or it can represent the frontal limb of a fault-propagation fold. In the latter case, the main thrust did not reach yet the surface, whereas the deformations of the shallow deposits, highlighted by geoelectrical surveys, may represent secondary structures.

Acknowledgments

Research activities have been carried out in the frame of the Italian PRIN Project (Research Projects of National Interest) “Fault segmentation and seismotectonics of active thrust systems: the Northern Apennines and Southern Alps laboratories for new Seismic Hazard Assessments in northern Italy (NASA4SHA)” (PI R. Caputo, UR Responsible A. Tibaldi), of the CRUST - Interuniversity Center for 3D Seismotectonics with Territorial Applications, and under the aegis of the International Lithosphere Program, Task Force II. We acknowledge PetEx that provided the Move 2019.1 suite software license and we thank Daniele Spallarossa and his colleagues for providing us the waveforms of the Regional Seismic Network of Northwestern Italy RSNI.

Corresponding author: alessandro.tibaldi@unimib.it

Integrated analysis of geophysical data: a case study from Central Italy

M.M. Tiberti[1], F.E. Maesano[1], M. Buttinelli[1], P. De Gori[1], F. Ferri[2], L. Minelli[1], M. Di Nezza[1], C. D'Ambrogi[2]

[1] Istituto Nazionale di Geofisica e Vulcanologia, Rome, Italy
[2]Istituto Superiore per la Protezione e la Ricerca Ambientale, Servizio Geologico d'Italia, Rome, Italy

We performed a 2D gravity modeling across the Central Apennines, spanning from the Tyrrhenian coast to the Adriatic Sea, in the area affected by the Amatrice-Visso-Norcia earthquakes.

The cross-section was built exploiting the results of the 3D model proposed by the RETRACE 3D project (*www.retrace3d.it*) and aimed at completing and verifying the crustal geometries resulting from the project itself.

The results were checked against the velocity model provided by local tomography (LET), adding further details, and, finally, against seismicity recorded during the 2016-2017 sequence.

The results indicate that the geometries proposed in the RETRACE 3D model fit well with the Bouguer anomalies, except for some local misfits.

We were also able to determine some new elements in the surroundings of the RETRACE study area, where the cross-section length exceeds the 3D model.

In addition, the gravity model allowed us to investigate the nature of the basement top and its relationship with seismotectonics.

Corresponding author: mara.tiberti@ingv.it

On-fault earthquake energy density partitioning from an exhumed seismic mid-crustal fault

G. Toffol[1], G. Pennacchioni[1], L. Menegon[2], D. Wallis[3], M. Faccenda[1], A. Camacho[4], M. Bestmann[5]

[1] Department of Geosciences, University of Padova, Padva, Italy
[2] Department of Geosciences, University of Oslo, Oslo, Norway
[3] Department of Earth Sciences, University of Cambridge, Cambridge, UK
[4] Department of Geological Sciences, University of Manitoba, Winnipeg, Canada
[5] Department of Geology, University of Vienna, Wien, Austria

The energy released during an earthquake is mostly dissipated in the fault zone and subordinately as radiated seismic waves. The on-fault energy budget is partitioned into frictional heat, generation of new grain surface by microfracturing, and crystal-lattice distortion associated with dislocation defects. The energy partitioning strongly influences earthquake mechanics; however, the relative contribution of the on-fault components is debated and difficult to assess.

Exhumed fault rocks bearing pseudotachylytes (quenched coseismic frictional melts, the geological record of earthquake failure) represent a fundamental source of information to understand earthquake mechanics. We used high-resolution scanning-electron-microscopy techniques to analyse shocked garnets in a fault wall-rock, to provide the first estimate of all three energy components for a seismic fault patch exhumed from midcrustal conditions. Fault single-jerk seismicity is recorded by the presence of pristine quenched frictional melt. The estimated value of energy per unit fault surface is ~ 13 MJ/m2 for heat, which is predominant with respect to both surface energy (up to 0.29 MJ/m2) and energy associated with crystal lattice distortion (0.02 MJ/m2).

Corresponding author: giovanni.toffol@unipd.it

Are productive gas fields anticorrelated with large seismogenic faults? Implications for hydrocarbon exploitation and seismic hazard

G. Valensise[1], F. Donda[2], A. Tamaro[2], S. Parolai[3]

[1] INGV, Rome, Italy
[2] OGS, Trieste, Italy
[3] University of Trieste, Italy

Thrust faulting earthquakes are an inherent occurrence in hydrocarbon-bearing active regions dominated by crustal shortening: they may be generated by regional-scale tectonic processes, but also triggered at all stages of hydrocarbon exploitation activities. Their occurrence, however, is highly heterogeneous, as earthquakes often appear scattered across relatively homogeneous tectonic trends. For instance, investigations of the seismicity of the Zagros region (southern Iran: Nissen et al., 2011), one of the largest oil and gas reserves worldwide, revealed (a) that thrust faulting earthquakes are less frequent than strike-slip events, despite the characteristic and actively deforming fold-and-thrust structure of the region; and, more importantly, that (b) the observed seismicity accounts for a small fraction of the region's shortening estimated from geodetic observations.

In a frictional regime, the fraction of fault slip that is released in earthquakes is generally referred to as seismic coupling, or *c*, a dimensionless parameter introduced in the 1970s based on observations of great earthquakes of the circum-Pacific belt (Kanamori et al., 1971). Investigations of the compressional domains encircling the Italian peninsula, most of which host important oil and gas reservoirs, have already suggested that the average *c* is about 50% (Carafa et al., 2017); half than that estimated for the extensional domains straddling the Apennines chain, which is close to 1.0. Is this the result of episodically aseismic behaviour of the large thrust faults occurring beneath Italy's hydrocarbon reservoirs? How else could it be exaplained?

These questions were initially addressed by Mucciarelli et al. (2015), moving from the evidence offered by the 20 and 29 May 2012, M_w 5.9-6.0, Emilia earthquakes. These workers focused on the 2D spatial relationships between some known seismogenic sources supplied by the DISS database (DISS Working Group, 2021), and the distribution of 455 gas fields falling in a ~ 10,000 km^2 portion of the central-southern Po Plain, using data supplied by the "Visibility of Petroleum Exploration Data in Italy" (ViDEPI) database run by the Italian Ministry of Economic Development (https://www.videpi.com/videpi/pozzi/pozzi.asp). Based on this exercise, they proposed the existence of an anticorrelation between productive reservoirs and the presence of relatively large seismogenic faults, i.e., faults capable of M_w 5.5 + earthquakes.

Later on, Valensise et al. (2022) investigated in 3D the spatial relationships among 18 known seismogenic faults and 1,651 wells drilled for gas exploitation in the main hydrocarbon province of northern-central Italy, based on the same DISS and ViDEPI databases. Together these data comprise a unique dataset worldwide. They adopted a robust statistical technique implemented in a GIS, and again found a significant anticorrelation between the location of productive wells and that of the considered seismogenic faults, which are often overlain or encircled by unproductive wells.

Their findings led to the following conclusions:

(a) over geological time, earthquake ruptures encompassing much of the upper crust may cause gas to be lost to the atmosphere from the potential reservoir formations;

(b) reservoirs underlain by smaller or aseismic faults are more likely to be intact. This implies that the May 2012 shocks may simply have been the most recent events released by faults having a long earthquake history; and

c) the limited seismic coupling observed by previous investigators does not just indicate diffuse aseismic behavior, but rather suggests that about 50% of the large thrust faults occurring beneath the Po Plain hydrocarbon province slip consistently in an aseismic fashion; the remainder are fully coupled, and hence capable of generating the largest possible earthquake allowed by their size. Recent works on the sources of the May 2012 Emilia earthquake suggested that stick–slip behaviour occurs only where previous tectonic histories caused high-stiffness rocks (e.g., Triassic and Jurassic limestones and dolostones) to be uplifted and brought in contact across the fault plane, up to the characteristic 3–10 km depth of local upper crustal thrust faults (Bonini et al., 2014).

These results, which are of inherently global relevance, have crucial implications for future hydrocarbon exploitation; for the public acceptance of energy-related facilities in tectonically active areas; and for or assessing the seismic–aseismic behaviour of large thrust faults, leading to a more accurate estimation of the local seismic hazard. They also suggest that in earthquake-prone areas, any facility for natural gas, hydrogen or CO_2 storage should (a) be located away from proven seismogenic faults, and (b) take full advantage of depleted gas reservoirs: in itself, the pre-exploitation performance of such reservoirs proves they can sustain the typical pressures of an intact gas-field, and should be free from the risk of being damaged by a large earthquake.

References

Bonini L., Toscani G., Seno S.; 2014: *Three-dimensional segmentation and different rupture behaviour during the 2012 Emilia seismic sequence (Northern Italy)*. Tectonophysics, 630, 33–42, DOI: 10.1016/j.tecto.2014.05.006.

Carafa M. M. C., Valensise G., Bird P.; 2017: *Assessing the seismic coupling of shallow continental faults and its impact on seismic hazard estimates: a case-study from Italy*. Geophys. J. Int., 209(1), 32–47, DOI: 10.1093/gji/ggx002.

DISS Working Group; 2021: Database of Individual Seismogenic Sources (DISS), Version 3.3.0: A compilation of potential sources for earthquakes larger than M 5.5 in Italy and surrounding areas. Istituto Nazionale di Geofisica e Vulcanologia (INGV), DOI: 10.13127/diss3.3.0.

Kanamori, H. Great earthquakes at island arcs and the lithosphere. Tectonophysics, 12, 187–198 (1971).

Mucciarelli M., Donda F., Valensise G.; 2015: *Earthquakes and depleted gas reservoirs: which comes first?* Natural Hazards and Earth System Sciences, 15(10), 2,201-2,208, DOI: 10.5194/nhess- 15-2201-2015.

Nissen E., Tatar M., Jackson J. A., Allen M. B.; 2011: *New views on earthquake faulting in the Zagros fold-and-thrust belt of Iran*. Geophys. J. Int., 186, 928–944, DOI: 10.1111/j.1365246X.2011.05119.x.

Valensise G., Donda F., Tamaro A., Parolai S.; 2022: *Gas fields and large shallow seismogenic reverse faults are anticorrelated*. Scientific Reports, 12(1), 1,827, DOI: 10.1038/s41598- 022-05732-8.

Corresponding author: gianluca.valensise@ingv.it

Investigating the Influence of Coulomb Stress Transfer in the Activity of the Central Apennine Fault System (CAFS) Over the Last Millennium

G. Valentini[1,2.], T. Volatili[1], P. Galli[3,4], E. Tondi[1,2]

1. School of Science and Technology - Geology Division, University of Camerino, Italy.
2. National Institute of Geophysics and Volcanology, Rome, Italy
3. Dipartimento Protezione Civile, Rome, Italy
4. Consiglio Nazionale delle Ricerche, Istituto di Geologia Ambientale e Geoingegneria, Rome, Italy

The active Central Apennine Fault System (CAFS) witnessed several destructive seismic events over the last millennia. Although numerous investigations have highlighted the role of Coulomb Stress Transfer (CST) in the onset of some of the most devastating earthquakes globally, there is limited scientific documentation pertaining to its specific impact within the CAFS. This research delves into and thoroughly examines the effects of CST on both historical and instrumental seismic events of significant magnitude associated with the CAFS.

15 seismic events within the CAFS region dating from 1279 to present with magnitudes higher than Mw 6.0 were selected. Specifically, 9 were selected for the CST investigation, based on their proximity to subsequently activated faults both spatially and temporally. Beyond analyzing the static stress transfer for each individual seismic event, the cumulative CST of recent instrumental earthquakes was also examined to provide a comprehensive overview of the current stress scenario. Leveraging an innovative approach, faults were modeled in three dimensions, adopting an ellipse as the most accurate representation of their 2D geometry. Considering the CST's sensitivity to strike variations, a variable strike three-dimensional elliptical model was therefore implemented, ensuring enhanced calculation accuracy.

Valentini et al. (2023) identify three prominent periods where most of the seismic moment was released. The initial phase spans from ~1300 CE to ~1400 CE, followed by a surge around 1700 CE, and the most recent phase extends from 1979 to 2016 with 300-350 years intervals. However, the scale of the released seismic moment varies across these distinct seismic periods. The first seismicity window cumulative seismic moment is approximately 1.35 times greater than the second phase and about 2.31 times that of the third phase. With the current data in consideration, it seems plausible to hypothesize the existence of a notable seismic gap in the ongoing historical period. Should this gap exist, it implies the need for a seismic event substantial enough to bridge this gap. Herein we will examine the factors that may influence this seismic gap and identify which

faults could potentially bridge it, in light of the Coulomb Stress Transfer analysis and the distribution of seismicity over the last millennium.

In recent times, there has been a renewed focus on investigating the tectonic and seismic features of the CAFS. This intensified commitment has fostered a deeper understanding of fault dynamics, stress interactions between them, and forecasts for future seismic activities. Given the intricate tectonic nature of the CAFS and its pronounced seismicity, the imperative for consistent research and monitoring in this domain becomes clear. A cornerstone in seismic risk assessment is grasping the Coulomb stress transfer mechanism among faults. This study delves into this particular facet within the CAFS, accounting for the most significant seismic events over the last 750 years. Both historic earthquakes and recent seismic occurrences are analyzed to determine potential future seismic scenarios. By evaluating both the magnitude and the proximity to other fault lines that ruptured shortly after the primary event, we have chosen to concentrate on 9 of these earthquakes in relation to the Coulomb stress transfer (CST). The comprehensive list of these earthquakes, along with their specific attributes, is presented in Table 1, highlighting the ones selected for the CST analysis. The seismic occurrence of 1349 AD was re-evaluated and updated based on the recent findings by Galli et al. (2022).

Within the framework of our research, we've operated under the assumption that subsequent to seismic activity on a specific fault, Coulomb stress can propagate to neighboring faults. If this stress is positive, it might encourage fault rupture, whereas if negative, it could deter it (King et al., 1994). Numerous factors, including the distance between the causative fault and its neighboring one, their shapes, positions, dynamics, and the slip of the source fault, influence the Coulomb stress changes. Utilizing the "Coulomb 3.4" software, we derived the CST using the equation (Lin and Stein, 2004; Toda et al., 2005):

$$\Delta CST = \Delta\tau s + \mu \Delta\sigma n$$

In this equation, ΔCST represents variations in Coulomb Stress Transfer, $\Delta\tau s$ corresponds to shifts in shear stress, while μ stands for the friction coefficient, and $\Delta\sigma n$ signifies alterations in normal stress. We adopted a friction coefficient of 0.6 (Galderisi and Galli, 2020) and opted for default spatial parameters with a Poisson's ratio of 0.25 and a Young's modulus of 800,000 bar.

Regarding the three-dimensional portrayal of faults within CST calculations, we leaned on the methodology proposed by Valentini et al., (2023). We integrated a three-dimensional model featuring strike variations and an elliptical shape into our CST algorithm, believing that an accurate representation of the CAFS is pivotal to reducing potential computational inaccuracies. In advancing with the CST simulations, we endeavored to mirror the real seismic rupture dynamics, factoring in variables such as the slip distribution or the partial or entire rupture.

To ensure sharp graphical detail and enhanced bar value precision, we established a 1 km grid for the fault modeling. Faults, perceived in an elastic half-space, were outlined as lines with variable strike and segmented into 1 km units. This intricate segmentation proved to be a balanced choice between output detail and modeling duration, deviating from the more typical practice of using 2 km segments for CST modeling. Subsequently, using the "Faults 3D" software (Mildon et al. 2016),

we were able to construct 3D fault models, drawing from actual traces and determining a slip distribution for each fault. We chose to compute the Coulomb stress for each fault segment, maintaining a consistent friction coefficient. Where available, we used actual slip data for recent earthquakes. For less documented seismic events, we assumed a centered slip distribution, reminiscent of a bull's eye pattern, depending on the relative seismic moment. In instances where the fault width wasn't specified in the reviewed literature, we used standard geometric relationships (Gupta and Scholz, 2000) to determine it, basing our calculations on a 1.5 aspect ratio (length/width). For faults with an extended length, their maximum depth was aligned with the thickness of the seismogenic layer, approximately 15 km (Gasparini et al., 1985; Chiarabba and De Gori, 2016). To optimize CST data comprehension, we crafted three distinct representations. Initially, a traditional CST map was produced at a depth of 5 km, in plan view, providing an approximation of CST distribution within the surrounding crust. This information was then translated to KML format for georeferenced visualization on Google Earth Pro. Lastly, we crafted cross-sections perpendicular to fault strikes and developed a 3D model of the fault planes, obtaining the CST values for each 1 km fault segment, thus ensuring heightened precision in the assessment of stress for each individual segment.

In many of the case studies, CST may have played an influential role within the CAFS (Fig. 1 and Fig.2), catalyzing the activation or inhibition of its faults. Several instances highlight fault reactivation following high stress transfer in short periods, some examples are described below:

- The 1279 Colfiorito earthquake positively stressed the northern tip of the Norcia fault, that ruptured in 1328.
- The 1703 Norcia earthquake positively stressed the Pizzoli fault, where few days later a huge earthquake nucleated, provoking a cascade effect engaging the Pettino and Paganica faults.
- The 24th august and 26th October 2016 earthquakes seems to have stressed the bends and the central portion of the Vettore fault, probably facilitating the 30th October complete rupture.
- The Colfiorito fault system stored conspicuous amount of positive stress from each of the earthquakes generated by the Norcia fault system probably influencing its reactivation in 1997.
- The 1703 Norcia earthquake generated a huge positive stress lobe towards the Fabriano area, where 38 years later a destructive earthquake struck.

Conversely, certain scenarios illuminate the calming effect of stress shadows. Some examples include:

- The Vettore fault generated only one earthquake during the last millennium, this could be linked to the parallel Norcia fault that ruptured 4 times in the same time span, transferring negative CST on the Vettore fault.

- The same hypothesis could be applicable on the Gran Sasso fault that ruptured in 1349, this is the only event in the last millennium. The Paganica fault generated 3 earthquakes that transferred negative Coulomb stress on the Gran Sasso fault.

The nuanced understanding of CST achieved through this research has both concrete and academic implications. By illuminating the interaction between faults in previous seismic episodes, it provides valuable insights into possible future earthquake sequences. Such awareness is essential: by anticipating seismic sequences, targeted risk mitigation tactics can be formulated, thereby protecting local communities from the catastrophic consequences of earthquakes.

Year	Month	Day	Epicentral Area	Lat	Lon	Io	Mw	ErrorMw	TMw	SOURCE
1279	4	30	Colfiorito	43.093	12.872	9	6.2	0.16	Mdm	CPTI15
1328	12	4	Valnerina	42.857	13.018	10	6.4	0.28	Mdm	CPTI15
1349	9	9	Gran Sasso	42.334	13.613	10	7.0	ND	Mdm	Galli et al., 2022
1461	11	27	L'Aquila	42.308	13.543	10	6.5	0.46	Mdm	CPTI15
1599	11	6	Cascia	42.724	13.021	9	6.0	0.24	Mdm	CPTI15
1639	10	7	Laga Mountains	42.639	13.261	9-10	6.2	0.15	Mdm	CPTI15
1703	1	14	Valnerina	42.708	13.071	11	6.9	0.1	Mdm	CPTI15
1703	2	2	L'Aquila	42.434	13.292	10	6.6	0.11	Mdm	CPTI15
1730	5	12	Valnerina	42.753	13.120	9	6.0	0.1	Mdm	CPTI15
1979	9	19	Valnerina	42.73	12.956	8-9	5.8	0.1	InsO	CPTI15
1997	9	26	Colfiorito	43.014	12.853	8-9	5.9	0.07	InsO	CPTI15/ISIDe
2009	4	6	L'Aquila	42.309	13.510	9-10	6.2	0.07	InsO	CPTI15/ISIDe
2016	8	24	Laga Mountains	42.698	13.233	10	6.0	0.07	InsO	CPTI15/ISIDe
2016	10	26	Valnerina	42.904	13.090		5.9	0.07	InsO	CPTI15/ISIDe
2016	10	30	Valnerina	42.83	13.109	11	6.5	0.07	InsO	CPTI15/ISIDe

Table 2 List of historical (Mw≥6) and instrumental (Mw≥5.8) seismic events from 1279 to 2016 caused by CAFS (from CPTI15; Rovida et al., 2022 and ISIDe seismic catalogues). The seismic events selected for simulations are highlighted in green.

Moreover, the complexity of the CAFS, observed in light of past seismic episodes like those in 1997, 2009, and 2016, underscores the intricate nature of stress patterns. These patterns emerge from interactions between seismic events, with stress lobes intertwining in ways that amplify, nullify, or diversify their impacts on nearby faults. It is noteworthy that while historically and currently seismic-active regions such as Fabriano and Sulmona have remained relatively quiescent, their potential for future activity and associated risks should not be overlooked. This research highlights the complex dynamics at play in a high-seismic-activity region like the CAFS. Through rigorous analyses and innovative modeling techniques, we offer insights that can guide future investigations and pragmatic strategies for seismic risk mitigation. This study stands as a testament to the profound ability of CST to influence the seismic narrative of a region and emphasizes the need for continued research in this field.

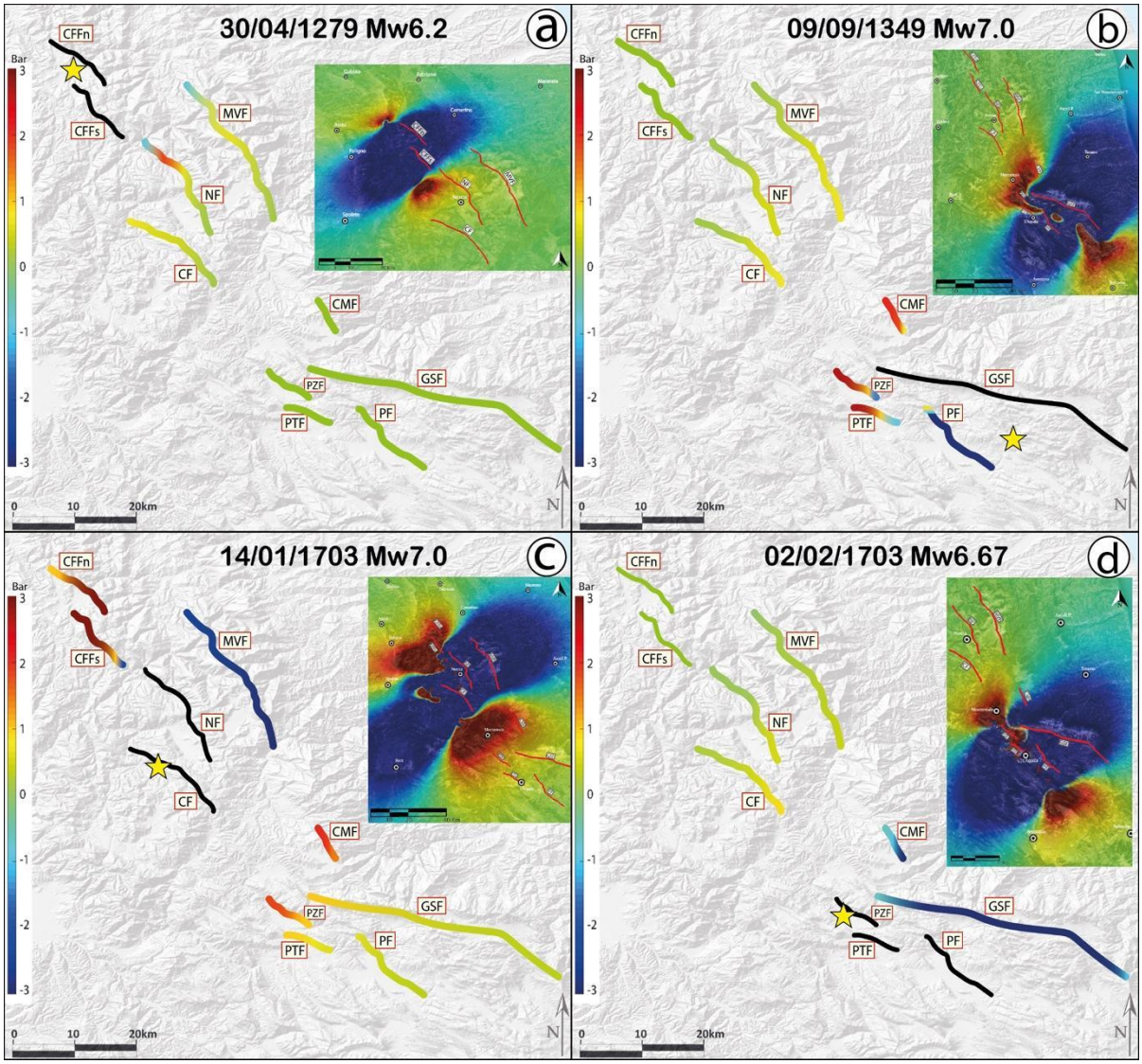

Figure 9 Summary visualization of the Calculated CST at a Depth of 5 km among the faults of the CAFS for each of the analyzed historical earthquakes. a) CST generated by the Colfiorito Fault System in April 1279. b) CST generated by the Gran Sasso Fault in September 1349. c) CST generated by the Norcia and Cascia Faults in January 1703. d) CST generated by the Paganica, Pizzoli, and Pettino Faults in February 1703. The fault traces drawn in black represent the causative faults. The insets of each figure illustrate the spatial distribution of the CST within the crust on a plane located at a depth of 5 km.

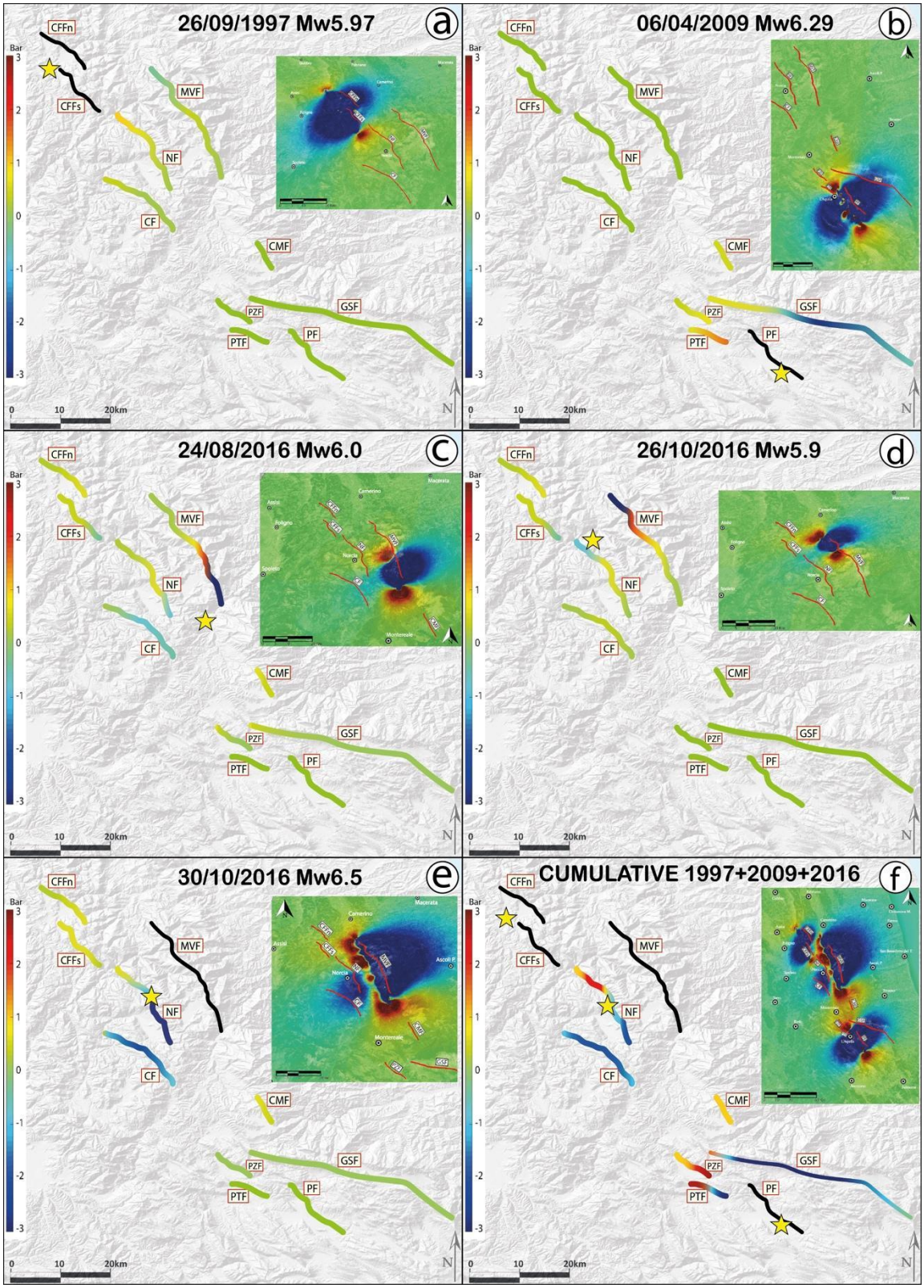

Figure 10 Summary visualization of the Calculated CST at a Depth of 5 km among the faults of the CAFS for each of the analyzed instrumental earthquakes. a) CST generated by the Colfiorito Fault System in September 1997. b) CST generated by the Paganica Fault in April 2009. c) CST generated by the southern portion of the Mt. Vettore fault in August 2016. d) CST generated by the northern portion of the Mt. Vettore fault in October 26th 2016. e) CST generated by the complete rupture of the Mt. Vettore fault in October 30th 2016. f) Cumulative CST from the last five instrumental earthquakes. The fault traces drawn in black represent the causative faults. The insets of each figure illustrate the spatial distribution of the CST within the crust on a plane located at a depth of 5 km.

Acknowledgments

We would like to acknowledge Dr. Zoë Mildon and Dr. Manuel-Lukas Diercks for their kind assistance in using the "3D-Faults" MATLAB code. This work was supported by the FAR Unicam project “Novel Approach for Seismic Hazard Analysis—NoHard'', responsible Emanuele Tondi.

References

Chiarabba C. and De Gori P.; 2016: *The seismogenic thickness in Italy: constraints on potential magnitude and seismic hazard*. Terra Nova, 28(6), 402-408.

Galderisi A. and Galli P.; 2020: *Coulomb stress transfer between parallel faults. The case of Norcia and Mt Vettore normal faults (Italy, 2016 Mw 6.6 earthquake)*. Results in Geophysical Sciences, 1, 100003.

Galli P., Galderisi A., Messina P. and Peronace E.; 2022: *The Gran Sasso fault system: Paleoseismological constraints on the catastrophic 1349 earthquake in Central Italy*. Tectonophysics, 822, 229156.

Gasparini C., Iannaccone G. and Scarpa R.; 1985: *Fault-plane solutions and seismicity of the Italian peninsula*. Tectonophysics 117, 59–78.

Gupta A. and Scholz C. H.; 2000: *A model of normal fault interaction based on observations and theory*. Journal of structural Geology, 22(7), 865-879.

ISIDe Working Group; 2007: *Italian Seismological Instrumental and Parametric Database (ISIDe)*. Istituto Nazionale di Geofisica e Vulcanologia (INGV). https://doi.org/10.13127/ISIDE

King G. C., Stein R. S. and Lin, J.; 1994: *Static stress changes and the triggering of earthquakes*. Bulletin of the Seismological Society of America, 84(3), 935-953.

Lin J. and Stein R. S.; 2004: *Stress triggering in thrust and subduction earthquakes and stress interaction between the southern San Andreas and nearby thrust and strike-slip faults*. Journal of Geophysical Research: Solid Earth, 109(B2).

Mildon Z. K., Toda S., Faure Walker J. P. and Roberts G. P.; 2016: *Evaluating models of Coulomb stress transfer: Is variable fault geometry important?*. Geophysical Research Letters, 43(24), 12-407.

Rovida A., Locati M., Camassi R., Lolli B., Gasperini P. and Antonucci A.; 2022: *Catalogo Parametrico dei Terremoti Italiani CPTI15, versione 4.0.*

Toda S., Stein R. S., Richards-Dinger K. and Bozkurt S. B.; 2005: *Forecasting the evolution of seismicity in southern California: Animations built on earthquake stress transfer*. Journal of Geophysical Research: Solid Earth, 110(B5).

Valentini G., Volatili T., Galli P. and Tondi E.; 2023: New methodological approach in the evaluation of faults interaction: insights from the central Apennine fault system. Bulletin of Geophysics and Oceanography.

Corresponding author: giorgio.valentini@unicam.it

Microseismicity and infrasonic monitoring at the Mefite d'Ansanto deep-CO_2-rich gas emission site (Southern Apennines, Italy)

L. Valoroso[1], S. Cianetti[2], P. De Gori[1], C. Giunchi[2], L. Improta[1], D. Piccinini[2], L. Zuccarello[1], F. Di Luccio[3]

[1] Istituto Nazionale di Geofisica e Vulcanologia (INGV), Osservatorio Nazionale Terremoti, Rome (Italy)
[2] Istituto Nazionale di Geofisica e Vulcanologia (INGV), Sezione di Pisa (Italy)
[3] Istituto Nazionale di Geofisica e Vulcanologia (INGV), Roma 1 (Italy)

The role of fluids in the earthquake nucleation process as well as in the evolution of aftershocks and swarms in space and time is well-documented, yet it is still an important issue for the seismological community to understand the physics governing the earthquakes. In particular, numerous studies evidence the primary role that mantle-derived fluids play in the generation of moderate to large upper crustal destructive earthquakes in extensional domains, where crustal-scale faults act as preferential hydraulic pathways.

In this study, we focus on the Mefite d'Ansanto degassing site (Southern Apennines, Italy) which is the largest low-temperature non-volcanic CO_2-rich gas emission site in the world, located at the northern tip of the Mw6.9 1980 Irpinia fault system. The study area experienced strong historical earthquakes (1702, 1732 and 1930 M6+ earthquakes) but it is characterised by a relatively low background seismicity rate with respect to the nearby Sannio and Irpinia regions.

To collect high-quality microseismicity data in this key sector of the southern Apennine extensional belt and investigate the relationship among seismicity, crustal fluids, and physical-hydraulic properties of the crust, we conducted a two years temporary experiment (June 2021 to May 2023) by installing a dense temporary network of 10 seismic stations equipped with short-period velocimeters (Lennartz 5sec). The temporary network covers an area of approximately 30x30 km^2 surrounding the Mefite d'Ansanto site and integrates with the numerous permanent stations of the INGV and ISNet permanent networks located at the boundary of the survey area. Within the Mefite area, we also deployed a temporary seismo-acoustic dense array to study two CO_2 degassing vents.

We show first results of the analysis of the seismicity recorded by the temporary network applying both standard (STA/LTA) detection algorithms or innovative enhanced techniques such as cross-correlation based template-matching algorithms (Chamberlain et al., 2018) and/or Deep-Learning-Phase-Recognition methods (Zhu and Beroza et al., 2018).

The activities are developed in the framework of the multidisciplinary project FURTHER (https://progetti.ingv.it/en/further).

References

Chamberlain C. J., Hopp C. J., Boese C. M., Warren-Smith E. , Chambers D., Chu S. X., Michailos K., Townend J. (2018). EQcorrscan: Repeating and Near-Repeating Earthquake Detection and Analysis in Python. Seismological Research Letters 2017; 89 (1): 173–181. https://doi.org/10.1785/0220170151

Zhu, W., & Beroza G. B. (2018). PhaseNet: A Deep-Neural-Network-Based Seismic Arrival Time Picking Method. Geophysical Journal International, 216(1), 261-273.

Corresponding author: luisa.valoroso@ingv.it

Vertical distributions of underground pore pressures from boreholes in the Southern Apennines and their seismotectonic implications

E. Vitagliano, N. D'Agostino, L. Improta, L. Pizzino

Istituto Nazionale di Geofisica e Vulcanologia (Rome, Italy)

Understanding subsurface pore pressures and crustal permeabilities is crucial for both resource exploitation and the mitigation of natural hazards. The pressure gradients inherent in the Earth's crust play an essential role in expelling geofluids and, more generally, in the underground fluid flows (groundwater, carbon dioxide, methane, etc.). Intensity and duration of the forces responsible for the pressure gradients are predominantly influenced by crustal permeability (Vannoli et al., 2021). In this context, unravelling the intricate dynamics of the pore pressure not only contributes to effective resource management but also enhances our ability to comprehend and address potential risks associated with seismic hazards.

The reconstruction of pore pressure regimes is normally inferred on the basis of indirect geophysical methods like the velocity ratios (e.g., Amoroso et al., 2017), which are suitable for large-scale studies and provide regional patterns often integrated with the geo-structural interpretation of the subsurface. However, these methods are limited, because they rely on certain assumptions about the subsurface, and their accuracy is contingent on the validity of these assumptions and can be influenced by the geological complexity of the study area. Conversely, direct pore pressure measurements from well data provide reliable information on in situ pressure conditions. These measures can be retrieved from formation and production tests and also derived from well logging by applying a properly calibration and validation procedure (e.g., Zhang, 2011).
Although future research will be addressed to combine both these approaches and thus providing a more comprehensive understanding of subsurface pressure conditions, in the present research we systematically investigate the vertical pressure trends using borehole data (mud weights, formation test and drill stem test pressures).

The proposed study is developed in the framework of the FLUIDS Project, funded by the Italian Ministry for Research with the aim at developing and applying an integrated multi-parametric and multi-disciplinary approach to image and track crustal fluids in different environments (e.g., tectonic, exploitation, volcanic). It deals with fluid movements, pore fluid-pressure diffusion and analysis of their correlation with the induced/triggered seismicity.

Moreover, our study focuses on the Irpinia and Sannio area, located in the northern part of the Southern Apennines. The Apennines has been generally explored in the last decades by many researchers to examine the relationship among tectonic processes, fluid movement and seismic

activity (e.g., Di Luccio et al., 2022). Regarding these topics, although many structural and geological aspects of the upper and lower crust of this chain are still unclear (e.g. Improta and Corciulo, 2006), it is overall accepted that the extensional tectonics has a primary role on CO_2 Earth degassing and that CO_2-rich fluids of mantle-origin is distributed in concomitance of the destructive Apennines seismic sequences (e.g., Chiodini et al., 2020 and references therein). The fluids, including CO_2, may contribute to the earthquake preparation, nucleation and evolution.

In the study area, the fold-and-thrust belt was under tectonic compression until the Pleistocene and is currently under extension (e.g., Improta et al., 2003). Moreover, the chain is nowadays the site of groundwater flow, natural gas circulation and seismicity (e.g., Fiorillo et al., 2010; Chiodini, 2014; D'Agostino et al., 2018). In particular, the fluids migrate across the crust, moving downward and upward through the orogenic wedge, whose upper part is composed by foredeep deposits and sediments formed in shallow, transitional, and deep-water environments. These sequences overlap with the carbonates of the Apulian Platform. Gas emissions collected at the Mefitiniella, Mefite, Malvizza and Telese sites testify that gas rises from great depths through the complex geological setting (e.g., Minissale, 2004). Moreover, in 1962 and 1980, two earthquakes of magnitude Mw>6 hit the region (Rovida et al., 2020; 2022), leading to the destruction of several municipalities in the provinces of Benevento and Avellino, and resulting in numerous fatalities, homeless people and extensive damages.

In the current work, 30 exploration wells available on open source (VIDEPI website) and drilled between 1961 and 1982 have been analysed. The pore pressures data were initially extracted from the well profiles, including mud weight and formation test pressures. Subsequently, the obtained pressures were normalized to a hydrostatic profile to better compare the pressure values at varying depths and different sites. Finally, observed hydrostatic and abnormal trends were compared to the fluids found at well sites to verify possible correlations.

Approximately half of the analysed wells identified carbon dioxide levels, either in sandy and calcareous formations across the hole or at the bottom hole reservoirs, such as the carbonates of the Apulian Platform. Since these boreholes allow us to extract pore pressure measurements up to a depth of 6 km, these wells offer a unique opportunity to investigate subsurface pore pressures and their interaction with the different fluid types (groundwater, hydrocarbons, carbon dioxide).

The study unveils that the CO_2 levels found in several wells (e.g., Circello 1 and Benevento 2) within the permeable layers of the Apulian Platform carbonates are in hydrostatic conditions, thus indicating that the storage of CO_2 is not necessarily correlated with the overpressures. Similarly, the CO_2 gas cap found in Monte Forcuso 1 and Monte Forcuso 2 wells is in hydrostatic conditions, thus suggesting that the CO_2 rising to the surface can occur without the generation of overpressures. In addition, moderate to high overpressured gradients are predominantly identified within allochthonous Miocene shaly-rich sequences, including the Irpinia/Sannio Units and the formations of the Rapolla Group, also associated with groundwater-fed levels, as evidenced by Panizza 1 and other wells.

References

Amoroso O., Russo G., De Landro G., Zollo A., Garambois S., Mazzoli S., Parente M., Virieux J.; 2017: From velocity and attenuation tomography to rock physical modeling: Inferences on fluid-driven earthquake processes at the Irpinia fault system in southern Italy. Geophys. Res. Lett., 44, 6752–6760.

Chiodini G., Cardellini C., Di Luccio F., Selva J., Frondini F., Caliro S., Rosiello A., Beddini G., Ventura G.; 2020: Correlation between tectonic CO2 Earth degassing and seismicity is revealed by a 10-year record in the Apennines, Italy. Sci. Adv., 6, eabc2938.

Chiodini G.; 2014: Gas emissions and related hazard in Italy. Mem. Descr. Carta Geol. d'It., XCVI, 189-194. In Italian

D'Agostino N., Silverii F., Amoroso O., Convertito V., Fiorillo F., Ventafridda G., Zollo A.; 2018: Crustal deformation and seismicity modulated by groundwater recharge of karst aquifers. Geophys. Res. Lett., 45, 12, 253–262.

Di Luccio F., Palano M., Chiodini G., Cucci L., Piromallo C., Sparacino F., Ventura G., Improta L. et alii; 2022: Geodynamics, geophysical and geochemical observations, and the role of CO2 degassing in the Apennines. Earth-Science Reviews, 234, 104236.

Fiorillo F., Guadagno F.M.; 2010: Karst spring discharges analysis in relation to drought periods, using SPI. Water Resource Manage, 24:1867-1884.

Improta L., Bonagura M., Capuano P., Iannaccone G.; 2003: An integrated geophysical investigation of the upper crust in the epicentral area of the 1980, Ms=6.9, Irpinia earthquake (Southern Italy). Tectonophysics, 361, 139-169.

Improta L., Corciulo M. (2006): Controlled source nonlinear tomography: A powerful tool to constrain tectonic models of the Southern Apennines orogenic wedge, Italy. *Geology*, 34 (11): 941–944.

Minissale A.; 2004: Origin, transport and discharge of CO2 in central Italy. Earth Sci. Rev. 66, 89–141.

Rovida A., Locati M., Camassi R., Lolli B., Gasperini P.; 2020: The Italian earthquake catalogue CPTI15. Bulletin of Earthquake Engineering, 18(7), 2953-2984.

Rovida A., Locati M., Camassi R., Lolli, B., Gasperini P., Antonucci A.; 2022: Catalogo Parametrico dei Terremoti Italiani (CPTI15), versione 4.0. Istituto Nazionale di Geofisica e Vulcanologia (INGV).

Vannoli P., Martinelli G., Valensise G.; 2021: The Seismotectonic Significance of Geofluids in Italy. Front. Earth Sci., 9:579390.

VIDEPI website, available at: https://www.videpi.com/videpi/videpi.asp. Accessed on 15 December 2023

Zhang J.; 2011: Pore pressure prediction from well logs: methods, modifications, and new approaches. Earth-Science Reviews, 108, 50-67.

Corresponding author: eleonora.vitagliano@ingv.it

The ‘Many’ Seismogenic Sources of the 1706, Mw=6.8, Maiella Earthquake: New Insights from Source Modelling

T. Volatili[1], V. Gironelli[1, 5], L. Luzi[2], P. Galli[3], M. M. C. Carafa[4], E. Tondi[1, 5]

1 Scuola di Scienze e Tecnologie – Sezione di Geologia, Università di Camerino, Italy
2 Istituto Nazionale di Geofisica e Vulcanologia, Milano, Italy
3 Presidenza del Consiglio dei Ministri, Dipartimento della Protezione Civile, Servizio Rischio Sismico - Roma, Italy
4 Istituto Nazionale di Geofisica e Vulcanologia, Sezione di Sismologia e Tettonofisica, L’Aquila, Italy
5 Istituto Nazionale di Geofisica e Vulcanologia, Sezione di Sismologia e Tettonofisica, Camerino, Italy

Introduction

Inner Abruzzi (central Italian Apennines), rank among the highest seismic hazard regions of Italy (Akinci et al., 2009; Petricca et al., 2015). All along the Apennines divide, a well-studied system of SW-dipping normal faults has been active both historically and in recent times, as evidenced by moderate-to-large earthquakes (Mw ≥ 5.5. Galadini and Galli, 2000). The most recent destructive seismic sequence occurred on April 6, 2009, (Mw = 6.3), known as the L’Aquila earthquake.

Following the events of 2009, there has been a growing interest in assessing the seismogenic potential of active faults in this region. Numerous studies have been conducted to identify active and potentially seismogenic structures. However, there are areas like the Maiella Massif, where both historical and instrumental seismicity are elusive, notwithstanding the occurrence of two strong events on November 3, 1706, and September 26, 1933, with Mw ~6.8 and 5.9, respectively (Rovida et al., 2022). According to Galli and Pallone (2019) and the Italian Macroseismic Database (DBMI15; Locati et al., 2022), these earthquakes caused severe damage over a wide area, with maximum epicentral intensities on the Mercalli-Cancani-Sieberg (MCS) scale reaching X-XI and IX, respectively. Despite being labelled as the Maiella earthquakes, the seismogenic structure responsible for these events remains controversial.

Various hypotheses have recently been proposed in the literature regarding the source of the 1706 earthquake. Before mentioning these hypotheses, it is worth noting that Pomposo and Pizzi (2009) have hypothesized that the area east of the Morrone-Porrara fault alignment is undergoing active compression, based on morphotectonic evidence of active anticline growth in the Orsogna area, suggesting a relationship with another strong event of the area (1881, Mw 5.4).

Galli and Pallone (2019), who re-evaluated the macroseismic intensity distribution on the basis of previously unknown historical sources, have suggested the activation of a blind backthrust that developed during Early-Middle Pleistocene in the footwall of the Maiella anticline as the potential

source for both the 1933 and 1706 earthquakes (labelled GALLI19 in Fig. 1). These authors also documented possible surface ruptures that occurred during the 1933 earthquake related with the Caramanico fault, a 26 km-long structure bounding westward the Maiella Massif. Although this surface evidence has been attributed to a likely passive slip of the Caramanico fault (Galli and Pallone 2019) we decided to test it anyway for the sake of completeness (labelled CARAMANICO in Fig. 1).

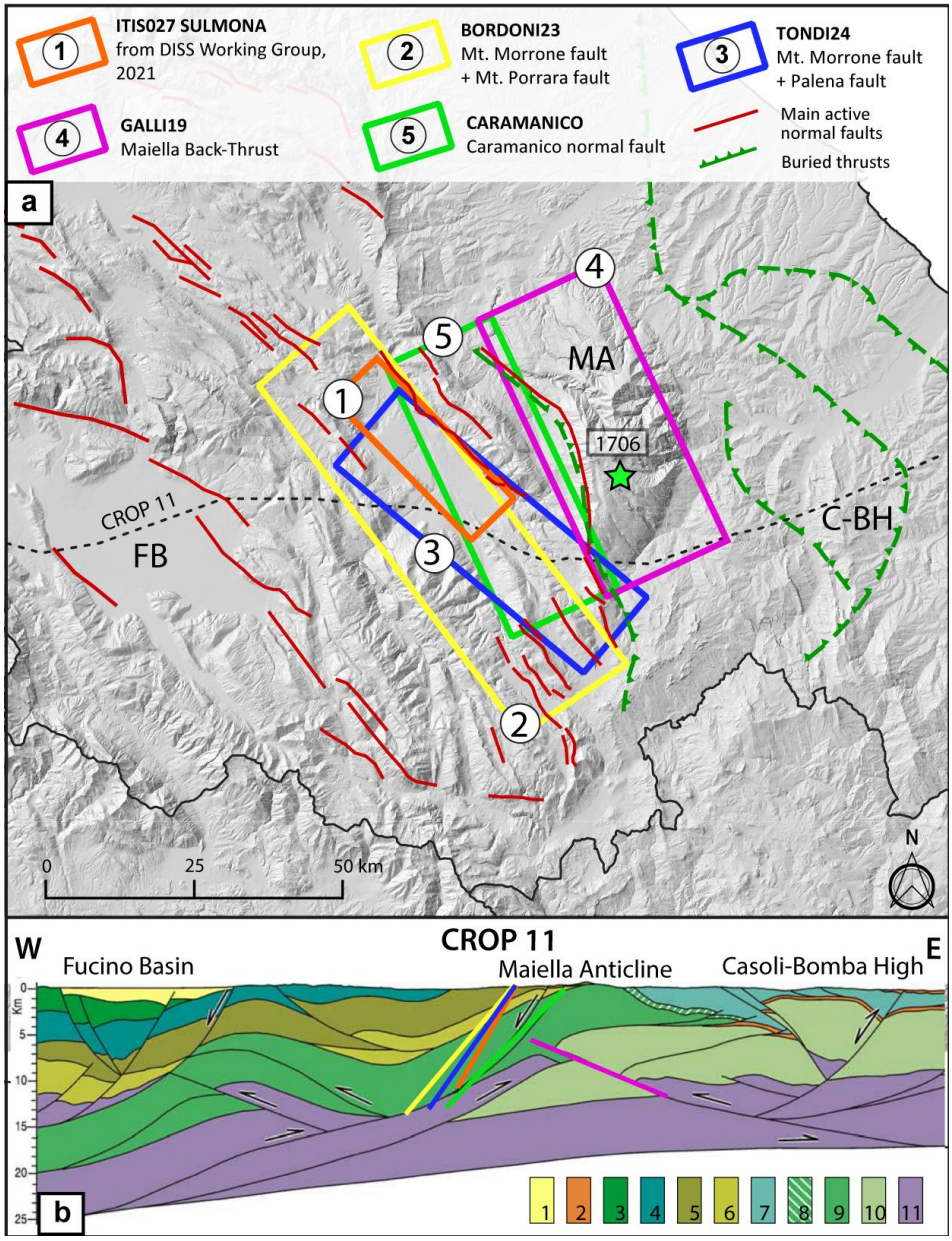

Figure 1. (a) Map showing the main tectonic structures of the study area (Galadini and Galli, 2000; Galli and Pallone, 2019) and the source models adopted for the simulations. (1) Seismogenic source "ITIS027" Sulmona from DISS (DISS Working Group, 2021); (2) Maiella back-thrust from Galli and Pallone (2019) for the 1933 earthquake; (3) Maiella back-thrust calibrated for the 1706 (Mw 6.8) earthquake, and (4) Non-Linear normal fault geometry proposal. (b) part of CROP-11 line interpreted by Patacca et al. (2008): 1, Pliocene-Quaternary continental deposits of intramontane basins; 2, Pliocene marine deposits conformably overlying the Apulia carbonates; 3, Western Marsica-Meta Unit; 4, Mount Genzana unit; 5, Mount Morrone-Porrara unit; 6, Upper Cretaceous-Pliocene Mount Queglia unit; 7, Molise units; 8, Lower Pliocene flysch of Maiella unit; 9, Mesozoic-Tertiary carbonates of Maiella unit; 10, Mesozoic-Tertiary carbonates of Apulia Platform; 11, Paleozoic-Triassic deposits.

Conversely, in the Database of Individual Seismogenic Sources (DISS – DISS Working Group, 2021; Basili et al., 2008) the 1706 earthquake, being the only meaningful seismic event in that area may relate with the largest and proximal individual seismogenic source labelled ITIS027 (see Fig. 1), associated with the Mt. Morrone fault. This consist of a dip-slip structure with surface expression consistent with a maximum magnitude of 6.7±0.1 (Galli et al., 2015), being composed by two major sub-parallel WSW-dipping splays, extending approximately 24 km across the western slope of Mt. Morrone. Lastly, Bordoni et al., (2023) presented a seismic scenario where the synchronous activation of both the Mt. Morrone fault and the Mt. Porrara fault, with a 43 km total fault length at surface and an 806 km2 maximum rupture area, would generate an earthquake consistent with the 1706 (labelled BORDONI23 in Fig. 1).

In this study we provide a comprehensive review of various hypotheses concerning the 1706 seismic source, along with another possible causative structure implying the dip-slip re-activation of the Mt. Morrone fault plus the Palena fault (labelled TONDI24 in Fig.1). As far as the Palena fault, Pizzi et al. (2010) hypothesized its Quaternary activity that, with an almost pure dip-slip kinematics, represents an inherited Pliocene syn-orogenic oblique structure. The results of this study, combined with the development of a shaking scenario, are expected to offer valuable insights to the earthquake geology community involved in studies on seismic risk assessment in this area.

Source Modelling

In our pursuit to identify the most likely source of 1706 Maiella earthquake, based on intensity data, we applied the procedure outlined by Gironelli et al. (2023) and schematised in the workflow in Figure 2. This methodology offers the advantage of testing various potential sources and conducting a quantitative interpretation of the earthquake-fault association.

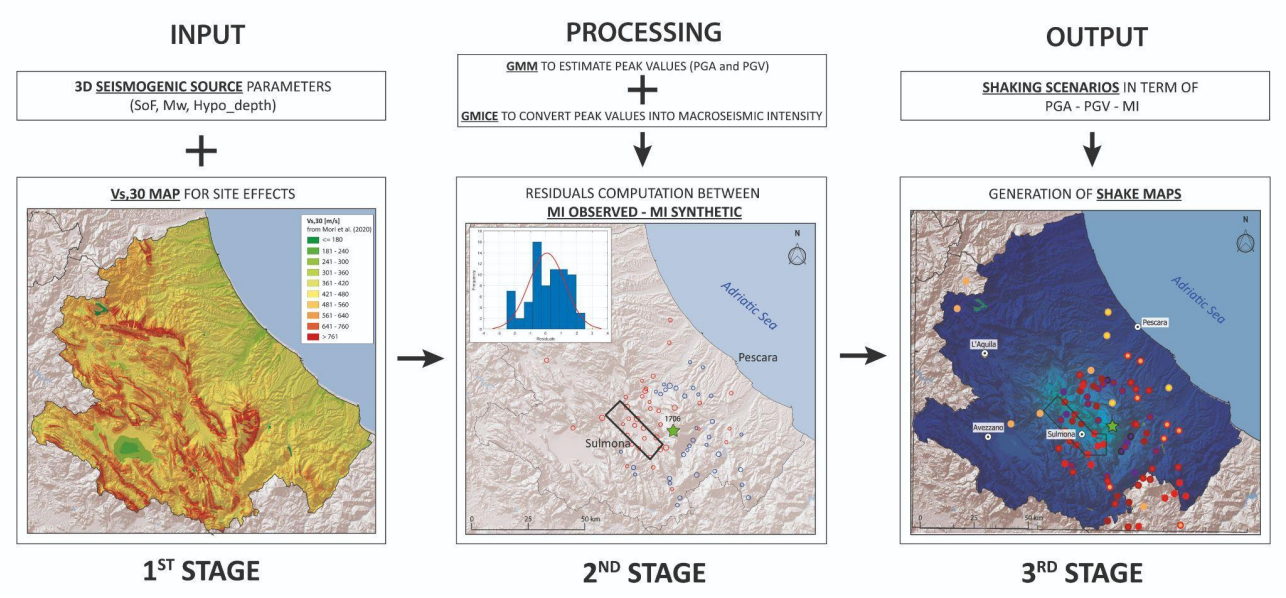

Figure 2. Summary workflow showing the main stages following Gironelli et al., 2023.

The analysis involves the creation of 3D seismogenic source models, considering the available geological and geophysical information. By varying individual source parameters such as dip angle and hypocentral depth, we estimate seismic scenarios in terms of macroseismic intensity. This is achieved by calculating synthetic peak ground motion values, including peak ground acceleration (PGA) and peak ground velocity (PGV), for each point within the 1706 macroseismic field (i.e., site). These peak values are subsequently converted into intensities using empirical relationships. This procedure incorporates site amplification effects into the synthetic ground motion calculations at each site within the macroseismic field. For this purpose, Vs,30 data representative of site effects are obtained from the more recent Vs,30 map proposed as a reference for Italy by Mori et al. (2020).

The determination of the best source model involves assessing the misfit (residuals) between the simulated macroseismic intensities and the observed ones. The accuracy of the simulated macroseismic field in reproducing the real field is evaluated by calculating the residual mean and the root-mean-square error (RMSE). The residual mean is deemed reliable if it is less than 0.1.

Our analysis shows a general fair matching between the synthetic and observed macroseismic field, especially using BORDONI23 and TONDI24 source models. However, the last surface rupture documented by paleoseismological survey in the northwestern sector of the Mt. Morrone fault dates back to the 2nd cent. CE (Galli et al., 2015), with no evidence at all of further activity (i.e., 1706 and 1933 events). Furthermore, the distribution of the macroseismic field, with the highest intensities surrounding the Maiella relief does not support the rupture of a normal fault dipping SW. On the other hand, the distribution of the macroseismic field may be biased by the settlement distribution itself, its characteristics, and relative site effects. In conclusion, it is evident that despite the possibility that this study might shed light on this open issue within the Apennine seismicity, there is still room for discussion and hopefully improvements to better constrain the seismic hazard of this region.

References

Akinci, A., Galadini, F., Pantosti, D., Petersen, M., Malagnini, L., & Perkins, D. (2009). Effect of time dependence on probabilistic seismic-hazard maps and deaggregation for the Central Apennines, Italy. Bulletin of the Seismological Society of America, 99(2A), 585-610.

Basili, R., Valensise, G., Vannoli, P., Burrato, P., Fracassi, U., Mariano, S., ... & Boschi, E. (2008). The Database of Individual Seismogenic Sources (DISS), version 3: summarizing 20 years of research on Italy's earthquake geology. Tectonophysics, 453(1-4), 20-43.

Bordoni, P., Gori, S., Akinci, A., Visini, F., Sgobba, S., Pacor, F., ... & Doglioni, C. (2023). A site-specific earthquake ground response analysis using a fault-based approach and nonlinear modeling: The Case Pente site (Sulmona, Italy). Engineering Geology, 314, 106970.

Galadini, F., & Galli, P. (2000). Active tectonics in the central Apennines (Italy)–input data for seismic hazard assessment. Natural Hazards, 22, 225-268.

Galli, P., Giaccio, B., Peronace, E., & Messina, P. (2015). Holocene paleoearthquakes and early–late pleistocene slip rate on the Sulmona fault (central Apeninnes, Italy). Bulletin of the Seismological Society of America, Vol. 105, No. 1, pp. 1–13, February 2015, doi: 10.1785/0120140029

Galli, P., & Pallone, F. (2019). Reviewing the intensity distribution of the 1933 earthquake (Maiella, Central Italy). Clues on the seismogenic fault. Alpine and Mediterranean Quaternary, 32(2), 93-100.

Gironelli, V., Volatili, T., Luzi, L., Brunelli, G., Zambrano, M., & Tondi, E. (2023). Ground motion simulations of historical earthquakes: the case study of the Fabriano (1741, Mw= 6.1) and Camerino (1799, Mw= 6.1) earthquakes in central Italy. Bulletin of Earthquake Engineering, 21(13), 5809-5830.

Gori, S., Giaccio, B., Galadini, F., Falcucci, E., Messina, P., Sposato, A., & Dramis, F. (2011). Active normal faulting along the Mt. Morrone south-western slopes (central Apennines, Italy). International journal of earth sciences, 100, 157-171.

Locati M., Camassi R., Rovida A., Ercolani E., Bernardini F., Castelli V., Caracciolo C.H., Tertulliani A., Rossi A., Azzaro R., D'Amico S., Antonucci A. (2022). Database Macrosismico Italiano (DBMI15), versione 4.0. Istituto Nazionale di Geofisica e Vulcanologia (INGV).

Mori, F., Mendicelli, A., Moscatelli, M., Romagnoli, G., Peronace, E., & Naso, G. (2020). A new Vs30 map for Italy based on the seismic microzonation dataset. Engineering Geology, 275, 105745.

Patacca, E., Scandone, P., Di Luzio, E., Cavinato, G. P., & Parotto, M. (2008). Structural architecture of the central Apennines: Interpretation of the CROP 11 seismic profile from the Adriatic coast to the orographic divide. Tectonics, 27(3).

Petricca, P., Barba, S., Carminati, E., Doglioni, C., & Riguzzi, F. (2015). Graviquakes in italy. Tectonophysics, 656, 202-214.

Pomposo, G., & Pizzi, A. (2009). Evidenze di tettonica recente ed attiva nel settore esterno sepolto dell'Appennino centrale abruzzese. In Rendiconti online della Società Geologica Italiana (Vol. 5, pp. 176-178). Società Geologica Italiana.

Rovida A., Locati M., Camassi R., Lolli B., Gasperini P., Antonucci A. (2022). Catalogo Parametrico dei Terremoti Italiani (CPTI15), versione 4.0. Istituto Nazionale di Geofisica e Vulcanologia (INGV). https://doi.org/10.13127/CPTI/CPTI15.4

*Corresponding author: tiziano.volatili@unicam.it

Interplay Between Fault Ruptures and Man-Made Structures Related With the 2023 Mw 7.8 and 7.5 Turkey Earthquakes

T. Volatili[1], A. Dall'Asta[2], S. Mazzoli[1], F. Micozzi[2], F. Stimilli[1], G. Valentini[1], M. Tümay[3], B. Aksay[3], A. Beycioğlu[3], E. Tondi[1, 4]

1 School of Science and Technology – Geology Division, University of Camerino, Italy
2 School of Architecture and Design, University of Camerino, Italy
3 Adana Alparslan Türkeş Science and Technology University, Turkey
4 National Institute of Geophysics and Volcanology, Seismology and Tectonophysics Division, Camerino, Italy

The February 6, 2023, earthquake twins, Mw 7.8 and 7.5, which struck Turkey and Syria on February stimulated scientific research on their geological and societal implications. Such destructive events, causing ca. 60'000 confirmed casualties, according to the Disaster and Emergency Management Authority (AFAD), was triggered by the partial re-activation of the Eastern Anatolian fault. Specifically, the southernmost segment of this left-lateral strike-slip structure produced fault ruptures at surface extending for ca. 500 km. Most of such fault expressions, clearly observable even from satellite images, were mapped soon after the mainshocks (Mai et al., 2023; Reitman et al., 2023).

The present study delved into the aftermath of this seismic upheaval: in 7 days of intense field survey (from 04/07/23 to 10/07/23), a total of 334 fault records were collected (Fig. 1) employing a multifaceted approach that combined traditional structural geology surveys with aero photogrammetric techniques. Covering the whole extent of the fault rupture at the surface, this research aimed to elucidate the manifold effects of surface faulting on both natural landscapes and human-built infrastructures and settlements.

Through meticulous structural geology surveys, the study catalogued the surface manifestations of the fault rupture, providing insights into the characteristics and behaviours of the ruptured fault segments. This in-depth analysis facilitated a comprehensive understanding of fault dynamics and their implications for seismic hazard assessments in the region. Moreover, the integration of aero photogrammetric surveys significantly expanded the scope and precision of the investigation. High-resolution aerial imagery enabled detailed mapping and three-dimensional reconstruction of fault rupture in key-zones. This comprehensive visualization proved instrumental in discerning fault displacement patterns and delineating the most susceptible areas to seismic activity.

Figure 1. a) spatial distribution of collected data from field (b) and drone (c) surveys. Surface ruptures highlighted in red.

One of the focal points of this study revolved around evaluating the impact of surface faulting on man-made structures and infrastructural facilities. Through meticulous field assessments and detailed analyses, the research documented the structural damage incurred by buildings, roads, bridges, and other vital infrastructures. By correlating the observed damage patterns with fault characteristics and ground motions, valuable insights were gleaned into the vulnerability of various structures (i.e., public, and private buildings) to seismic events of this magnitude. The findings of this study offer contributions to the fields of seismology, structural geology, and earthquake engineering. By elucidating the complex interactions between surface faulting and infrastructure vulnerability, the research provides a robust foundation for enhancing seismic risk assessments, informing urban planning strategies, and bolstering disaster preparedness and mitigation efforts in earthquake-prone regions.

In summary, this comprehensive investigation, blending traditional structural geology surveys with advanced aero photogrammetric techniques, presents a holistic understanding of the M7.8 and 7.5 Turkey earthquakes surface rupture effects. The implications of this study extend far beyond understanding the geological aspects, offering insights into the intricate interplay between seismic

events and the built environment, thus paving the way for more resilient and earthquake-resistant buildings and infrastructures in vulnerable regions worldwide.

References

Mai, P. Martin; Aspiotis, Theodoros; Aquib, Tariq Anwar; Cano, Eduardo Valero; Castro-Cruz, David; Espindola-Carmona, Armando; Li, Bo; Li, Xing; Liu, Jihong; Matrau, Rémi; Nobile, Adriano; Palgunadi, Kadek Hendrawan; Ribot, Matthieu; Parisi, Laura; Suhendi, Cahli; Tang, Yuxiang; Yalcin, Bora; Klinger, Yann; Jónsson, Sigurjón (2023). "The Destructive Earthquake Doublet of 6 February 2023 in South-Central Türkiye and Northwestern Syria: Initial Observations and Analyses". The Seismic Record. 3 (2): 105–115. doi:10.1785/0320230007

Reitman, Nadine G, Richard W. Briggs, William D. Barnhart, Jessica A. Thompson Jobe, Christopher B. DuRoss, Alexandra E. Hatem, Ryan D. Gold, John D. Mejstrik, and Sinan Akçiz (2023) Preliminary fault rupture mapping of the 2023 M7.8 and M7.5 Türkiye Earthquakes. DOI: https://doi.org/10.5066/P985I7U2

Corresponding author: tiziano.volatili@unicam.it

The role of long-range correlations and memory in earthquake occurrence

D. Zaccagnino[1*], L. Telesca[2], C. Doglioni[1,3]

[1] Sapienza University, Earth Sciences Department, Rome, Italy
[2] Institute of Methodologies for Environmental Analysis, National Research Council, Tito, Italy
[3] Istituto Nazionale di Geofisica e Vulcanologia (INGV), Rome, Italy.

Seismicity occurs because of strain accumulation in the brittle crust due to the action of tectonic forces. However, this background process is just one of numerous ones affecting earthquake occurrence. In the long run it controls the frequency of large events (Neely et al., 2023); conversely, at our time scales it is likely one of the less impactful. The spatial and temporal evolution of seismic sequences has been proposed to be driven by fluid migration and frictional instability and to be affected by stress perturbations as well as anthropic activities, rheology, structural properties of fault systems and by the tectonic regime (e.g., Rice & Cocco, 2007; Ellsworth, 2013; Ross & al., 2017). Consequently, several empirical relationships have been found connecting properties of seismicity with geophysical observables (pore pressure, differential stress, static friction etc.). We suggest that local variability of some routinely investigated parameters can be clarified considering few all-encompassing physical principles instead of advocating several hardly testable physical mechanisms. To provide an observational example, we analyse a high-definition regional seismic catalogue of seismicity in Central Italy (Tan et al., 2021). We identify a chain of relationships, starting with the properties of inherited structures and tectonic stress gradients directly affecting the fractal properties of fault systems, which, in turn, have an impact on the frequency-magnitude scaling of earthquakes. It produces implications for the duration of seismic sequences, complexity of the seismogenic source and the composition of moment tensors (Zaccagnino & Doglioni, 2022). Our approach has the advantage to be valid regardless of the specific rheology, lithology, tectonic setting, and state of stress. In this regard, we guess that such connections between seismicity and structural properties of fault systems are universal, being due to the action of feedback mechanisms and memory processes.

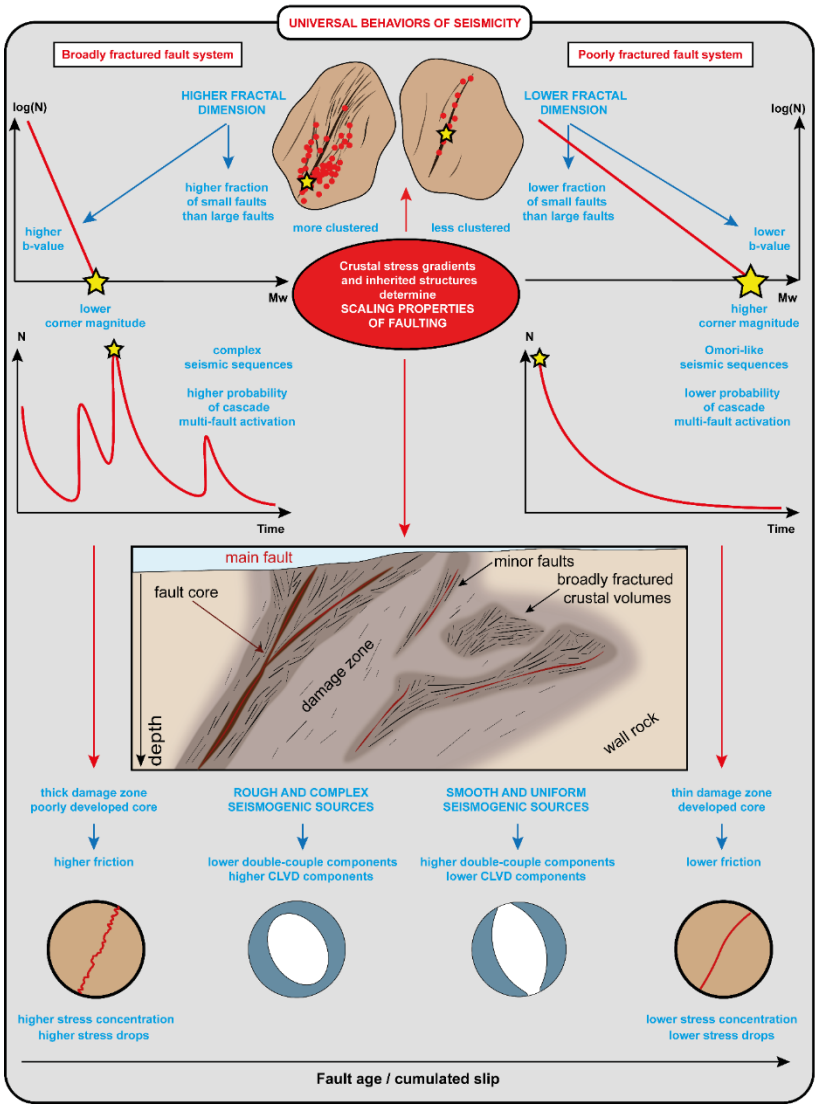

Fig. 1 - Universal properties of seismicity. Crustal stress gradients and inherited structures determine the scaling properties of seismicity, hence, the spatial organization of faults and fractures and its scaling properties. Higher fractal dimension of fractures and hypocenters produces strongly clustered seismicity in space with steeper Gutenberg-Richter law and lower corner magnitudes; hence, lower maximum magnitude and vice versa. Moreover, more developed fracturing with thicker damage zones and complex seismogenic sources promote stress accumulation because of higher internal friction within the boundary interface and, also, larger stress drops (magnitude fixed) during seismic events. At last, the interaction of fault planes with different spatial orientation is more likely in complex fault systems, which decreases the double-couple component of moment tensors of earthquakes.

References

Ellsworth W. L.; 2013: *Injection-induced earthquakes*. Science, 341(6142), 1225942.

Neely J. S., Salditch L., Spencer B. D. and Stein S.; 2023: *A More Realistic Earthquake Probability Model Using Long-Term Fault Memory*. Bull. Seismol. Soc. Am., 113(2), 843-855.

Rice J. R. and Cocco M.; 2007: *Seismic fault rheology and earthquake dynamics.* Tectonic faults: Agents of change on a dynamic earth, 99-137.

Ross Z. E., Hauksson E. and Ben-Zion, Y.; 2017: *Abundant off-fault seismicity and orthogonal structures in the San Jacinto fault zone*. Sci. Adv., 3(3), e1601946.

Tan Y. J., Waldhauser F., Ellsworth W. L., Zhang M., Zhu W., Michele M., ... and Segou M.; 2021: *Machine-learning-based high-resolution earthquake catalog reveals how complex fault structures were activated during the 2016–2017 Central Italy sequence*. The Seismic Record, 1(1), 11-19.

Zaccagnino D. and Doglioni C.; 2022: *The impact of faulting complexity and type on earthquake rupture dynamics*. Commun. Earth Environ., 3(1), 258.

Corresponding author: davide.zaccagnino@uniroma1.it

The 1783 Calabria earthquake sequence: a review of the coseismic effects on the natural environment

C. Zei[1,2], C. Ciuccarelli[1], M.G. Bianchi[1], G. Tarabusi[1], D. Mariotti[1]

[1] Istituto Nazionale di Geofisica e Vulcanologia, Italy
[2] Università degli Studi di Ferrara - Dipartimento di Fisica e Scienze della Terra, Italy

The primary goal of the initial versions of the CFTI (Boschi et al. 1995, 1997 and 2000) was to define the effects of strong earthquakes on the built environment. Consequently, the effects on the natural environment (EE) were not extensively studied but were considered as additional information.

In recent years, starting from the CFTI5med (Guidoboni et al, 2018 and 2019), special attention has been devoted to the retrieval and analysis of the EE.

Here we present a review of the effects on the natural environment of the 1783 Calabria earthquake sequence, starting from the data already included in the CFTI database.

The earthquake sequence began on 5 February 1783 and lasted for over three years, featuring five main shocks with a magnitude between 5.9 and 7.0 (5 February, 6 February, 7 February, 1 March, and 28 March 1783) and several hundred smaller shocks, which had cumulative devastating effects over an area of several thousand square kilometers. Within two months, from 5 February to 28 March, the earthquake activity migrated from the foothills of the Aspromonte to the area between the Golfo di Sant'Eufemia and the Golfo di Squillace.

Before this review, for the 1783 earthquake sequence the CFTI5med reported 222 EE, grouped into 14 different categories based on the observed natural phenomena. The most frequently observed typologies were landslides (67 observations), ground cracks (57 observations), and water effects (38). Only 2% of the 222 EE were assigned to a specific earthquake of the sequence. Other recent reviews (Cucci 2022) pointed attention to specific types of effects instead, in this work, we collected all the effects on the natural environment reported.

We focused on the review of 22 historical sources coeval with the earthquake, already archived in the CFTI5Med. These sources are the most reliable for the sequence, as many such as Vivenzio (1783) and Sarconi (1784), describe the effects on the natural environment after their survey of the epicentral area.

The CFTIvisual dataset (Bianchi et al., 2022) plays a central role in this work as it supplies over thirty historical original drawings that can be used to identify and locate the EE: indeed, they show

the coseismic effects in the territory as it appeared at the time, including cracks, landslides, effects on surface waters, liquefactions, appearance of ponds, etc. The detailed visual representation of the effects allowed for a better attribution to the correct effect category, compared to only consulting historical sources. Moreover, since in many cases it was possible to georeference the drawings accurately, we were able to improve the location of the effects.

As an in-depth part of this work, we also conducted a specific analysis of the Historical Earthquake-Induced Landslides (HEILs), in order to include new data in the CFTI Landslide (Zei et al., 2023). Our goal was to achieve a more accurate location and definition of the slope movement types of the HEILs, whenever the descriptions of the historical sources or drawings allowed it, through a geographical comparison with data of different origins. When possible, these effects were associated with the individual landslides reported in the IFFI database (https://www.progettoiffi.isprambiente.it/).

Our review led to a 120% increase in the pre-review number of effects, totalling 494 elements. Over 67% of the effects are now connected to a specific earthquake in the sequence, compared to the previous 2%.

The most numerous effects are those affecting the ground (69% of the total); within this class, the more common are landslides (59% of ground effects). Furthermore, the review returned effects related to seven EE categories for which there were no data (figure 1).

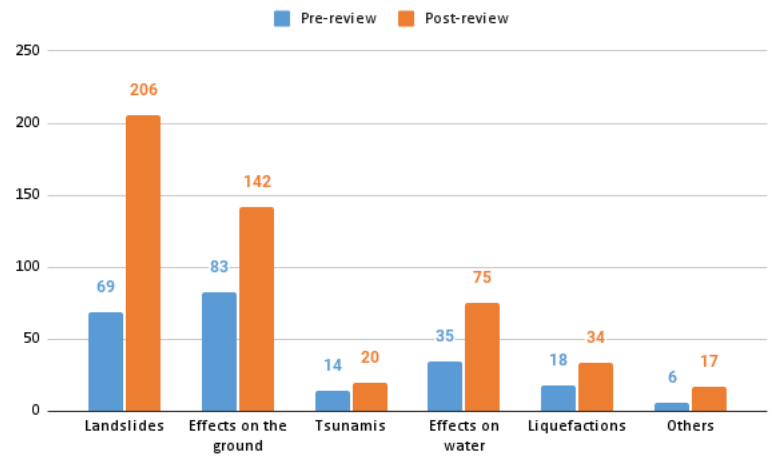

Fig.1 Pre- and post-review effects on the natural environment collected for the 1783 Calabria earthquake sequence.

Regarding HEILs, 36% of them have excellent/good location accuracy. All earthquake-induced landslides, along with their improvements in number, movement type and location, are now collected into the CFTILandslides database (Zei et al., 2023).

Acknowledgments

Part of the activities have been supported by a grant from Italy's Presidenza del Consiglio dei Ministri-Dipartimento della Protezione Civile. Nevertheless, the views and conclusions reported are the sole responsibility of the authors, and should not be interpreted as necessarily representing official policies, either expressed or implied, of the Dipartimento della Protezione Civile.

References

Bianchi M.G., Tarabusi G., Ciuccarelli C., Maresci M., Baranello S., Taccone R.C., Ferrari G.; 2022: *CFTIvisual, Atlante delle fonti visive dei terremoti italiani*. Istituto Nazionale di Geofisica e Vulcanologia (INGV). https://doi.org/10.13127/cfti/visual

Boschi E., Guidoboni E., Ferrari G., Mariotti D., Valensise G., Gasperini P. (eds); 200: *Catalogue of Strong Italian Earthquakes from 461 B.C. to 1997*. Annali di Geofisica, 43, 4, 609-868.

Boschi E., Ferrari G., Gasperini P., Guidoboni E., Smriglio G., Valensise G. (eds); 1995: *Catalogo dei forti terremoti in Italia dal 461 a.C. al 1980*. ING-SGA, Bologna, 970 pp.

Boschi E., Guidoboni E., Ferrari G., Valensise G. and Gasperini P. (eds.); 1997: *Catalogo dei forti terremoti in Italia dal 461 a.C. al 1990*, vol. 2. ING-SGA, Bologna, 644 pp.

Cucci L.; 2022: *NW-dipping versus SE-dipping causative faults of the 1783 M7.1 Southern Calabria (Italy) earthquake: The contribution from the analysis of the coseismic hydrological changes.* Front. Earth Sci. 10:987731. doi:10.3389/feart.2022.987731

Guidoboni E., Ferrari G., Mariotti D., Comastri A., Tarabusi G., Sgattoni G., Valensise G.; 2018: *CFTI5Med, Catalogo dei Forti Terremoti in Italia (461 a.C.-1997) e nell'area Mediterranea (760 a.C.-1500)*. Istituto Nazionale di Geofisica e Vulcanologia (INGV). https://doi.org/10.6092/ingv.it-cfti5

Guidoboni E., Ferrari G., Tarabusi G., Sgattoni G., Comastri A., Mariotti D., Ciuccarelli C., Bianchi M.G., Valensise G.; 2019: *CFTI5Med, the new release of the catalogue of strong earthquakes in Italy and in the Mediterranean area*, Scientific Data 6, Article number: 80. https://doi.org/10.1038/s41597-019-0091-9

Istituto Superiore per la Protezione e la Ricerca Ambientale (ISPRA); *IFFI, Inventario dei Fenomeni Franosi in Italia.* https://www.progettoiffi.isprambiente.it/

Sarconi M.; 1784: *Istoria de' fenomeni del tremoto avvenuto nelle Calabrie, e nel Valdemone nell'anno 1783 posta in luce dalla Reale Accademia delle Scienze e delle Belle Lettere di Napoli*, Napoli.

Tarabusi G., Ferrari G., Ciuccarelli C., Bianchi M.G., Sgattoni G., Comastri A., Mariotti D., Valensise G., Guidoboni E.; 2020: *CFTILab, Laboratorio Avanzato di Sismologia Storica. Istituto Nazionale di Geofisica e Vulcanologia (INGV)*. https://doi.org/10.13127/CFTI/CFTILAB

Vivenzio G.; 1783: *Istoria e teoria de' tremuoti in generale ed in particolare di quelli della Calabria, e di Messina del MDCCLXXXIII,* Napoli.

Zei C., Tarabusi G., Ciuccarelli C., Mariotti D., Baranello S., Sgattoni G., Burrato P., CFTI working Group; 2023: *A new database of historical earthquake-induced landslides in Italy*, 41st National Conference of the GNGTS, Bologna https://gngts.ogs.it/atti/GNGTS2023/HTML/212/

Corresponding author: caterina.zei@ingv.it